CVD OF CERAMIC COATINGS IN A HOT WALL AND FLUIDISED BED REACTOR

A thesis submitted for the degree of

Masters of Applied Science

by

Despina Papazoglou B.Sc.(Hons)

Department of Chemical Engineering

The University of Adelaide

Adelaide, SA 5001

AUSTRALIA

1994

To my children

John & George

TABLE OF CONTENTS

DECLARATION

This thesis contains no material which has been accepted for the award of any other degree or diploma in any University or other tertiary institution and, to the best of my knowledge and belief, this thesis contains no material previously published or written by another person, except where due reference has been made in the text of the thesis or where common knowledge is assumed.

The author consents to the thesis being made available for loan and photocopying, when deposited in the University Library.

Signature _____ Date 13/9/94

ACKNOWLEDGMENTS

I wish to express my sincere gratitude to Dr. Vinod Puri, my DSTO supervisor and my external supervisor Prof. P.K. Agarwal, Department of Chemical Engineering, University of Adelaide for their continual guidance, support and supervision throughout this research project.

Many thanks are due to Barry Jenkins, Jim Bulley and Dave Harris of Explosives Ordnance Division(EOD), Materials Research Laboratory(MRL), for their technical assistance in the construction of the furnace, Jim Trenorden of EOD/MRL, for his assistance with some of the technical drawings, Graham Fowler of Optoelectronics Division(OED), Surveillance Research Laboratory(SRL), for assisting in SEM and X-ray diffraction analyses, John Terlet and Hugh Rossen of CEMMSA, University of Adelaide for SEM and TEM analyses, and Corina Stamatiou of University of Adelaide for providing the Mass Spectrometry data. A special thanks is also due to Dr. Temi Linjewile for his useful suggestions during the designing and construction of the fluidised bed reactor. The financial support from Defence Science and Technology Organisation is gratefully acknowledged.

Finally, I would like to thank my husband Arthur and my parents for their encouragement and support.

ABSTRACT

Silicon based ceramic type compounds were chemically deposited by the decomposition of methyltrichlorosilane in a hot wall reactor and a fluidised bed reactor; using nitrogen and/or hydrogen as a carrier gas.

A hot wall reactor was designed and fabricated from a high purity carbon cylinder. This system was later converted to a fluidised bed unit. The coating was effected by injecting methyltrichlorosilane into the reactor at 973, 1073 and 1173 K. The other coating variables included methyltrichlorosilane feed rate and carrier gas (nitrogen and/or hydrogen) concentration. The effectiveness of varying reaction conditions were evaluated by examining the coatings under Scanning Electron Microscopy for coating thickness, coating uniformity and adherence to the steel plate. From this data, a comparative assessment was made on the efficiency and applicability of hot wall and fluidised bed reactor. The results clearly indicated that fluidised bed technique provided superior coatings in comparison with hot wall reactor.

Scanning Electron Microscopy and X-ray diffraction results also indicated that at applied temperatures silicon dioxide, silicon carbide, silicon and carbon were the most prevalent species.

Thermodynamic analysis of methyltrichlorosilane/nitrogen/hydrogen

system under varying reaction conditions was conducted using the CSIRO Thermal Chemistry System computer code CHEMIX, which is based upon the free energy minimisation method. In order to calculate the equilibrium composition of this system, 37 gaseous and 5 condensed species were taken into consideration. The thermodynamic variables included temperature (500°C-1000°C), mole ratios of nitrogen to methyltrichlorosilane and hydrogen to methyltrichlorosilane. Thermodynamic calculations were in good agreement with the experimental results except that formation of silicon dioxide was not predicted. Mass spectrometry, however, indicated the presence of hydroxy derivatives of silanes, which probably on decomposition resulted in the formation of silicon dioxide. Kinetics of the reaction were performed using PE DSC 7, and also from the deposition rates. Lower activation energies (14.19kJ/mole) indicate that the reaction is not temperature dependant.

Based on the Mass Spectrometry data and the information obtained from thermodynamic calculations, an attempt was made to predict the chemistry of the system. A plausible reaction mechanism is proposed under studied experimental conditions. It is believed that silicon carbide, silicon, and silicon dioxide are the main species deposited. Formation of silicon dioxide is possible, in the presence of water molecules. It is presumed that the water vapour was absorbed by methyltrichlorosilane, a highly hygroscopic material, during feeding. The formation of carbon can

be avoided by selecting the operating conditions which favour the formation of silicon carbide, i.e., higher temperature and higher concentrations of hydrogen.

LIST OF FIGURES

LIST OF TABLES

CHAPTER 1

INTRODUCTION

1.1 BACKGROUND

The class of materials that are neither metallic nor organic are classified as ceramics[1]. The early ceramics were the low firing earthwares that appeared some 10,000 years ago. With the advent of sophisticated firing technology, the quality of ceramic product improved dramatically. However, until recently the word ceramics only meant pottery, roofing tiles, clay pipes and bricks. But, today ceramic products are widely used such as magnets in television, optical fibres for telecommunications, insulators in electronics, heating elements, and substrates for integrated circuits. As engineering ceramics they appear in engines and cutting tools.

O'Bannon[2] defines ceramics as:

> **"any of a class of inorganic, nonmetallic products which are subjected to a temperature of 540°C and above during manufacture or use, including metallic oxides, borides, carbides, or nitrides, and mixtures or compounds of such materials."**

A more precise definition, however, was given by W.W. Perkins[3], editor of the American Ceramic Society's Ceramic Glossary. According to Perkins[3], ceramics can be defined as:

> **"any of a class of inorganic, nonmetallic products which are subjected to a high temperature (>540°C) during manufacture or use. Typically, but not exclusively, a ceramic is a metallic oxide, bromide, carbide, or nitride, or a mixture or compound of such materials, i.e., it includes anions that play important roles in atomic structures and properties."**

These definitions are general and do not include some of the products currently manufactured because of advances in technology. In recent years, terms like crystalline ceramics, new ceramics, fine ceramics, technical ceramics, engineering ceramics, high technology ceramics, structural ceramics, hydrothermal ceramics, and bioceramics have been used extensively [1].

The modern advanced ceramics differ from conventional ceramic consumer goods in that they are made from extremely pure, microscopic powders that are consolidated at high temperatures to yield a dense and durable structure. Compared with general structural metals, advanced ceramics have superior wear resistance, high temperature strength, and chemical stability. Also, they generally have lower electrical and thermal conductivity and lower toughness. The low toughness of ceramics causes them to fail suddenly when the applied stress is sufficient enough to propagate cracks that originate at flaws in the material. This unpredictable failure phenomenon caused by poor control over flaw

populations hinders the use of ceramics in load bearing applications[1].

Over the years several techniques have been suggested that can reduce the sensitivity of ceramics to flaw. These include incorporation of ceramic particulates, whiskers, or continuous fibres in a ceramic matrix. An alternative approach is the application of a thin ceramic coating to a metal substrate. The coated component thus exhibits the surface properties of a ceramic combined with the high toughness of metal in the bulk. Also advanced ceramic components with minimal flaws are more expensive than metal components they would replace. Therefore, in many applications, coatings of an advanced ceramic (high performance ceramic) on a metal substrate may offer the best compromise between cost and performance.

The coating approach offers several advantages. Firstly, it provides the possibility of independently optimising the properties- of the surface region and those of the base material for a given application- necessary for the efficient functioning of the component over the required lifetime. Secondly, there can be significant cost savings by replacing expensive exotic materials only for thin coatings and not for the manufacture of bulk components. Thirdly, coatings can contribute to the conservation of strategically critical materials.

Coated metallic components are gaining widespread acceptance in

industry. For instance, coatings of titanium nitride, titanium carbide, and alumina have been extensively used to enhance the useful life of tungsten carbide on high speed steel cutting tools by a factor of two to five[4].

Over the decade, many different processes have been used in the fabrication of ceramic coatings and in the modification of surfaces of various substrates. Table 1 lists the most common processes which have been widely investigated, some of which are used in industrial applications. The choice of a particular coating process depends largely on the desired surface characteristics. Other factors which can influence the choice of coating process include purity, physical state and toxicity of the material to be deposited, deposition rate, substrate temperature limits, substrate modification techniques to obtain required adhesion, and finally cost.

Coating technology has advanced rapidly in the past thirty years and it has greatly assisted in meeting complex demands placed on materials. The important coating methods for high technology applications can be broadly divided into two groups: 1) processes which involve a droplet mode of transfer; and 2) processes involving an atom-by-atom mode of transfer.

In the first type, the deposition is obtained via the transfer of material by the action of heat and high velocity gas. Thermal spraying is the generic

Table 1 : Categorisation of Coating Techniques[18A]

I.. Atomic Deposition

- **A. Chemical Vapour Environment**
  - Chemical Vapour deposition
    - Reduction
    - Decomposition
    - Plasma Enhanced
    - Deposition
    - Spray Pyrolysis
    - Infiltration
    - Laser assisted
    - Metal organic
- **B. Electrolytic Environment**
  - Electroplating
  - Electroless Plating
  - Fused Salt Electrolysis
  - Chemical Displacement
- **C. Plasma Environment**
  - Sputter deposition
    - Diode
    - Triode
    - Reactive
  - Evaporation
    - Direct
    - Activated Reactive
  - Ion plating
    - Hot cathode discharge
    - Reactive
  - Diffusion
  - Plasma polymerisation
- **D. Vacuum Environment**
  - Vacuum evaporation
  - Ion beam deposition
  - Ion implantation
  - Molecular Beam epitaxy

II. Particulate Deposition

- **A. Fusion Coatings**
  - Electrostatic
  - Electrophoretic
  - Sol-Gel
- **B. Impact Plating**
- **C. Thermal Spraying**
  - Plasma spraying
    - Low press plasma spray
    - Laser assist plasma spray
  - Flame spraying
  - Detonation gun
  - Electric Arc spraying

III. Bulk Coatings

- **A. Mechanical**
  - Co-extrusion
  - Explosive cladding
  - Roll bonding
  - Electromagnetic impact bonding
- **B. Electrostatic spraying**
  - Printing
  - Spin coating
- **C. Overlaying**
  - Laser glazing
  - Brazing
  - Weld coating
    - Oxy-acetylene
    - Powder welding
    - Manual metal arc
    - Metal inert-gas
    - Tungsten inertgas
    - Submerged arc
- **D. Diffusion**
  - Diffusion bonding
  - Hot isostatic pressing
- **E. Wetting Processes**
  - Dipping
  - Enamelling
  - Painting
  - Spraying
  - Thick film

IV. Surface Modification

- **A. Chemical Conversion**
- **B. Chemical (liquid)**
  - Oxidation
- **C. Chemical (vapour)**
  - Thermal
  - Plasma
- **D. Electrolytic**
  - Anodization
  - Fused salts
- **E. Leaching**
- **F. Ion Implantation**
- **G. Mechanical**
  - Shot peening
- **H. Sputtering**
- **I. Surface Enrichment**
  - Diffusion from bulk
- **J. Thermal**
  - Laser alloying
  - Quenching
  - Diffusion

term used for a particular type of coating technique in which the material to be sprayed is rapidly heated until substantially molten and propelled through a high velocity thermospray gun onto the prepared substrate surface. Flame spray[5] and plasma spray[6] processes, are the two main spraying techniques grouped under this category.

During flame spraying[5], the coating compound is melted in an environment of an oxy-fuel gas flame and the molten particles are propelled towards the substrate with the aid of compressed air. Suitable materials for coating may be available either in wire form or powder form and include pure elements such as Cu and Al, alloys and some composites. The plasma spraying[6] process involves the injection of powder particles into a plasma jet stream created by heating an inert gas in a constricted electric arc which passes from the central electrode in the torch through the nozzle. The particles injected into the plasma jet undergo simultaneous melting and are accelerated at high velocity towards the substrate. This method[7,8] is used for spray coating of metals and ceramics, free flowing powders, and some plastics. These methods are limited to those materials which melt below 3000°C.

In the second type, the deposition process involves the synthesis either in vapour phase or in solution from precursor materials, transport, and subsequent deposition on the target substrate. These include techniques based on Physical Vapour Deposition (PVD) and Chemical Vapour

Deposition (CVD). Processes based on vacuum evaporation[9,10], sputtering[11], and ion plating[12-14] are grouped under PVD.

Vacuum evaporation[9,10] involves the deposition of a single material via the condensation of a vapour of a compound or a pure element on a hot or cold base to form a solid deposit. This technique can be used for depositing metals, semiconductors, alloys and refractory compounds.

Sputtering[11] is a process whereby the coating material is passed into the vapour phase by ion bombardment and ejected towards the substrate to be coated. In this technique an energetic ion strikes a solid surface with sufficient momentum to remove one or more surface atoms, atomic clusters or molecules. The ejection of the source material is accomplished by the bombardment of the surface with high energy particles of an inert gas accelerated by high voltage. Materials such as metals, alloys, semiconductors, metal oxides, some sulphides, carbides, and cermets can be deposited using this technique[11].

Ion plating[12-14] involves the evaporation of atoms through an argon gas discharge directed towards the substrate. Materials such as metals, alloys, and ceramics can be deposited using this technique.

Electrochemical[15-17] processes are mainly used in the deposition of metals and alloys and occur in solution rather than in vacuum. The

technique has been successful in the deposition of Pt, Rh, Ru, Cu, Ni, Cr, Fe, Ag and Au[18A], while difficulties have been encountered in the deposition of Al, Mo, Si, W, Ti, Ta, Zr, Nb and Ir[18A].

CVD uses chemical processes occurring between the gaseous compounds when in contact with a heated substrate. Deposition takes place as long as the reaction produces a solid. Substrate temperature governs the deposition rate, resultant microstructure and properties of the coating. The chemical vapour deposition process finds its greatest application in the production of coated materials that are not easily fabricated by conventional means. The process is particularly useful for the deposition of coatings in difficult to reach sites. The CVD process offers the deposition of alloys, carbides, oxides and nitrides.

1.2 OBJECTIVES OF THE PRESENT STUDY

The aim of the present investigation was to determine the feasibility of hot wall and/or fluidised bed reactor for the deposition of ceramic type coatings from organosilane precursor materials at lower temperatures (<1273 K) using CVD technique.

The principal objectives of the present study are:

- To design and construct a carbon based hot wall reactor and a

fluidised bed reactor that will safely operate up to 1350 K;

- To evaluate and screen precursor materials for obtaining a desirable ceramic type coating;
- To develop suitable priming methods to achieve optimum adhesion;
- To optimise processing parameters to obtain a coating of desirable surface characteristics;
- To understand the chemistry of the system by the application of thermodynamics and from reaction kinetic studies;
- To assess the suitability of hot wall and/or fluidised bed reactor for the decomposition of organosilane compounds and subsequent deposition of silicon based products;
- To select and possibly recommend optimal reaction conditions for obtaining a desirable surface coating.

Literature review on the chemical vapour deposition process is given in Chapter 2. This includes a general description of the deposition equipment, process control parameters and structure of CVD deposits.

Chapter 3 presents a detailed description of the furnace construction, materials and methods utilised, and experimental detail.

Thermodynamics and chemical kinetics are given in chapters 4 and 5 respectively. Results and discussion of experimental results are presented in Chapter 6.

CHAPTER 2

CHEMICAL VAPOUR DEPOSITION

2.1 INTRODUCTION

CVD may be defined as a technique in which a solid film or a coating is deposited by the condensation of a compound or compounds as a result of chemical reactions in the gas phase either on, at, or near the substrate surface. The CVD technique probably existed for a long time. Even the caveman used soot formed by the condensation of firewood to paint his cave and to draw figures on the walls. Obviously, this is an application of pyrolytic carbon[19].

The first documentary evidence of the CVD process was a patent granted in 1893, to de Lodyguine[20], which described the deposition of tungsten on carbon lamp filaments by hydrogen reduction of tungsten chloride.

For many years CVD remained a laboratory curiosity, however, in recent years it has become an indispensable tool of modern technology. There has been a widespread use of surface modified products using CVD technique particularly in specialised areas of nuclear, space, and microelectronic technologies.

The interest in CVD has increased dramatically in the last three decades and there is an abundance of literature available covering various aspects of this technology. Its capacity to improve the surface characteristics of a number of materials used in high tech industry has given CVD research a

major impetus. Some of the prominent areas of applications[21] include:

- deposition of superconducting, semiconducting and insulating films for integrated circuits;
- formation of very hard layers to reduce the wear of mechanical components;
- production of protective layers against corrosion or oxidation at high temperatures;
- diffusion barriers;
- thermal barriers;
- infiltration of porous materials;
- production of composite materials from elements which are difficult to sinter; and
- optical applications.

CVD technique has been known for its versatility as a variety of elements and compounds can be uniformly deposited on objects of complex shapes. A typical laboratory or industrial CVD system would include a source of precursor gases, a heated reaction chamber, and a system for the treatment and disposal of exhaust gases. The CVD process, as such, can be described in terms of system chemistry (chemical species, thermodynamics, kinetics, and reaction mechanism), mass transport, gas flow, and characterisation of deposited film and gaseous effluents.

2.2 CVD REACTORS

The design and operation of CVD reactors varies widely with application. The basic components of any CVD coating system, however, include a source of precursor gases, a heated reaction chamber, and a system for the treatment and disposal of exhaust gases. Although some reactors can be used for a group of reactions in which the volatility and chemical stability of the precursor materials are similar, there is no such thing as a universal CVD reactor. The variation in CVD reactors is well documented in the literature[22-25].

CVD coatings, however, are applied in reactors similar in principle to the laboratory reactors of the type shown in Fig. 1. The deposition system is generally designed to operate under variable conditions of temperature (1173 K to 2473 K), pressure (10^{-6} Torr to 1 atm.), and type of precursor material (liquid or solid). The various components of CVD reactors are discussed below.

2.2.1 FEED SYSTEMS

Feed systems are designed to transport precursor materials to the reaction chamber. Different options are used for the injection of gases, liquids and solids. Gaseous materials, which are commercially available in compressed form in tanks are fed directly into the reactors, and the feed

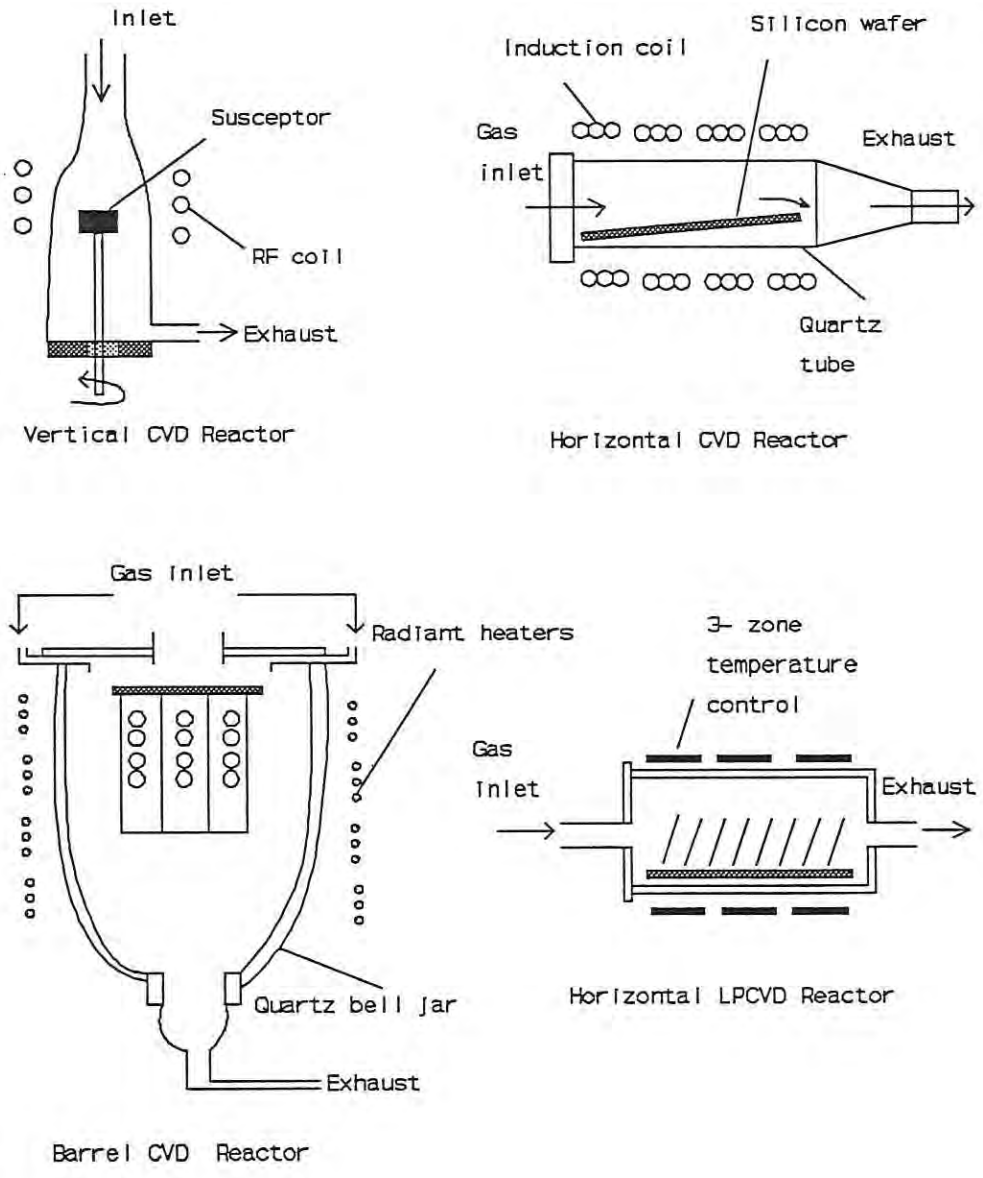

Figure 1 : Typical CVD reactors[146A]

rates are monitored by flow meters and pressure gauges. This method has been found useful for the handling of materials such as tungsten hexafluoride, which is injected into the reaction chamber under vacuum using H_2 as a carrier gas[26].

Similarly, carbon deposition on nuclear fuel particles has been obtained by the injection of gaseous hydrocarbons into the fluidised bed reactor[27,28].

However, when low vapour pressure reactants are used, the delivery procedures and control are more complicated. Two alternate methods which are generally employed include vaporisation and *in situ* generation. In addition , liquids or solids can be vaporised by passing an inert carrier gas through or over the material. The delivery rate in such cases is controlled by the source temperature and pressure and in addition by the flow rate of the carrier gas. An example of this type is the vaporisation of $TiCl_4$ at or near room temperature for CVD of TiO_2 or TiB_2. Although convenient, there is limited control on the reactant concentration, unless the carrier gas is fully saturated with the reactant. This is highly unlikely, particularly when the stream residence time in the vaporiser is too short, i.e., high flow rate and/or low surface area of reactant, or the reactant is entrapped in the form of liquid droplets. SiC coatings on carbon fibres have been obtained by bubbling H_2 through a vessel containing liquid methyltrichlorosilane (MTS) at a constant temperature. A reactant flow rate of 0.24 mole/h has been obtained[29].

Other methods of reactant feeding include metering liquid into the reaction chamber by a metering pump. Minato and Fukuda[30] used this technique for the transportation of pyrolytic MTS into a fluidised bed reactor for the deposition of SiC on carbon coated fuel particles. The liquid MTS is injected into the carrier gas stream of H_2 and Ar at a constant rate. The pumping technique has also been used for the CVD of SiC from silicon tetrachloride ($SiCl_4$[31]) and $SiCl_4$ and benzene[32].

In situ generation involves reacting a gas with a solid or liquid source, thus generating a new gaseous reactant and transporting it directly to the deposition zone. Chlorination of a metal is the most common *in situ* generation process, i.e.,

$$x/2\ Cl_2\ (g) + M(s) \rightarrow MCl_x\ (g)$$

The experimental conditions are controlled in such a way so that the vapour pressure of the generated reactant is greater than the system pressure. Under such conditions the reactant transport rate is proportional only to the input gas flow rate and is not dependant on the temperature and pressure. The chlorination of yttrium (Y) metal at approximately 1400°C for deposition of Y_2O_3 is an example of this technique. The most common technique to feed solid metal in vapour form is the conversion of metal to a metal halide by *in situ* halogenation, as halides so formed are either gases (BCl_3) or liquids ($TiCl_4$)[33-37].

Another method of reactant feeding of solid precursor materials requires the positioning of the material within the reaction chamber before the reaction is initiated. The chamber is then saturated with reactant gas under predetermined experimental conditions, to form a solid condensed phase. Coating of titanium nitride is obtained by the action of titanium dioxide in a nitrogen atmosphere at 673 K - 773 K. The powdered TiO_2 is placed in the reaction chamber before the reactant gas is introduced[38].

The CVD of SiC has also been obtained by using this technique whereby Si-crystals are placed in the reaction chamber, and the reactant gaseous vapours of methane are injected into the reaction chamber in conjunction with H_2/N_2 carrier gas at 1473 K[39].

Regulation of gas flow into the reactor is an important part of any feed system. Many types of flow meters are used. In addition to rotameters, electronically controlled flowmeters provide the best control as an electronic signal provides the measure of the cooling effect of the mass flow of gas on a hot wire. In more elaborate systems, items like known volume reservoirs; air operated valves and a programmer have also been used[24].

Carrier gas and reactant gas purity is of importance as it directly affects the quality of the coating. Units based on palladium or palladium-silver diffusion cells have been used to purify hydrogen. Hydrogen has also

been purified by passing over heated chips of copper or titanium or by flow through molecular sieves. The commonly used carrier gas, helium, has been purified by passing it through a liquid nitrogen trap and alternatively by flow over heated platinum wool followed by liquid nitrogen trapping[24].

2.2.2 REACTION CHAMBER

CVD reactors can be grouped according to the mode of operation. Reactor names such as a cold wall reactor, hot wall reactor, fluidised bed reactor and rotating drum reactors are commonly used in the literature.

In cold wall reactors, the wall temperature of the reaction chamber is considerably lower and is often close to ambient. The substrate in cold wall reactors is heated by induction (either directly or by using a susceptor), electrical resistance or infra-red heating. Resistance heating is however, limited to substrates of relatively small cross-sectional area and high electrical resistivity. Therefore, cold wall methods of heating are limited to a select group of substrates which can respond to the applied methods of heating. Temperature control of the substrate is also difficult in resistance or induction heating. Formation of hot spots has been reported on inductively heated mandrels, particularly where the shapes of the work coil and the mandrel are not exactly matched. Also semiconductors or insulators are difficult to heat by inductive methods

because of their high electrical resistivity. Infra-red heating techniques are limited to only low temperature coatings. If applicable this technique, however, is advantageous as the deposition occurs only on the desired surface. This is helpful in conserving the reactants and leads to lower overall maintenance for the reactor. This technique also minimizes the possibility of gas phase powder formation since the stream temperature is much lower than that of substrate. Such a reactor has been used for the deposition of heterogeneous phase systems of Si, SiC and Si_3N_4 by directly heating the graphite rod substrate[40], CVD of SiO_2 using SiH_4, O_2 and Ar or N_2 by direct contact of the substrate with a hot plate[41], and CVD formation of Si films in a vertical heated system[42]. A typical cold wall reactor is shown in Fig. 2[43].

In hot wall reactors the reaction chamber which is surrounded by the furnace, is heated indirectly by radiation. The temperature profiles can be achieved and the temperature control is relatively easy. This technique is not substrate selective as the deposition occurs on both the substrate and the walls of the reaction chamber. The technique can therefore be uneconomical particularly where costly reactants are used for deposition. Also, the technique poses maintenance problems. The depletion of vapour

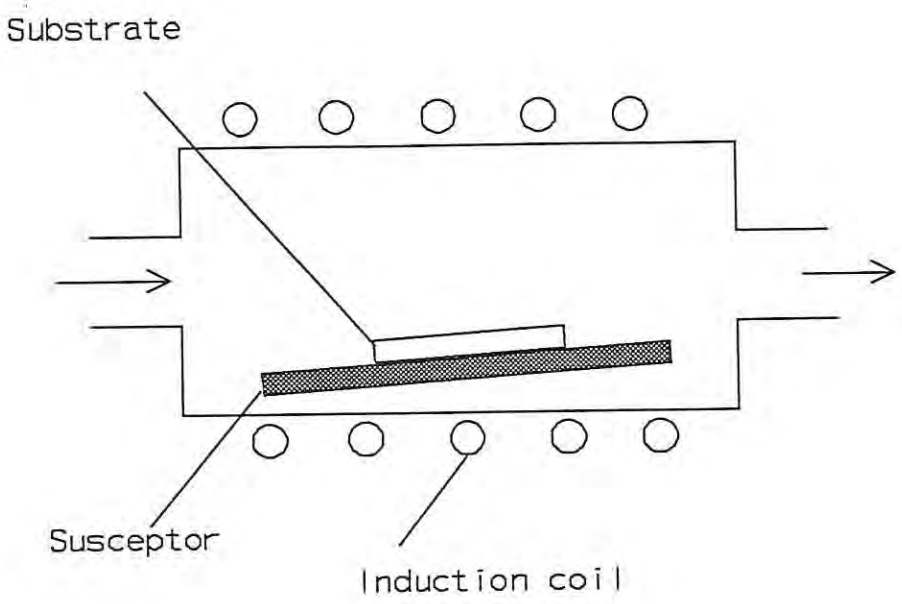

Figure 2 : A schematic diagram of a cold wall reactor[43]

with respect to reactants changes the deposition rate during transportation within the reaction chamber. This increases the risk of introducing contaminants from reactions occurring between the reactant vapours and the particles of the reactor wall and particle contamination from the reactor wall with increasing deposit thickness. Such a reactor has been used for the CVD of Si by the hydrogen reduction of either $SiCl_4$, $SiHCl_3$, $SiBr_4$, SiI_4, $Si(CH_3)_4$ or Si_2Cl_6 in a horizontal quartz reactor heated by r.f. induction coils mounted outside the tube[44], and the deposition of $Al_xO_yN_z$ from $AlCl_3$, CO_2 and NH_3 in nitrogen, in a resistively heated fused silica enclosure at temperatures between 1043 K - 1173 K[45]. A schematic diagram of a basic hot wall reactor is shown in Fig. 3[43]. This method has been extensively used for the deposition of ceramic type coatings from organometallic precursor materials[46].

Another variation of hot wall reactor is the fluidised bed reactor, in which either small particles in the form of granules are fluidised and coated[47], or coatings are applied to a dissimilar material either bulk[48] or particulate[49].

The application of fluid beds has increased dramatically in the field of CVD coating of powders and ceramics. CVD coating involves reaction of a vapour either with or in the presence of a solid substrate to deposit a coating of material on the substrate surface. CVD coatings using fluid bed technology have been shown to generate high purity coatings with good

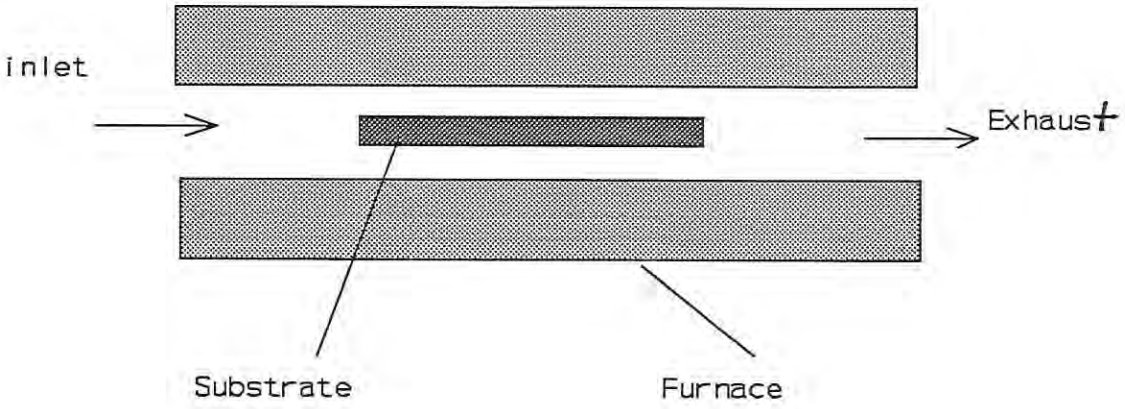

Figure 3 : A schematic diagram of a hot wall reactor[43]

adherence and uniform grain structure. Nuclear fuel particles have been successfully deposited with pyrolytic carbon using fluid beds[50-52].

CVD in a bed of fluidised particles has been demonstrated to be a very efficient means for conversion of gaseous compounds of silicon into solid silicon. Deposition efficiencies greater than 90% have been achieved at a deposition rate of 4-5 μm/min on the particles[30].

The efficiency of fluid bed reactors has been attributed to: a) rapid mixing of solids leading to nearly isothermal conditions throughout the reactor; b) higher heat and mass transfer rates; and c) uniformity of the coated surface[27]. A flow diagram of a fluidised bed unit used in CVD of pyrolytic carbon, silicon carbide or other ceramics is shown in Fig. 4[53].

2.2.3 EXHAUST SYSTEMS

Majority of the precursor materials, either on decomposition or during vapour phase reactions, produce gaseous by-products. Halides of metals or chlorosilanes tend to produce gaseous halides that are extremely corrosive particularly when they are hot. As CVD processes are either carried out at reduced pressure or at atmospheric pressure, it becomes paramount to protect vacuum pumps and any other equipment. As some of the compounds escaping

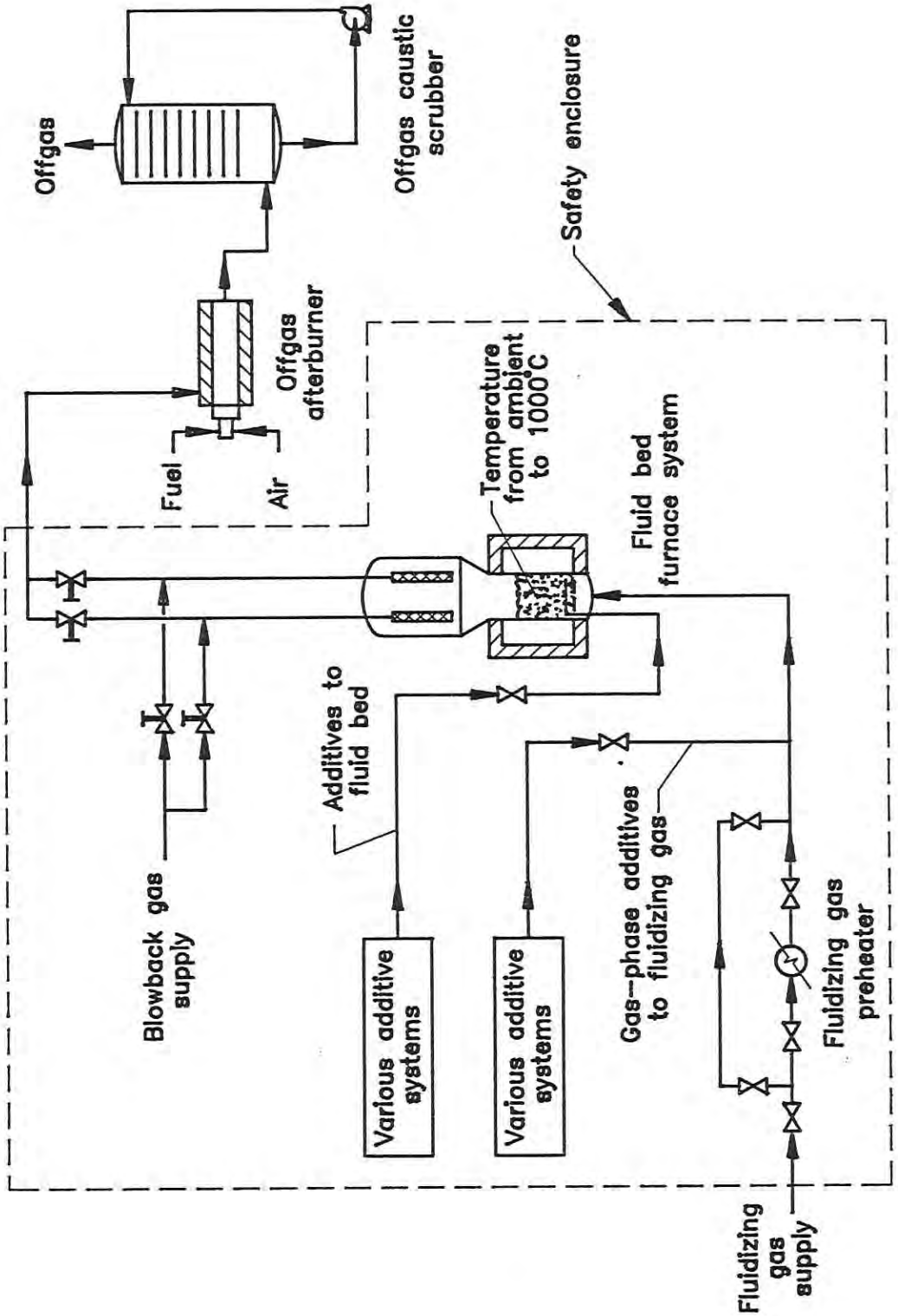

Figure 4 : Flow diagram of a fluidised bed unit[53]

the reactor could be toxic, it is advisable to entrap these compounds in chemicals rather than discharge them to the atmosphere.

Cold traps are frequently used to cool the exhaust gases which at high temperatures can cause abrasion problems. Chemical traps for other corrosive compounds have also been successfully used, e.g., sodium and calcium compounds have been used to neutralise hydrogen halides[54,55].

Another system, a decomposer, has also been used for the collection of residual precursor materials, e.g., metal carbonyl are passed over heated tubes with large surface areas for the deposition of metals, and the residue is passed through hydrocarbon supported burner to eliminate traces of carbonyl[50]. This precaution is necessary whenever the reactant is expensive. Finally, water scrubbers have been used to prevent any toxic effluents entering the atmosphere.

However, each CVD reaction, generates very different effluents and thus an efficient and viable exhaust system needs to be designed to overcome particular recycle and disposal problems.

2.3 BASIC PRINCIPLES OF CVD TECHNOLOGY

The deposition of a variety of coatings by CVD can be obtained by various chemical reactions and conditions[56].

In order to control chemical composition and morphology of the deposits and to determine the optimum deposition conditions, it is important to understand the basic principles involved in the formation of coatings using CVD. The gas phase reactions, where numerous gaseous species are involved to produce condensed phases and gaseous by-products are quite complex. Therefore, to develop an understanding of CVD processes, it is essential to have a fundamental knowledge of the equilibrium thermodynamic yields, possible chemical kinetic rate limiting mechanisms, mass transport processes and finally the chemistry of the system[56].

2.3.1 THERMODYNAMICS

Thermodynamic principles are generally applied at an early stage in order to determine the material to be deposited for a well-defined application, the nature of reactants, and the range of experimental parameters[57].

The thermodynamic approach has been used to assess the chances of successful deposition, determination of reactant gases and phases likely to be formed from the initial gas phase and also by reaction with the substrate and the furnace walls. It can provide a preliminary range of values which can be used to decide experimental parameters such as temperature, pressure, flow meter fluxes[58,59].

For many years several authors have used the thermodynamic approach to

the complex chemical equilibria involved in the multi-phase systems that prevail in CVD reactors[59-62].

Most of the thermodynamic calculations for CVD systems are based on the minimisation of the total Gibbs free energy of any system which can be expressed by the following equation:

$$\Delta G = \Delta G^{o} + RTlnK_{p}$$

where ΔG is the Gibbs free energy, $\Delta G°$ the standard free energy, R the gas constant at S.T.P., T the temperature (K), and K_p the equilibrium constant as a function of pressure. Its principles, as well as examples of its application to CVD, have been investigated by Bernard, et. al.[58], Ducarroir et. al.[63], Thebault et. al.[64], Schäfer[65], Spear[66,67], and Reisman and Sedgwick[68].

The technique is used for calculating the concentrations of all the gaseous and condensed species, at equilibrium, as a function of temperature, total pressure and initial composition of the vapour phase. The method is based on the supposition that all the chemical species present at equilibrium are known. The values of thermodynamic functions $G°_T - H°_{298}/T$ and $\Delta H°_{298}$ for a number of species have been reported in JANAF thermodynamic tables[69], and by Hűltgren, et. al.[70] and Hajiev and Agarunov[71].

Thermodynamic calculations can be used to show the ranges of input conditions for a CVD system which will produce a specific condensed phase(s) at equilibrium to the exclusion of others. Such representation of information is known as a CVD phase diagram[72].

The plots define a pressure-temperature region between two straight lines where a compound will preferentially deposit over another. The boundaries will therefore separate the ranges of input conditions necessary to give desired equilibrium products. In the B-C-H-Cl system several workers[73] have defined efficiencies in terms of boron containing species and carbon containing species.

Other examples of such analyses for the deposition of a diverse range of material include TiC[74], Ti-Si-C[75], $GaAs_{1-x}P_x$[76], $Al_xGa_{1-x}As$[77], $In_{1-x}Ga_xAs$[78], B_4C[58], GaAs[79], GaP[79], Si[80,81], and doped tungsten[82]. Efficiency diagrams are also useful in optimising a CVD process. They predict efficiency in producing the most favourable condensed phase under equilibrium conditions.

Although CVD reactions can be studied by a thermodynamic approach, this does not give by its very principle, any information on the CVD mechanism or on the deposition rate. As mentioned earlier, this approach is useful to point out the influence of the deposition parameters on the compositions of both the vapour and solid phases. Even then, such a

condition may not be fulfilled in every case.

2.3.2 MASS TRANSPORT AND REACTION KINETICS

Thermodynamic analysis of any CVD system is a useful tool in the prediction of limiting equilibrium composition of the gas phase, limiting deposition rates, and also the types of species to be expected in the condensed phases, but not what happens on the substrate. A knowledge of reaction rates is important to understand the actual reaction on the substrate surface and the rate at which the reaction proceeds. Kinetic data are useful in selection of experimental conditions for the synthesis of the desired coatings. For example, the reaction of oxygen with $AlCl_3$ to form Al_2O_3 is thermodynamically favourable, but kinetically exceptionally slow[83].

During CVD coatings, it has been shown that both the rate of deposition and the coating structure depend on the rate of transfer of precursor materials or reaction intermediates at the surface, and the surface diffusion of adsorbed species, before, during or after reaction to give the final product[84].

The structure of the deposit is temperature dependent[85] and for optimisation of CVD reaction, rate of deposition either has to be minimised or maximised depending on the ability to obtain the desired

structure, a problem which increases with increasing thickness of the coating.

Bryant[24] has shown the effect of temperature on deposition growth rate (Fig. 5). The areas labelled A, B, and C represent rate control by a reaction occurring at or near the substrate surface, rate controlled by mass transport in the gas stream, and rate limitation due to homogeneous gas phase nucleation of product respectively. Based on this, possibly the following process steps exist in any CVD system, which control the overall deposition:

(a) Transport of reactant(s) to the substrate;

(b) Adsorption of reactant(s) on the substrate;

(c) Chemical reaction/diffusion on the surface;

(d) Desorption of product gas(es); and

(e) Transport of product gas(es) from the surface.

The total CVD process is generally assumed to consist of these 5 steps occurring in a given sequence. The reaction steps referred to as (b), (c), and (d) are kinetic steps, while the mass transport steps include (a) and (e). The rate determining step (rate of deposition), is governed by both mass transport and surface kinetics. However, for a majority of systems one of these two mechanisms predominate.

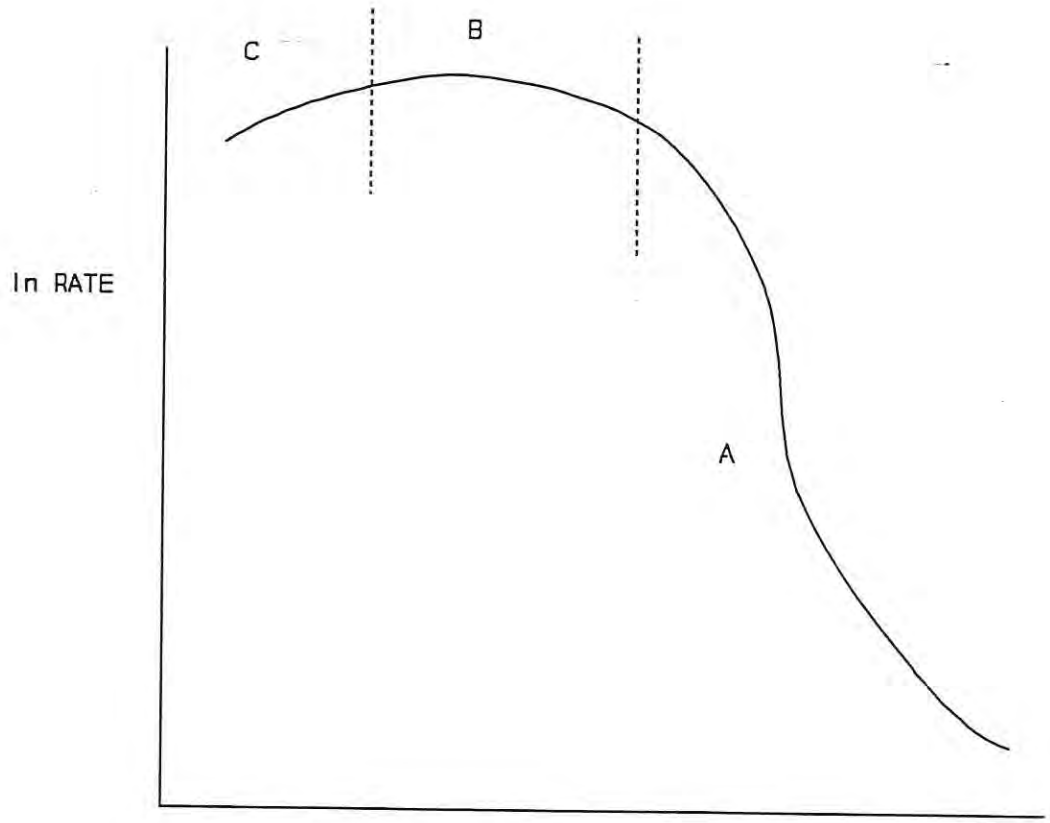

Figure 5 : Effect of temperature on the deposition rate[24]

The conditions that favour mass transport control, generally provide maximum deposition rates. These conditions can be determined from data of rate as a function of pressure, while maintaining a constant deposition temperature, gas compositions and flow rates. At both higher and lower mass flow rates the deposition rate is independent of mass flow indicating that the process is controlled by surface kinetics and natural convection.

Many CVD reactions have been investigated with due consideration to transport and kinetic phenomena. A simple example in which transport through the boundary layer occurs by interdiffusion of reactants and reaction products, the kinetic limitation occurs at very near the substrate, and the composition of the bulk gas stream changes in accordance with amount of material deposited. The typical example is the thermal decomposition of silane[86,87] although Coltrui et al.[88], have shown that limiting silicon deposition to the surface is not as simple. They describe the SiH_2 radical in the gas phase as an important intermediate species.

Oxley's[89] expression taking into consideration the diffusion flux through a boundary layer and mass transport by a simple first order chemical reaction at the surface, has been extensively used as a basis for the modelling of CVD reactions, i.e.,

$$J = \frac{1}{RT}\frac{(P_b - P_{eq})}{(\frac{\delta}{D} + \frac{I}{k})}$$

where J is the flux of deposition, P_b-P_{eq}, the difference between the reactant partial pressures at equilibrium and in the bulk gas stream, δ is the boundary layer thickness, D is the diffusivity of deposition species, k is the mass transfer coefficient, R is the gas constant, and T is the absolute temperature. When δ/D, the diffusional impedance is large relative to the kinetic impedance I/k, the reaction is said to be diffusion controlled. When the reverse is true, the reaction is said to be kinetically controlled.

Two types of models, a film model or a boundary layer model has been applied to determine the relation for deposition growth rate. Using a film model, the deposition rate, R is described by the relation:

$$R = \frac{M}{\phi} k_g \Delta Y$$

where M and Φ are the molecular weight and density of the deposit respectively, k_g is a mass transfer coefficient and ΔY is a diffusion potential. This model has been used to accurately represent the deposition of tungsten by the hydrogen reduction of WF_6 at high temperature and pressure[90]. Under these conditions mass transfer has been shown as a rate controlling step[91]. The boundary layer model takes into account the

effects of mass transfer and bulk flow on the thickness of the layer[92-95].

Although the deposition rates are higher under conditions of mass transport control, this is not always desirable. If however, sufficient depletion of reactant occurs, then uniform thickness over an extended substrate area, can only be obtained under conditions favouring surface kinetic control, e.g., as in the coating of the internal surfaces of a porous body such as carbon fibre yarn[96] or in the bonding of individual tungsten spheres held in a packed bed[97] and for infiltration of porous structures with BN[98].

Rate equations for surface kinetics can be promulgated either by relations based on Langmuir - Huishelwood adsorption isotherm relations[99] or on the basis of absolute reaction rate theory[100].

Surface reaction rates can be altered by the addition of gases. For example, the rate of tungsten deposition has been slowed by the addition of HCl, O_2, and water vapour[101] or either increased or decreased with the change in temperature by the addition of $MoCl_5$[102].

The kinetics of deposition of compounds and alloys are relatively more complex than those of single elements, e.g., the deposition of SiC and TiC follows two different paths. Si has been shown to be the intermediate species during the deposition of SiC, while elemental Ti is not formed

during TiC formation[103].

Solid state diffusion is often rate-limiting in CVD by which substrates provide one of the elements by diffusion into the deposit. This is applicable in the coating of the inner surfaces of graphite or carbon tubes of great length-to-bore ratio with carbides[104]. Solid state diffusion control, although slow, is an effective means of uniformly coating large substrate areas[105].

2.3.3 CHEMISTRY OF THE SYSTEM

CVD is an important high temperature synthesis technique for coatings. It involves the flow of reactant gases into a high temperature reactor where chemical reactions occur to produce a condensed phase plus various other gaseous products. In order to tailor the chemistry of CVD deposits for specific applications, understanding of the overall chemical reactions occurring in the deposition reactor is essential. This information is derived by the understanding of the combined equilibrium, kinetic, and transport processes.

Organometallic compounds, metallic halides, hydrides, hydrocarbons and ammonia complexes have commonly been used as precursor materials. The deposition of the desired species is then effected by thermal decomposition (pyrolysis), e.g., thermal decomposition of MTS at 800°C -

1200°C has been used in H_2/N_2 or Ar atmosphere to obtain coatings of SiC[106],

$$CH_3SiCl_3(g) \rightarrow SiC(s) + 3HCl(g)$$

or CVD of Si from silane at 850°C[107-111].

$$SiH_4(g) \rightarrow Si(s) + 2H_2(g)$$

Reduction of halides is very well investigated technique for the deposition of refractory metals. A typical example is the deposition of tungsten by the hydrogen reduction of WF_6:

$$WF_6(g) + 3H_2(g) \rightarrow W(s) + 6HF(g)$$

This reaction has been extensively studied as demonstrated by the number of papers presented in the first four CVD conference proceedings[112-115].

CVD of Si by the reduction of silicon halides is an important reaction which has received considerable attention because of its application in semiconductor technology[116], i.e.,

$$SiHCl_3(g) + H_2(g) \rightarrow Si(s) + 3HCl(g)$$
$$SiCl_4(g) + 2H_2(g) \rightarrow Si(s) + 4HCl(g)$$

Hydrolysis of metal halides has also been shown to produce thin films or crystals of metal oxides in a CVD reactor. The technique has its origin with the discovery of haematite (Fe_2O_3) single crystals in the throats of volcanoes[65]. The overall chemical reaction can be represented as:

$$2FeCl_3(g) + 3H_2O(g) \rightarrow Fe_2O_3(s) + 6HCl(g)$$

Another example that utilises this approach is the deposition of Al_2O_3 from $AlCl_3$[65].

$$2AlCl_3(g) + 3H_2O(g) \rightarrow Al_2O_3(s) + 6HCl(g)$$

Oxidative methods have also been used particularly for the synthesis of silicon oxide, a material which has been extensively used in semiconductor industry[41], e.g.,

$$SiH_4(g) + O_2(g) \rightarrow SiO_2(s) + 2H_2(g)$$
$$SiH_4(g) + 2O_2(g) \rightarrow SiO_2(s) + 2H_2O(g)$$

The use of CVD technique is more widespread and coatings such as oxides, carbides, nitrides, borides, silicides, and many others have been deposited. Bhat[117] has given a comprehensive list covering the deposition of various compounds using different precursor materials.

The overall reactions described above are oversimplified. In the deposition of many of the coatings, these reactions proceed through many intermediary species. The reaction mechanisms involve various chemical processes which are influenced by several factors, such as CVD reactor system design and process parameters. For example, it has been shown that the deposition of SiC from MTS proceeds through the formation of C, H_2, Si, $SiCl_2$, $SiCl_3$ and HCl species[30].

It has also been shown that the concentration of hydrogen directly influences the type of chemical species formed, as lower levels of hydrogen concentration are linked with the deposition of C; while higher hydrogen concentrations favour the formation of SiH_3Cl, SiH and SiH_4 species[30].

Similarly, it has been shown using *in situ* or quasi *in situ* vapour phase

probe techniques such as Raman Scattering and Mass Spectrometry that $SiCl_2$ is amongst the predominant species in atmospheric pressure reactors before Si(s) or SiC(s) is deposited from dichlorosilane/H_2 system[118-120]. Under reduced pressure however, the thermodynamic computation favour the greater predominance of $SiCl_2$ and $SiCl_4$ species. Amato et al.[121], using molecular beam apparatus coupled with the hot wall reactor, has described the possible reaction mechanism of the deposition of AlN from its organometallic precursor $(Al(CH_3)_2NH_2)_3$. They postulated that the deposition of AlN, occurs through formation of trimer-dimer from the precursor, or alternatively, the precursor may have already begun to decompose with the formation of CH_4 and a dimeric species, which decomposes to give AlN, e.g.,

1.

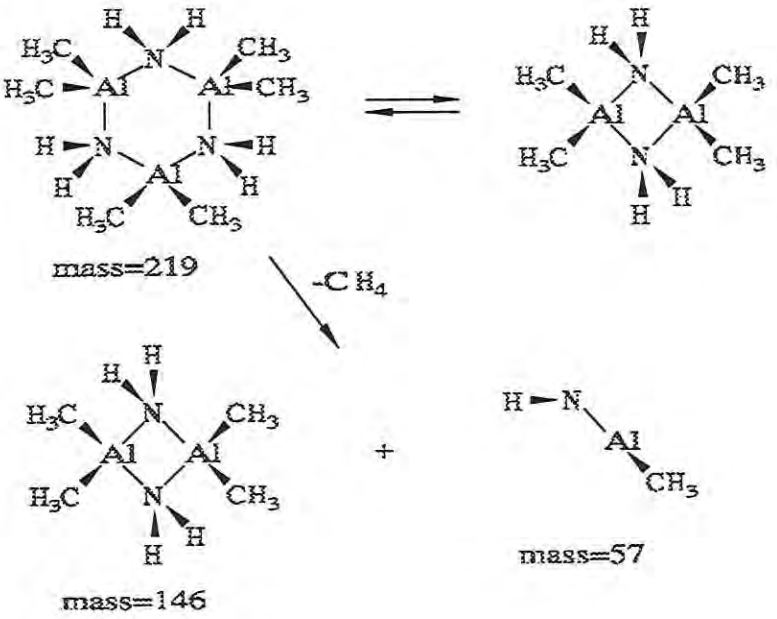
mass=219
-CH4
mass=146
+
mass=57

2.

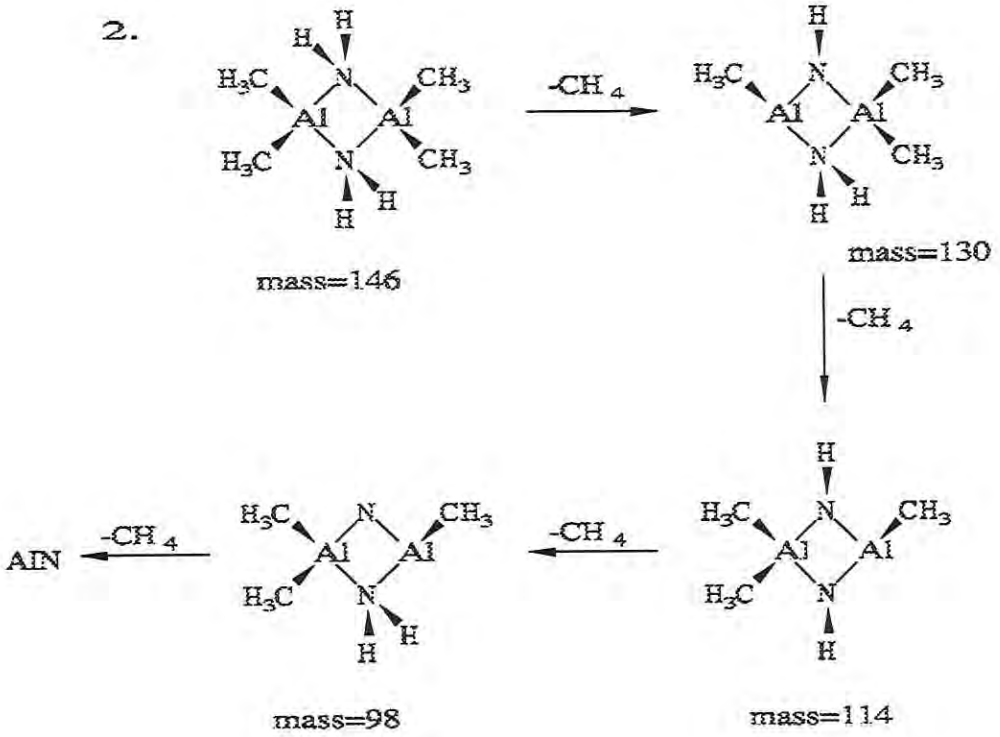
-CH4
mass=146
mass=130
-CH4
AlN
-CH4
-CH4
mass=98
mass=114

These studies clearly indicate that vapour phase synthesis involves a wide range of chemical processes in any CVD system, taking place in several regions of the reactor. These reactions are complex, and require careful analysis to predict the overall mechanism.

2.4 PROCESSING PARAMETERS

A number of workers has reported that in any CVD process, the deposition is influenced by a number of process parameters. These include: the precursor material, the base material, the shape of the sample and its locality within the reaction chamber, the reaction chambers' dimensions, flow rate of the carrier gas, temperature and temperature distribution within the reaction zone, pressure, gas composition and flow rate and concentration of various chemical species[122]. Literature clearly indicates that the optimisation of a CVD system for any specific application is a complex issue. A typical example is *in situ* formation of SiC by thermal decomposition of volatile silicon and carbon compounds. For ease of deposition, both elements should be present in equal amounts within the same molecule.

A number of variations of process parameters have been reported in the literature for the deposition of SiC from MTS, in a hot wall, cold wall(Table 2), and fluidised bed reactors(Table 3)[122].

Table 2 : A list of coating parameters for hot wall and cold wall reactors[122]

Precursor	Carrier Gas	Temp °C	Pressure kPa	Substrate	Product	Furnace	Growth rate µm/h	Gas Flow Rate cm^3/min
HOT WALL REACTOR								
CH_3SiCl_3	H_2	1100-1400	3-101	C-fibre	SiC-L	i.h.	40 (1400°C)	300..600
	H_2	900-1300		C-filament	SiC-L	d.h.		430
	H_2	1600-1700		C-rod	SiC-L	i.h.	300 (1600°C)	35
	H_2/Ar	1000-1500		C-plate	SiC + C-L	d.h.		16
	Ar	1400-1900	0, 3..6	C-tube	SiC-crystal	d.h.		700..1000
	H_2/Ar	1200-1300		SiO_2-plate/filament	SiC-L	i.h.	1400 (1200°C)	
COLD WALL REACTOR								
CH_3SiCl_3	H_2	1300-1400		C-tube	SiC-L	d.h.	360 (1400°C)	1000
	H_2	1100-1500		C-rod	SiC-L + C	i.h.	200-500 (1400°C)	30

	H_2	800-1200		porous SiC porous Si_3N_4		d.h.		300-400
	H_2/Ar	1400		SiC-L + Si	SiC-L + Si	i.h.		
	H_2/Ar	1200-1800		SiC-L	SiC-L	d.h.		5000
	H_2/He	1400		SiC-L + Si + C	SiC-L + Si + C	d.h.		1800
	H_2/N_2, Ar	1200-1400		SiC-L + Si	SiC-L + Si	d.h.	1200-3000 (1400°C)	700
	H_2	1500		SiC-whisker	SiC-whisker	i.h.		

d.h.--- direct heating
i.h.---indirect heating

Table 3 : A list of coating parameters in a fluidised bed reactor[122]

Precursor Material	Carrier Gas	Temp °C	Particles	Particle diameter µm	Product	Growth Rate µm/h	Gas Flow Rate cm^3/min
CH_3SiCl_3	H_2	1100-1900	C	625	SiC		6000
	H_2	1130-1850	C	260	SiC + Si	50-280 (1500°C)	2000
	H_2	1100-2000	UC_2	200-400	SiC + C	20 (1390°C)	
	H_2	1400-1800	C-disks		SiC-L	180 (1400°C)	
	H_2/Ar	1200-1700	UC	500	SiC SiC + Si		
	He	1375-1600	C		SiC + C	30-70 (1400°C)	8000...9000

The influence of the nature of the substrate has been reported to be detrimental in achieving the deposition[124]. The substrate, by itself, could be involved in chemical reactions, affecting the deposition process initially until the first coating layer is complete. In the case of CVD of Si onto an Fe substrate, the use of either $SiH_4/Ar/H_2$ or $SiH_4/SiCl_4/H_2/Ar$ precursor yields Fe_5Si_3 or FeSi[123].

The temperature and pressure of the system strongly influence the chemistry of the overall system. The nature of the chemical species at equilibrium depends on both temperature and the initial composition of the vapour phase.

The CVD of SiC from MTS and hydrogen mixtures within porous carbon-carbon composite materials at temperatures between 1000 K to 1600 K has been presented by Christian and co-workers[124]. They indicate that parameters such as chemical species present at equilibrium including initial compositions at equilibrium of the vapour phase, total pressure, flow rate of the inert carrier during reaction, the C/Si ratio present in the vapour phase, and the nature of the substrate strongly influence the overall deposition process. The decrease in total pressure during CVD of SiC from MTS at 1200 K, results in the increase of SiC deposit yield. The total pressure also affects the appearance of the silicon in the deposit. The effect of the addition of argon on the nature of the deposit, in the absence of H_2 lead to SiC co-deposition with C, due mainly to silicon chlorides in

the vapour phase which remain unreduced due to a lack of hydrogen. The nature of the substrate on the equilibrium composition, to avoid other deposition processes occurring, must be chemically inert towards the initial vapour phase. Carbon substrates are not chemically inert to MTS/H_2 mixtures. The C/Si ratio present in the initial composition also influences the deposition process, with $(CH_3)_2SiCl_2$ depositing SiC at higher H_2 concentrations compared with MTS.

Federer[125] reported that the density of SiC deposits obtained from CH_3SiCl_3/H_2 in a fluidised bed at 1850 K and 1 atm., is greatly influenced by initial gas composition.

Several workers reported the co-deposition of silicon with SiC from a MTS/H_2 gaseous precursor mixture at temperatures below 1673 K. Chin et. al.[61], found that silicon co-deposited with SiC for H_2 rich initial compositions, and these results are in agreement with the thermodynamic studies of Christian et.al.[124]

The structure-property relationship of deposition layers is best approached by a consideration of the mechanism of nucleation and growth in condensation from the vapour phase. For a given substrate-vapour combination, the nucleation and growth kinetics are determined by the supersaturation (concentration of adsorbed species on the surface) and temperature (determines the mobility). Blocher[85] described the

structural dependence on supersaturation and temperature of materials prepared by PVD and has presented a relational sequence as shown in Fig. 6. It indicates that different materials with different structures may be deposited on a base material. The same type of dependencies exist for CVD. For example, low supersaturation and high temperature result in epitaxial growth, while at the other extreme, high supersaturation and low temperatures result in powder deposition. One discrepancy exists for homogeneous gas-phase nucleation. For the preparation of Al_2O_3 by CVD the formation of powder was accomplished at low temperature[24].

2.5 STRUCTURE OF CVD DEPOSITS

CVD deposits may present different structures as detailed below.

2.5.1 POLYCRYSTALLINE DEPOSITS

Polycrystalline deposits comprise columnar grains with a high degree of preferred orientation. Growth of columnar grains is characteristic of some materials under certain ranges of conditions such as the deposition of tungsten at 500°C by hydrogen reduction of tungsten hexafluoride. This type of structure results from uninterrupted grain growth toward the source of supply.

Intercrystalline microporosity results at regions of preferred orientation if

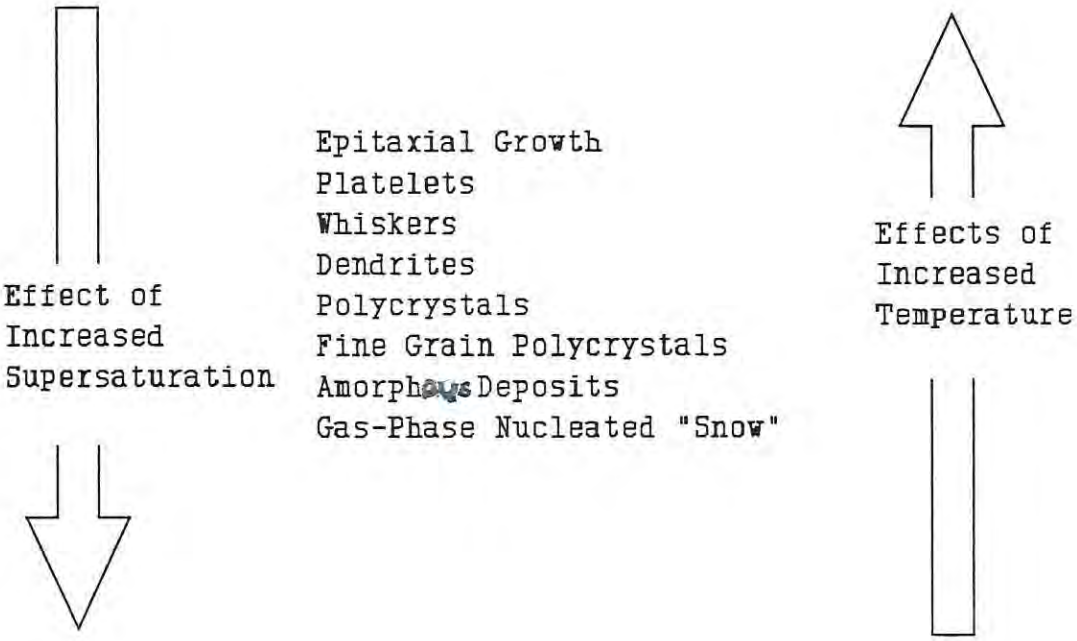

Figure 6 : **Effect of supersaturation and temperature on the structure of condensed materials[24]**

the growth rate is controlled by mass transport processes, whereas dense deposits result when the growth rate is controlled by the solid surface. The growth rate and reactant concentration are greatest at or near the apex of growing crystallites under favourable mass transport conditions, since the apex extends furtherest into the boundary layer of the gas stream over which a concentration gradient of reactant exits. These enhanced growth rates can therefore produce grown-in boundaries or dense deposits simply by surface reactant control[50].

The degree of preferred orientation is strongly dependent on the process parameters. Such effects have been examined for tungsten[126-128], silicon[129,130] and rhenium[131,132]. It has been found that the crystallographic orientation is strongly influenced by the flow conditions of the reactive gas mixture.

2.5.2 EPITAXIAL DEPOSITS

Epitaxial deposits are found usually in the growth of either single crystals or epitaxial layers, formed by nucleation and growth mechanisms. The growth mechanisms are merely speculative. These include the formation of a monolayer of which the contact angle between the coating and substrate is zero; the depositing atoms lacking sufficient mobility to diffuse over the surface substrate; or some hybrid mechanism of deposit formation. Epitaxy results from nucleation in a particular orientation

preferring lower free energy sites. With an increase in supersaturation however, nucleation rates of other orientations become pronounced enough to lose epitaxy[24].

2.5.3 POWDER FORMATION

At sufficiently high reactant concentration and gas temperature, nucleation and growth of a powder product can be achieved. High reactant temperatures lead to an increase in the molecular collisions capable of producing solid deposits. Powder formation is also detrimental to deposit density, deposition rate, and the maintenance of equipment. Powder formation however, can be used successfully in determining gas flow patterns in a CVD reactor.

2.5.4 OTHER STRUCTURES

The chemical vapour deposition process can produce structures such as whisker-like crystals and amorphous film deposits. Whisker-like crystal growth can be initiated by a screw dislocation in the substrate surface. Subsequent layers grow by adsorption followed by diffusion onto the whisker tip. The growth rate of the whisker is determined by its own set of parameters such as whisker geometry and concentration of adsorbed atom onto whisker. CVD whiskers have been used in solar energy cells[133].

Chemical vapour deposition is widely used in the preparation of insulating and passivating layers for use in the electronics industry. Films possessing such properties are known as amorphous deposits. Amorphous growth is a mode of heterogeneous nucleation which involves a slow surface diffusion of adatoms accompanying a high rate of formation of these adatoms. A newly created adatom will impinge on a specific site before the former has had a possibility to make a diffusional jump to an energetically more favourable crystallographic site. Amorphous deposits have been prepared from SiO_2[41,134], Si[135], Al_2O_3[136], aluminium oxynitride[45], phosphosilicate and borosilicate glasses[137,138]. An amorphous film can be converted to crystalline form simply by heating to above deposition temperature[139].

2.6 DEPOSIT-SUBSTRATE ADHERENCE

The interface between deposit and substrate surface is an important consideration in determining deposit adhesion. The substrate surface must be clean of contaminating species to avoid the formation of undesirable intermediate products or corrosion of the substrate surface prior to coating. The adhesion must be able to withstand in-stresses and stresses experienced by the cooling down of deposit temperature.

Coating substrates of active metals such as titanium or aluminium by hydrogen reduction of halides is certainly difficult because the active

metals are superior reducing agents. The surface would be eroded or a non-volatile intermediate halide can be formed which consequently results in a non-adherent coating. Typically an interlayer improves adhesion by either enhancing compatibility or protecting substrate from the atmosphere. A nickel coating using $Ni(CO)_4$ is used on ferrous alloys prior to coating of tungsten. TiC is an effective interlayer for tantalum coatings on ferrous alloys[140]. The deposit of cobalt onto a steel substrate in the deposition of TiC also proved to increase adhesion[141].

The deposit and substrate compatibility particularly at the deposition temperature is important. CVD temperatures below 800°C lead to coating substrate interdiffusion resulting in brittle interlayers and thus poor adhesion. Various surface cleaning and/or priming methods have been employed by various investigators and include pickling, grit blasting, and degreasing[50]. Metal surfaces, such as iron, whose oxides are reducible by hydrogen are pretreated by a gaseous hydrogen environment at or above the deposition temperature for a pre-defined length of time, prior to the introduction of the CVD reactants[24]. Oxide contaminated silicon surfaces to be coated epitaxially with doped silicon are generally etched in HCl(g) at 1000°C[50].

2.7 UNIFORMITY OF DEPOSITION

The major goals in CVD processing are: a) to obtain uniform surface coverage, and b) to avoid spurious growth of protrusion from the coating surface. The non-uniformity of deposit thickness has been reported particularly when an attempt is made to coat a substrate of considerable surface area[142]. Fig. 7 represents a deposit thickness profile reported by Bryant[24].

This non-uniformity is the result of the continual depletion of reactants and formation of the gaseous products, as the stream moves over the substrate. Van der Brekel and Jansen[143] and Jansen and Van der Brekel[144] have shown quantitatively that uniformity of deposition is promoted if the deposition is conducted in the kinetically limited regime. Surface irregularities, generally, result because of dust particles entering the reactor from a dirty gas stream or as particles of gas-phase-precipitated reaction product.

Other approaches involve altering the flow pattern of gas[145], rotating the substrate combined with gas flow reversal[146], or imposing the temperature gradient over the length of the substrate[92].

Another method[26] suitable in obtaining deposit thickness uniformity is to introduce reactant gases in a pulsating manner by injecting into a

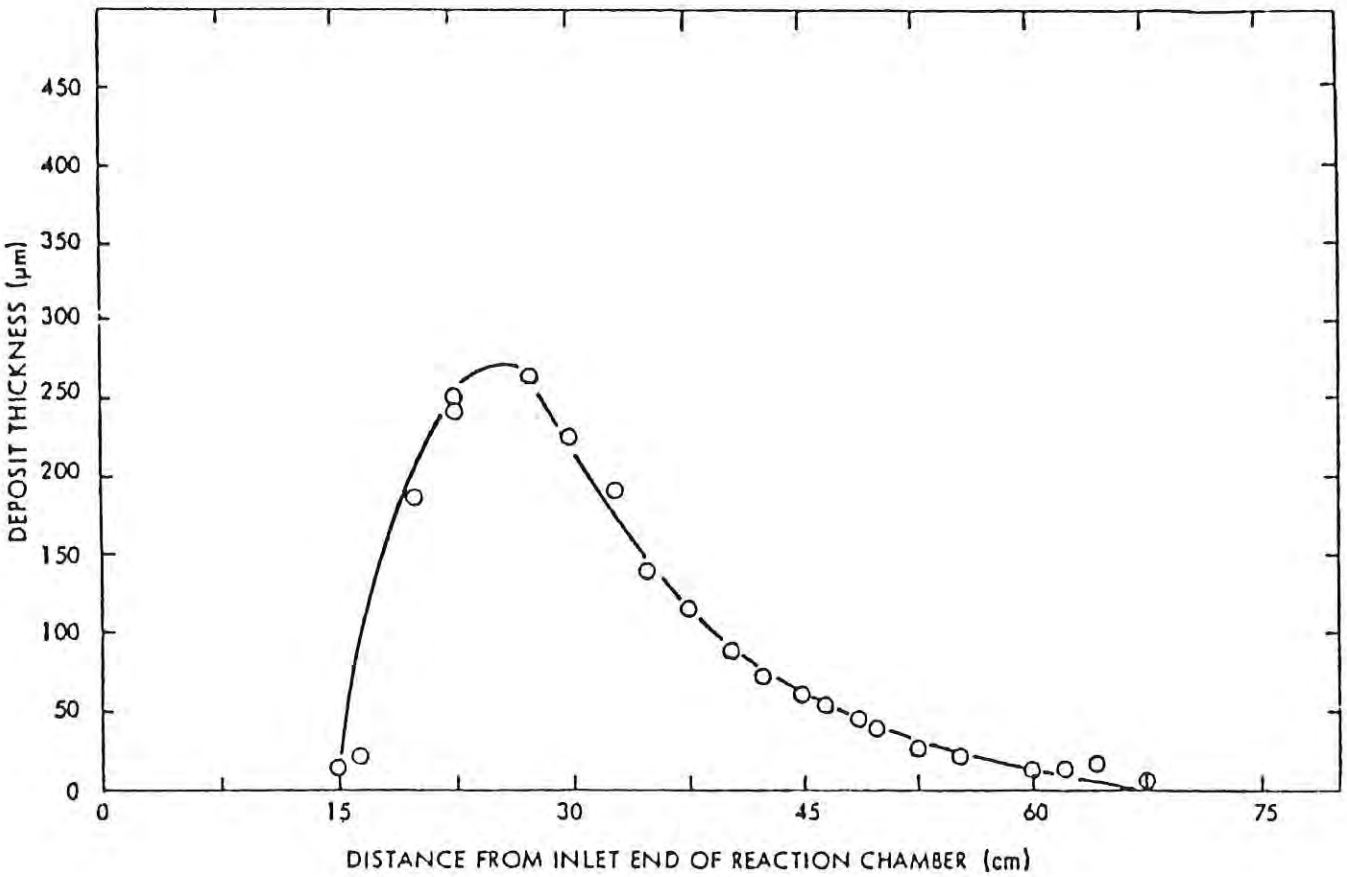

Figure 7 : Typical deposit thickness profile for flow through CVD reactor[24]

previously evacuated chamber. Although the composition changes with respect to time, the gaseous products are evacuated and fresh batches of reactant gases are reinjected, ensuring that the composition of gaseous species is constant over the substrate surface leading to coating thickness uniformity.

2.8 SCOPE OF THE PRESENT WORK

The silicon based ceramic coating such as Si, SiC and SiO_2, can be obtained by thermal decomposition of organosilanes. These coatings possess good mechanical properties, high wear and corrosion resistance as well as oxidation resistance. Volatile organosilanes have been widely investigated in cold wall and hot wall reactors at a very high temperature (900°C - 1500°C), particularly for the deposition of SiC. The simplest way to deposit the coating is by the thermal decomposition of CH_2SiCl_2 or CH_3SiCl_3. The aim of the present investigation was to determine the feasibility of hot wall and/or fluidised bed reactors for deposition of ceramic type coatings from organosilane precursor materials at lower temperatures (>1273 K) using CVD technique.

The outline of the present investigation is given below:

1) CVD Reaction System : A hot wall and fluidised bed reactor was designed and constructed which involved three major components, a liquid feed delivery mechanism, carbon based reaction chamber and exhaust treatment system.

2) Precursor Material : Methyltrichlorosilane (CH_3SiCl_3,MTS) was used as the precursor material because of its simplicity, commercial availability, economy and ease of understanding of a single component system.

3) System Analysis : a) A detailed thermodynamic analysis was conducted using a computer program CHEMIX, over the temperature range of 500°C -1000°C. The analysis was useful in providing information such as limiting equilibrium composition of the gas phase, identification of condensed and gaseous species, and limiting deposition rate; b) An attempt was made to understand the kinetics of the reaction using Perkin Elmer DSC and built in kinetics software and from deposition rate data. However, in DSC the studies were limited to maximum temperatures of 1000 K.

4) Substrate Selection and Deposition : the stainless steel plate was used in the experimental trials as a substrate. The coatings obtained under different experimental conditions were used in measuring deposition rates, while the deposit morphology and structure was determined using Scanning Electron Microscopy(SEM) and X-ray

diffraction(XRD).

5) Reaction Mechanism : Based on the data available a plausible reaction mechanism was proposed indicating the mode of decomposition of MTS and formation of a mixture of ceramic type components such as Si, SiC, and SiO_2.

6) The experimental data was also used to compare the value of hot wall reactor, against fluidised bed reactor for CVD of MTS.

CHAPTER 3

EXPERIMENTAL

3.1 CVD REACTOR SYSTEM

There is an abundance of literature describing the overall chemical reaction to produce CVD materials from organometallic precursors. However, the details of preparation for specific materials are not easily available. The equipment used for CVD reactions is either a hot or cold wall reactor, or a fluidised bed (modified hot wall reactor).

In this study, the experimental CVD reactor system designed to carry out the deposition of ceramic type thin films on a metallic substrate consisted of hot wall as well as a fluidised bed reactor chamber, a liquid feed system, exhaust neutralisation unit and effluent gas analysis equipment together with a data acquisition system. The details of the entire experimental system are described in the following sub-section.

3.1.1 LIQUID FEED SYSTEM

The precursor material was delivered to the reaction chamber either by vaporising the material and transporting the generated vapour with the aid of a carrier gas (Fig. 8), or by using a diaphragm positive displacement metering pump (Acromet 3000).

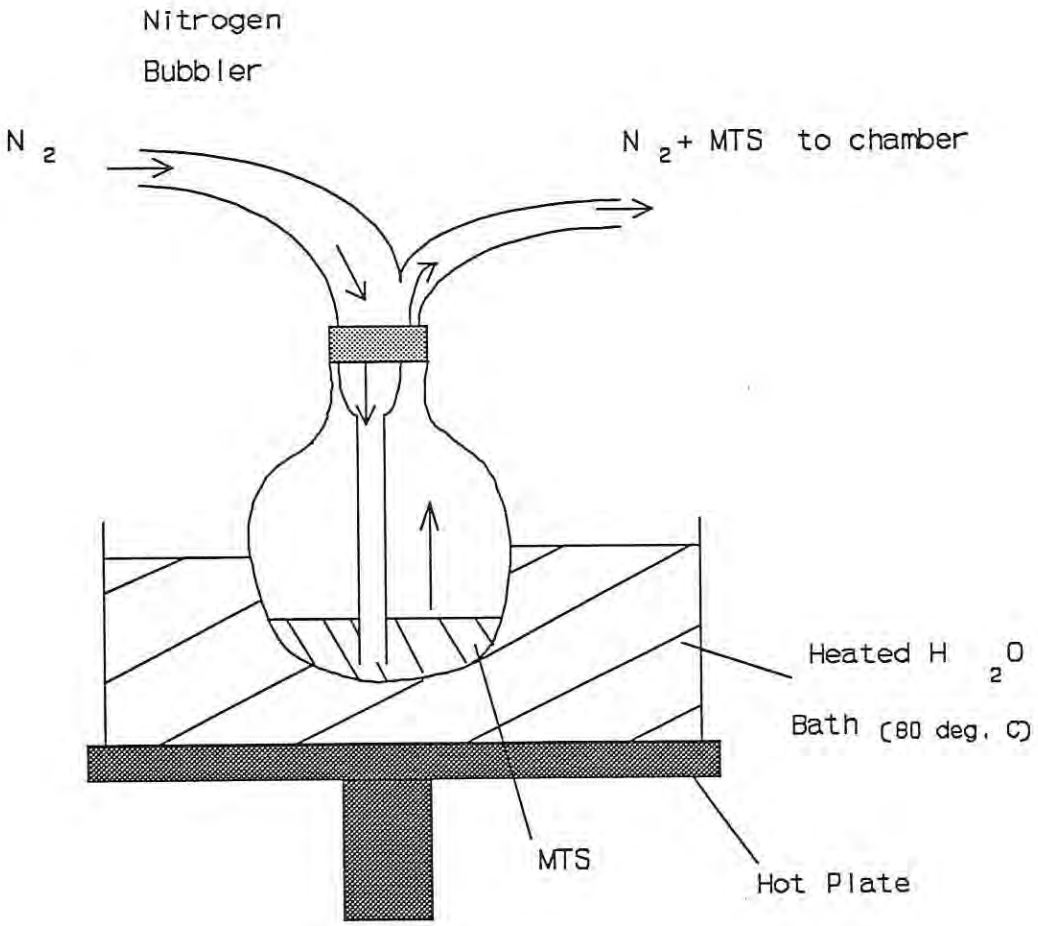

Figure 8 : A schematic diagram of the nitrogen bubbler

In the first delivery technique, a known quantity of the reactant was placed in a round-bottomed flask fitted with inlet and outlet tubes, as shown in the Fig. 8. The flask was placed in a hot water bath whose temperature was maintained at 353 K. The carrier gas N_2 was bubbled through the liquid, and the vapours of the reactant were carried to the reaction chamber by adjusting the flow of the carrier gas.

The second method used for the delivery of the reactant to the carrier gas stream involved a diaphragm positive displacement metering pump; commercial name, Acromet 3000; with a back pressure check valve of polypropylene and teflon. The maximum capacity of the pump was 20ml/min with a gear ratio of 46 strokes per minute.

3.1.2 GAS PREHEATER

The vaporised or liquid material was fed into the gas stream which passed through a preheater maintained at 373 K. The preheater consisted of an aluminium block with a 450W cartridge heater press-fitted into the centre. The delivery pipes were wound around the aluminium block which was covered with a stainless steel sheath. The heater was attached to a thermostat with a temperature controller for operation between 323 K and 573 K.

3.1.3 REACTION CHAMBER

Two types of reaction chambers were used: 1) a hot wall reaction chamber, and 2) a fluidised bed unit.

3.1.3.1 HOT WALL REACTION CHAMBER

The hot wall chamber was fabricated from carbon rod. It consisted of two modular units, a preheating chamber and a reaction chamber. The chambers had an ID of 0.12m and OD of 0.15m.

In the preheating chamber the incoming vapours were heated to the deposition temperature prior to the transfer to the reaction chamber. This chamber, which measured 0.4m in length was mounted with one type R thermocouple in the wall.

The reaction chamber, which represented the main section of the overall reactor system, measured 0.66m in length and was fitted with two type R thermocouples. The reaction chamber was also fitted with a gas distributor plate consisting of 800 holes of 1×10^{-3}m diameter arranged in a 1×10^{-2}m square pitch. A schematic diagram is given in Fig. 9.

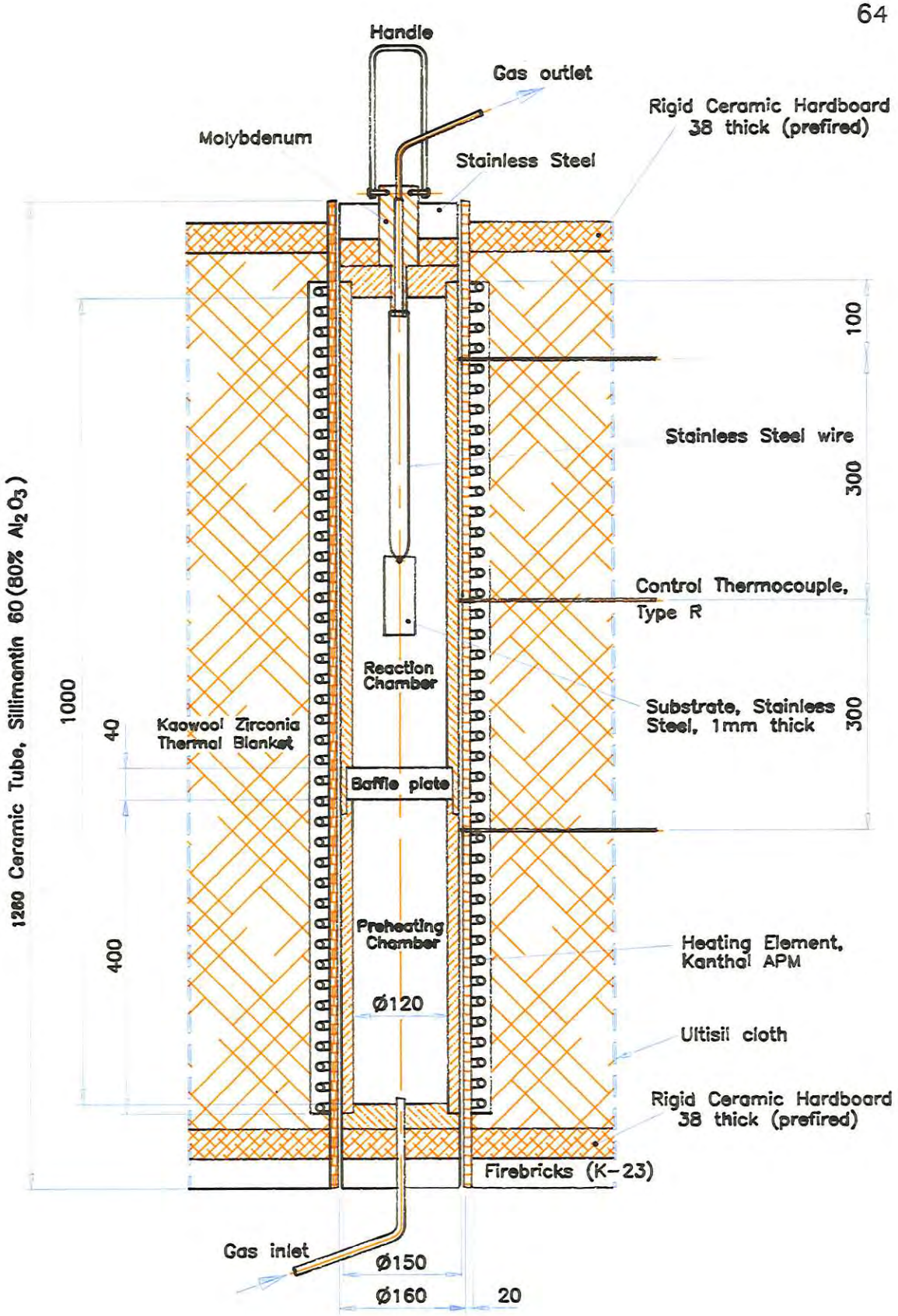

Figure 9 : A schematic diagram of the hot wall reactor

3.1.3.2 FLUIDISED BED REACTION CHAMBER

The fluidised bed reaction chamber had a very similar configuration to that of the hot wall reaction chamber, except that it was partitioned right through the middle with a 1 x 10^{-2}m thick carbon plate. The provision was made to attach the substrate to be coated onto one side of the partition, whereas the other side of the substrate was constantly bathed by fluidised material in the fluidised section. The precursor material with varying ratios of N_2 and H_2 gas was selectively fed into the side of the chamber containing the substrate, while the sand particles (average size 1 x 10^{-3}m) were fluidized in the other compartment. A schematic diagram representing the overall design and dimensions is shown in Fig. 10 and a flow diagram of the overall system is given in Fig.11.

3.1.4 ELECTRIC FURNACE

The electric furnace was constructed as a muffle tube furnace using silicon carbide elements (Kanthal APM element wire) with a total power output of 12 kW, (3 x 4 kW) with 240 Volts elements balanced over 3 phases. The maximum temperature attainable was 1673 K, however the experimental runs were conducted at 973, 1073, and 1173 K. The element wire was wrapped around the outside of a ceramic tube (Sillimantin 60, 80% Al_2O_3); this tube completely surrounded the carbon chamber. The element wire spanned the working hot zone (length 1.04m), and was fastened onto the

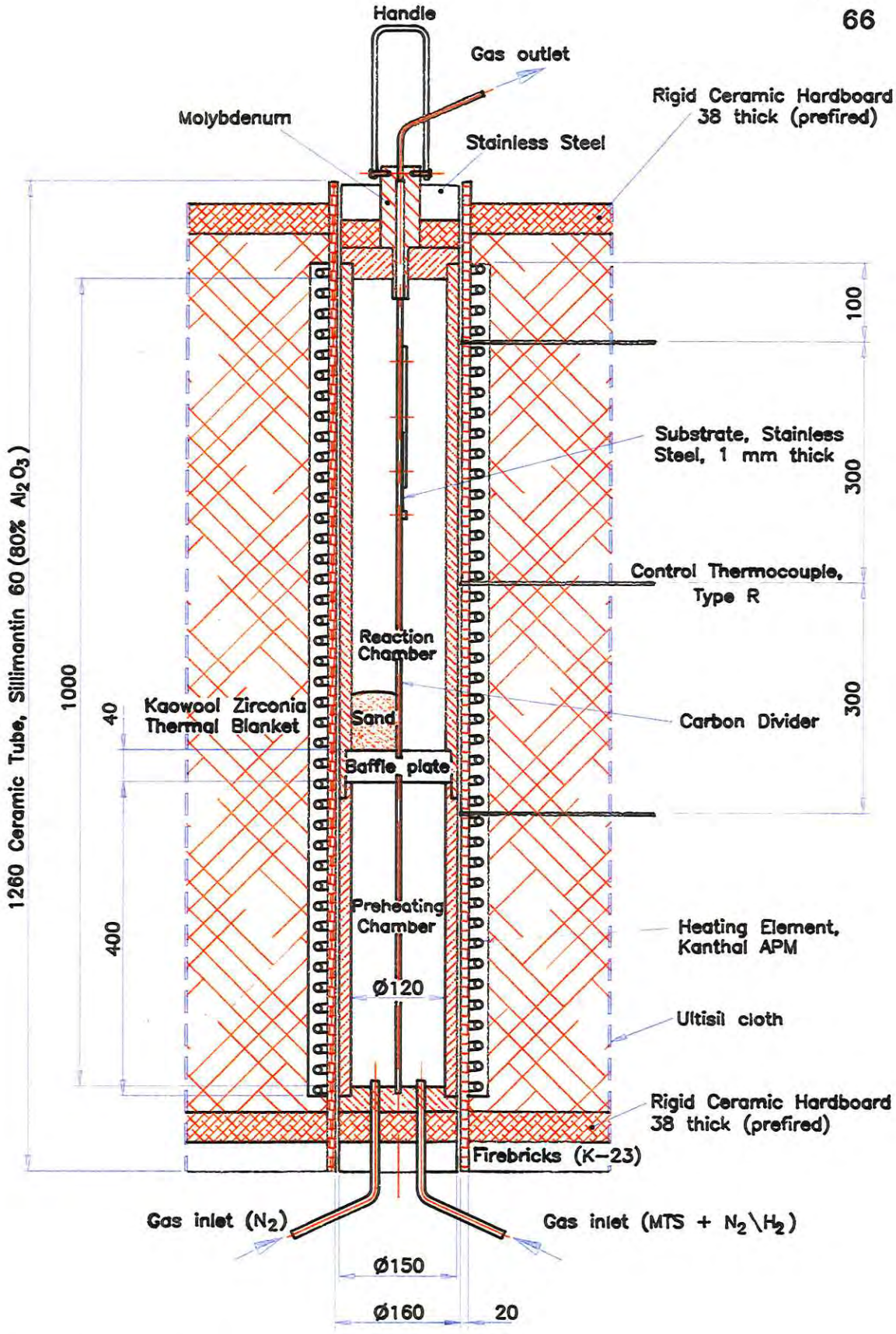

Figure 10: A schematic diagram of the fluidised bed reactor

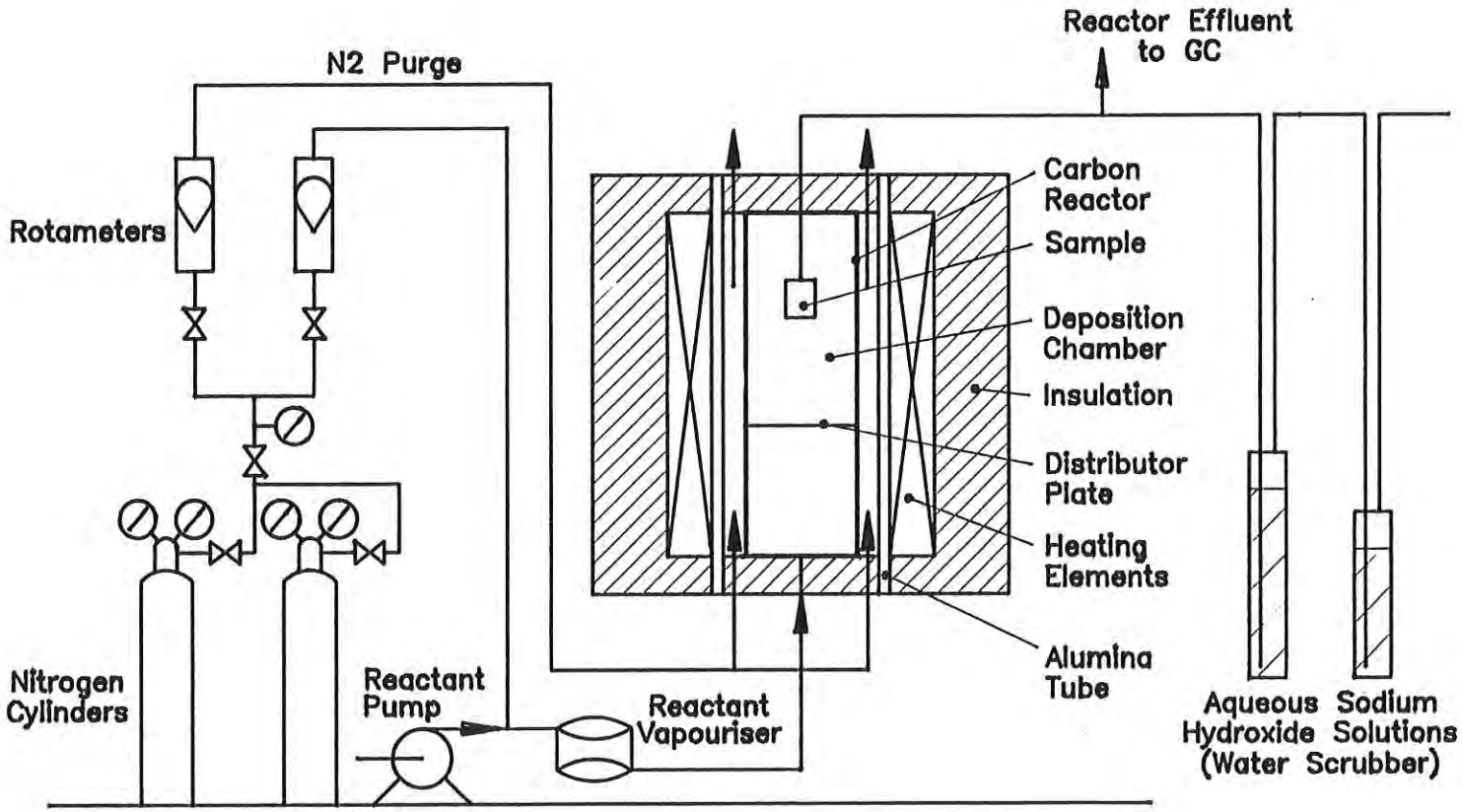

Figure 11 : Flow diagram of the hot wall/fluidised bed reactor system

ceramic tube using galvanised wire which was covered with bedding cement. Each element was connected to a PAC 25 thyristor power regulator, and a Shimaden SR temperature controller. Three type R thermocouples were positioned at 0.12m, 0.32m, and 0.72m from the top of the reaction chamber. Each thermocouple was mounted 1×10^{-2} m into the carbon work tube and covered by a protective ceramic sheath. The thermocouples were connected to a Shimaden KR 10 thermocouple switch which, in turn, was connected to a Shimaden SD 15 digital unit. The temperature of the furnace could be displayed easily on the display unit relating to any one site at a time. Thermocouple no. 2 was used as the control for monitoring the carbon chamber temperature. The furnace was heavily insulated using Kaowool ceramic fibre (zirconia blanket, 128 kg/m^3) and wrapped around the ceramic tube bearing the elements, yielding a thickness of 0.105 m. The final layer was covered with Ultisil cloth (high temperature silica fabric). This insulation system ensured that the outer surface temperature remained below 303 K. The whole system was supported on rigidised board 1260 and K23 firebricks which formed the base of the furnace.

3.1.5 EXHAUST TREATMENT SYSTEM

The gaseous effluents from the exhaust of the reaction chamber were directed through a 4m stainless steel tube of 9.5mm diameter into a water scrubber. The cooled gases were passed through two glass containers

filled with standard sodium hydroxide. The overall reaction indicated the formation of HCl as the major decomposition product of MTS therefore, every precaution was taken to neutralise the acid gas. The effluent gases were also taken as aliquot by an automatic sampler and passed through the gas chromatograph to monitor the traces of any unreacted reactant. The sodium hydroxide solution was back-titrated with standard acid to measure the quantity of HCl produced.

3.2 MATERIALS

The materials used in the present investigation are given below:

3.2.1 METHYLTRICHLOROSILANE

Methyltrichlorosilane (MTS), an organosilane with a boiling point of 66°C and density 1.273 g/ml (@25°C) was used as the precursor material, and supplied by Crown Scientific Pty. Ltd.

3.2.2 NITROCELLULOSE

Commercial grade nitro-cellulose was used as a standard for the determination of kinetic parameters. It has a nitrogen content of 12.6% and was obtained from Australian Defence Industries, Mulwalla.

3.2.3 EPOXY RESIN

Commercial grade epoxy resin no. 828 was obtained from Shell Chemicals (Australia) Pty. Ltd. and was used as a standard for the comparison of kinetic parameters.

3.2.4 HYDROCHLORIC ACID

Ampoules of HCl were diluted to 1 litre to produce a solution of 0.1N were obtained from Selbys.

3.2.5 SODIUM HYDROXIDE PELLETS

Sodium hydroxide pellets with a minimum assay of 99.0% were obtained from Selbys.

3.3 METHODS

3.3.1 SAMPLE PREPARATION

Stainless steel plates, measuring 0.05m x 0.10m prepared with a hole punched out at the top for passing the suspending wire through, were prepared. The sample surface was primed by two methods. The first involved grit blasting the surface with a mixture of sand plus grit particles at 85 psi, to clean and roughen the surface. The second method involved

chemically etching the surface in a solution of sulphuric acid, potassium fluoride and a commercial surfactant Fluorad FC-99. The specification of the stainless steel plate is given in Table 4.

3.3.2 CALIBRATION OF LIQUID FEED PUMP

A diaphragm positive displacement metering pump (Acromet 3000) was calibrated for MTS delivery. The pump was primed with MTS using a back pressure check valve to establish and maintain continual delivery. The volume of MTS was measured by collection into a measuring cylinder over 1 minute, to give a flow rate in ml/min. at minimum and maximum pump settings. Other pump settings of interest were determined in the same way. A graph indicating the delivery rates with variable pump settings is given in Fig. 12.

3.3.3 CALIBRATION OF THE REACTION CHAMBER

The reaction chamber was calibrated at temperatures ranging from 773 K to 1173 K. The furnace was purged with high purity nitrogen at a flow rate of 5.66×10^2 l/h, for 10 minutes prior to commencement of heating. A rod containing three lengths of type R thermocouple wire (0.14m, 0.34m, 0.54m), was suspended from a central locality at the top of the furnace. The temperature at each position was measured using a telatemp thermocouple thermometer (115) measuring unit. A graph of the furnace set points against the measured temperatures is given in Fig. 13.

Table 4 : Specification of stainless steel substrate

ELEMENT	PLATE OR SHEET	BAR
Carbon	0.07%	0.06%
Manganese	-	1.7%
Nickel	12%	12%
Chromium	17%	17%
Molybdenum	2.25%	2.25%

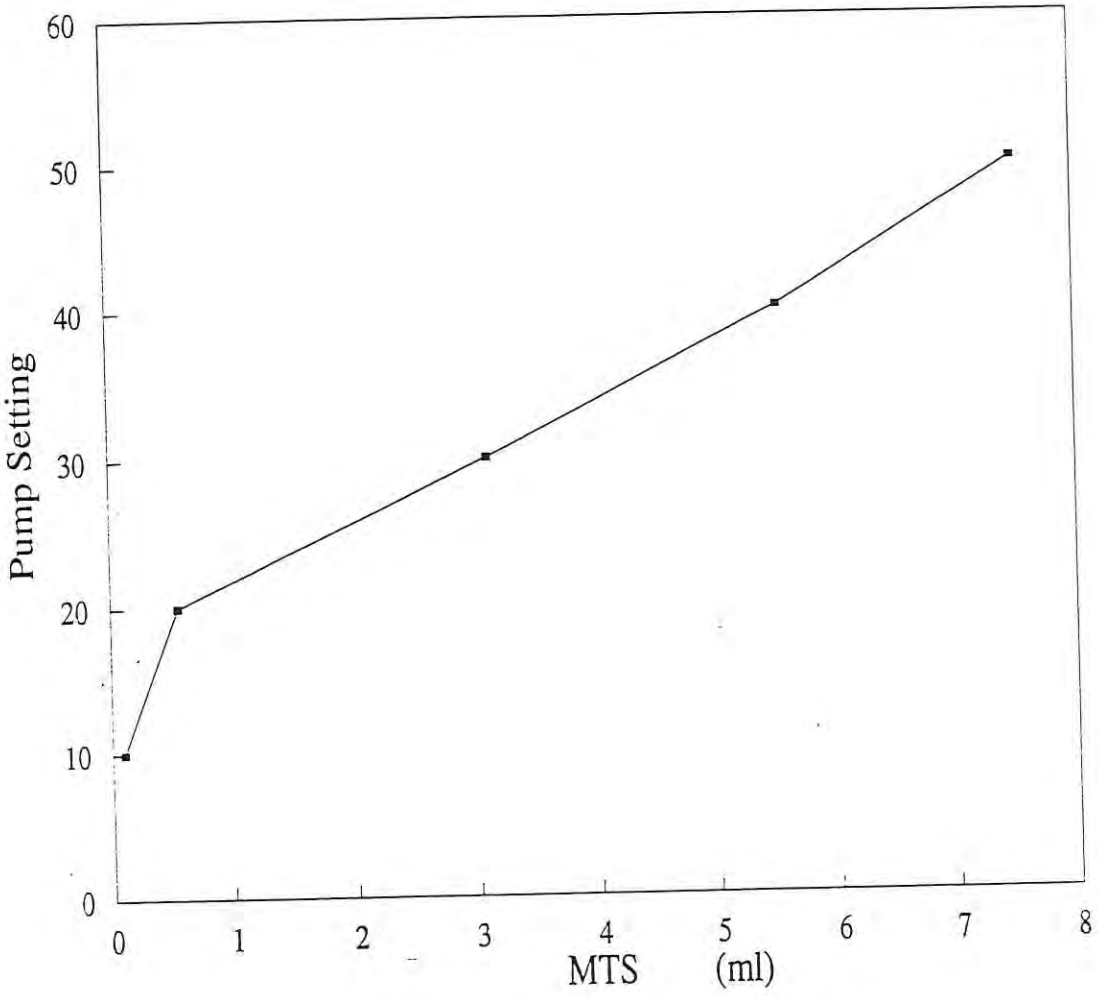

Figure 12 : Calibration curve for the diaphragm liquid metering pump

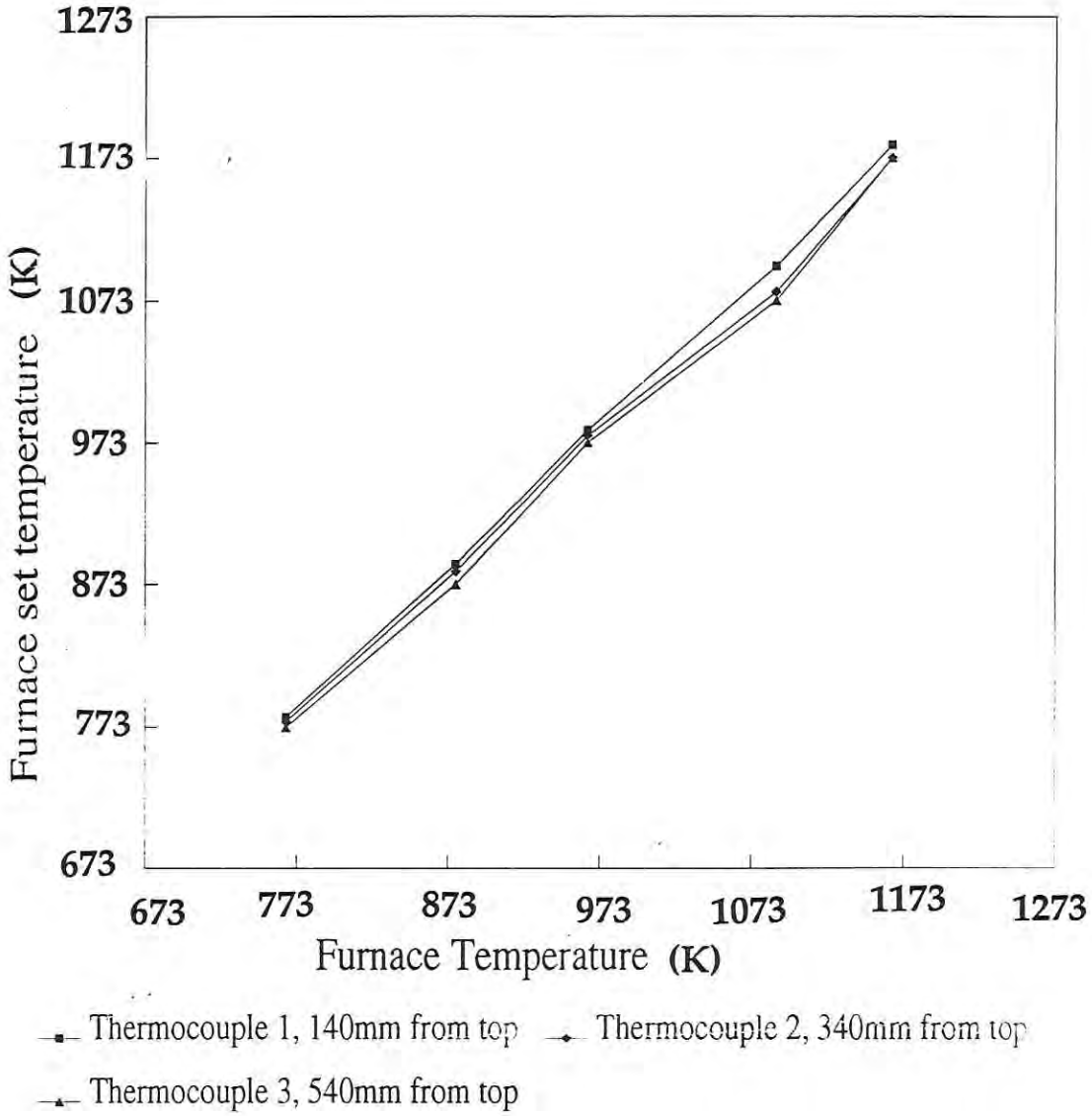

Figure 13 : Calibration curve for the hot wall reactor

The wall temperatures of the carbon furnace were measured by three type R thermocouples which were permanently mounted into the wall ($1x10^{-2}m$) of the reaction chamber. The temperature readings were displayed on a Shimaden SD 15 digital unit. A graph of the furnace set points against the furnace wall temperatures is given in Fig. 14.

3.3.4 DEPOSITION METHOD IN HOT WALL REACTOR

The pre-treated substrate was suspended from a stainless steel wire, within the reaction chamber, 0.3m from the lid (0.1m above the gas distribution plate). The lid was held down using a stainless steel block (0.05m wide) fastened with bolts on either side. The furnace was purged with high purity N_2 gas, both internally and externally at a flow rate of 5.66×10^2 l/h for 10 minutes prior to furnace heating. The furnace was set to the desired deposition temperature (not exceeding 1173 K). The temperature of the furnace was monitored and it took about two hours to obtain temperature stability inside the reaction chamber. The gas preheater was set to 373 K to ensure complete volatilisation of the precursor material. The temperature of the furnace was measured by three type R thermocouples mounted into the wall. The precursor material, MTS, was transported into the reaction chamber using two different methods. In the first method, MTS vapours were carried by a N_2 carrier gas into the reaction chamber via the preheating chamber. Table 5 lists the varying experimental conditions with the deposition

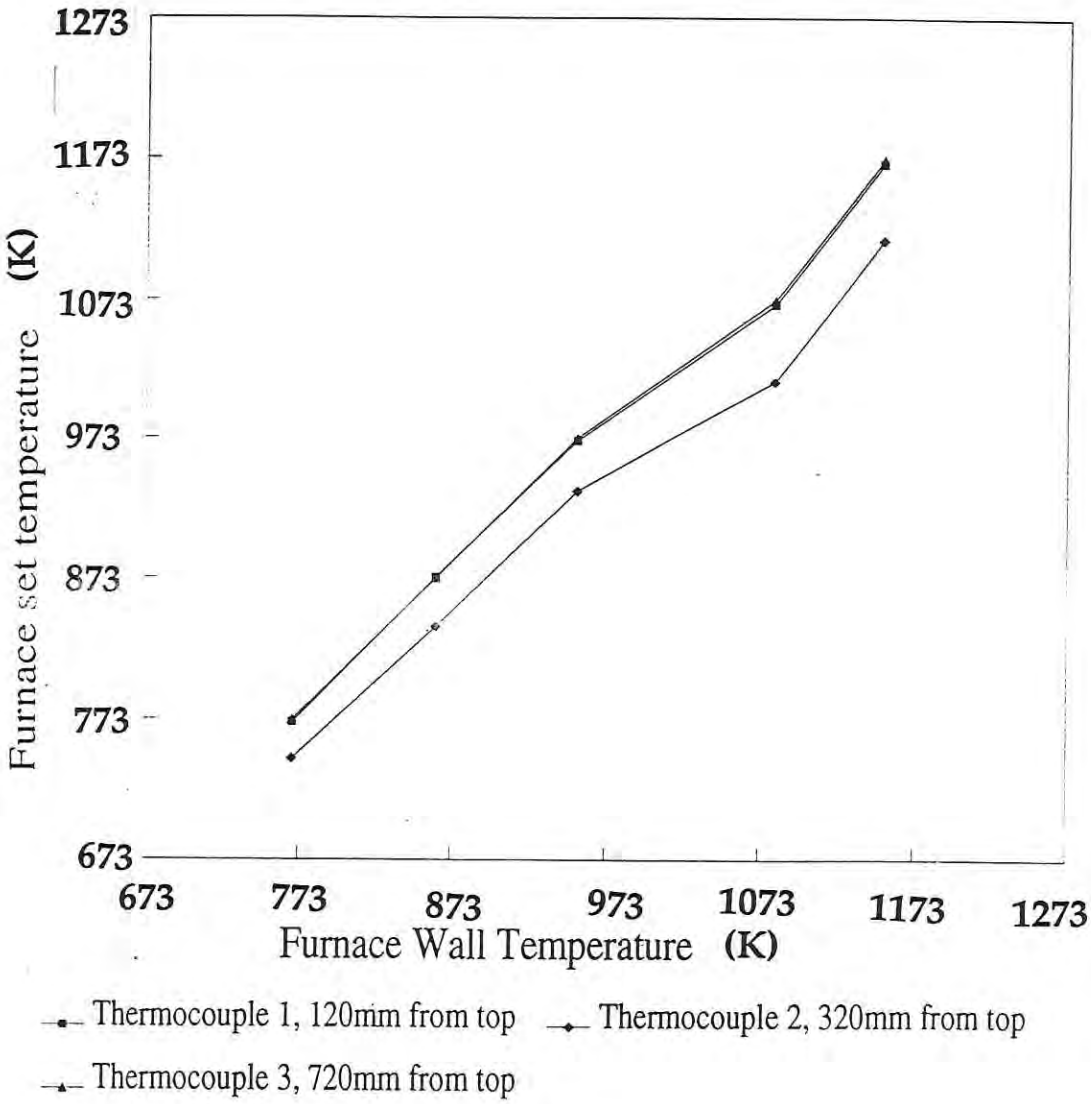

Figure 14 : Calibration curve for measuring the reactor wall temperature

Table 5 : Deposition rate in a Hot Wall Reactor using a nitrogen bubbler

No	Temp K	MTS ml/min	N_2 ml /min	Deposit mg	HCl yield %	Thick-ness µm	Deposition Rate mg/m^2s
1	973	1.6	10	6.05	35	10	2.05
2	1073	1.7	10	65.43	50	10	27.3
3	1173	1.8	10	70.7	48	15	18.3

rates. In the second method, MTS was fed directly into either a N_2, H_2 or N_2/H_2 carrier using a diaphragm positive displacement pump at various feed flow rates via the preheating chamber. Tables 6 & 7 list the varying conditions and deposition rates. For each experimental trial, a total of 20ml of MTS was utilised. The effluent gases were passed through two glass containers filled with standard sodium hydroxide. This solution was back-titrated with standard acid to measure the quantity of HCl produced. Aliquot of effluent gas was passed through the gas chromatograph to monitor unreacted precursor material. The coated substrate was removed from the reaction chamber after cooling down to 423 K. Rapid cooling was achieved by increasing the flow rate of the N_2 through the reaction chamber.

3.3.5 DEPOSITION METHOD IN FLUIDISED BED REACTOR

The fluidising reaction chamber was a hot wall reaction chamber containing a 1×10^{-2}m carbon partition. The fluidising media was 1×10^{-3}m sand particles. One kilogram of sand was placed into one side of the fluidising chamber. Provision was made on the partition to enable attachment of the substrate to the other side of the deposition chamber. The furnace was purged with high purity N_2 gas, both internally and externally, at a flow rate of 5.66×10^2 l/h for 10 minutes. Separate inlet tubes were positioned on either side of the chamber. The fluidising gas

Table 6 : Deposition Rate in a Hot Wall Reactor using a liquid metering diaphragm pump and N_2 as a carrier gas

No	Temp K	MTS mol/ h	Carrier Gas (N_2) Flow Rate L/h	Coating Deposit mg	HCl Yield %	Deposition Rate mg/m²s
1	973	1.4	$2.83x10^2$	8.46	40.47	$1.93x10^{-2}$
			$4.24x10^2$	4.9	43.05	$1.12x10^{-2}$
			$5.66x10^2$	8.43	37.30	$1.92x10^{-2}$
			$7.08x10^2$	5.27	25.80	$1.20x10^{-2}$
		2.81	$2.83x10^2$	6.02	32.30	$1.41x10^{-2}$
			$4.24x10^2$	0.71	38.75	$3.25x10^{-3}$
2	1073	1.4	$2.83x10^2$	49.42	38.37	$1.12x10^{-1}$
			$4.24x10^2$	72.01	46.49	$1.64x10^{-1}$
			$5.66x10^2$	55.08	32.50	$1.24x10^{-1}$
		2.81	$2.83x10^2$	196.37	25.00	$8.99x10^{-1}$
			$4.24x10^2$	34.9	40.47	$1.59x10^{-1}$
3	1173	1.4	$2.83x10^2$	122.4	36.16	$2.79x10^{-1}$
			$4.24x10^2$	107.3	24.11	$4.91x10^{-1}$
			$5.66x10^2$	139.9	24.11	$3.19x10^{-1}$
		2.81	$4.24x10^2$	91.4	47.8	$4.18x10^{-1}$

Table 7 : Deposition rate in a Hot Wall Reactor using a liquid metering diaphragm pump and N_2 and/or H_2 as a carrier gas

No	Temp K	MTS mol /h	N_2 l/h	N_2:H_2 mole ratio	Deposit mg	HCl Yield %	Deposition Rate mg/m^{2}s
1	973	1.4	$2.83x10^2$	1:1	4.84	15.5	1.105
			$2.83x10^2$	1:4	8.47	11.7	1.93
			0	0:H_2	5.2	10.2	1.18
2	1073	1.4	$2.83x10^2$	1:1	126.8	26.6	28.9
			$2.83x10^2$	1:4	60.36	56.1	13.8
			0	0:H_2	139.8	29.3	31.9
3	1173	1.4	$2.83x10^2$	1:1	101.68	41.7	23.2
			$2.83x10^2$	1:4	102.4	43.6	23.4
			0	0:H_2	23.69	33.6	54

was high purity N_2 gas, the flow of which was maintained high enough to attain minimum fluidisation. The precursor material was fed into the reaction chamber using a diaphragm positive displacement pump, with varying concentrations of N_2 and H_2 gas. For each experimental trial, a total of 20ml of MTS was utilised. The effluent gases were passed through two glass containers filled with standard sodium hydroxide and the solution was back-titrated with standard acid to measure the quantity of HCl produced. Aliquot of effluent gas were passed through the gas chromatograph to monitor unreacted precursor material. Table 8 lists the varying experimental conditions and deposition rates obtained using the fluidising technique.

3.3.6 GAS CHROMATOGRAPHY

The effluent gases, representing the decomposition products of MTS, were analysed dynamically using gas chromatography. Dynamic sampling methods assure uniformity in replicate measurements and minimise memory efforts in the sampling volume. A Perkin-Elmer Autosystem Gas Chromatograph (GC), fitted with a flame ionisation detector (FID) was used in the analysis. This system was connected to the exit lines of the furnace. The exhaust gases were cool (30°C) prior to entry into the GC. Aliquot samples were abstracted periodically using a gas sampling valve, at 2, 4, and 6 minutes from commencement of precursor material feed into the reactor. The GC column was an SGE teflon column, poropak Q 80-

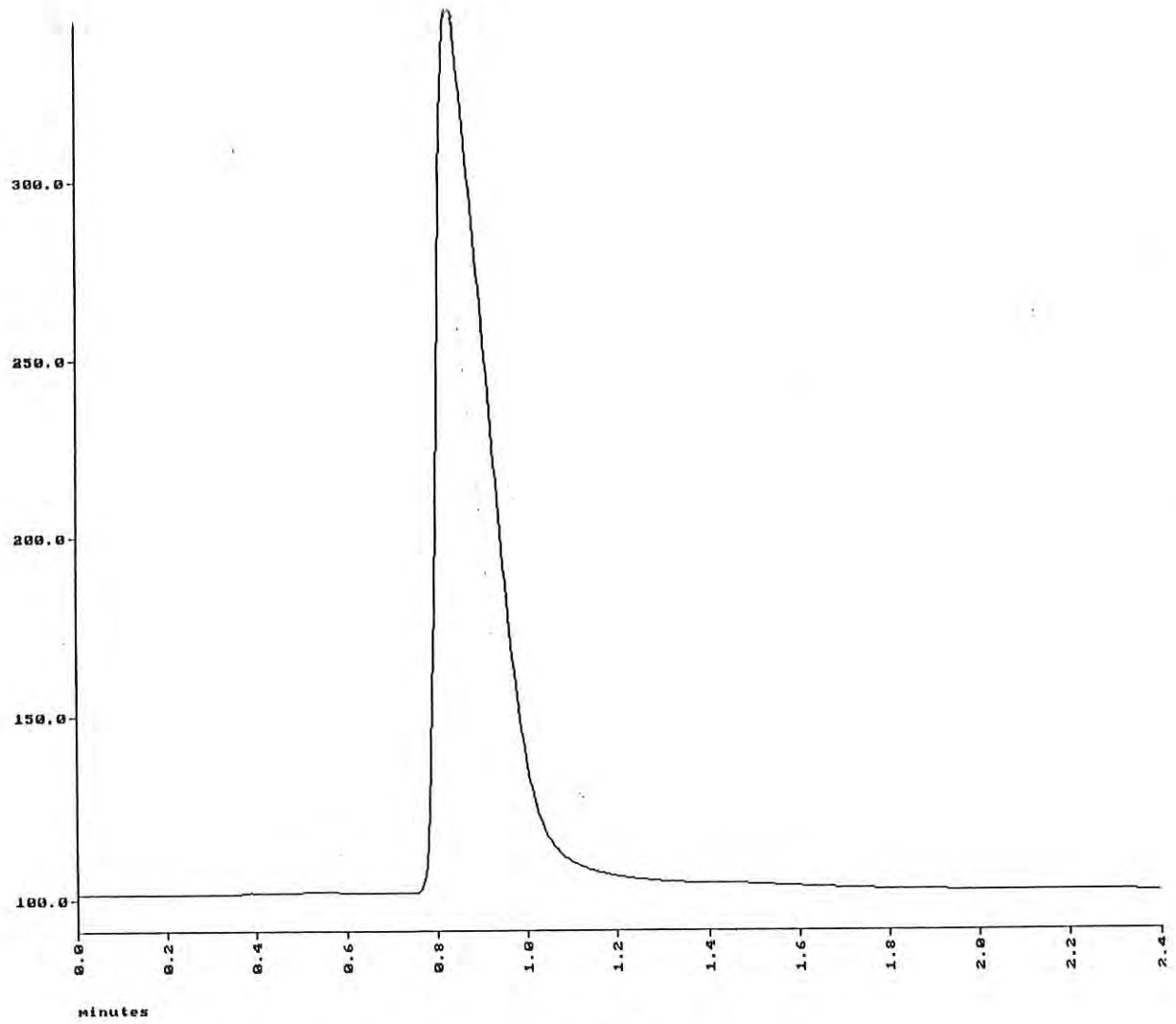

Figure 15 : Gas Chromatogram for MTS

Table 8 :Deposition rate in a Fluidised Bed Reactor using N_2 as a carrier gas

No	Temp K	MTS mol/h	N_2 l/h	N_2:H_2 mole ratio	Deposit mg	HCl Yield %	Deposit Rate mg/m^{2}s
1	1073	1.4	$4.24x10^2$	1:4	26.66	3.26	32.6
			$5.66x10^2$	1:4	5.2	2.19	2.38
			0	0:H_2	6.83	6.03	3.12
2	1173	1.4	$4.42x10^2$	1:4	30.3	6.7	
			$5.66x10^2$	1:4	13.0	4.2	5.94
			0	0:H_2	13.8	0.55	6.3

100#, capable of MTS detection. The column was standardised for MTS detection. The chromatogram indicating the Rt is given in Fig. 15. Helium was used as the carrier gas. The oven, injector and FID were set at 200°C, 200°C, and 250°C respectively.

3.3.6.1 DATA ACQUISITION SYSTEM

A Perkin-Elmer Nelson 1020S Personal Integrator was connected to the PE Autosystem Gas Chromatograph for data collection.

3.3.7 SCANNING ELECTRON MICROSCOPY

A Jeol 35 Scanning Electron Microscope with a Tracor Northern Energy Dispersive X-ray Analyser was used for analysing the coating topography and thicknesses of the coatings. The analysis was carried out using an Image Acquisition and Processing Program and Energy Dispersive Analysis to give X-ray Imaging, Line Scans and Image Enhancement photographs for the coated surface.

A Jeol 200 FX operated in the STEM mode as a Scanning Electron Microscope with a Tracor Northern TN 5502 Energy Dispersive Analyser, was used in the analysis of several coating surfaces.

3.3.8 X-RAY DIFFRACTOMETRY

A PW1710/00 Philips automated powder diffractometry system was used to determine the types of coatings on the substrate. The basic function of the X-ray spectrometer is to separate the polychromatic beam of radiation into individual wavelengths. The spectrometer consists of a primary collimator and a goniometer. The primary collimator selects an almost parallel beam of radiation from the sample and directs this onto the plane surface of the analysing crystal. Here the radiation is diffracted in accordance with Bragg's law: $\mathbf{n\lambda = 2d \sin\theta}$, which gives the relationship between the wavelength(λ), the (2d) spacing of the diffracting crystal and the angle(θ) through which the radiation is diffracted. The function of the goniometer is to accurately control the 2:1 rotation of the detector and the crystal. The spectrometer is also fitted with a primary excitation source (a sealed X-ray tube) powered by an ultra high stability high voltage generator. The function of the primary excitation source is to excite characteristic radiation from the specimen. Finally, the spectrometer is fitted with a detection system comprising a gas flow proportional counter(for wavelengths greater than 2**Å**) and a scintillation counter(for wavelengths greater than 2**Å**). The detector converts the X-ray photons into voltage pulses, which are then amplified before passing to the scaling circuitry.

3.3.9 THERMAL ANALYSIS

A Perkin-Elmer Differential Scanning Calorimeter DSC-7 was used to mimic the reaction *in situ* and for measuring parameters such as heat of reaction (enthalpy change), decomposition temperature and kinetic parameters (such as activation energy, order of reaction and pre-exponential factor) for the overall decomposition process. The samples were placed in hermetically sealed high pressure capsules. Nitrocellulose, epoxy resin and polyethylene were scanned using DSC and used as standards. The measurements were performed in dynamic temperature program mode ranging from 303 K to 998 K (@ 5, 10, 20 & 40 K/min scanning rates). Baseline corrections were made for each sample run at the same conditions.

CHAPTER 4

THERMODYNAMICS

4.1 METHOD

Thermodynamic analysis provides the basic information such as: (a) limiting equilibrium composition of the gas phase; (b) identification of the condensed phase; and (c) their limiting deposition rates. This information although useful in describing possible reaction mechanism, neither provides information on CVD mechanism nor on the deposition rate. The present study was concerned with the thermodynamic analysis of Si-C-H-Cl vapour system in order to define optimum conditions for the deposition of ceramic type films when MTS is used as the main reactant with or without the presence of H_2 gas.

A number of methods have been reported in the literature for computing thermodynamic equilibrium compositions. All the reported techniques are based upon the minimisation of the total free energy of the system[147,148]. The method required the writing of a series of chemical reactions and the computation of their respective equilibrium constants.

The technique developed by White et. al.[149] was relatively simple and direct for computing chemical equilibria and involved minimising the sum of the free energies of all the species. Ericksson[150] extended this further to include systems containing more than one condensed phase. He devised a computer code called SOLGAS, which was later modified and renamed SOLGASMIX for performing thermodynamic calculations.

The basic equilibrium calculations are based upon the free energy minimisation method where the quantity

$$(G/RT) = \sum_{n_i} (g^o/RT)_i + \ln a \qquad (1)$$

is minimised with respect to variables n_i for constant temperature and pressure. In equation (1), G represents the total free energy of the system, R the gas constant, T the thermodynamic temperature, n_i the amount of the i^{th} substance, g^o the standard chemical potential, and a the activity coefficient.

Under ideal conditions in each phase, equation 1 can be expressed as:

$$\begin{aligned} G/RT = & \sum_{p=1}^{I} \sum_{i=1}^{m_p} n_{pi}[(g^o/RT)_{pi} + \ln P + \ln(n_{pi}/N_p)] \\ & + \sum_{p=2}^{q+1} \sum_{i=1}^{m_p} n_{pi}[(g^o/RT)_{pi} + \ln(n_{pi}/N_p)] \\ & + \sum_{p=q+2}^{q+s+1} \sum_{i=1}^{m_p} n_{pi}(g^o/RT)_{pi} \end{aligned} \qquad (2)$$

where n_{pi} is the moles of species i in phase p, N_p the total moles of species in phase p, m_p the number of species in phase p, and P the total pressure. In equ. (2): p=1 corresponds to the gaseous phase, p=2-(q+1) to the condensed phase, and p=(q+2)-(q+s+1) to the invariant condensed phases. It is evident that in order to calculate the total free energy of a system using above equations, the value of (g^o/RT) has to be specified for all species condensed. This quantity can be calculated either by the

expression:

$$(g^o/RT) = \Delta_f G^o/RT \qquad (3)$$

where $\Delta_f G°$ denotes the Gibbs free energy of formation from the elements in their chosen reference state, or by the expression

$$(g^o/RT) = (1/R)[G^o - H^o_{298}/T] + \Delta_f H^o_{298}/RT \qquad (4)$$

where $G° - H°_{298} / T$ is the free energy function and $\Delta_f H°_{298}$ is the heat of formation at 298 K.

In the present investigation, the thermodynamic calculations were performed using CHEMIX[151], developed by CSIRO. This program is based on similar principles as that of Ericksson's SOLGASMIX code, described above. This code a part of the thermochemistry system, includes a data-base of thermodynamic property data for a wide range of chemical species.

4.2 RESULTS

To calculate the equilibrium composition of $MTS/N_2/H_2$ system, 37 gaseous and 5 condensed species were taken into consideration (Table 9).

Table 9 : A list of possible intermediates/products from the thermal decomposition of MTS used in the Chemix model

Gaseous Products			
$SiCl_3CH_3$	Si_2	C_2Cl_4	CH_4
$Si(CH_3)_4$	Si	C_2Cl_2	CH_3
SiC_2	HCl	C_2ClH	CH_2
SiC	Cl_2	C_4	CH
$SiCl_4$	CCl_4	C_3	C
$SiCl_3H$	CCl_3	C_2H_6	H_2
$SiCl_3$	CCl_2	C_2H_4	
$SiCl_2$	CCl	C_2H_2	
SiCl	CCl_3H	C_2H	
Si_3	C_2Cl_6	C_2	
Condensed Products			
SiC(s,alpha)	Si(l)	C(s)	
SiC(s,beta)	Si(s)		

Thermodata for these species were taken from the thermochemistry CPDJANDAT database which is based on the data from the JANAF thermochemical compositions[69].

The thermodynamic variables, for MTS/N_2 or MTS/N_2/H_2 or MTS/H_2 system, were temperature and mole ratios of the gases to MTS. The pressure was fixed at 1 atm. and temperature ranged from 773 K - 1273 K, in 25° intervals. The data on variations of gaseous mole ratios to MTS is given in Tables 10-13. The CVD efficiency diagrams for the system investigated with variable conditions are given in Figs. 16 - 36.

4.2.1 THE CH_3SiCl_3-N_2 SYSTEM

The variables taken into consideration for the computation of thermodynamic data include temperature for this system which was varied from 773 K - 1273 K at 25° intervals. The CVD phase diagrams are given in Figs. 16 - 20. These diagrams provide information on the formation of gaseous species and the specific condensed phases at equilibrium under input conditions. As can be seen from Fig. 16, two condensed phases, C and SiC, are predicted along with the formation of gaseous species (HCl, CH_4, $SiCl_4$ and H_2). The species distribution of C, H, Si, and Cl is separately plotted in Figs. 17 - 20. Fig. 17 clearly indicates that H_2 and CH_4 are the two gaseous species formed below 973 K. The concentration of methane decreased with an increase in

Table 10 : Thermodynamic distribution of major species from the decomposition of MTS in nitrogen atmosphere

Calculation basis	1 mole SiCl3CH3 0 mole H2							
TEMP, °C	HCl(g)	CH4(g)	SiHCl3(g)	SiCl3(g)	SiCl4(g)	H2(g)	C (s)	SiC (s,1)
525	0.0242	0.3856	0.0136	0.0000	0.7338	0.7100	0.3618	0.2526
525	0.0337	0.3285	0.0156	0.0000	0.7299	0.8183	0.4170	0.2545
550	0.0457	0.2736	0.0176	0.0000	0.7253	0.9211	0.4694	0.2570
575	0.0604	0.2231	0.0196	0.0001	0.7202	1.0138	0.5167	0.2602
600	0.0778	0.1785	0.0215	0.0001	0.7144	1.0933	0.5574	0.2641
625	0.0981	0.1407	0.0232	0.0002	0.7079	1.1580	0.5907	0.2687
650	0.1212	0.1096	0.0249	0.0002	0.7009	1.2077	0.6164	0.2740
675	0.1473	0.0847	0.0263	0.0004	0.6932	1.2437	0.6351	0.2801
700	0.1762	0.0652	0.0277	0.0005	0.6848	1.2676	0.6478	0.2870
725	0.2079	0.0501	0.0288	0.0008	0.6758	1.2814	0.6553	0.2946
750	0.2425	0.0385	0.0299	0.0011	0.6661	1.2867	0.6586	0.3029
775	0.2798	0.0297	0.0308	0.0015	0.6558	1.2853	0.6585	0.3118
800	0.3197	0.0230	0.0315	0.0021	0.6448	1.2785	0.6556	0.3215
825	0.3622	0.0178	0.0322	0.0028	0.6331	1.2672	0.6505	0.3317
850	0.4071	0.0139	0.0327	0.0038	0.6207	1.2524	0.6436	0.3425
875	0.4542	0.0109	0.0331	0.0049	0.6077	1.2346	0.6353	0.3538
900	0.5034	0.0085	0.0334	0.0064	0.5940	1.2146	0.6259	0.3656
925	0.5543	0.0067	0.0335	0.0081	0.5797	1.1926	0.6156	0.3777
950	0.6069	0.0053	0.0335	0.0102	0.5647	1.1691	0.6046	0.3900
975	0.6607	0.0043	0.0334	0.0127	0.5491	1.1444	0.5932	0.4026
1000	0.7156	0.0034	0.0332	0.0157	0.5329	1.1188	0.5815	0.4152

Table 11 : Thermodynamic distribution of major species from the decomposition of MTS under hydrogen in a ratio of 1:2

Calculation basis	1 mole SiCl3CH3 2 mole H2							
TEMP., °C	HCl(g)	CH4(g)	SiHCl3(g)	SiCl3(g)	SiCl4(g)	H2(g)	C (s)	SiC (s,1)
500	0.0356	0.7474	0.0252	0.0000	0.7222	1.9748	0.0000	0.2526
525	0.0511	0.7433	0.0245	0.0000	0.7189	1.9755	0.0000	0.2567
550	0.0718	0.7380	0.0237	0.0000	0.7142	1.9763	0.0000	0.2620
575	0.0968	0.6515	0.0253	0.0001	0.7068	2.1360	0.0807	0.2679
600	0.1262	0.5368	0.0278	0.0001	0.6975	2.3493	0.1886	0.2746
625	0.1607	0.4349	0.0301	0.0002	0.6871	2.5347	0.2825	0.2826
650	0.2004	0.3476	0.0323	0.0003	0.6755	2.6885	0.3605	0.2920
675	0.2452	0.2750	0.0342	0.0004	0.6628	2.8104	0.4224	0.3026
700	0.2950	0.2161	0.0358	0.0006	0.6489	2.9024	0.4693	0.3146
725	0.3497	0.1692	0.0373	0.0008	0.6340	2.9682	0.5029	0.3279
750	0.4092	0.1323	0.0384	0.0012	0.6180	3.0116	0.5253	0.3424
775	0.4732	0.1036	0.0394	0.0016	0.6009	3.0366	0.5384	0.3580
800	0.5416	0.0813	0.0401	0.0022	0.5828	3.0466	0.5440	0.3748
825	0.6141	0.0640	0.0406	0.0029	0.5637	3.0447	0.5435	0.3925
850	0.6904	0.0506	0.0409	0.0038	0.5437	3.0332	0.5382	0.4112
875	0.7701	0.0402	0.0410	0.0050	0.5228	3.0141	0.5291	0.4308
900	0.8529	0.0320	0.0409	0.0063	0.5010	2.9890	0.5169	0.4510
925	0.9382	0.0257	0.0405	0.0079	0.4785	2.9592	0.5024	0.4719
950	1.0256	0.0207	0.0400	0.0098	0.4554	2.9257	0.4862	0.4931
975	1.1146	0.0168	0.0393	0.0120	0.4317	2.8895	0.4686	0.5146
1000	1.2045	0.0137	0.0385	0.0145	0.4075	2.8512	0.4501	0.5362

Table 12 : Thermodynamic distribution of major species from the decomposition of MTS under hydrogen in a ratio of 1:4

Calculation basis	1 mole SiCl3CH3 4 mole H2							
TEMP, °C	HCl(g)	CH4(g)	SiHCl3(g)	SiCl3(g)	SiCl4(g)	H2(g)	C (s)	SiC (s,1)
500	0.0426	0.7497	0.0414	0.0000	0.7083	3.9585	0.0000	0.2503
525	0.0611	0.7448	0.0402	0.0000	0.7046	3.9598	0.0000	0.2552
550	0.0858	0.7383	0.0389	0.0001	0.6993	3.9610	0.0000	0.2617
575	0.1180	0.7300	0.0377	0.0001	0.6922	3.9623	0.0000	0.2700
600	0.1589	0.7194	0.0364	0.0001	0.6828	3.9635	0.0000	0.2806
625	0.2102	0.7063	0.0352	0.0002	0.6709	3.9647	0.0000	0.2937
650	0.2662	0.6068	0.0363	0.0003	0.6560	4.1352	0.0858	0.3074
675	0.3264	0.4842	0.0383	0.0004	0.6393	4.3492	0.1939	0.3219
700	0.3933	0.3835	0.0400	0.0006	0.6212	4.5162	0.2783	0.3382
725	0.4667	0.3025	0.0414	0.0009	0.6016	4.6410	0.3414	0.3561
750	0.5462	0.2382	0.0425	0.0012	0.5807	4.7293	0.3862	0.3756
775	0.6314	0.1876	0.0433	0.0017	0.5584	4.7874	0.4158	0.3966
800	0.7219	0.1481	0.0437	0.0022	0.5350	4.8209	0.4329	0.4189
825	0.8174	0.1173	0.0439	0.0029	0.5104	4.8347	0.4401	0.4425
850	0.9171	0.0933	0.0437	0.0038	0.4849	4.8329	0.4395	0.4672
875	1.0205	0.0746	0.0434	0.0049	0.4584	4.8189	0.4326	0.4928
900	1.1270	0.0599	0.0427	0.0061	0.4312	4.7953	0.4210	0.5191
925	1.2356	0.0484	0.0418	0.0076	0.4035	4.7645	0.4057	0.5459
950	1.3456	0.0393	0.0406	0.0092	0.3753	4.7282	0.3876	0.5730
975	1.4560	0.0321	0.0393	0.0110	0.3470	4.6881	0.3677	0.6002
1000	1.5658	0.0264	0.0377	0.0130	0.3187	4.6454	0.3466	0.6270

Table 13 : Thermodynamic distribution of major species from the decomposition of MTS under hydrogen in a ratio of 1:8

Calculation basis	1 mole SiCl3CH3 8 mole H2							
TEMP., °C	HCl(g)	CH4(g)	SiHCl3(g)	SiCl3(g)	SiCl4(g)	H2(g)	C (s)	SiC (s,1)
500	0.0538	0.7526	0.0640	0.0000	0.6886	7.9360	0.0000	0.2474
525	0.0771	0.7462	0.0620	0.0000	0.6842	7.9380	0.0000	0.2538
550	0.1082	0.7380	0.0600	0.0001	0.6779	7.9399	0.0000	0.2620
575	0.1484	0.7275	0.0581	0.0001	0.6693	7.9419	0.0000	0.2726
600	0.1995	0.7142	0.0561	0.0002	0.6579	7.9438	0.0000	0.2858
625	0.2631	0.6978	0.0540	0.0003	0.6435	7.9458	0.0000	0.3022
650	0.3408	0.6779	0.0520	0.0004	0.6256	7.9479	0.0000	0.3221
675	0.4338	0.6541	0.0498	0.0005	0.6038	7.9500	0.0000	0.3459
700	0.5429	0.6263	0.0475	0.0007	0.5781	7.9521	0.0000	0.3737
725	0.6656	0.5828	0.0456	0.0009	0.5488	7.9789	0.0125	0.4048
750	0.7773	0.4618	0.0462	0.0012	0.5201	8.1646	0.1057	0.4324
775	0.8960	0.3661	0.0463	0.0017	0.4899	8.2966	0.1719	0.4619
800	1.0206	0.2909	0.0461	0.0022	0.4585	8.3849	0.2161	0.4930
825	1.1501	0.2319	0.0454	0.0029	0.4261	8.4385	0.2428	0.5253
850	1.2833	0.1857	0.0444	0.0036	0.3930	8.4648	0.2557	0.5586
875	1.4188	0.1494	0.0430	0.0045	0.3594	8.4702	0.2580	0.5925
900	1.5551	0.1209	0.0412	0.0055	0.3257	8.4599	0.2524	0.6266
925	1.6905	0.0985	0.0392	0.0066	0.2924	8.4382	0.2410	0.6605
950	1.8234	0.0807	0.0369	0.0078	0.2597	8.4084	0.2255	0.6938
975	1.9520	0.0665	0.0344	0.0090	0.2282	8.3737	0.2076	0.7259
1000	2.0746	0.0552	0.0318	0.0102	0.1982	8.3363	0.1883	0.7565

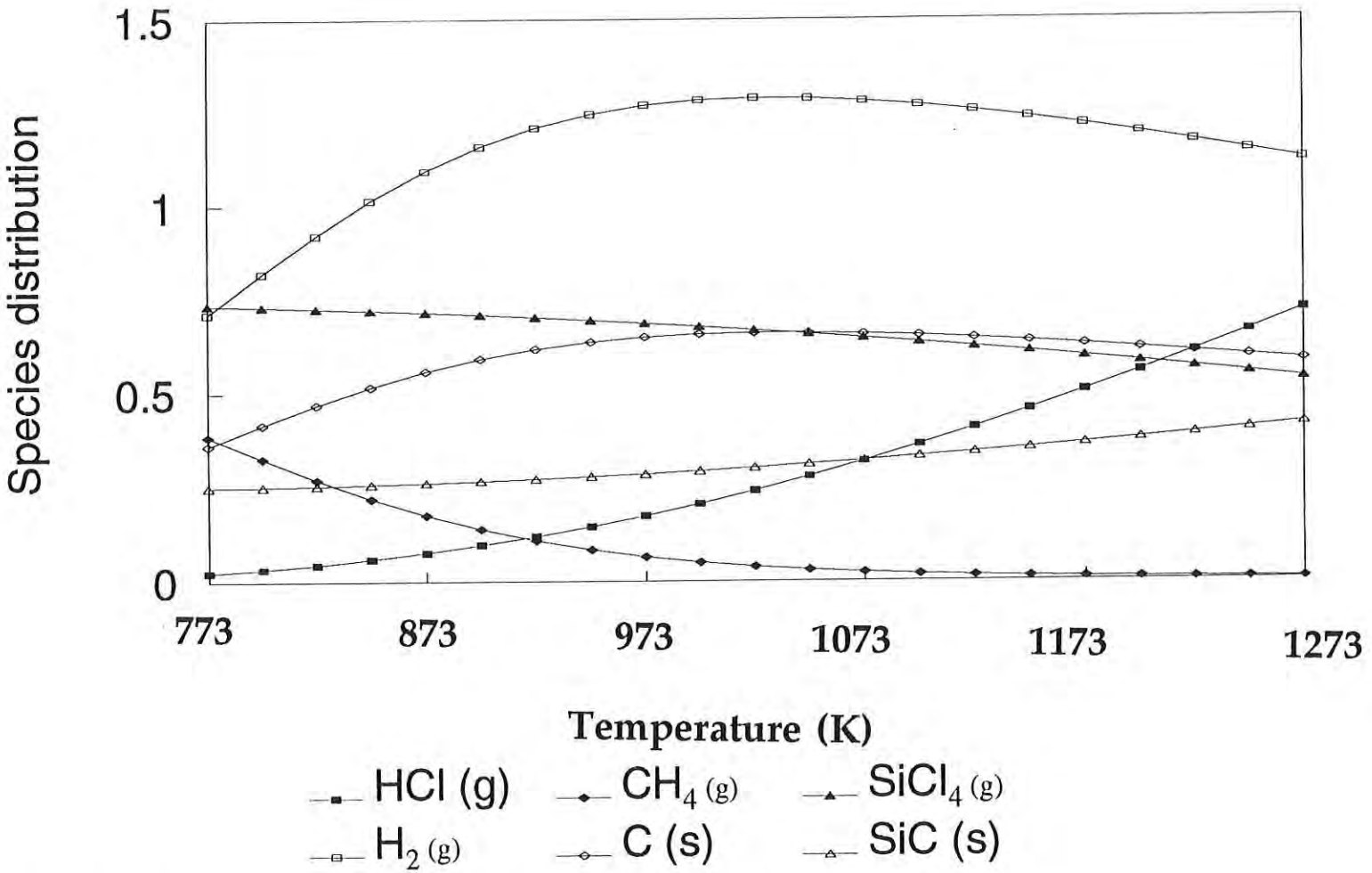

Figure 16 : Distribution of species from the thermal decomposition of MTS
Basis: 1 mole $SiCl_3CH_3$

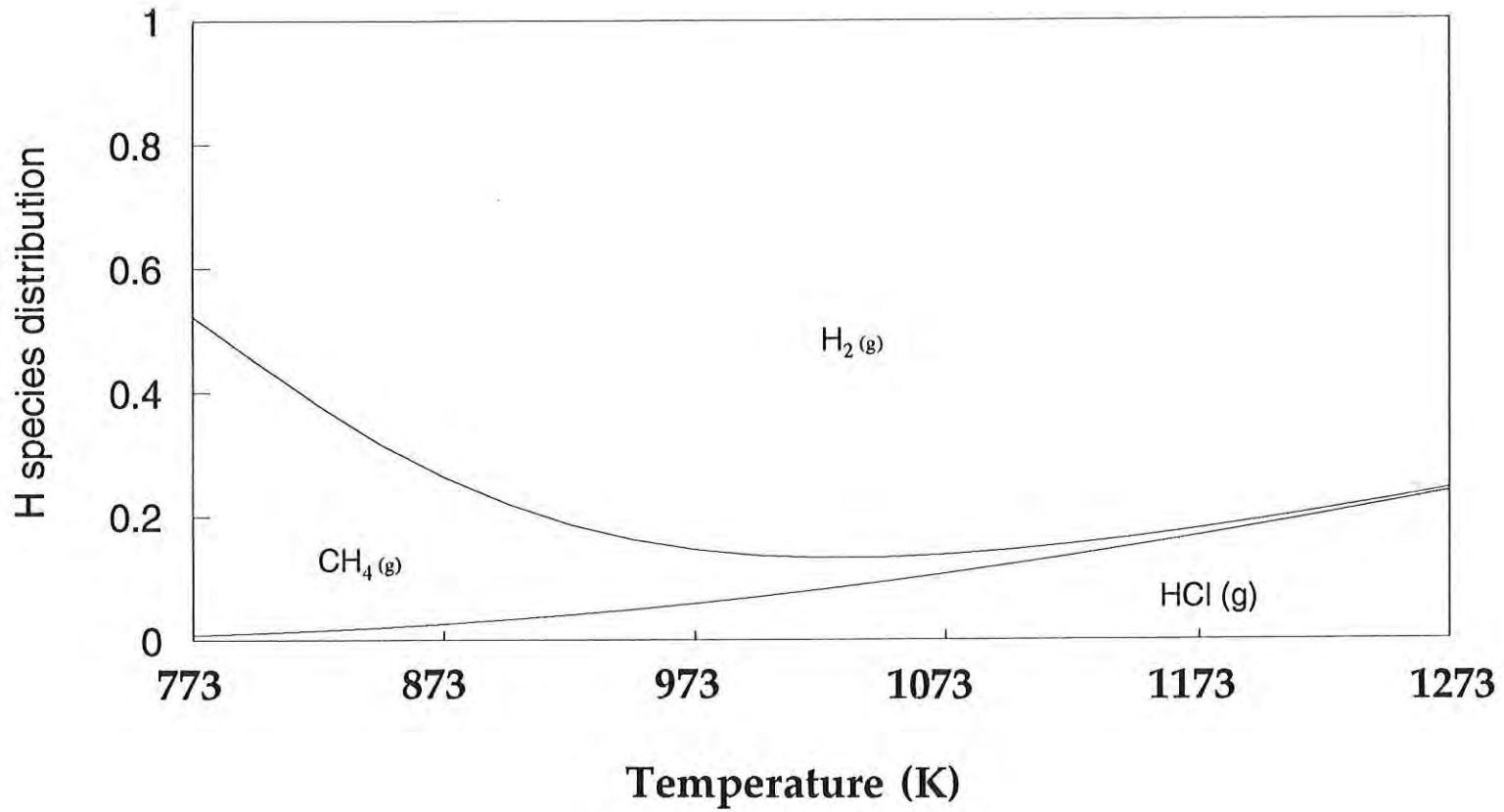

Figure 17: Area graph showing distribution of hydrogen species from the thermal decomposition of MTS

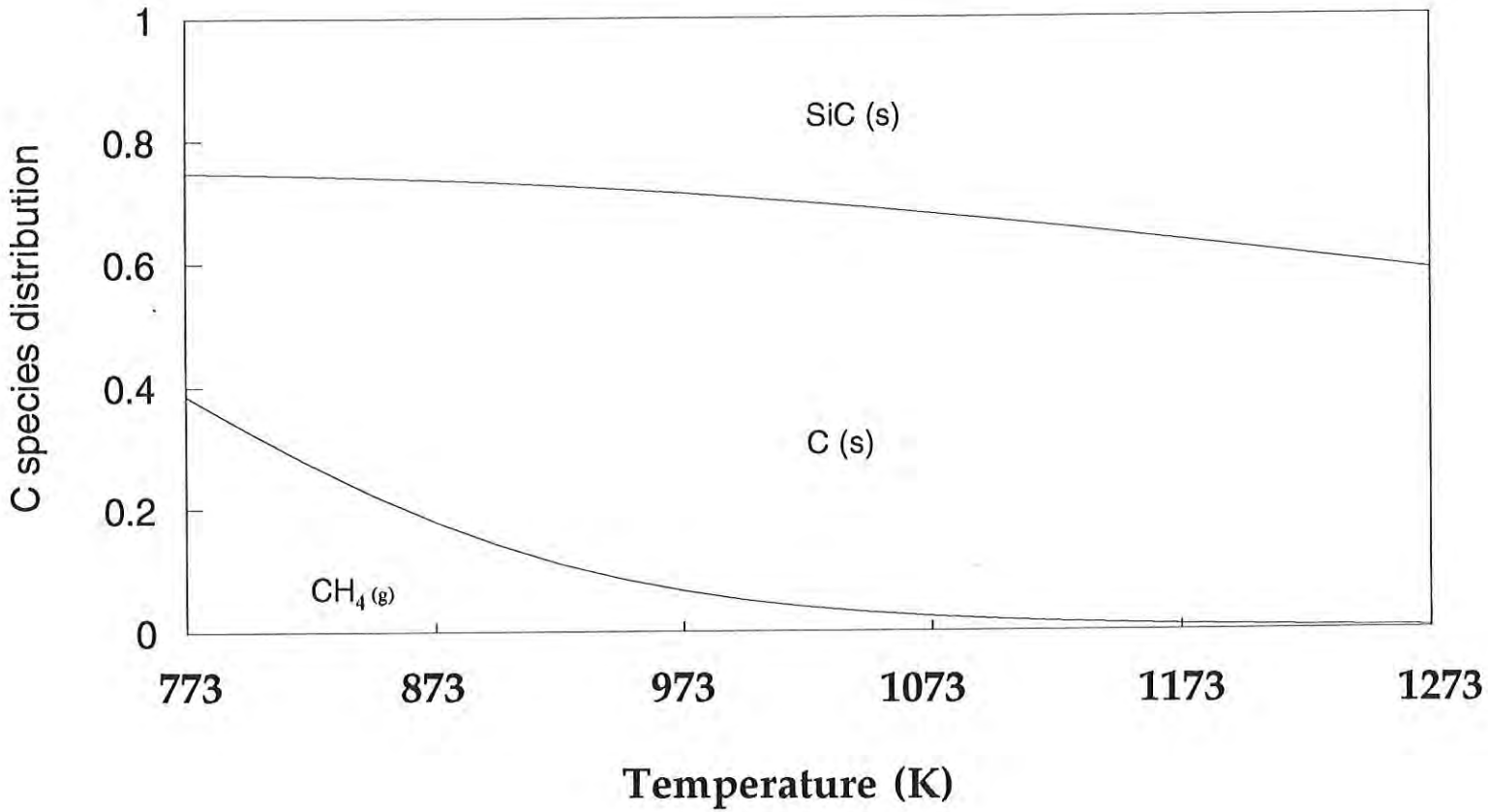

Figure 18 : Area graph showing distribution of carbon species formed from the thermal decomposition of MTS

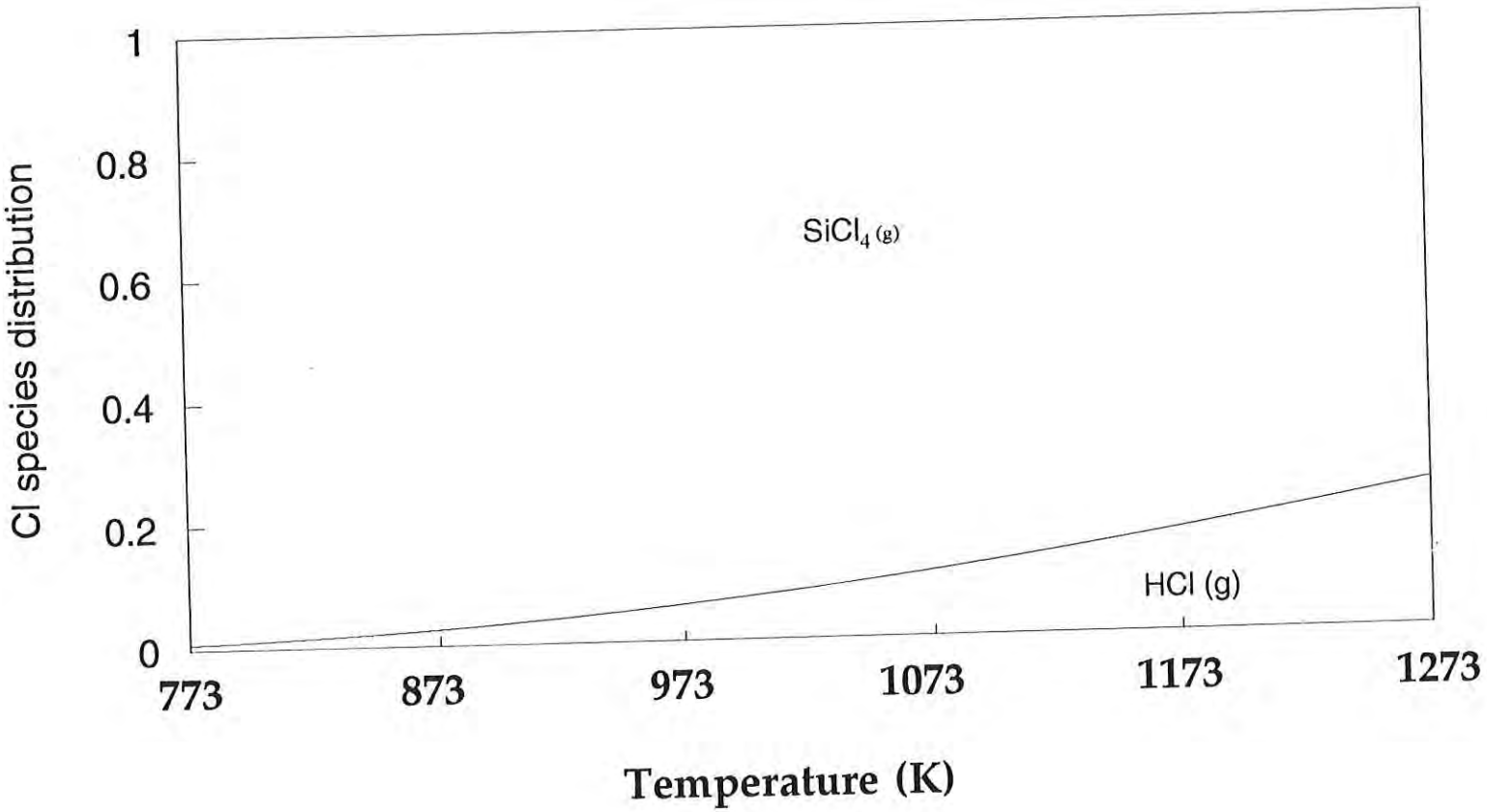

Figure 19 : Area graph showing distribution of chlorine species formed from the thermal decomposition of MTS

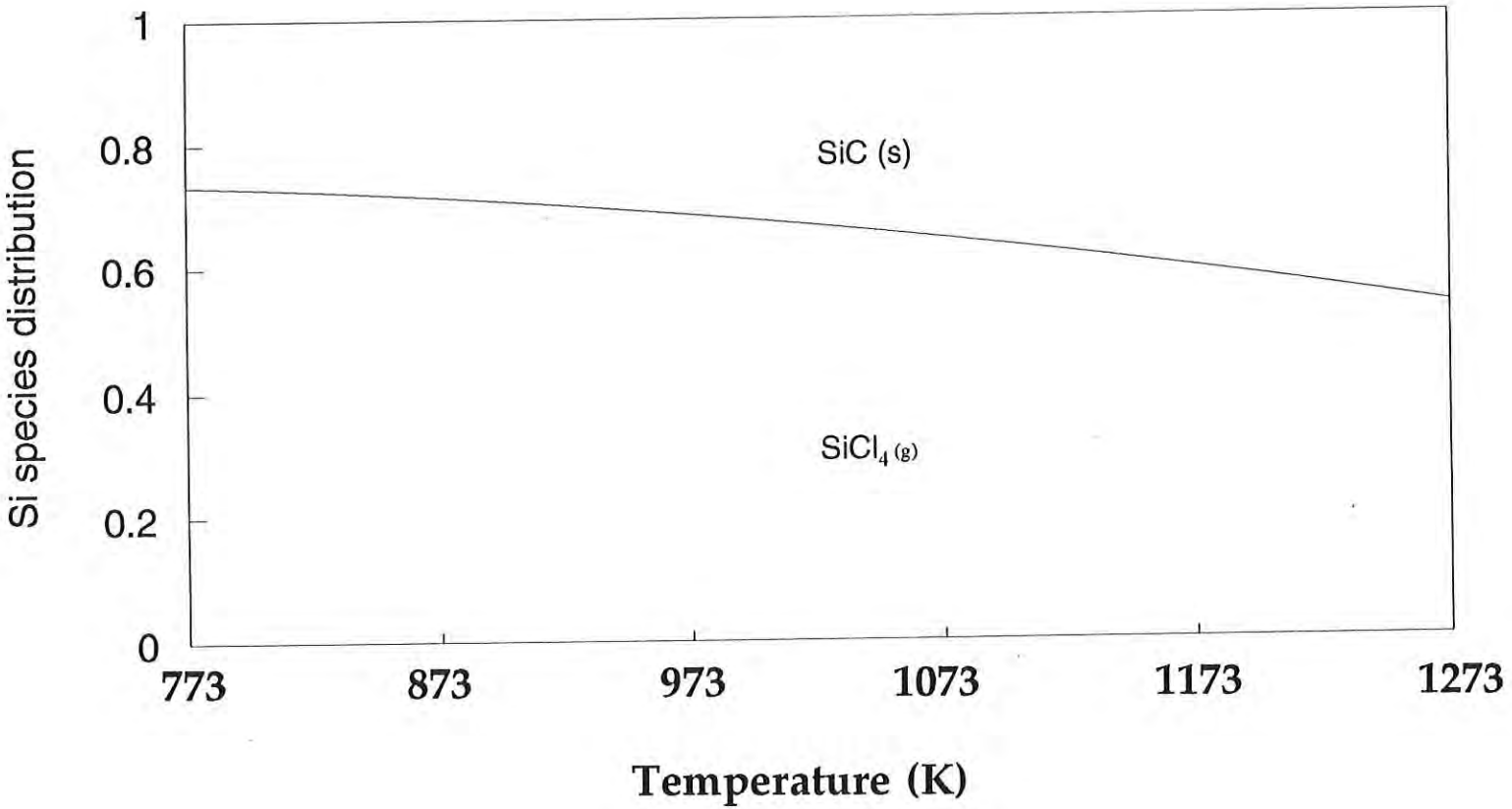

Figure 20 : Area graph showing distribution of silicon species formed from the thermal decomposition of MTS

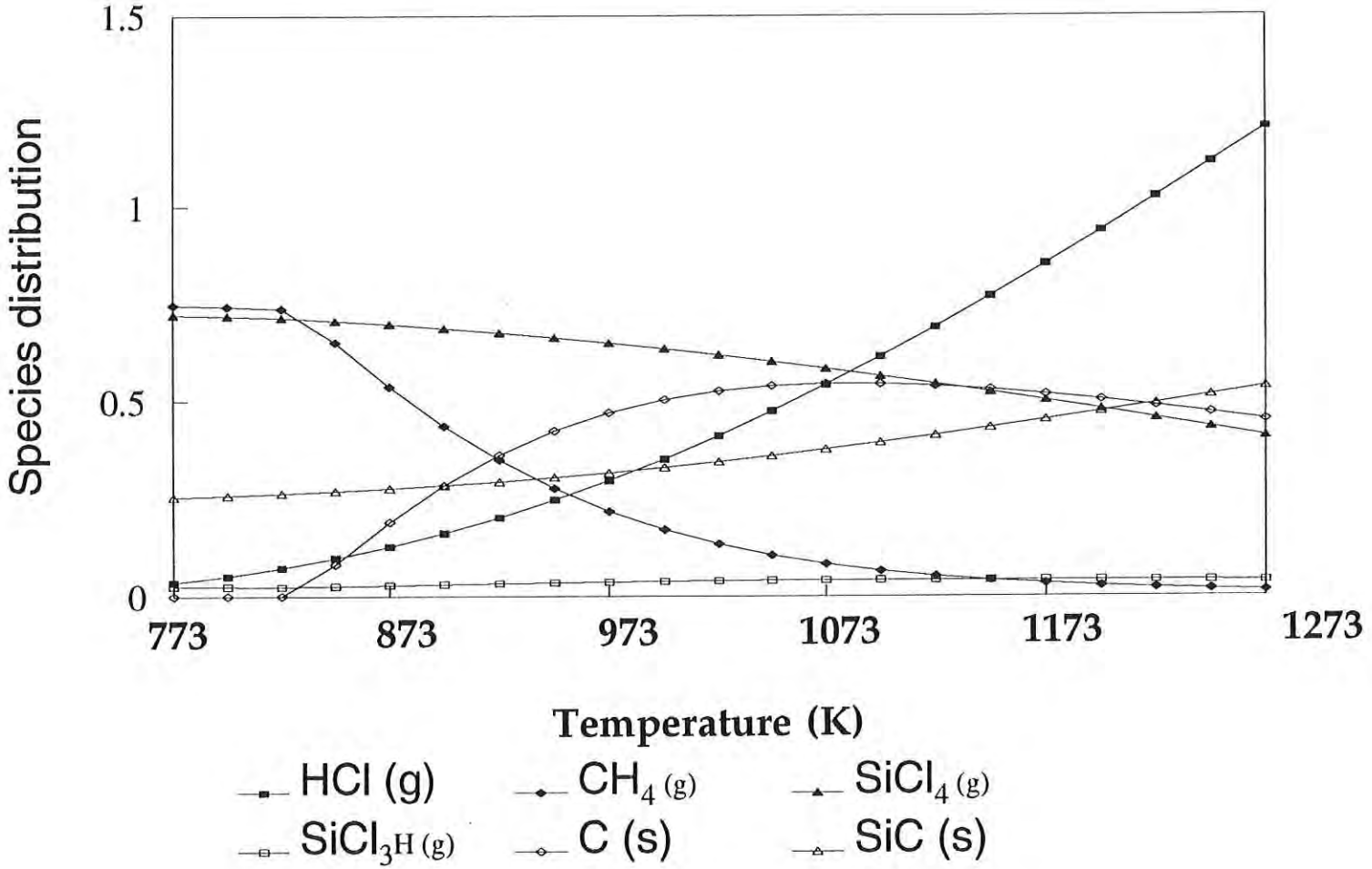

Figure 21 : Distribution of species from the thermal decomposition of MTS
Basis: 1 mole $SiCl_3CH_3$; 2 moles H_2

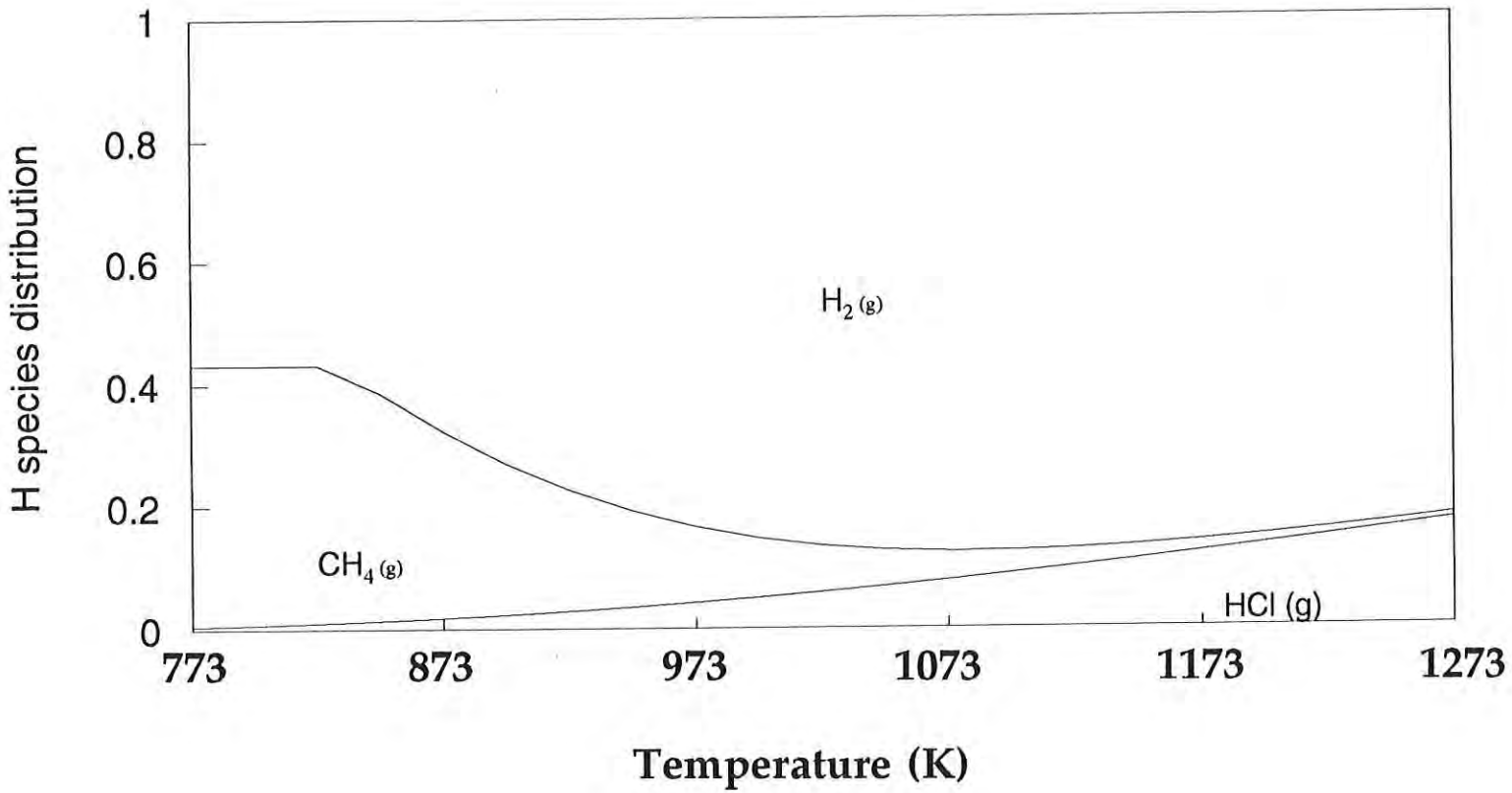

Figure 22: **Area graph showing distribution of hydrogen species formed from the thermal decomposition of MTS Basis: $SiCl_3CH_3$ to H_2 ratio 1:2**

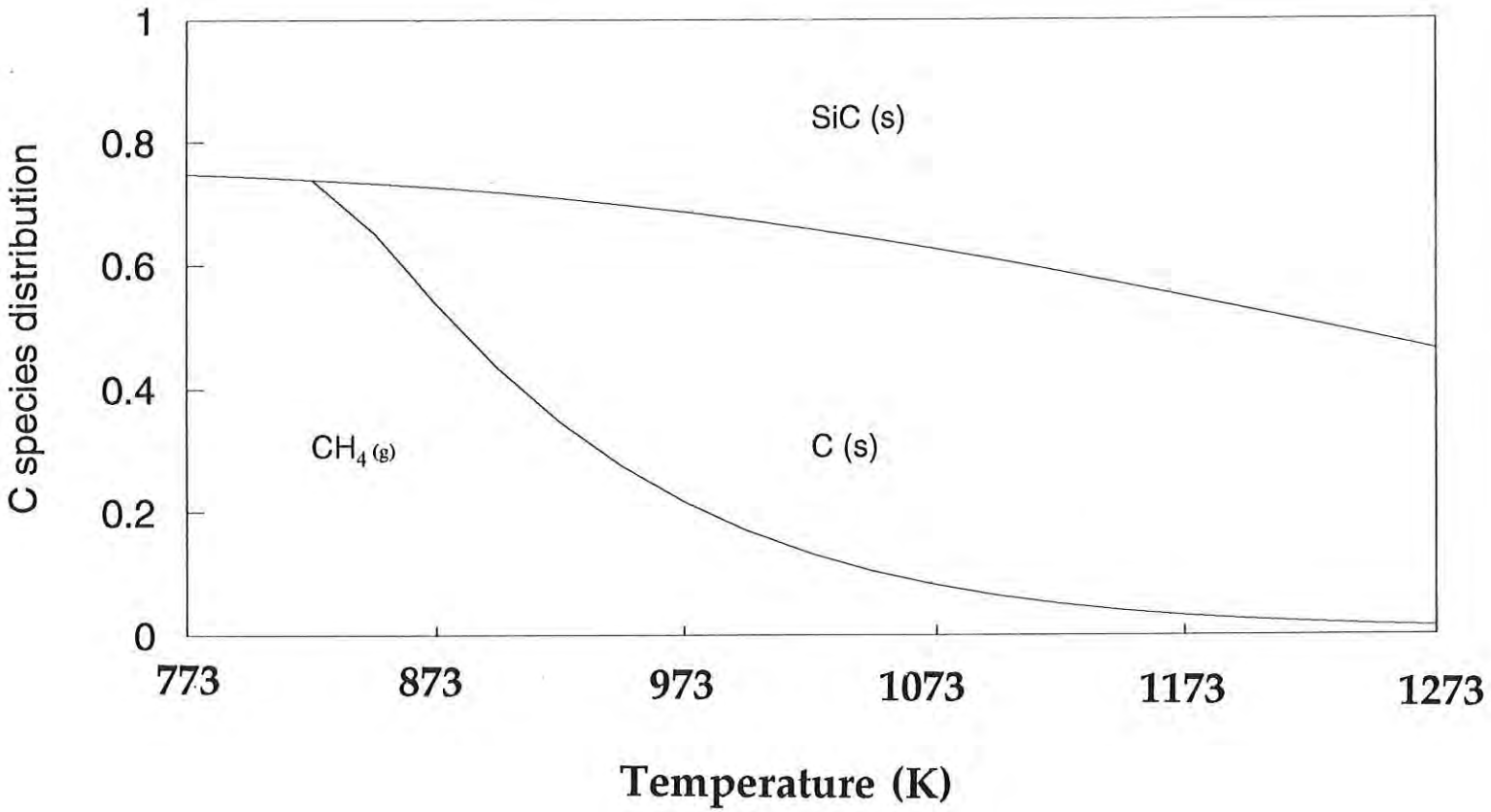

Figure 23: **Area graph showing distribution of carbon species formed from the thermal decomposition of MTS Basis: $SiCl_3CH_3$ to H_2 ratio 1:2**

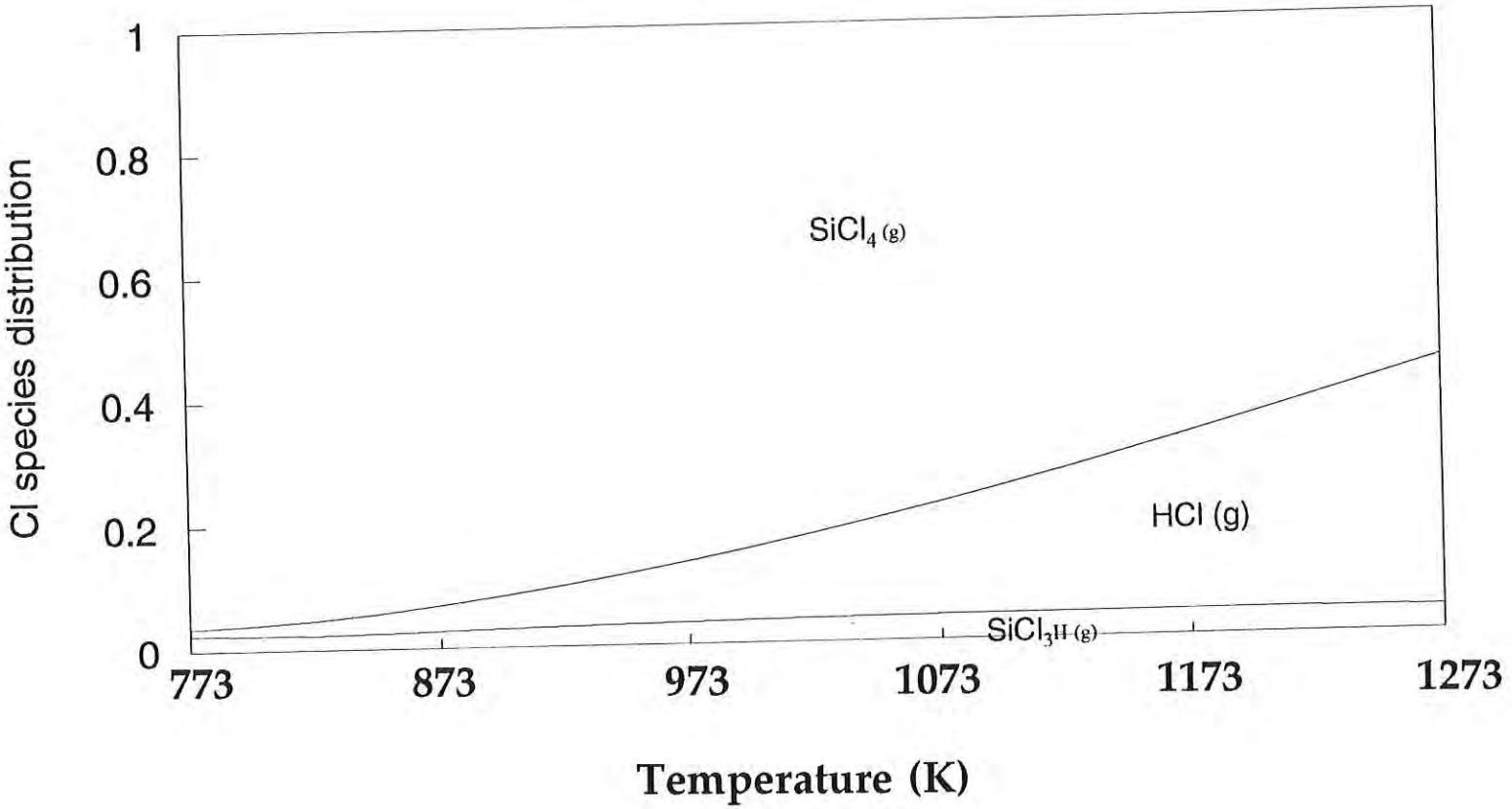

Figure 24: **Area graph showing distribution of chlorine species formed from the thermal decomposition of MTS Basis: $SiCl_3CH_3$ to H_2 ratio 1:2**

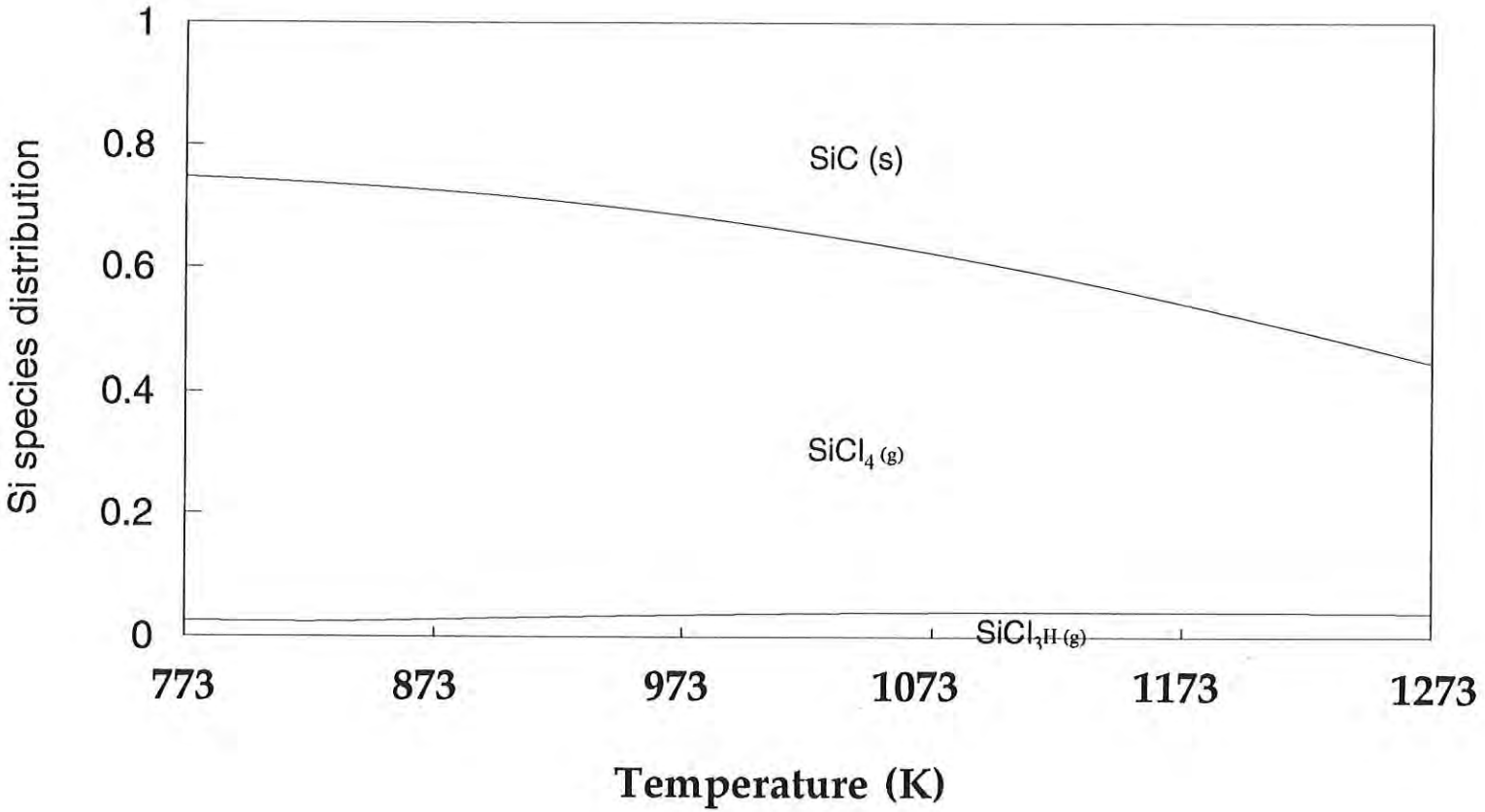

Figure 25: **Area graph showing distribution of silicon species formed from the thermal decomposition of MTS Basis: $SiCl_3CH_3$ to H_2 ratio 1:2**

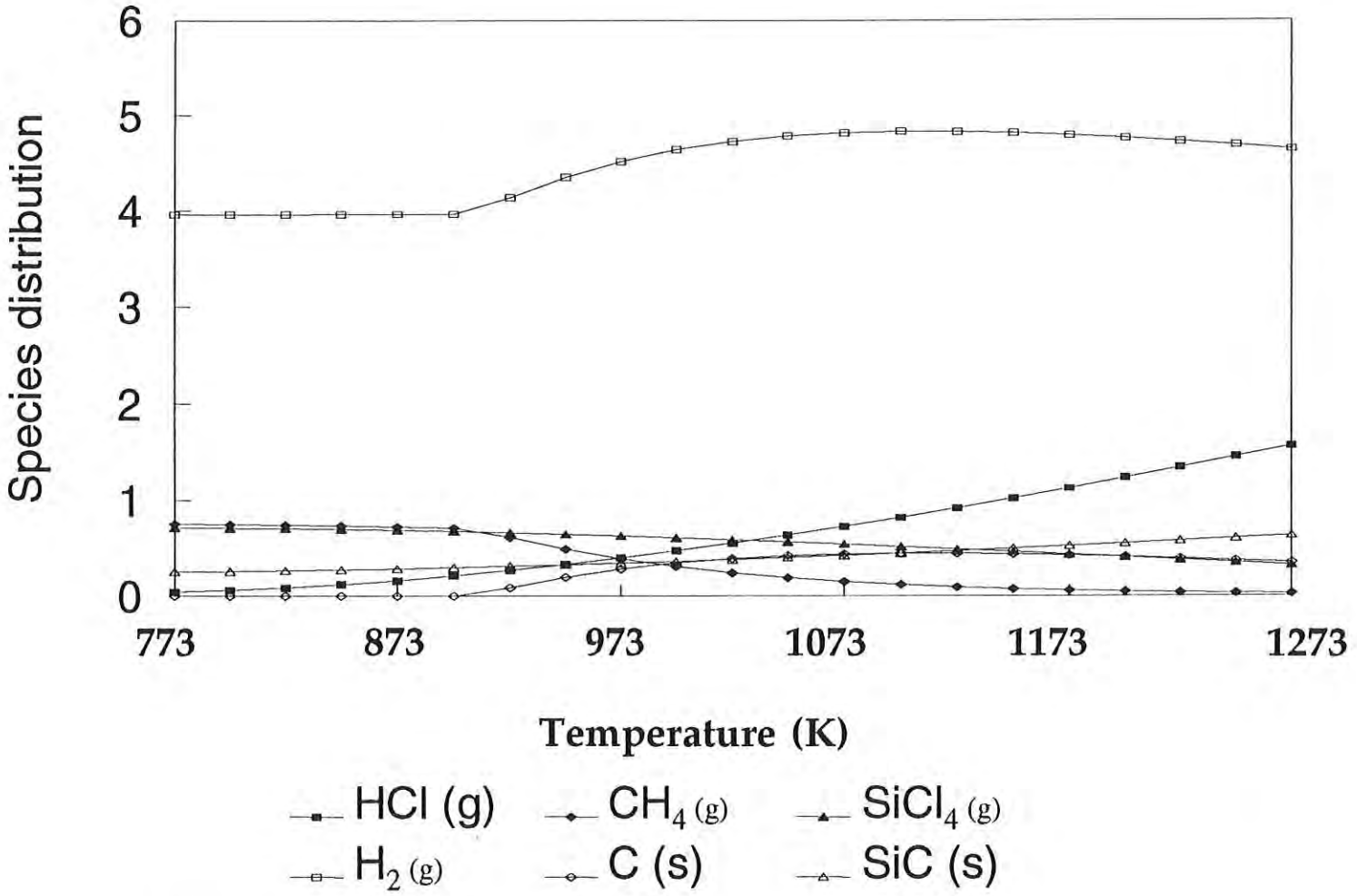

Figure 26: **Distribution of species from the thermal decomposition of MTS**
Basis: 1 mole $SiCl_3CH_3$: 4 moles H_2

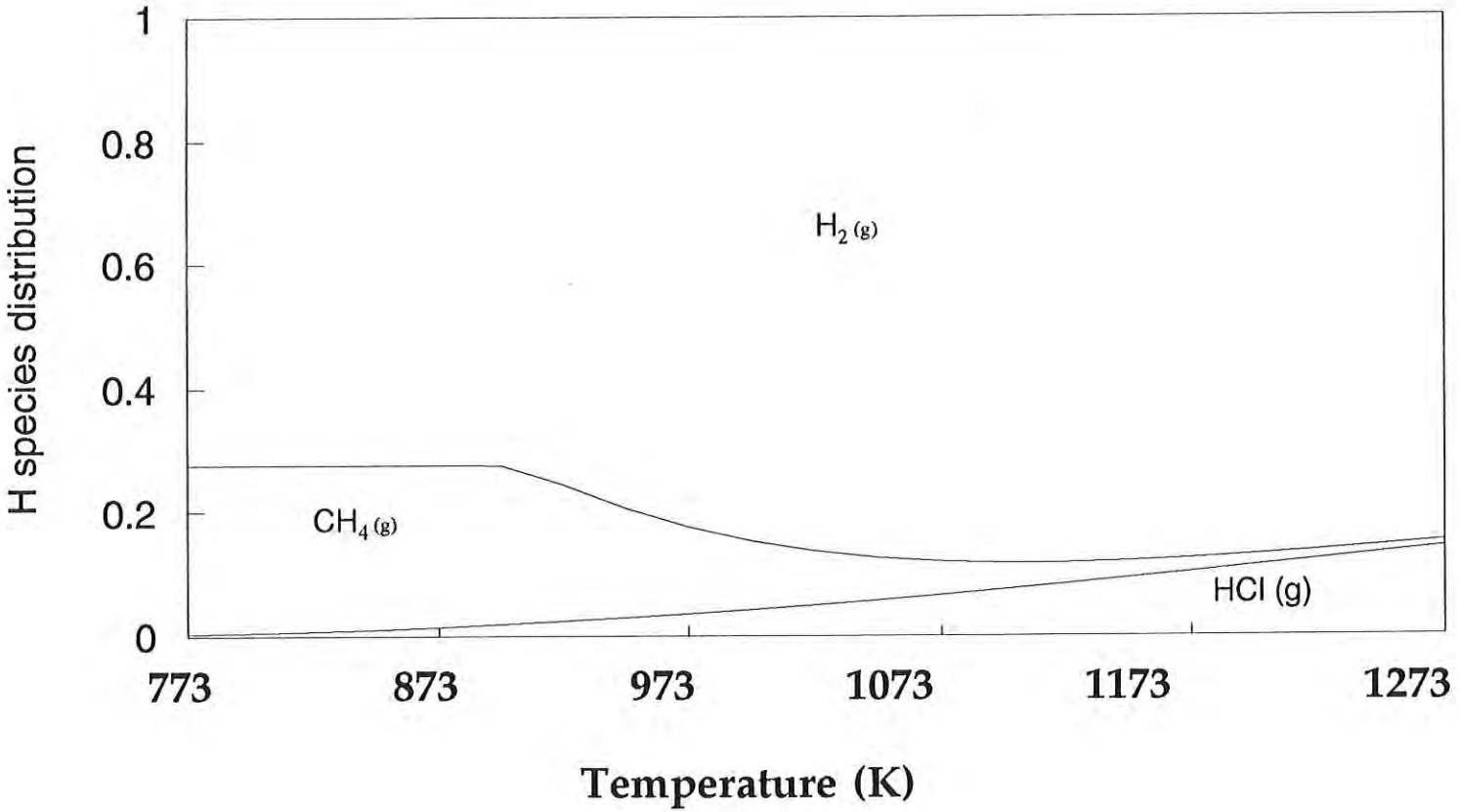

Figure 27: **Area graph showing distribution of hydrogen species formed from the thermal decomposition of MTS Basis: $SiCl_3CH_3$ to H_2 ratio 1:4**

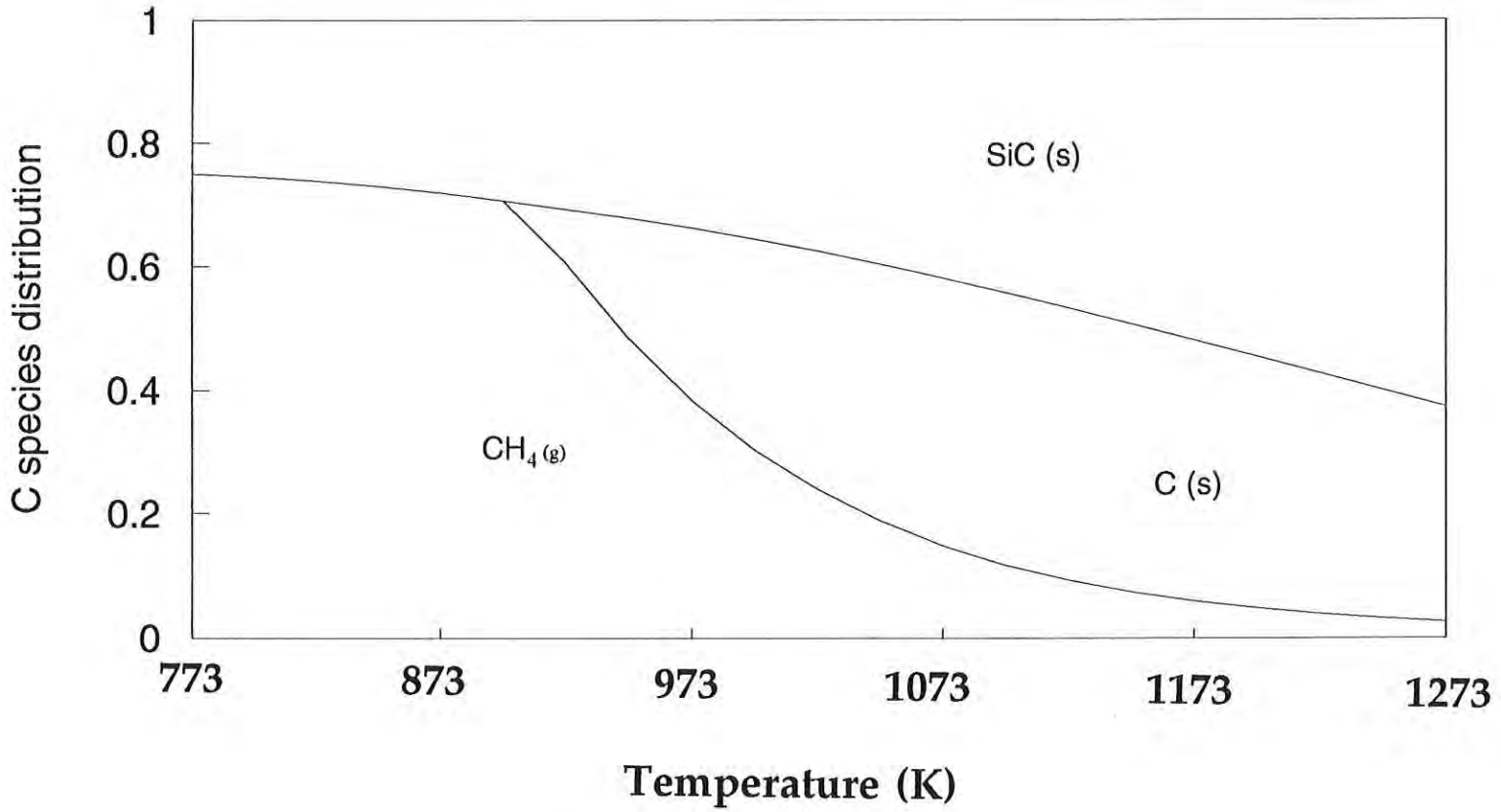

Figure 28: **Area graph showing distribution of carbon species formed from the thermal decomposition of MTS Basis: $SiCl_3CH_3$ to H_2 ratio 1:4**

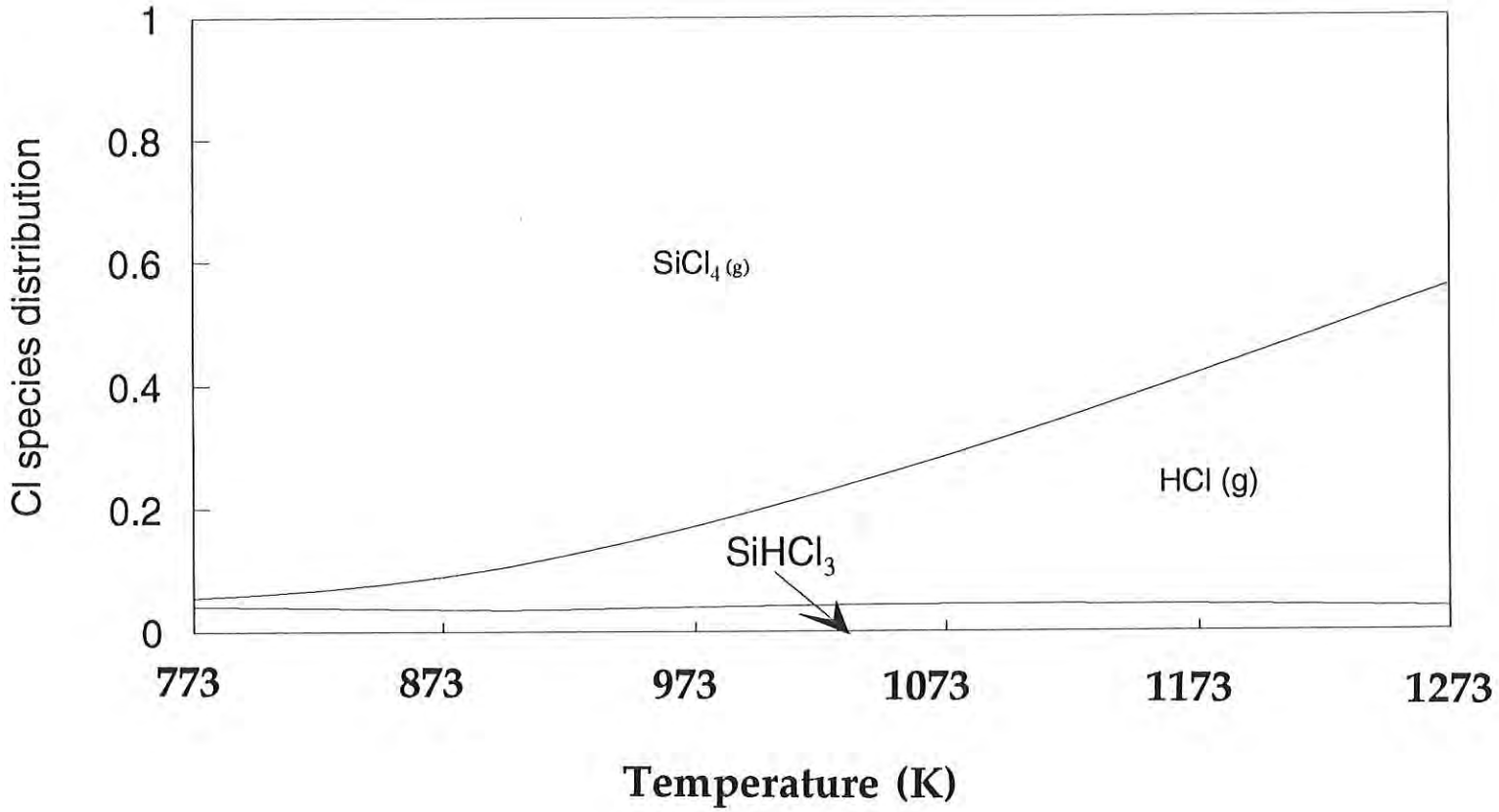

Figure 29: **Area graph showing distribution of chlorine species formed from the thermal decomposition of MTS Basis: $SiCl_3CH_3$ to H_2 ratio 1:4**

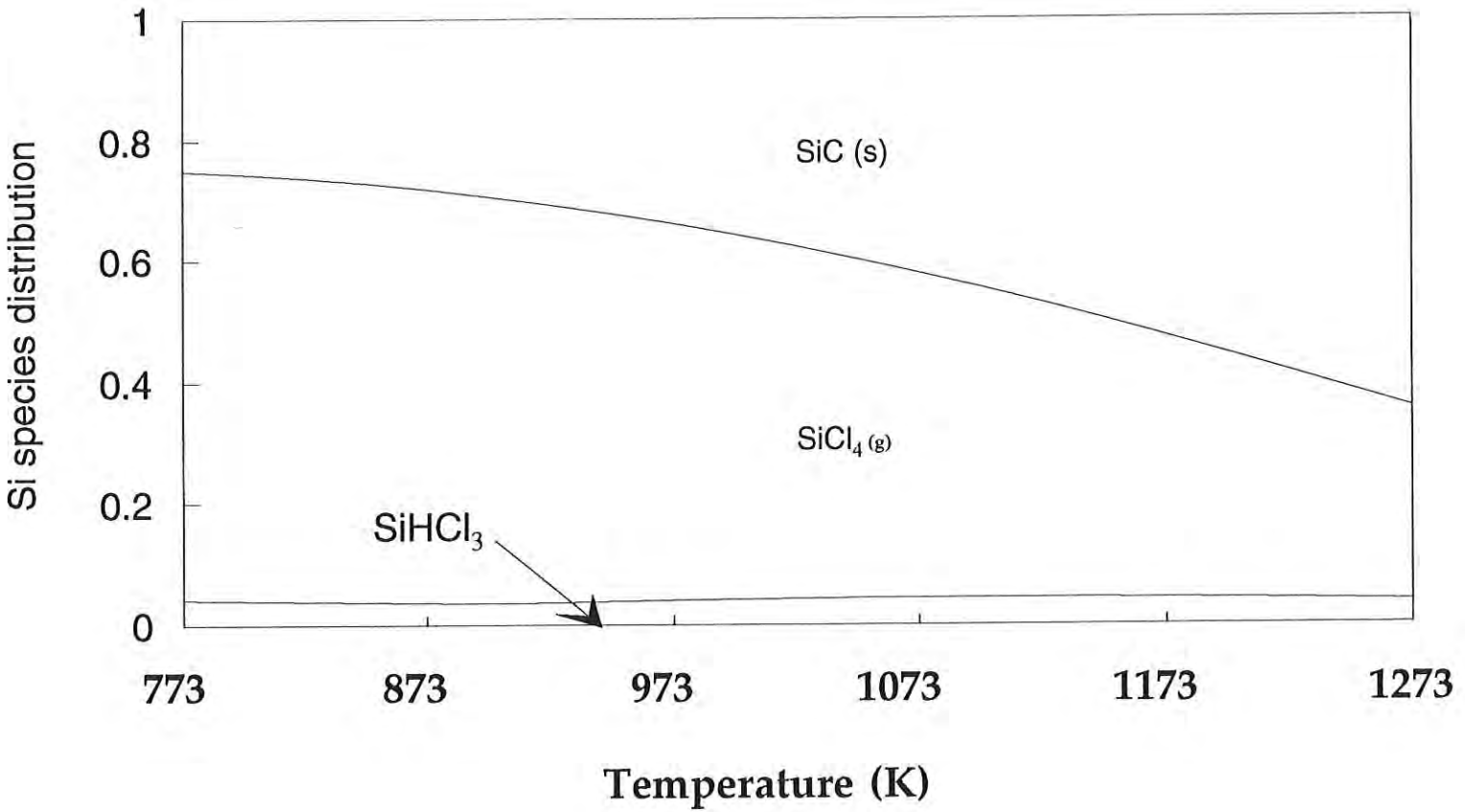

Figure 30: **Area graph showing distribution of silicon species formed from the thermal decomposition of MTS Basis: $SiCl_3CH_3$ to H_2 ratio 1:4**

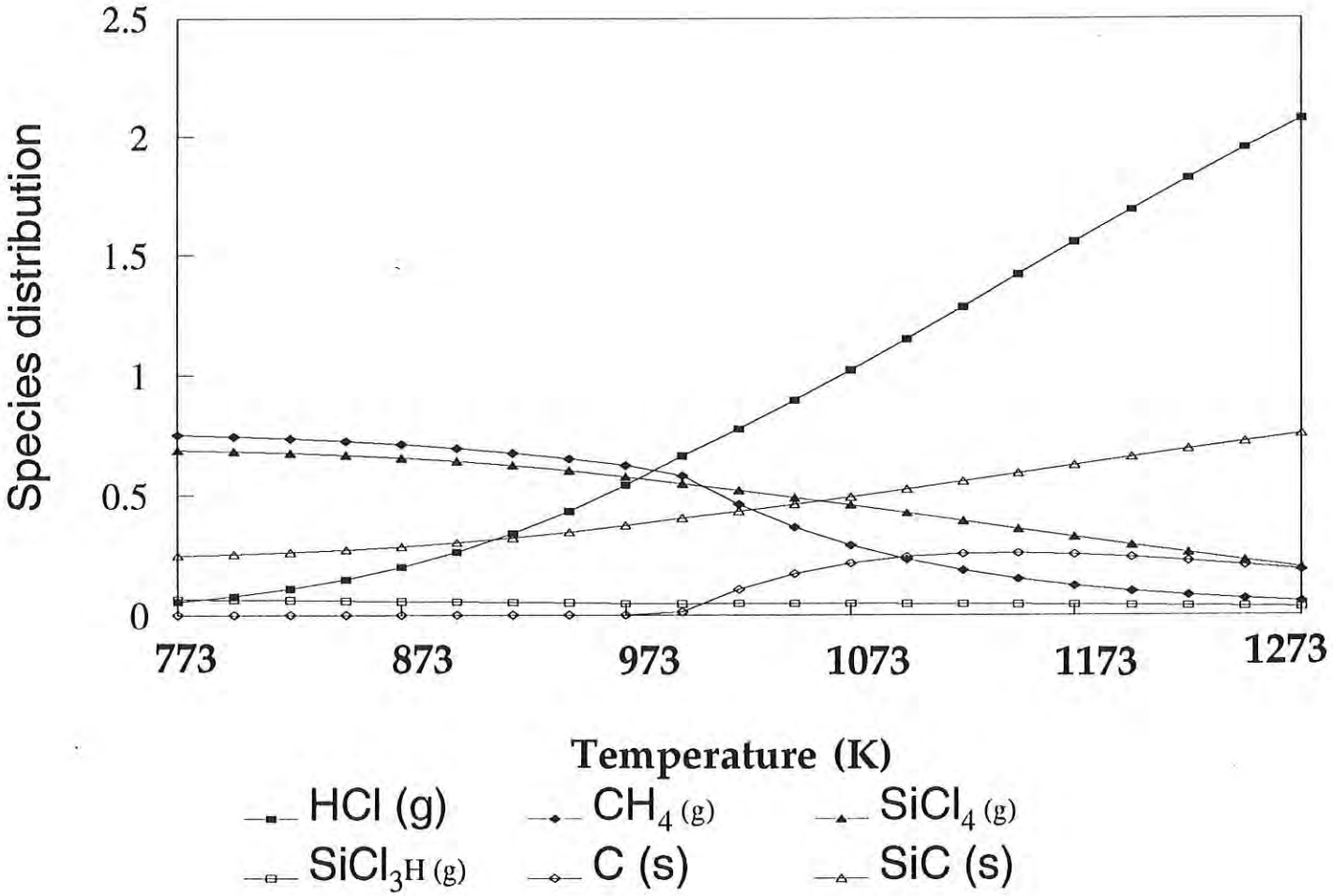

Figure 31: **Distribution of species from the thermal decomposition of MTS**
Basis: 1 mole $SiCl_3CH_3$: 8 moles H_2

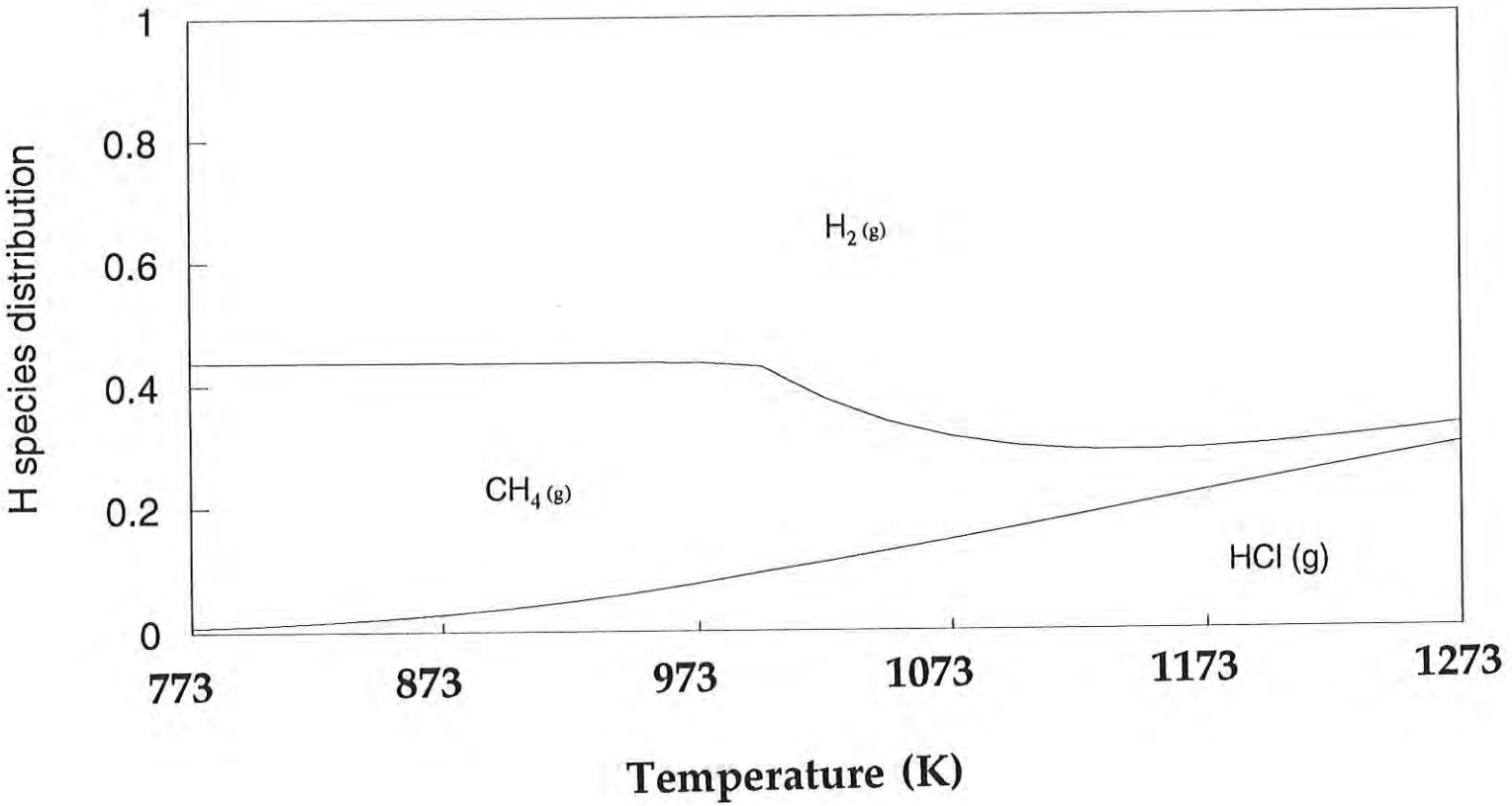

Figure 32: **Area graph showing distribution of hydrogen species formed from the thermal decomposition of MTS Basis: $SiCl_3CH_3$ to H_2 ratio 1:8**

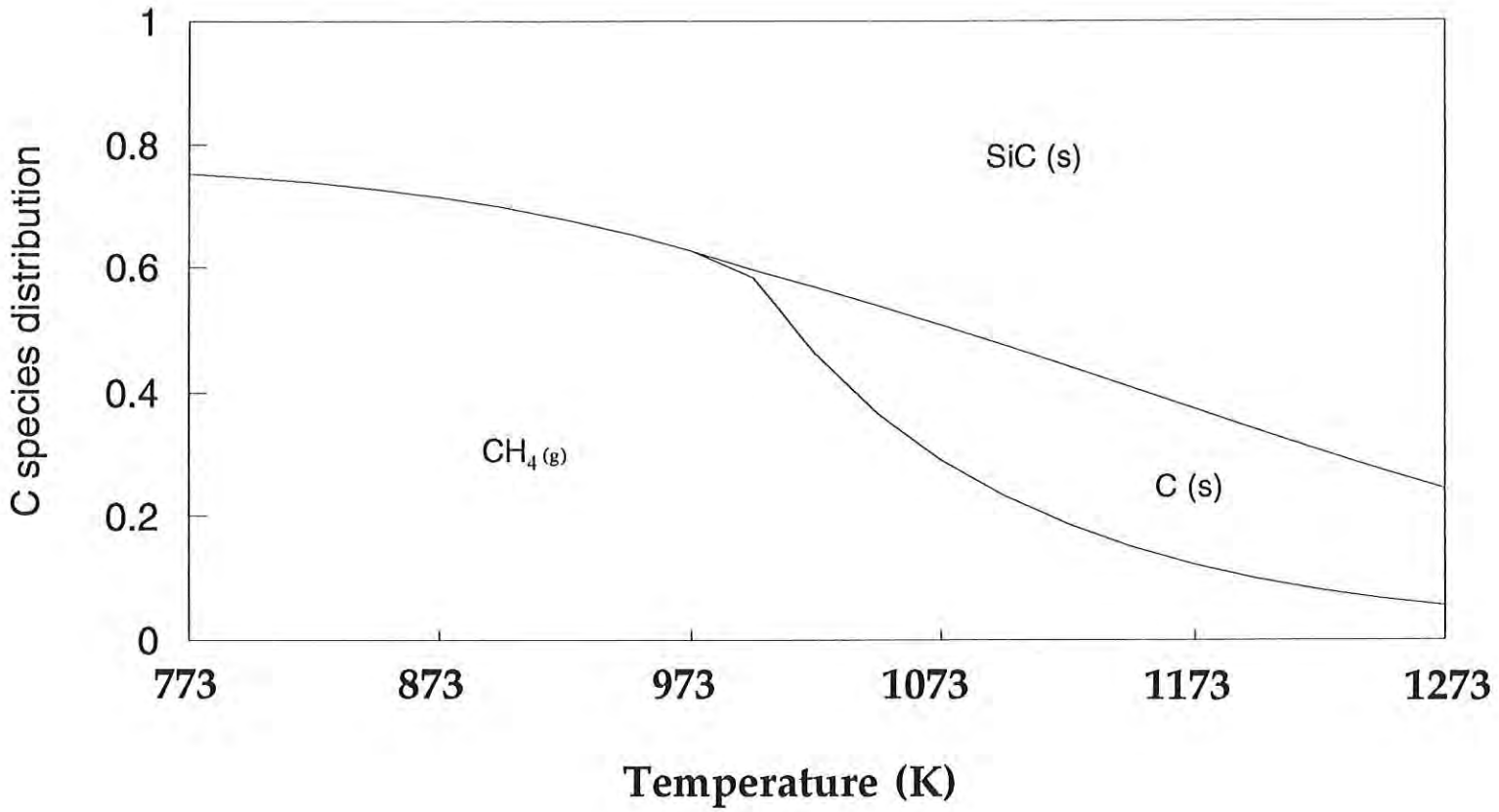

Figure 33: **Area graph showing distribution of carbon species formed from the thermal decomposition of MTS Basis: $SiCl_3CH_3$ to H_2 ratio 1:8**

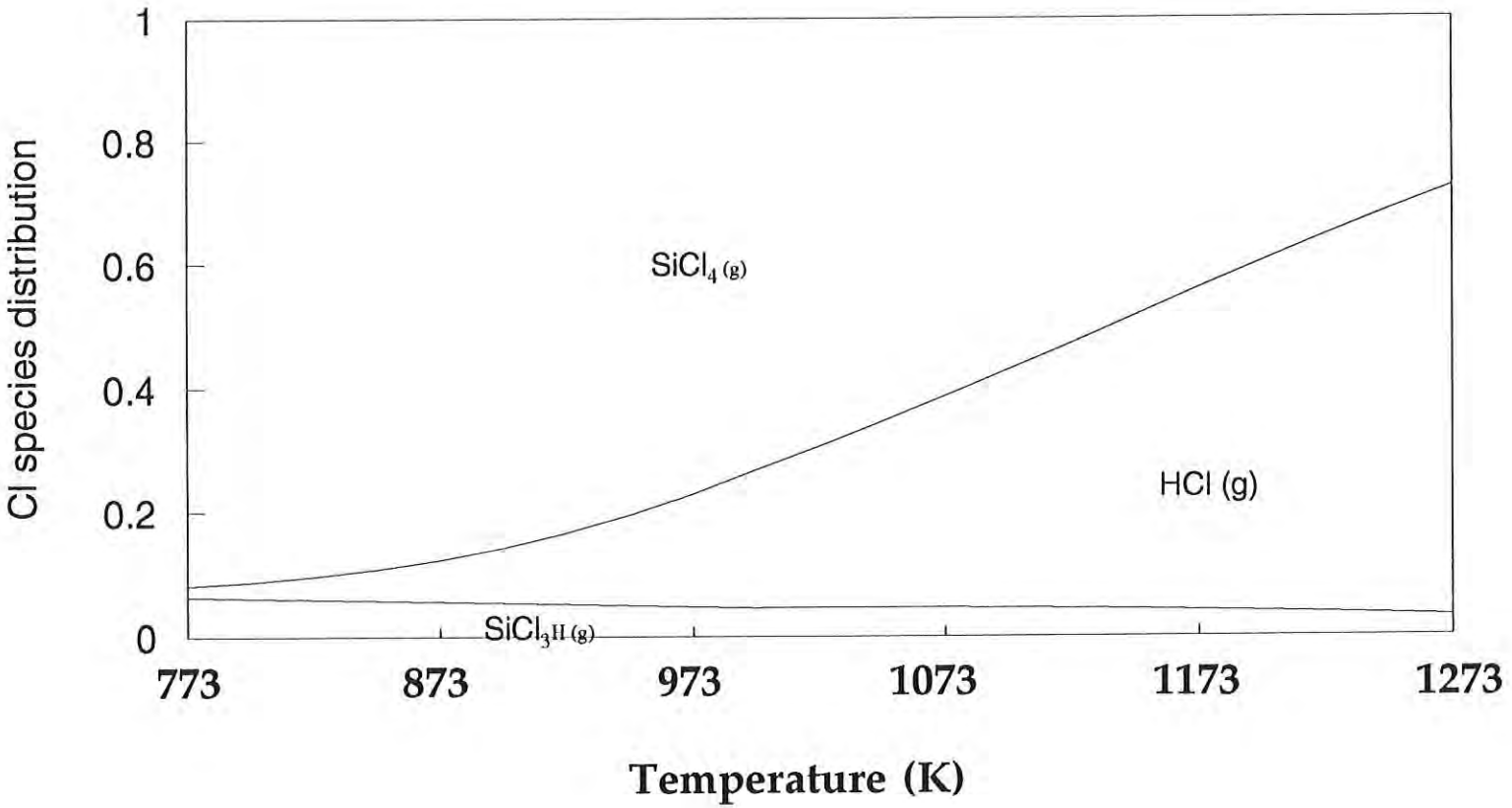

Figure 34: **Area graph showing distribution of chlorine species formed from the thermal decomposition of MTS Basis: $SiCl_3CH_3$ to H_2 ratio 1:8**

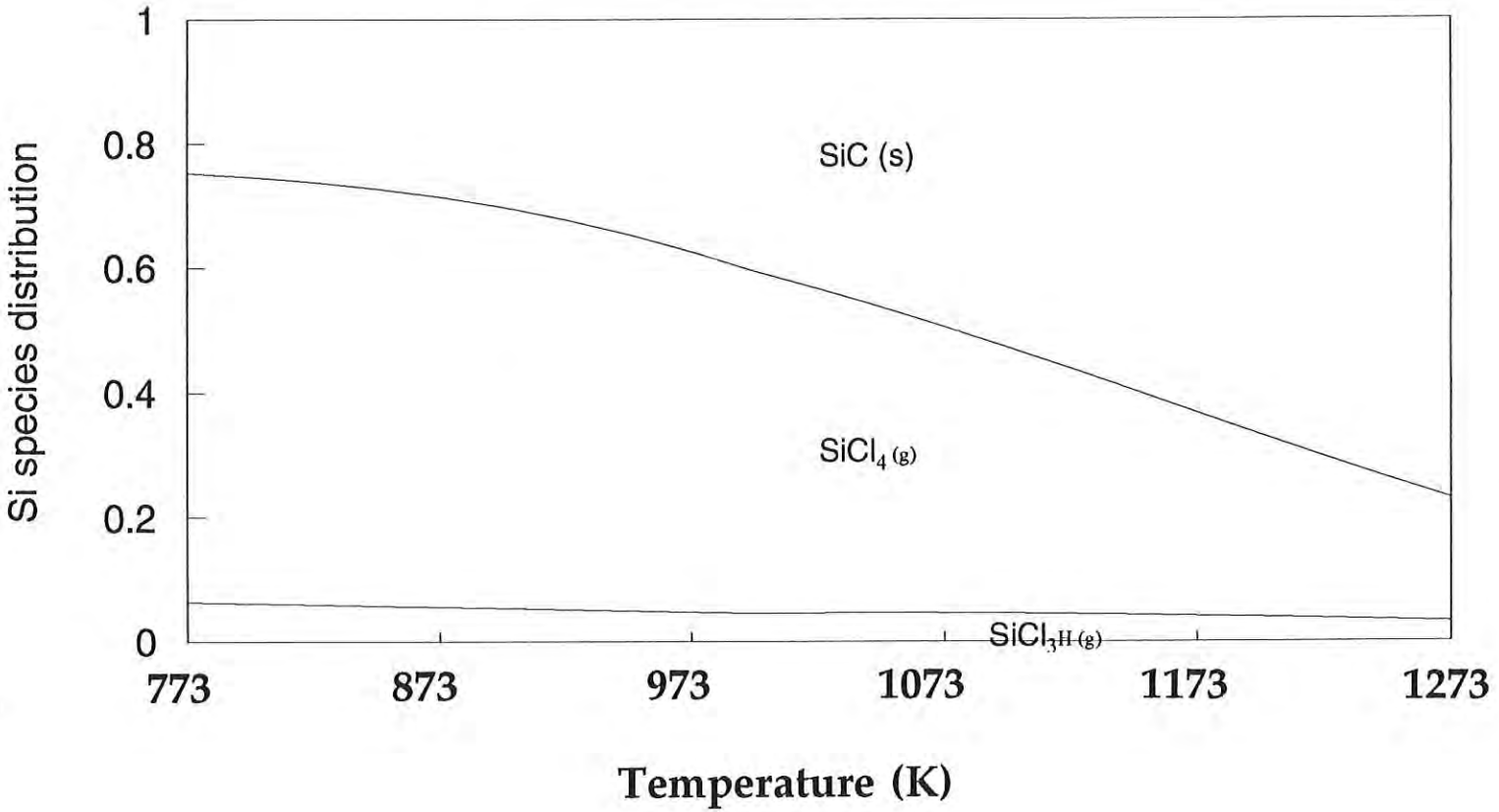

Figure 35: **Area graph showing distribution of silicon species formed from the thermal decomposition of MTS Basis: $SiCl_3CH_3$ to H_2 ratio 1:8**

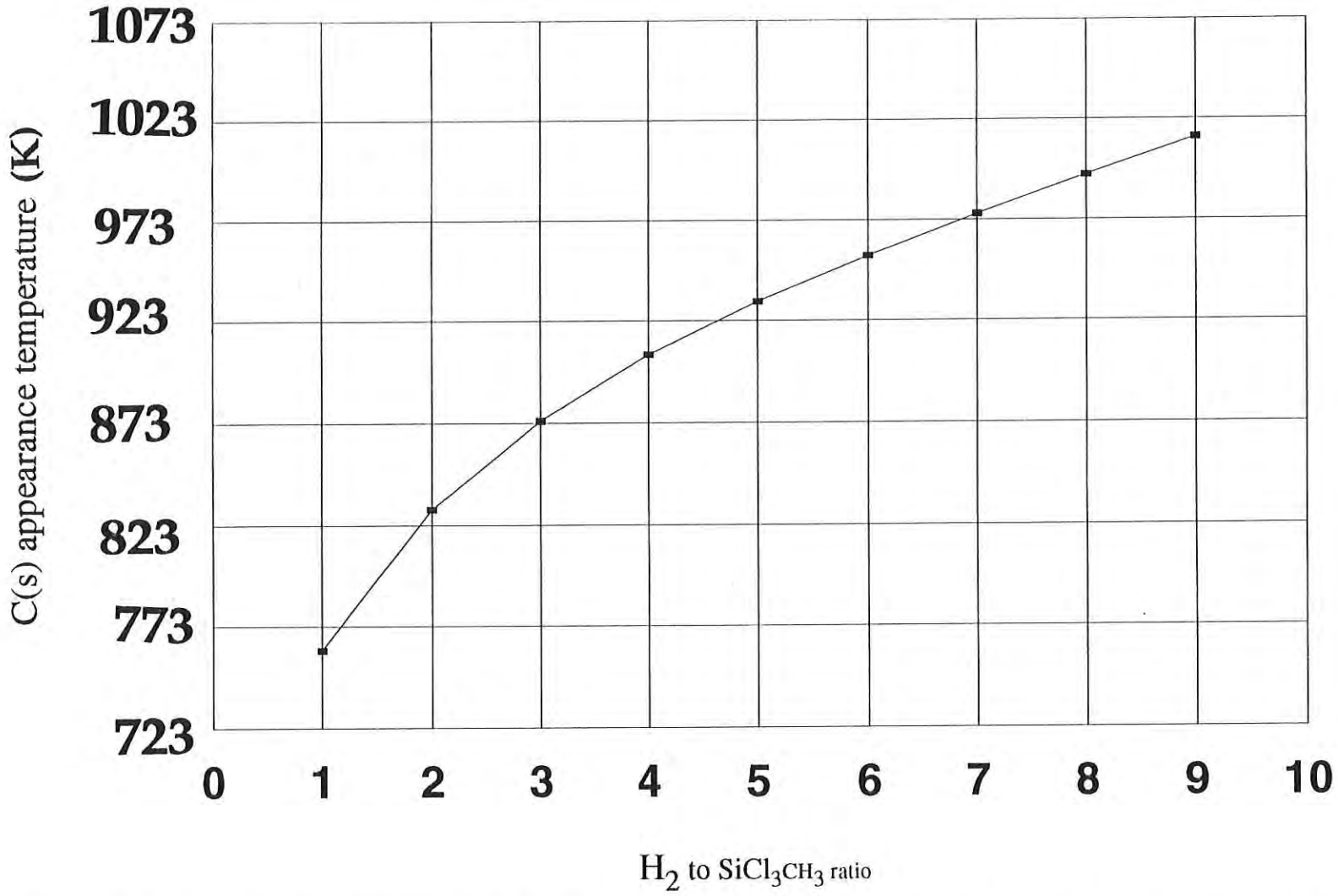

Figure 36: Calculated temperature at which $C_{(s)}$ formation begins from the thermal decomposition of MTS

temperature to a minimum at ~973K. The decrease in CH_4 concentration is limited with the formation of HCl at higher temperatures (973 K - 1273 K). Fig. 18 represents the area graph showing distribution of C-species. A slight decrease in SiC is predicted, with an increase in temperature. C co-deposition with SiC is predicted over the entire temperature range. The major chlorine species predicted is $SiCl_4$(g), along with HCl and traces of $SiHCl_3$ (Fig. 19). Area graph (Fig. 20) shows the distribution of silicon species. The two major species over the entire range of temperature included $SiCl_4$(g) and SiC(s).

4.2.2 THE CH_3SiCl_3-H_2 SYSTEM

Variables taken into consideration in this system include the mole ratio of H_2 to CH_3SiCl_3, and temperature. The pressure was maintained at 10^5 Pa (≈ 1 atm.). The temperature was varied from 773 K - 1273 K at 25° intervals and CH_3SiCl_3 to H_2 ratios of 1:2, 1:4, and 1:8 were considered. Under these conditions the main gaseous species predicted are CH_4, H_2, $SiCl_4$ and HCl with small amounts of $SiCl_3H$ and $SiCl_3$ (approx. 1% by volume). The distribution of these species for the specified conditions are given in Tables 11 - 13. The distribution pattern of the species involving C, H, Si and Cl are given in Figs. 21 - 36. A comparison of Figs. 21, 26 and 31 clearly indicates that with increase in H_2 concentration in the reaction chamber, there should be an increase in HCl concentrations with increasing temperature. Formation of CH_4 declined above 973 K. The C

co-deposition is reduced with increasing concentrations of H_2. It is evident from area graphs Figs. 23, 28 and 33, that an increase in H_2 concentration reduced the C deposition resulting in an overall increase in the deposition of SiC(s), particularly at higher temperatures (1173 K - 1273 K). Area graphs (Fig. 24), (Fig. 29) and (Fig. 34) indicate that an increase in H_2 concentration in the reactor results in the reduction of $SiCl_4(g)$ concentration, while increasing HCl formation. Area graphs (Fig. 25), (Fig. 30) and (Fig. 35) also indicate that an increase in H_2 concentration and temperature results in an increase in β-SiC deposition.

CHAPTER 5

REACTION KINETICS

5.1 METHOD

The reaction kinetics is the study of the rates of chemical reactions and how reaction conditions such as reactant concentration, temperature, pressure, flow rate, and gaseous dilution factors influence the reaction rate. MTS undergoes decomposition at a higher temperature (>700 K), and the vapour reaction between decomposed species is slow at lower temperatures; however, the reaction velocities increase with the increase in temperature.

The reaction rates are classified according to the molecularity and the order of reaction. The molecularity is the number of atoms or molecules taking part in each act leading to a chemical reaction. The order of reaction however, expresses the experimentally determined dependence of the reaction rate on the concentration of the reactants. The rate at which reaction is proceeding is proportional to the product of the specific rate constant and fraction of unreacted material raised to the n^{th} power.

A general rate equation can therefore be expressed as :

$$\frac{d\alpha}{dt} = k(1-\alpha)^n \qquad (5)$$

where

α	=	concentration of the reactant
t	=	time
k	=	rate constant
n	=	order of the reaction

Rearranging this equation and integrating

$$-\int_{\alpha_0}^{\alpha} \frac{d\alpha}{\alpha} = k\int_0^t dt \qquad (6)$$

where

α	=	concentration of reactant at time t
α_o	=	concentration of reactant at time zero

Since

$$\int \frac{d\alpha}{\alpha} = \ln\alpha \tag{7}$$

equation (7) can be further expressed as

$$\ln\alpha = -kt + \ln\alpha_o \tag{9}$$

then

$$-[\ln\alpha]_{\alpha_0}^{\alpha} = [kt]_0^t \tag{8}$$

Borchardt and Daniels[152] first described the application of Differential Thermal Analysis (DTA) to study the reaction kinetics of benzenediazonium chloride in water. Parameters such as activation energy (E_a), order of reaction (n), pre-exponential factor (k_o), and heat of reaction (ΔH) were determined from a DTA curve. This method was found useful for reactions in solution only, and could not be applied to reactions occurring in solid state and vapour phase because of the following incorrect assumptions:

- that the temperature of the sample is always uniform;
- that the heat capacity of the system remains constant throughout the course of the reaction; and,

- that the peak temperature of DTA corresponds to the maximum rate of reaction.

The use of Differential Scanning Calorimetry (DSC) has been shown to overcome these problems[153]. It measures enthalpy changes by directly measuring the heat flux of the sample as a function of temperature. From the decomposition curve E_a, n and k_o can be calculated. Perkin Elmer's DSC 7 has a built-in kinetics software program which is based on the following theoretical principle. When a sample is subjected to a controlled temperature ramp, a peak is recorded on the DSC scan representative of a conversion by the following reaction:

where:

$$A \xrightarrow{k} B + \Delta H \qquad (10)$$

A = precursor material

B = product material

k = Arrhenius rate constant

ΔH = heat of reaction

The constant k as a function of temperature can be calculated once the two primary kinetic constants (E_a and k_o) have been evaluated from the

following equation:

$$k = k_o \exp\left(-\frac{E_a}{RT}\right) \tag{11}$$

where

k_o = pre-exponential factor (sec^{-1})

R = gas constant ($JK^{-1}mol^{-1}$)

T = temperature (K)

Combining equations (5) & (11) we derive the following expression

$$\frac{d\alpha}{dt} = k_o \exp\left(-\frac{E_a}{RT}\right)(1-\alpha)^n \tag{12}$$

Combining equations (5), (11) & (12), the following relation can be derived:

$$\ln\frac{(d\alpha)}{(dt)} = \ln k_o - \frac{E_a}{RT} + n\ln(1-\alpha) \tag{13}$$

These expressions were derived by Gray[154], and Freeman and Carroll[155] to determine kinetic parameters using DSC data. By using multiple linear regression analysis (MLR), the kinetic parameters k_o, E_a, and n can be determined, while $d\alpha/dt$, T, and α are measured from the DSC scan. The validity of the kinetic results determined by DSC 7 and using the PE kinetic software was verified by measuring the E_a of standard materials using the well known technique of Ozawa[157].

According to this method, the chemical reaction of MTS, Epoxy 828, and Nitrocellulose was followed independently using DSC dynamic temperature mode over the temperature range 30°C to 725°C. The heating rates (β) were varied between 2.5°C and 40°C per minute. The heating rate is representative of the DSC scanning rate and T_{max} is the peak temperature representing the maximum rate of reaction. T_{max} was determined using DSC 7 peak analysis software, from the peak of curve. E_a of the materials used in this investigation was determined from the slope of the graph of a plot of log β vs. $1/T_{max}$ in Ozawa method. The E_a results obtained using Ozawa method are given in Table 14 along with E_a values determined by using DSC 7 kinetic software program.

Table 14 : Comparison of Activation Energies

Sample	Ea kJ/mol[1]	Ea kJ/mol[2]	Ea kJ/mol[3]
Nitrocellulose	10.8	9.78	10.05
Epoxy 828	54.96	67.47	51.57
Methyl-trichlorosilane	15.49	18.21	14.19

1. Ozawa[157]
2. Literature values
3. PE DSC 7

5.2 KINETIC RESULTS

DSC has been used for the kinetic determinations of the decomposition process of MTS, Nitrocellulose and Epoxy 828. This technique measures enthalpy changes by directly measuring the heat flux of the sample as a function of temperature. The decomposition curve, as depicted in Fig. 37, 37a and 37b, represents heat flow to sample (mW) vs. Temperature (°C). The experimental scan was conducted at 5°C/min scanning rate, for maximum sensitivity, over a temperature range of 30°C - 725°C. The application of DSC 7 kinetics software calculates the kinetic parameters which include activation energy, order of reaction and pre-exponential factor. This information leads to the possible mechanisms of the process. From this data, additional kinetic parameters were determined. These include:

1) An Arrhenius plot of the rate coefficients for the decomposition of MTS which indicates the quality of the kinetics data and the fit of the data to the rate equation, (Fig. 38) ;
2) A plot of the Rate Constant vs. Temperature, which gives the variation of the rate coefficient with temperature for the decomposition of MTS, (Fig. 39);
3) A plot of the Percent Concentration vs. Time (min.), elucidated using partial areas from the DSC scan of MTS, which determines the rate at which the precursor material is depleting, (Fig. 40);

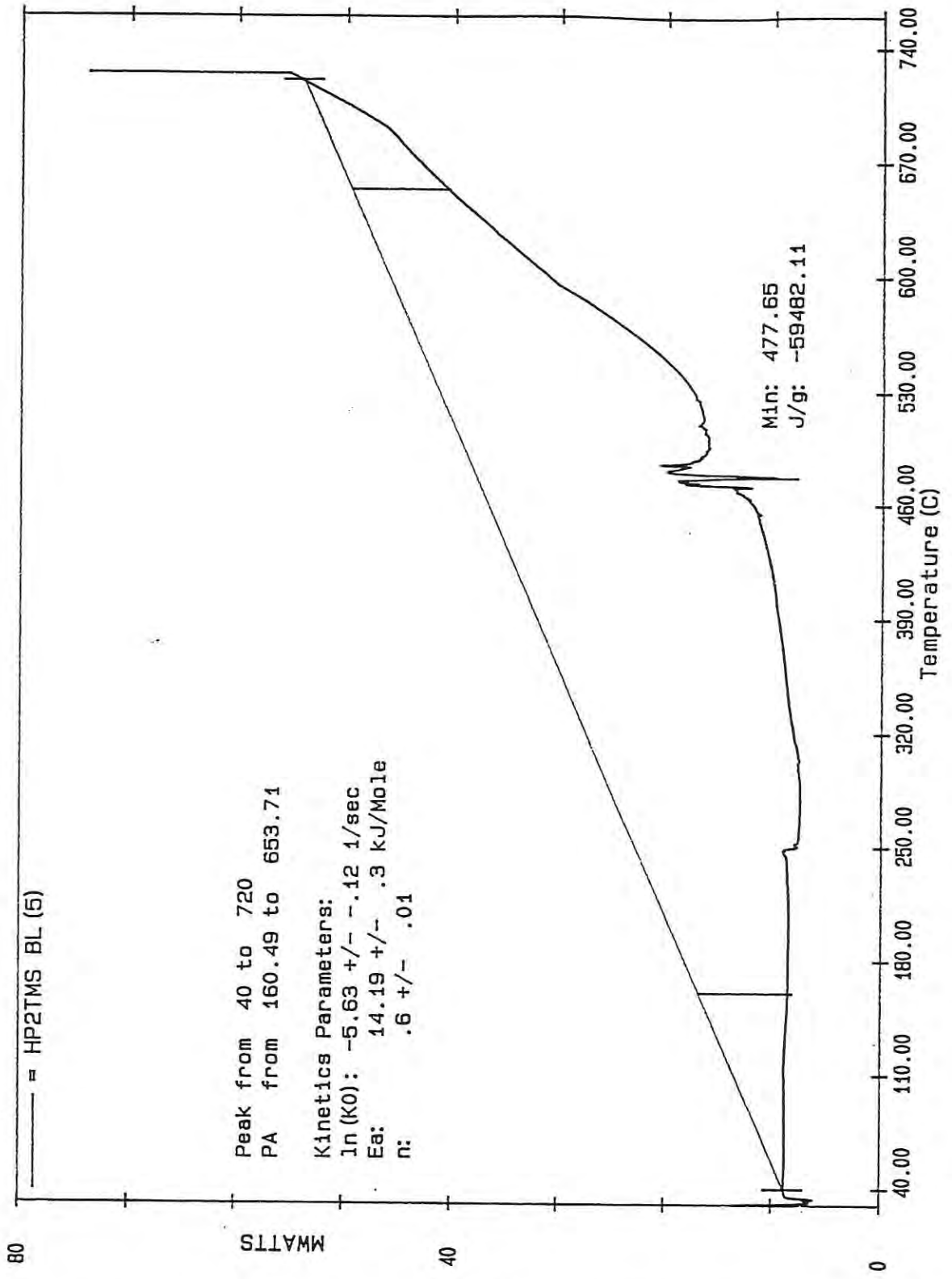

Figure 37 : DSC thermogram for MTS over temperature range of 40°C to 720°C at 5°C/min scanning rate showing kinetic parameter calculations

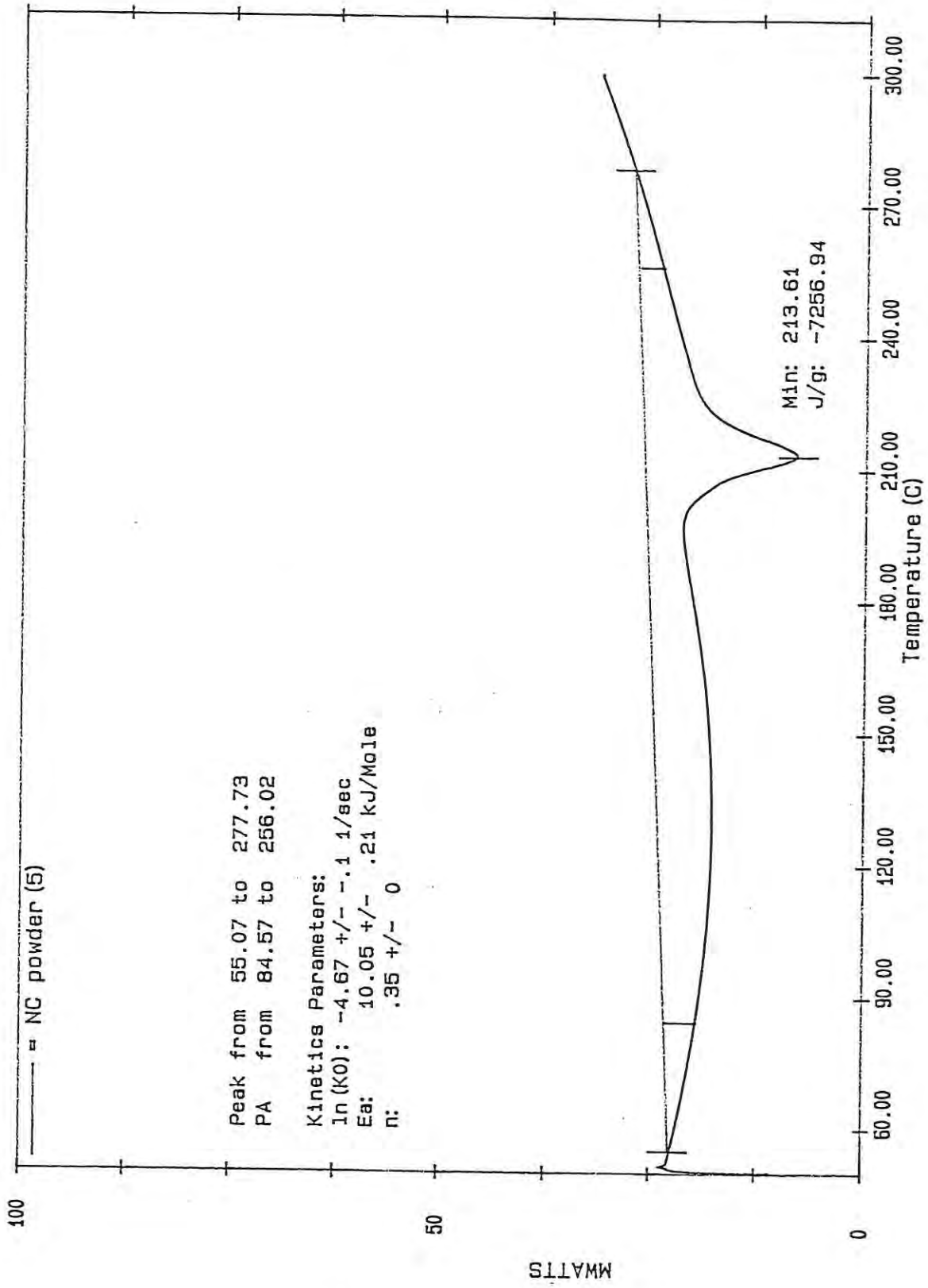

Figure 37a : DSC thermogram showing kinetic parameter calculations for nitrocellulose

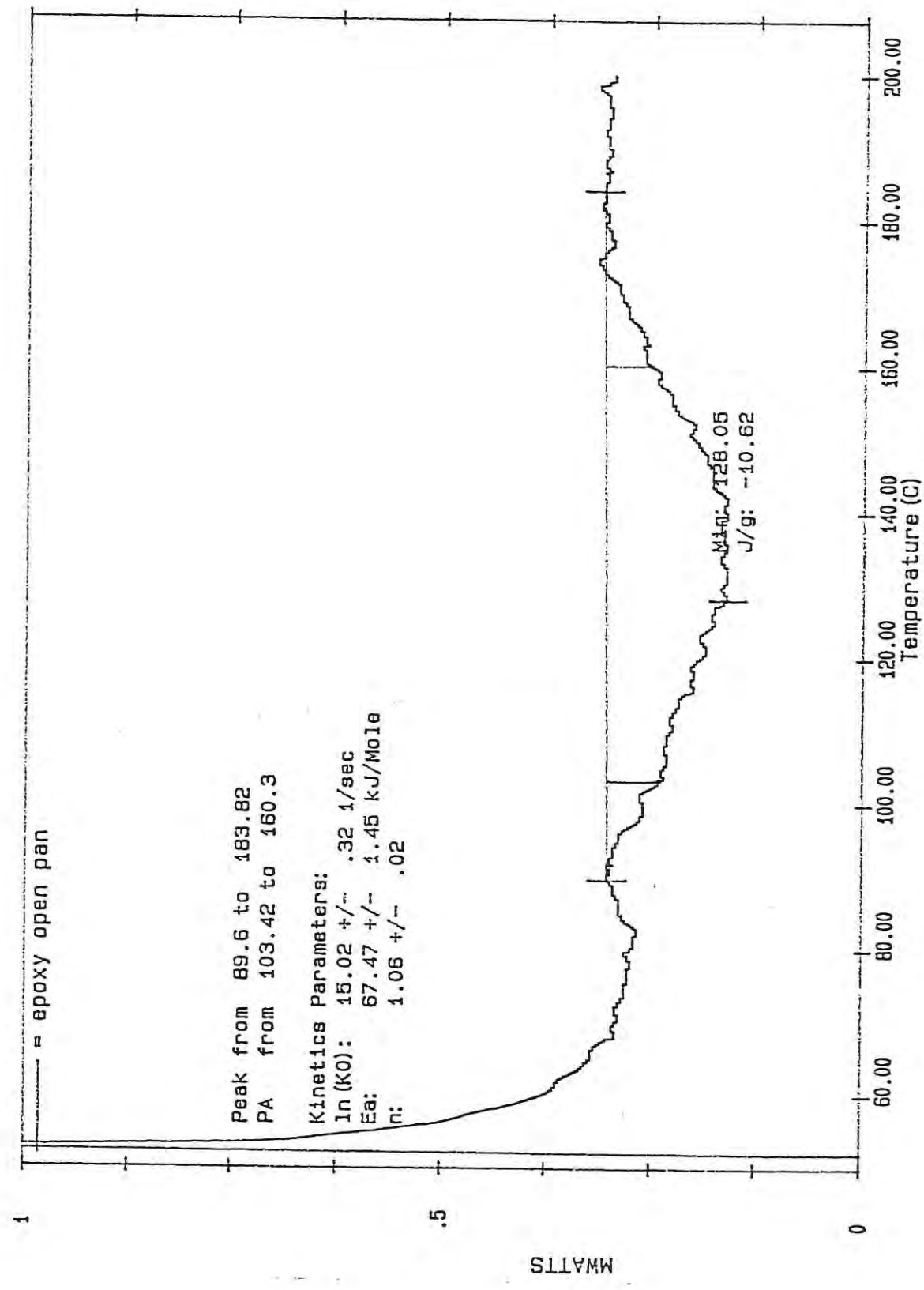

Figure 37b : DSC thermogram showing kinetic parameter calculations for Epoxy 828

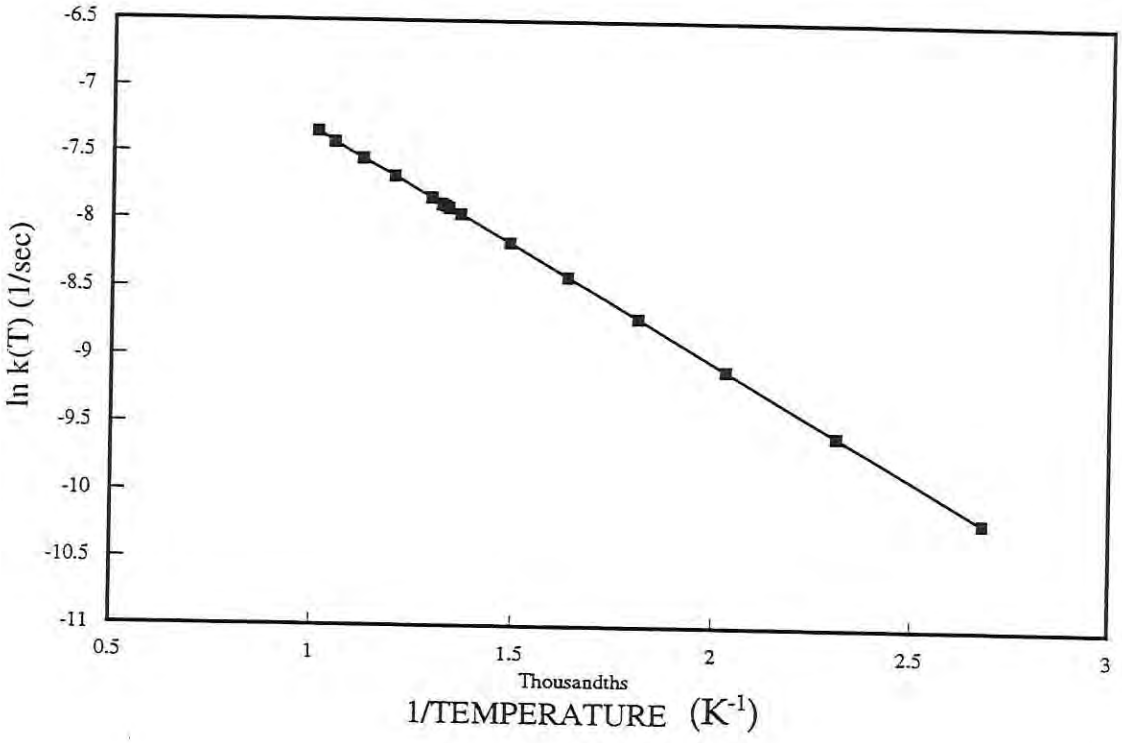

Figure 38 : Rate co-efficient as a function of inverse absolute temperature

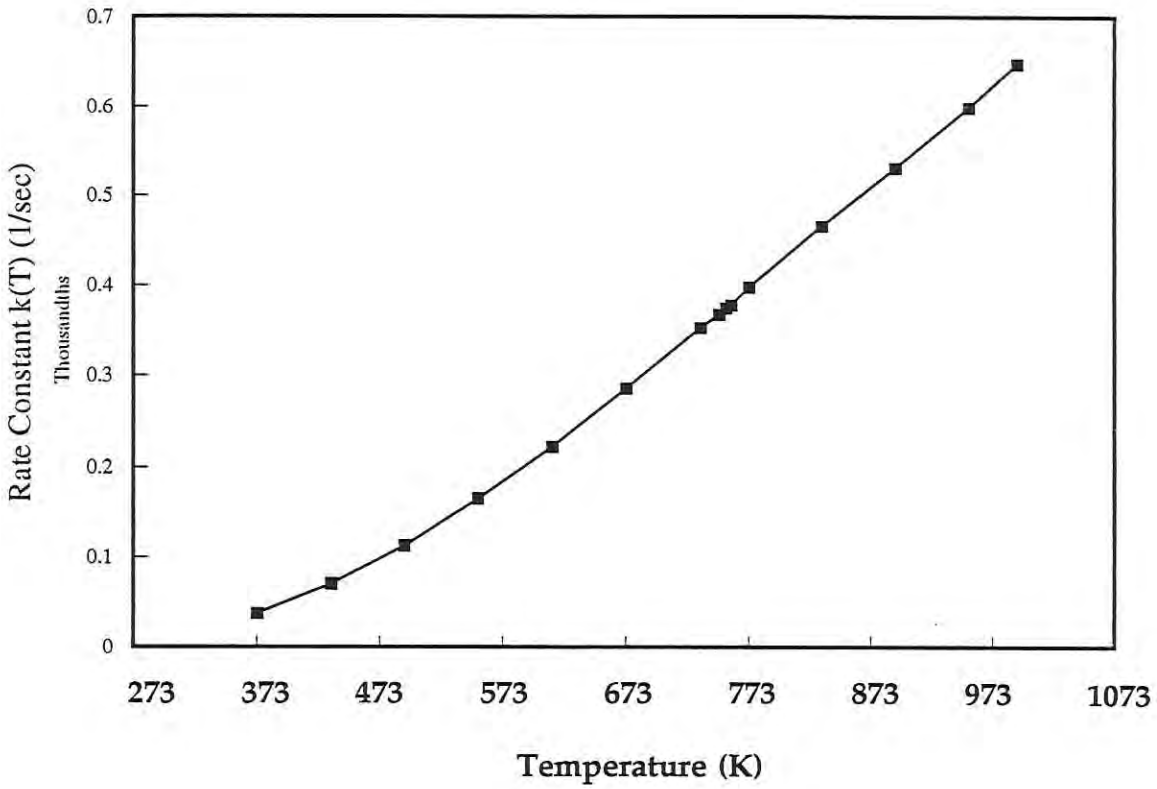

Figure 39: Arrhenius rate constant as a function of temperature

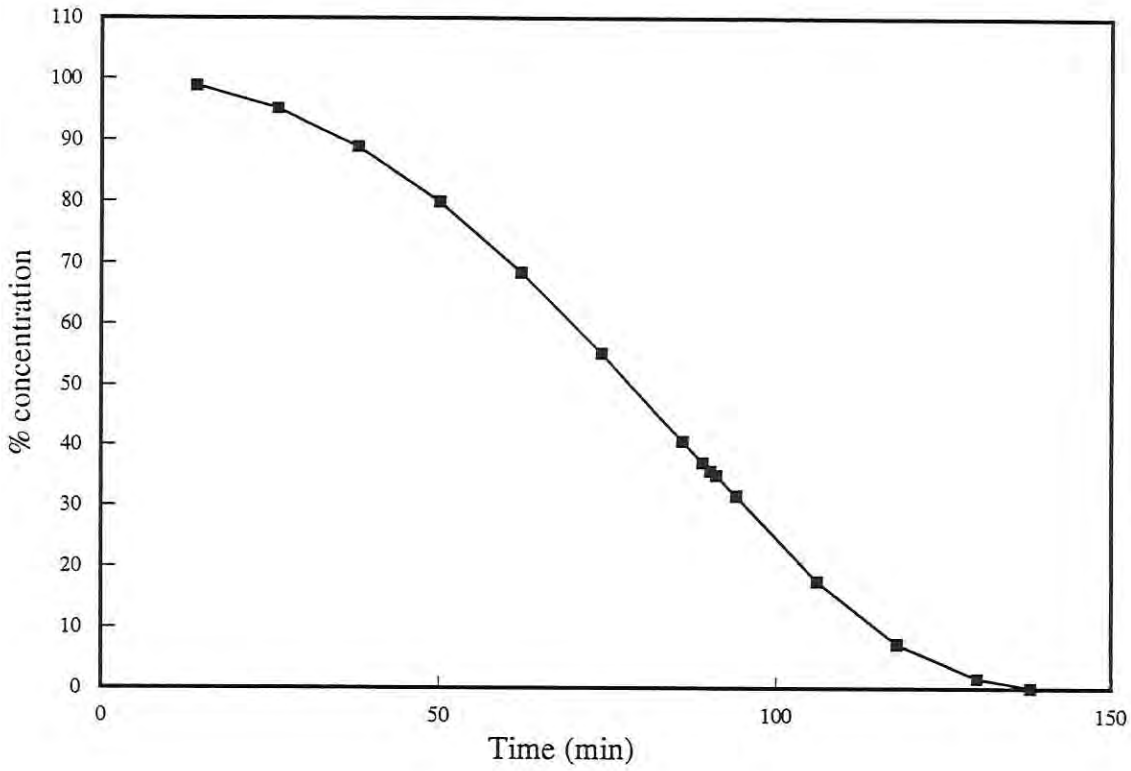

Figure 40: Percent concentration of MTS as a function of time (min)

4) A plot of percentage of MTS Reacted vs. Time (min.), also generated from partial area calculations (Fig. 41).

Other methods exist which allow the determination of E_a and k_o. In order to determine the validity of the kinetic calculations and the DSC software, standard samples which include Nitrocellulose, Epoxy 828, and Polyethylene were trialled using the Ozawa[157] method and deposition rate data obtained from the experimental runs.. The Ozawa plots of log β vs. $1000/T_{max}$ (K^{-1}) for MTS, Nitrocellulose, Epoxy 828, and Polyethylene are given in Figs. 42 - 44. E_a has been calculated from the slope of the graph. The sample temperature T_{max} for each sample corresponds to the peak temperature representative of the maximum rate of the reaction. Each value of T_{max} was determined from a single DSC experimental trial. Figs. 45 - 47, 48 - 52, and 53 - 56 give plots of heat flow to sample (mW) versus Temperature (°C) for MTS, Nitrocellulose, and Epoxy 828 respectively.

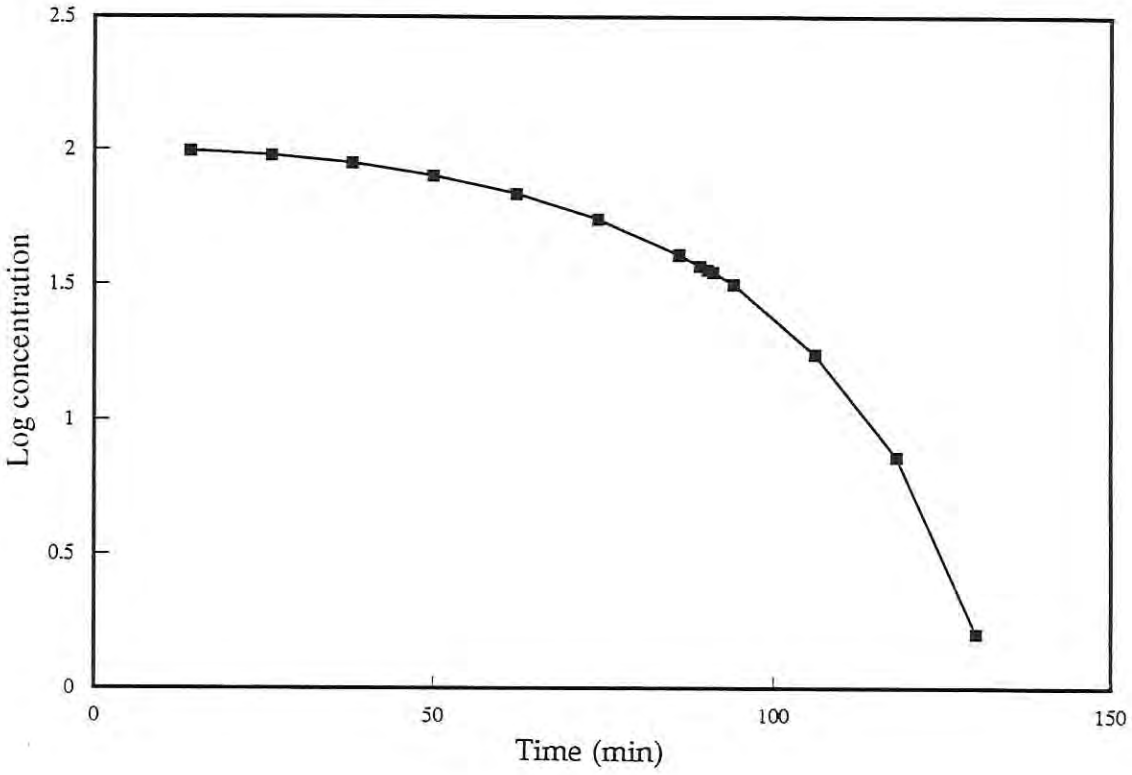

Figure 41 : Concentration MTS as a function of time (min)

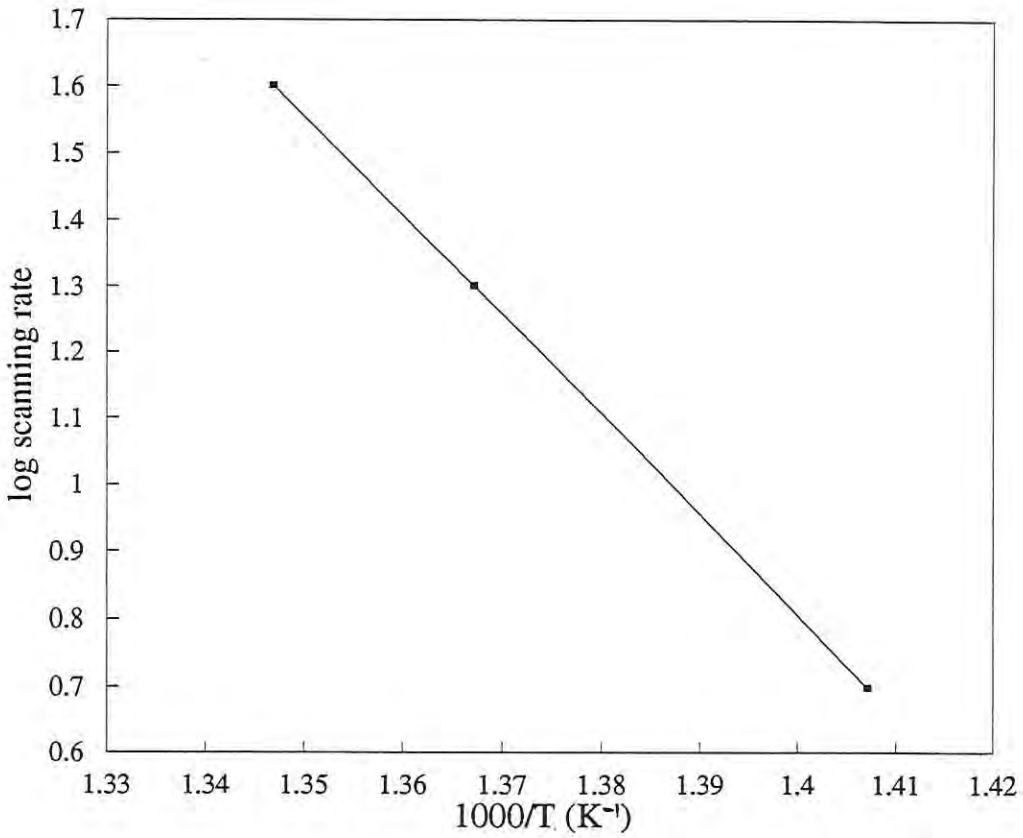

Figure 42 : Ozawa's plot for MTS : log. scanning rate as a function of inverse absolute temperature

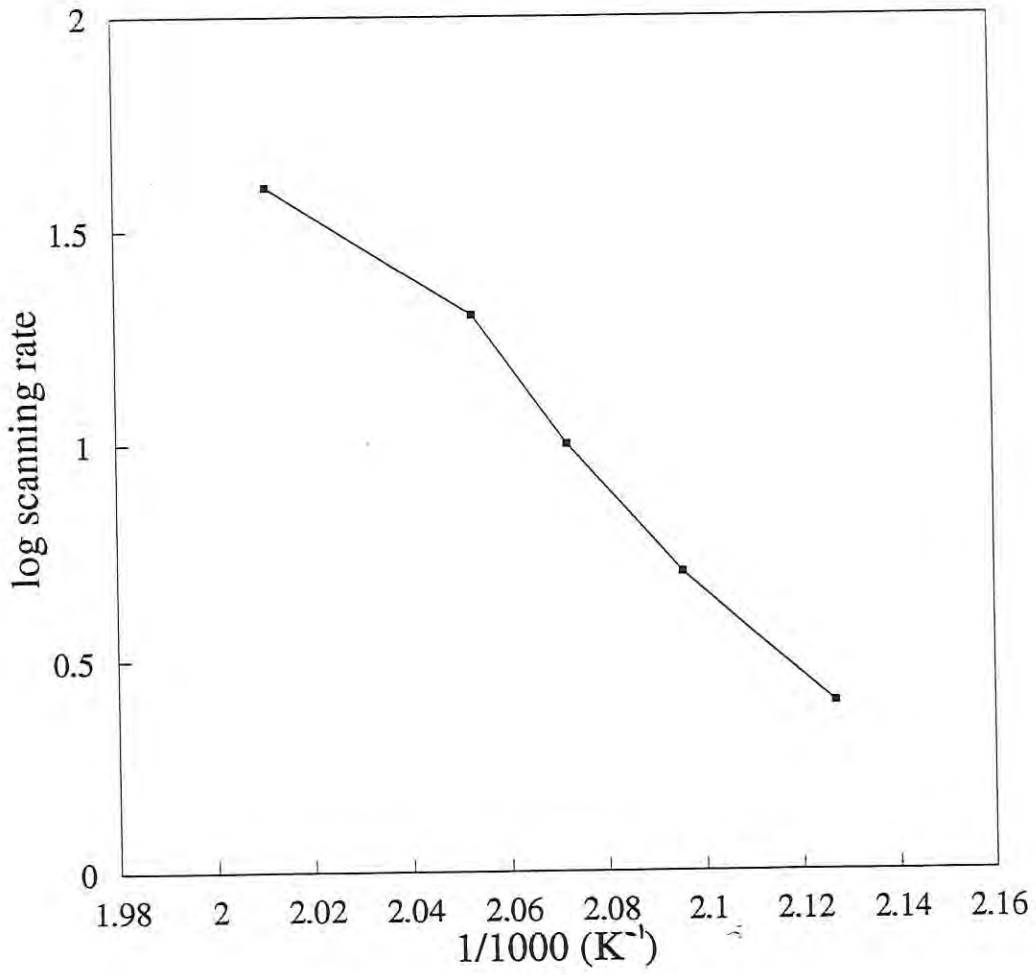

Figure 43 : Ozawa's plot for nitrocellulose - log. scanning rate as a function of inverse absolute temperature

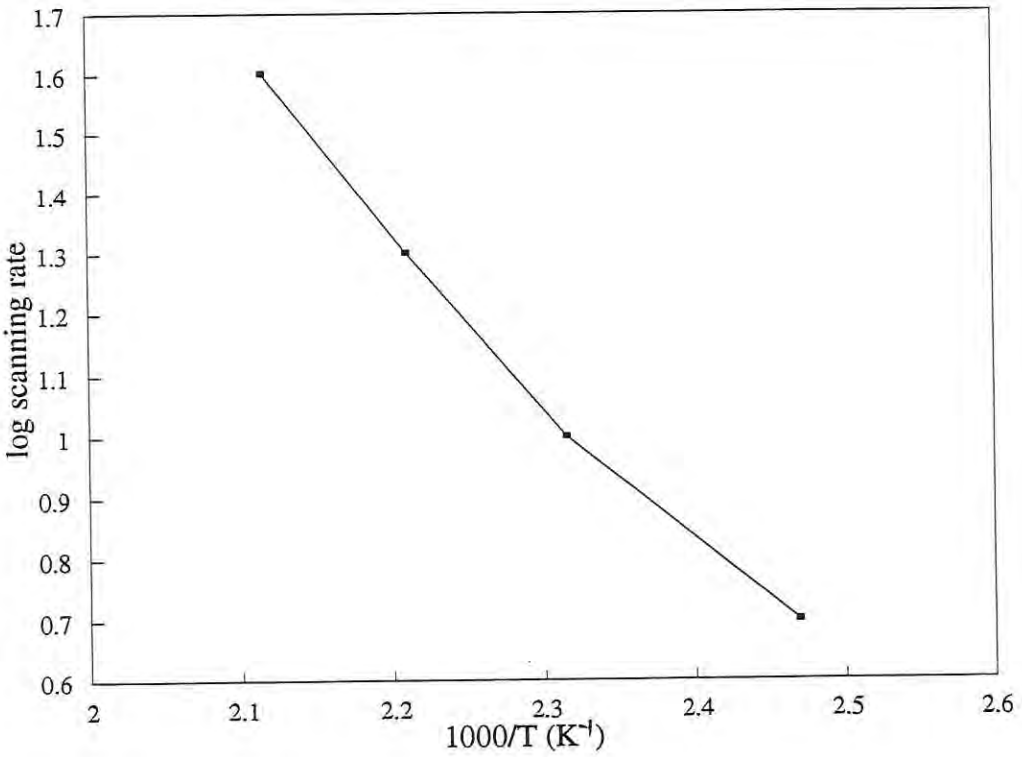

Figure 44 : Ozawa's plot for Epoxy 828 : log. scanning rate as a function of inverse absolute temperature

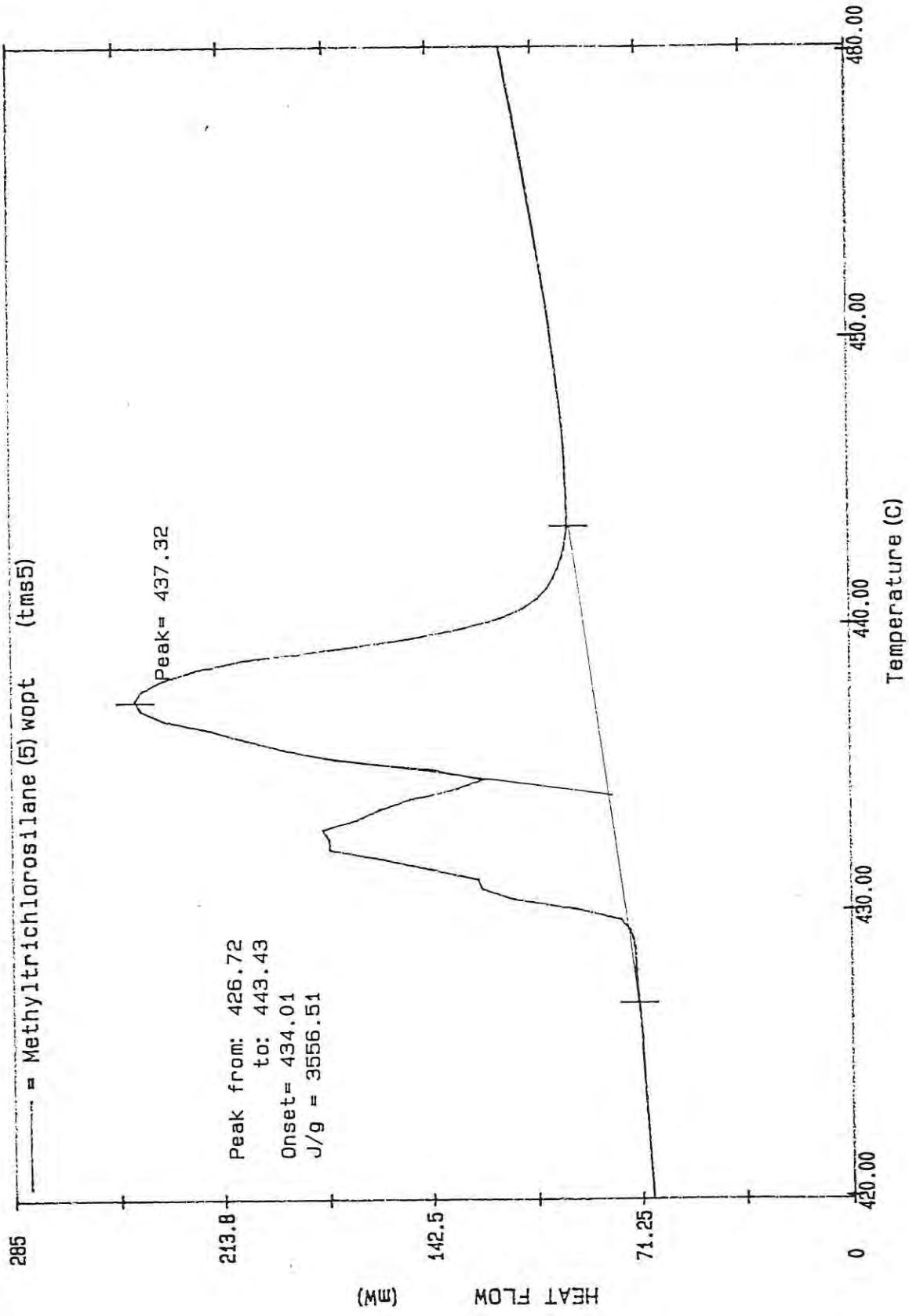

Figure 45 : DSC thermogram for MTS at a scanning rate of 5°C/min showing peak temperature at 437.32°C

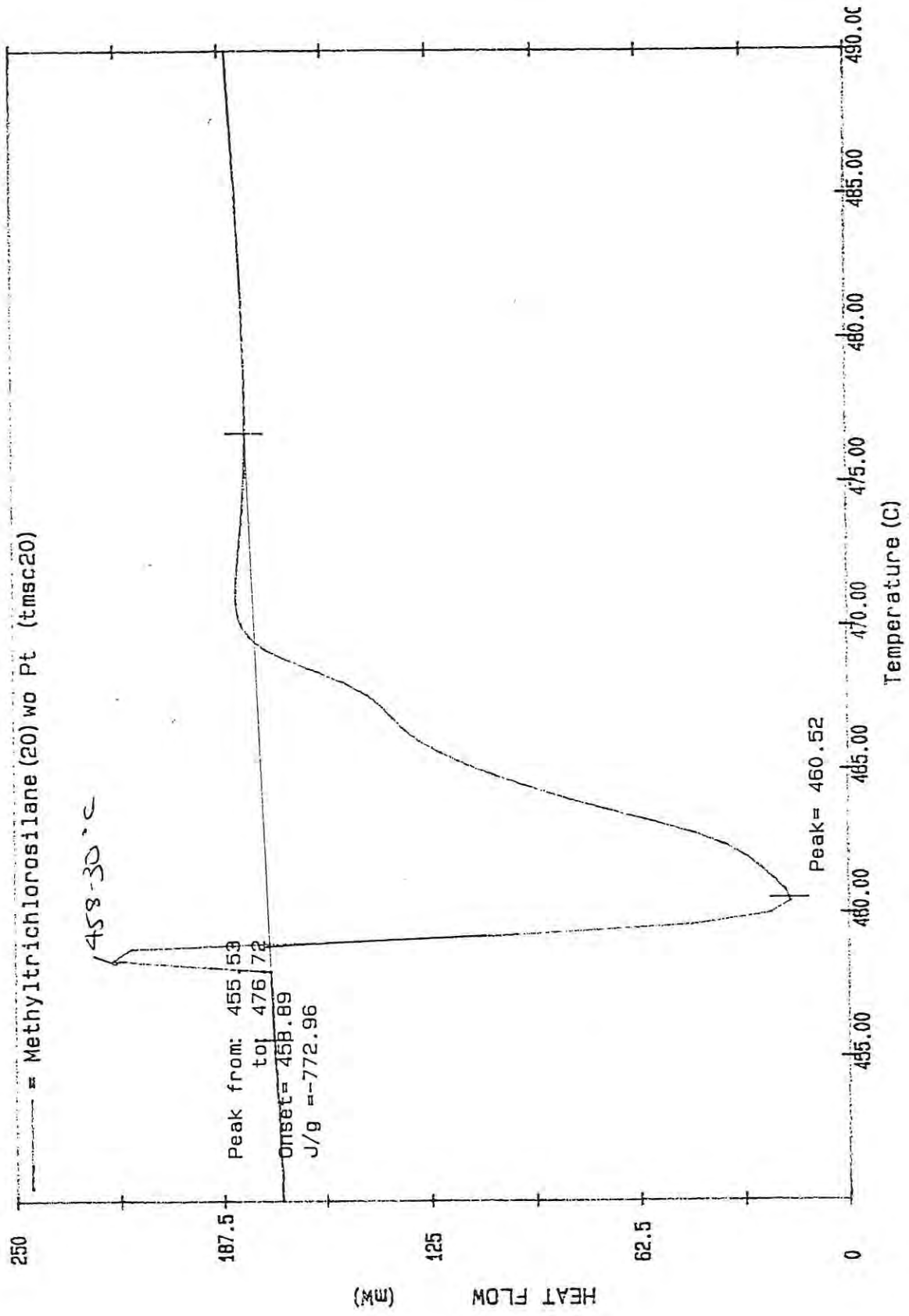

Figure 46 : DSC thermogram for MTS at a scanning rate of 20°C/min showing peak temperature at 458.30°C

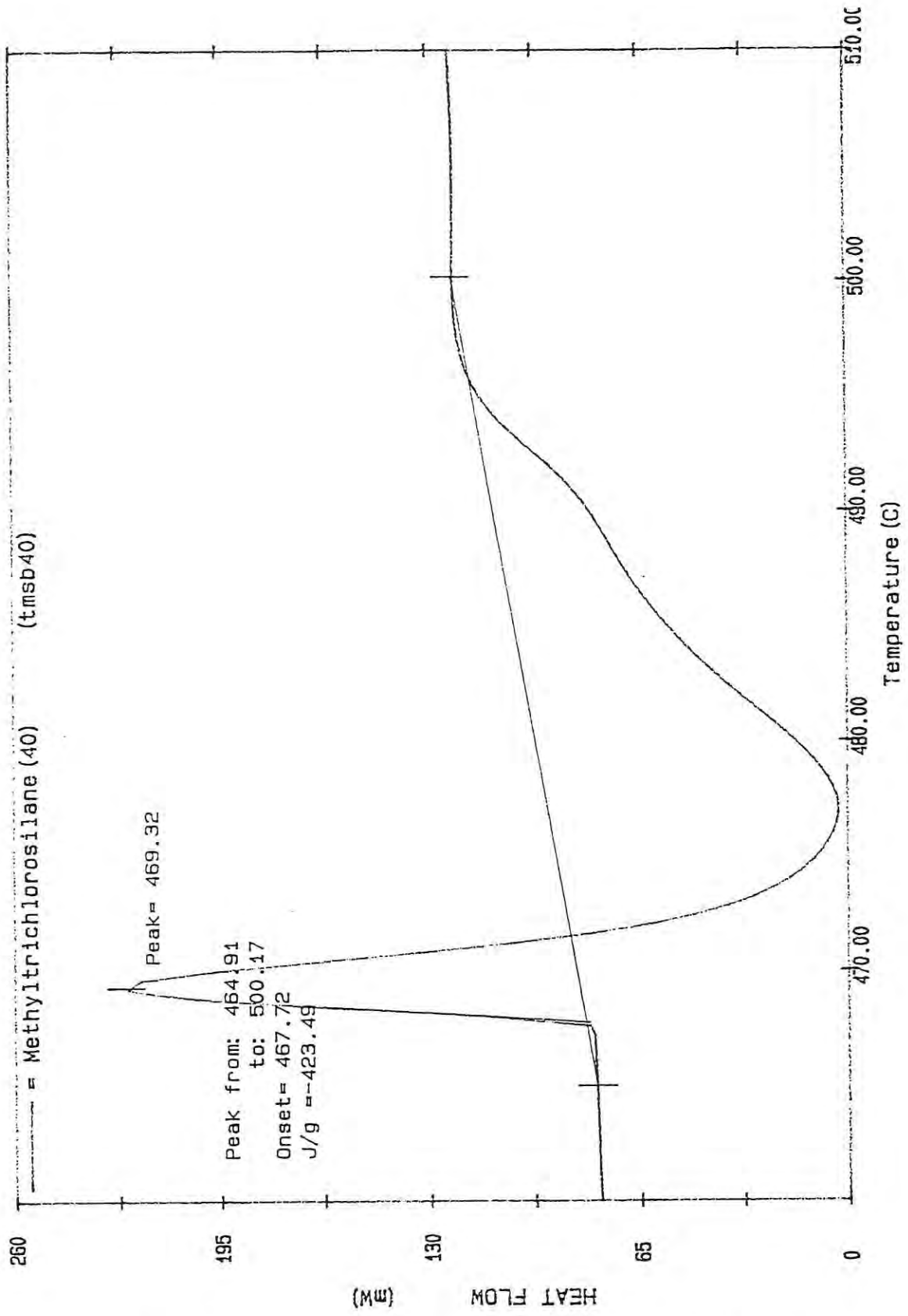

Figure 47 : DSC thermogram for Methyltrichlorosilane at a scanning rate of 40°C/min showing peak temperature at 469.32°C

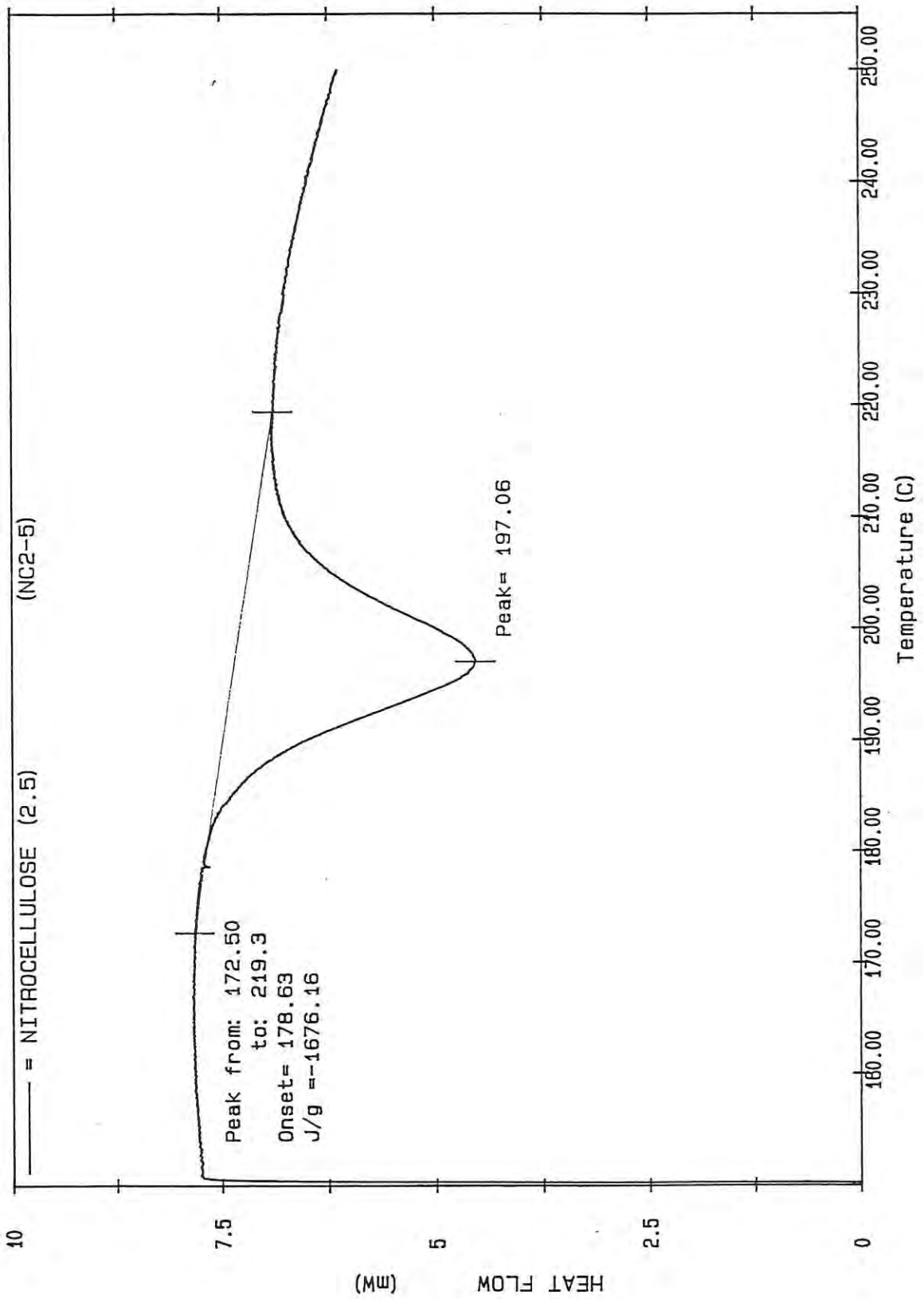

Figure 48 : DSC thermogram for Nitrocellulose at a scanning rate of 2.5°C/min showing a peak temperature of 197.06°C

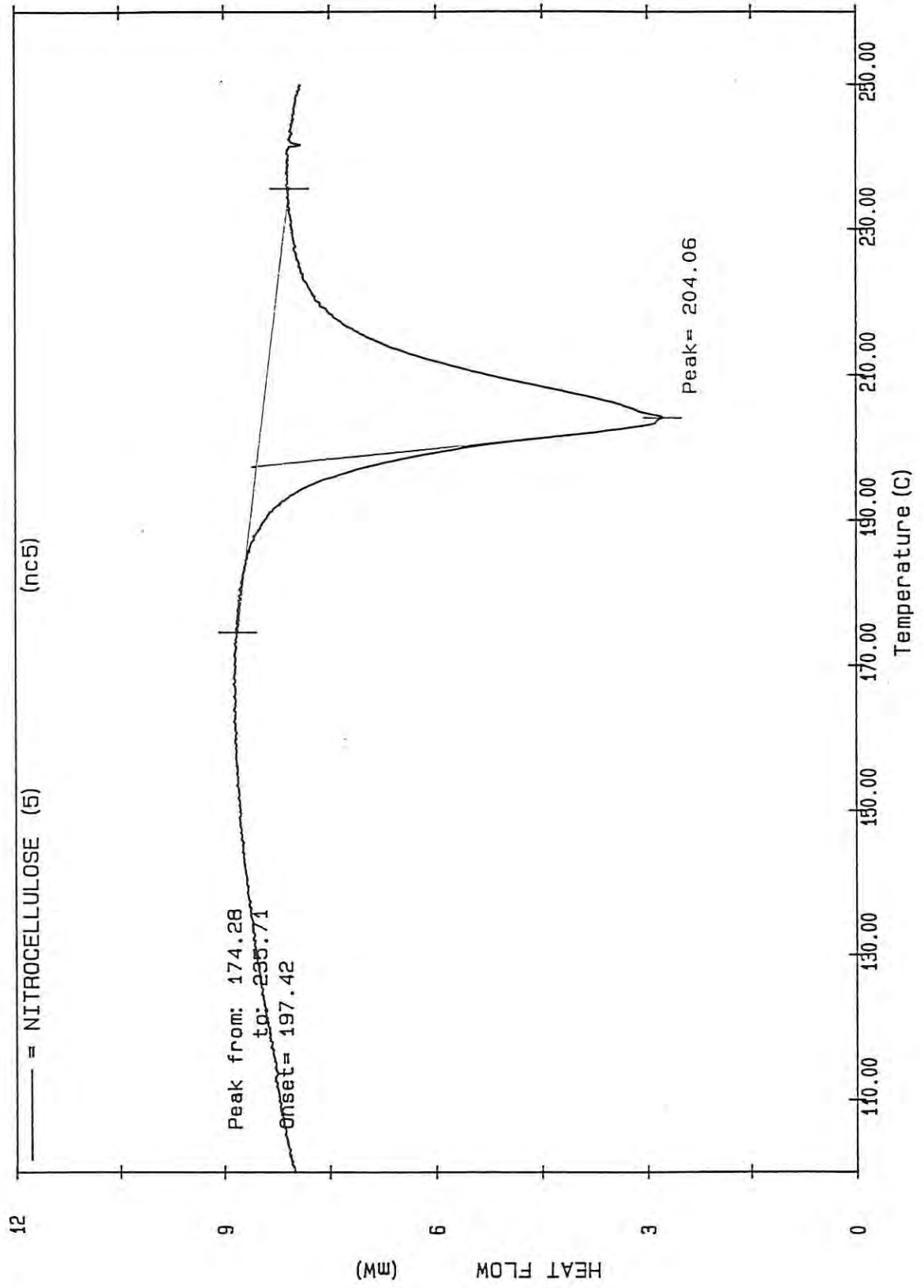

Figure 49 : DSC thermogram for Nitrocellulose at a scanning rate of 5°C/min showing peak temperature at 204.06°C

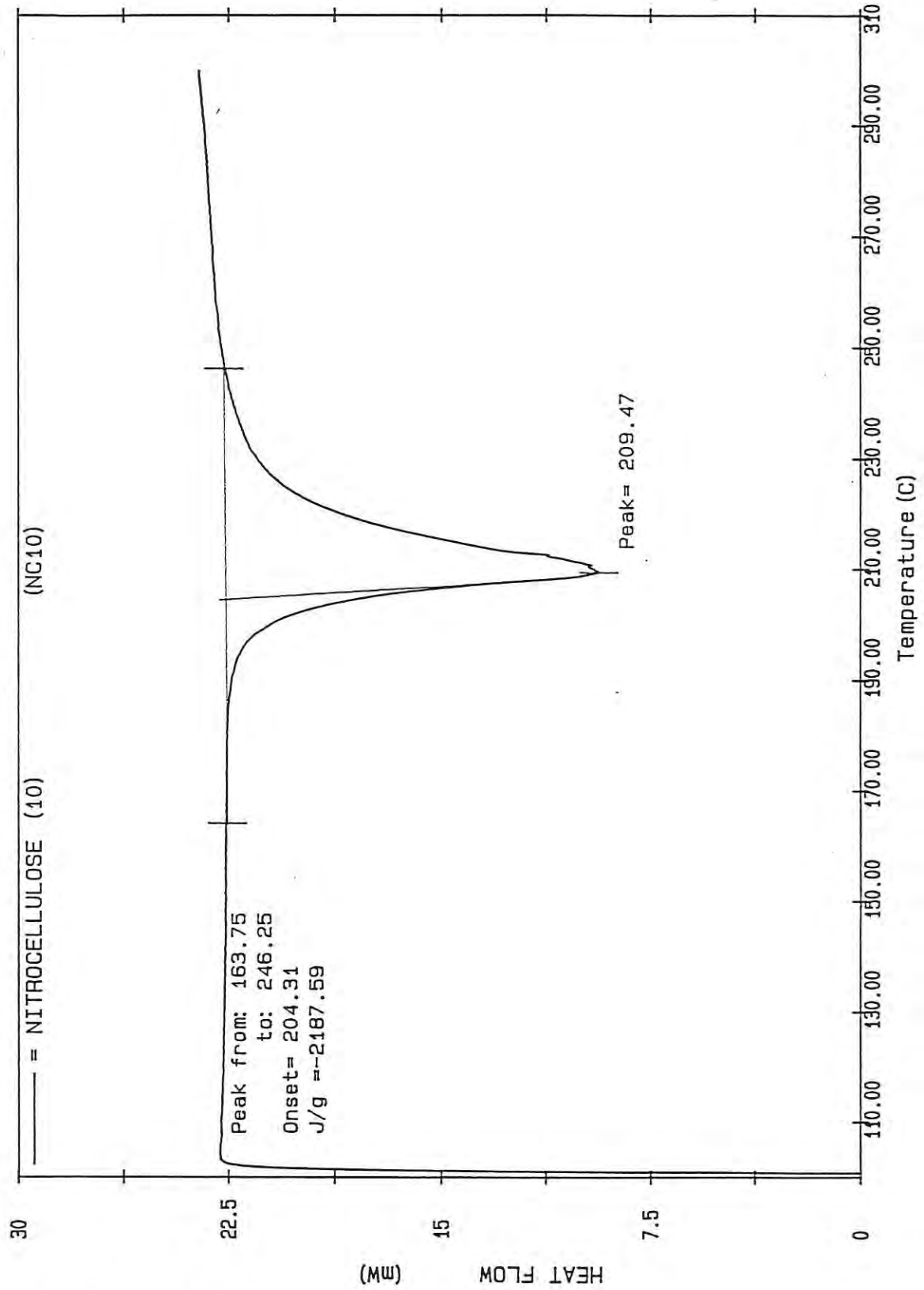

Figure 50 : DSC thermogram for Nitrocellulose at a scanning rate of 10°C/min showing peak temperature at 209.47°C

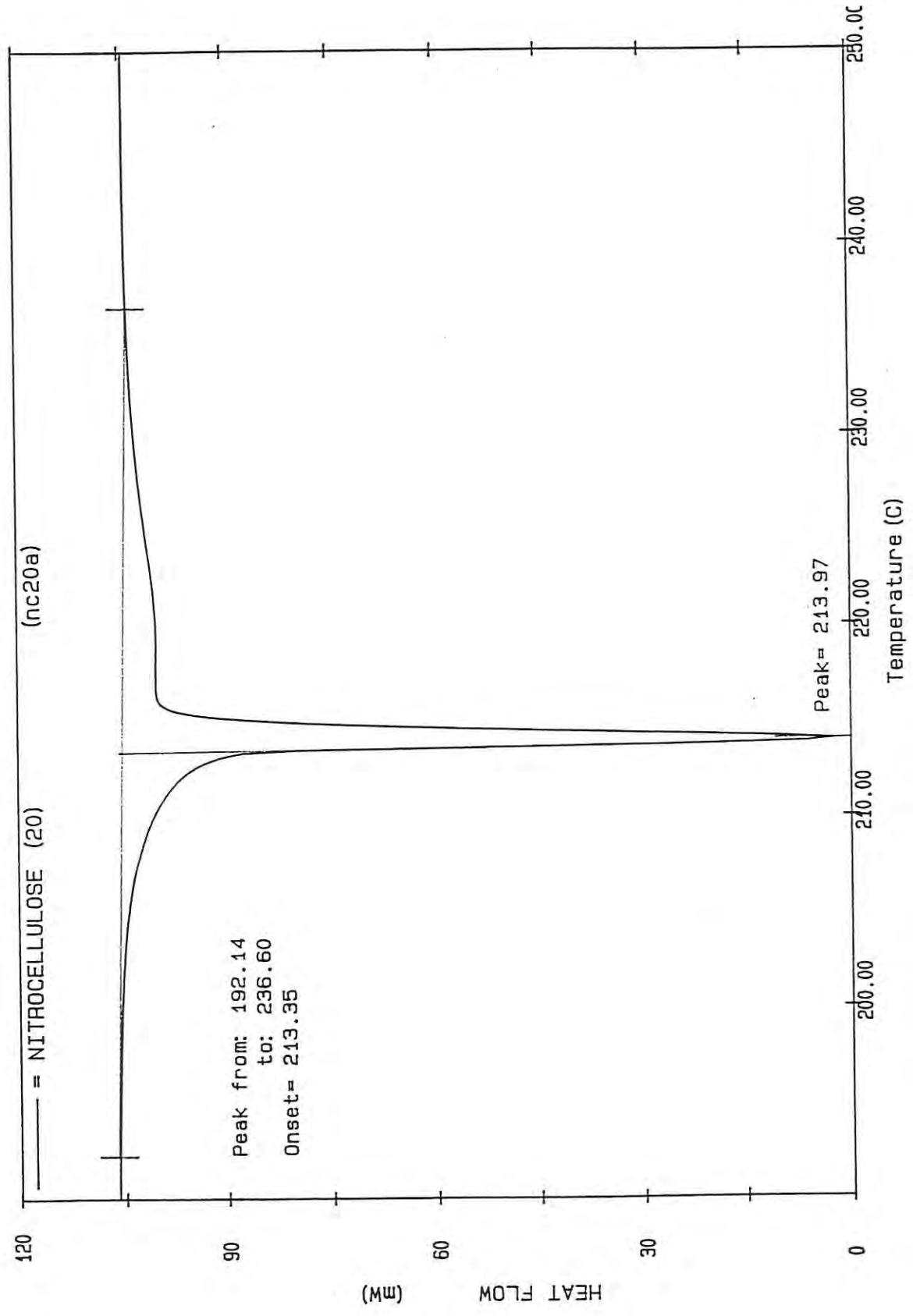

Figure 51 : DSC thermogram for Nitrocellulose at a scanning rate of 20°C/min showing peak temperature at 213.97°C

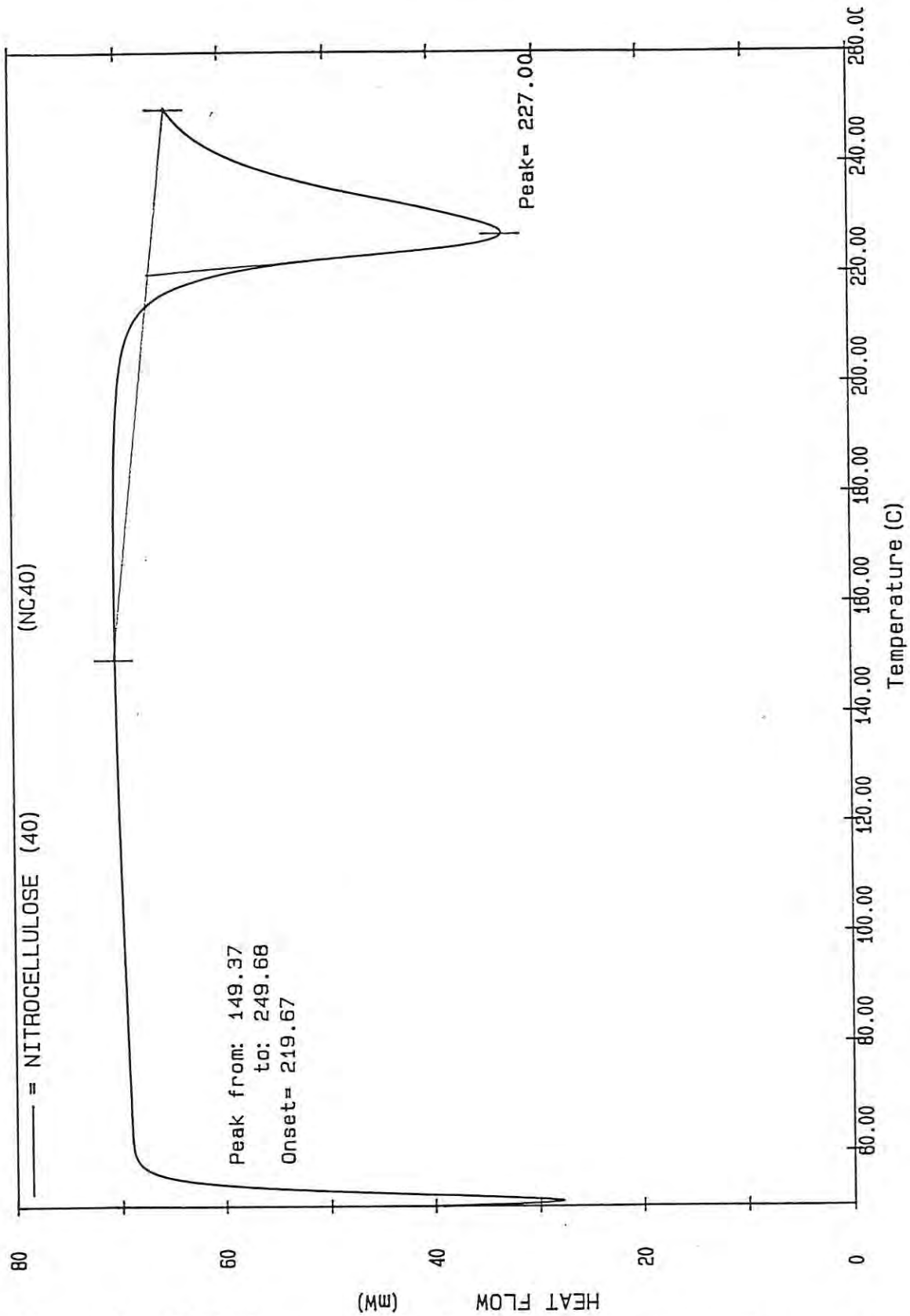

Figure 52 : DSC thermogram for Nitrocellulose at a scanning rate of 40°C/min showing peak temperature at 227.0°C

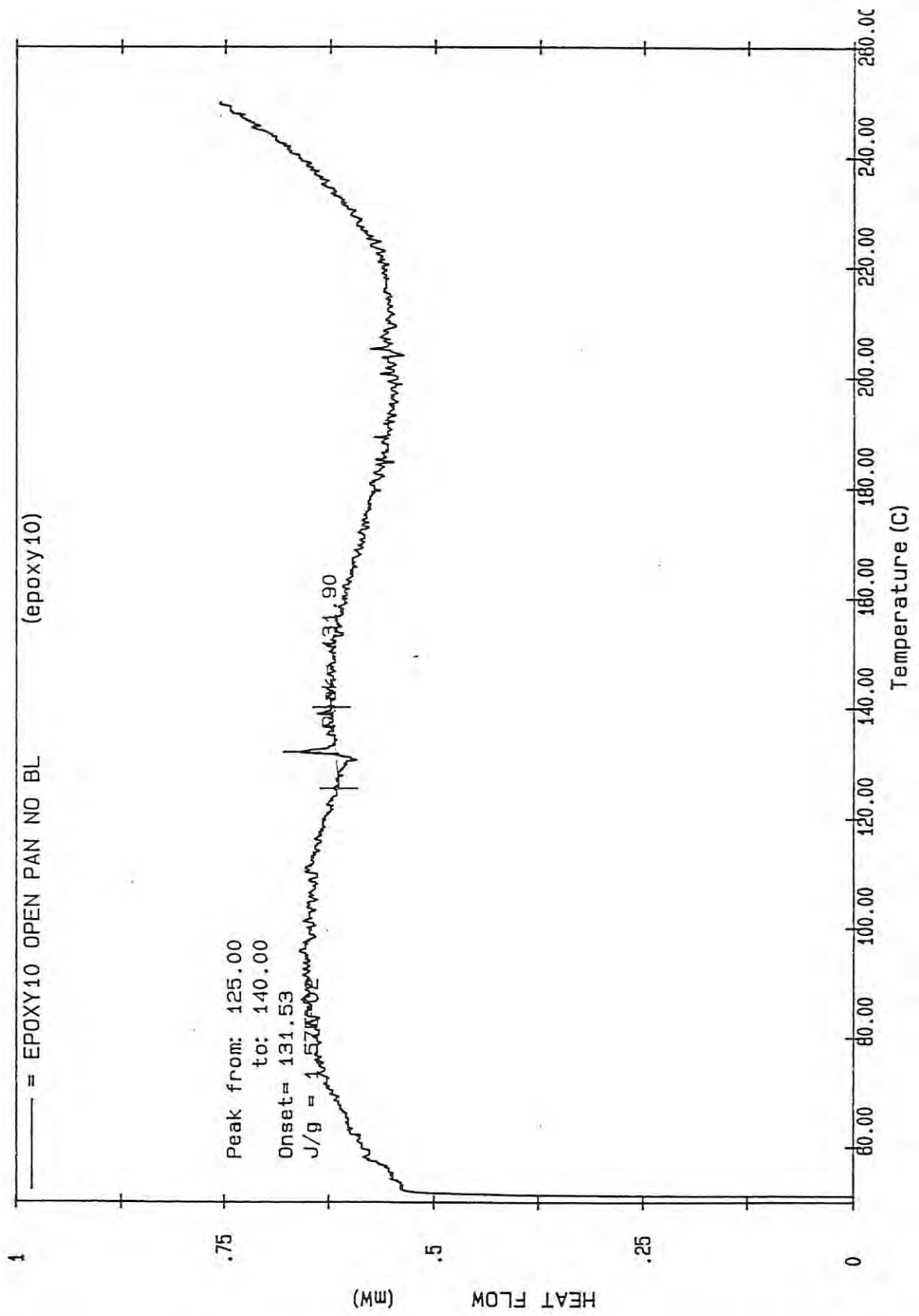

Figure 53 : DSC thermogram for Epoxy 828 at a scanning rate of 5°C/min showing peak temperature at 131.90°C

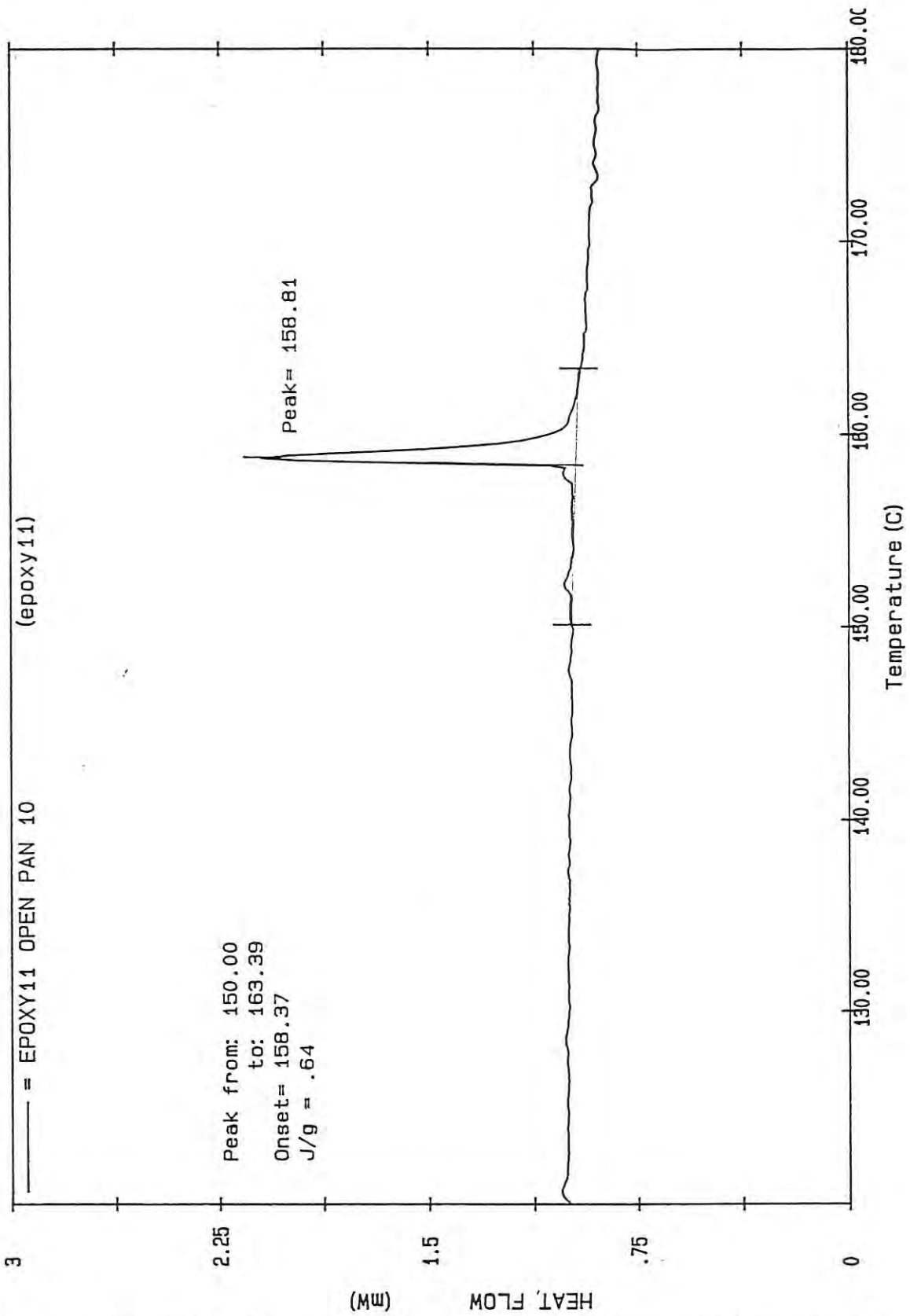

Figure 54 : DSC thermogram for Epoxy 828 at a scanning rate of 10°C/min showing peak temperature at 158.81°C

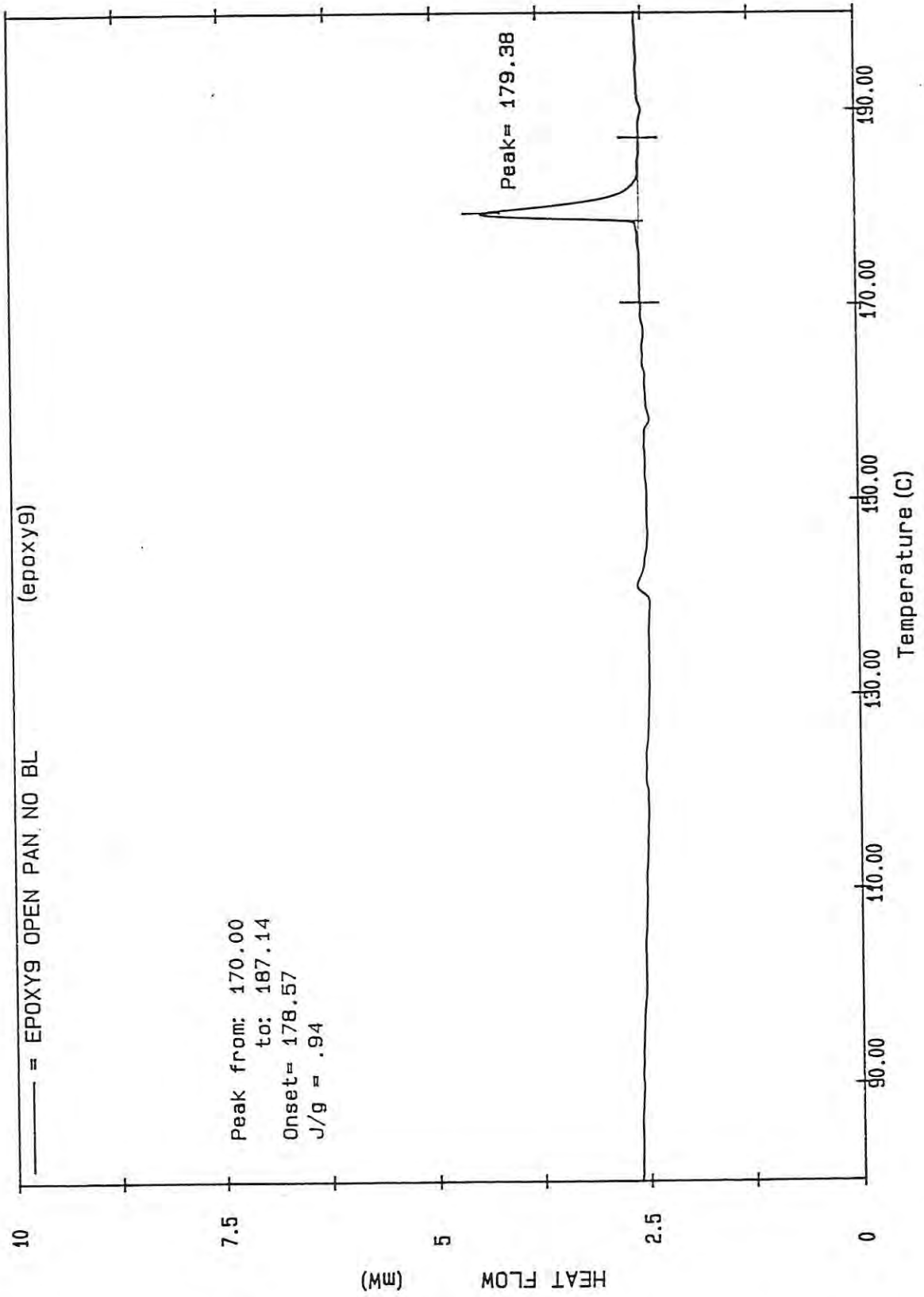

Figure 55 : DSC thermogram for Epoxy 828 at a scanning rate of 20°C/min showing peak temperature at 179.38°C

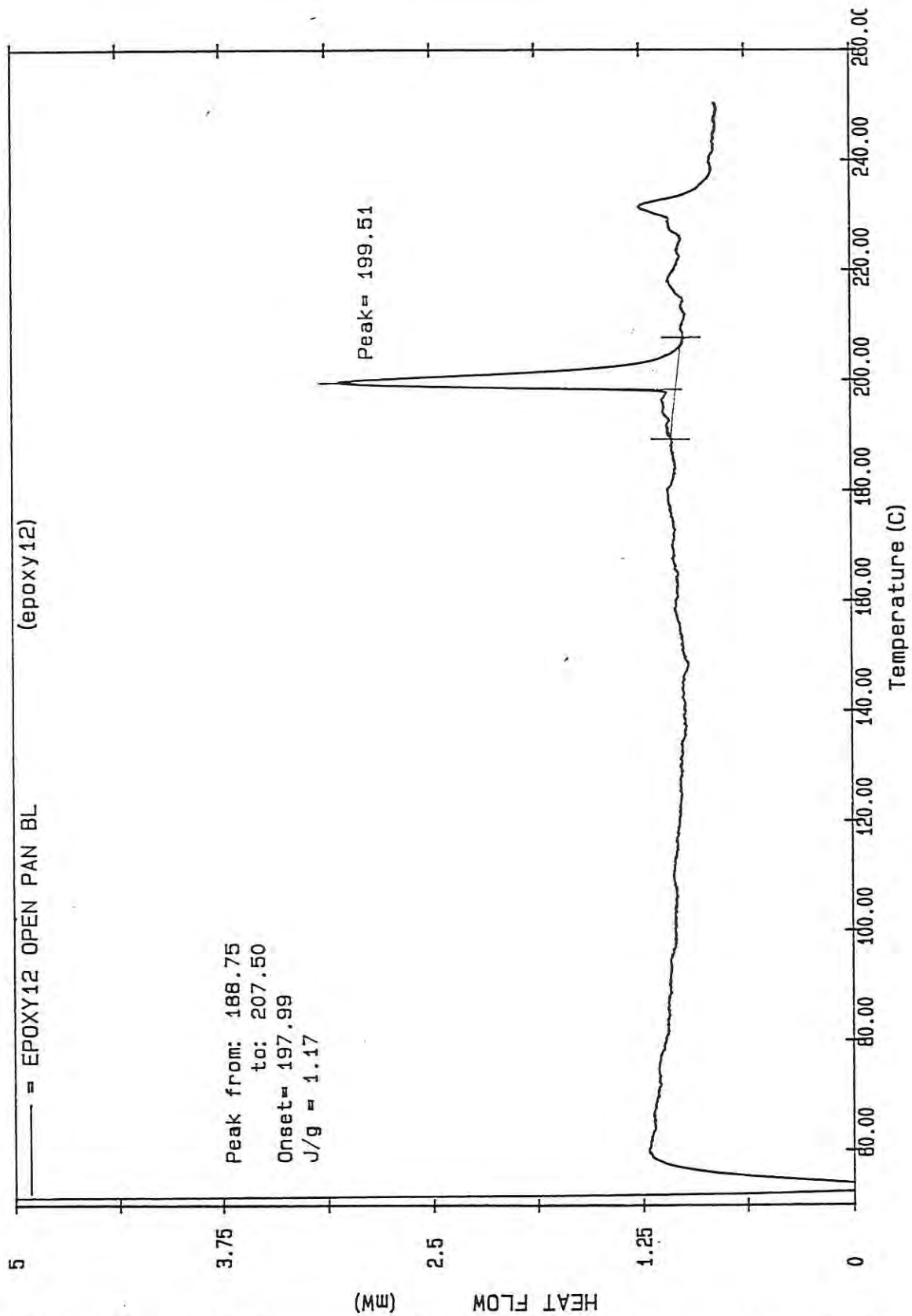

Figure 56 : DSC thermogram for Epoxy 828 at a scanning rate of 40°C/min showing peak temperature at 199.51°C

CHAPTER 6

DISCUSSION

6.1 PRECURSOR MATERIAL

A number of silicon and carbon containing materials have been used to form ceramic coatings by CVD technique. Hydrocarbons and silicon halides are commonly used for the synthesis of SiC[32,158].

Organosilanes containing both silicon and carbon in the same molecule are attractive because these compounds provide Si and C in equal ratios. MTS based one-component system has been extensively investigated for the deposition of SiC[122].

In the present investigation, MTS was used as a precursor material. This material was selected because of its ready availability, cost and ease of operation. Gaseous phase syntheses are quite complex. So in order to keep the system simple, MTS was considered to be an ideal precursor material for the production of silicon based compounds. MTS, though highly toxic and hygroscopic, can be handled easily using a liquid metering pump for delivery into the reactor. Also MTS can be vaporised at a relatively low temperature (339 K) and it decomposes at 733 K. It was envisaged that it may be possible to synthesise high temperature silicon based species from MTS below 1273 K.

6.2 CVD REACTOR SYSTEM

Two types of reactor systems are used in the present study. A hot wall reactor, in which external heat source is used to heat the walls of the reaction chamber from which heat radiates to the substrate, and the fluidised bed reactor, where the reaction chamber is heated in a similar way, but in addition sand particles of 1 x 10^{-3} m OD were placed on the gas distributor plate. As indicated earlier (Chapter 3, Fig. 10), the fluidised bed reactor was designed in such a way whereby the reactant gases entered only that side of the reactor, which contained the substrate to be coated. The fluidising media, i.e., sand particles, were fluidised with nitrogen gas. This type of reactor design is a unique design and has not been reported previously for the coating of metallic substrates. Fluidised bed technique has been recommended [27,159,160-165] for the coating of nuclear fuel particles; microspheres of uranium carbide or oxide that constitute this fuel for high temperature gas cooled reactors, have been successfully coated in fluidised beds with SiC from gas mixtures containing an organosilane, hydrogen, and usually an inert diluting gas. Methyltrichlorosilane is the most commonly used organosilane for such purposes[61,166-170]. Deposition temperatures in the range of 1200°C - 1800°C have been reported. Graphite reactors are generally used for such applications.

In the present study, the fluidising media has been separated from the

reaction chamber. The fluidised bed techniques are particularly well suited for the coating of particles because of its ability for obtaining high rates of heat transfer to the substrate, which is crucial for successful reaction on the surface of the substrate.

The principle used in the hot wall reactor is very similar to that reported in the literature. A large number of investigators[125,171-173] have reported on the CVD of SiC, and the process is now very well known. It is however very difficult to find the ideal method of application, the design of reaction chamber and correct processing parameters. Deposition overall, is largely dependant on variables such as: furnace type, the furnace dimensions, shape and size of specimen, and its location inside the reactor.

The size of the hot wall and fluidised bed reactor used in this investigation was based on such considerations as the type of materials to be coated, adequate residence time for the gaseous species moving through the reactor, and ease of operation.

There are certain advantages and disadvantages of using hot-wall reactor arrangements.

Hot wall reactors are generally reliable and can be assembled from readily available materials. Also, a reasonably high degree of precision in

temperature control is attainable. However, the major disadvantage is the high consumption of the costly precursor materials as all the inner surfaces of the reactor compete with the substrate for deposition.

Alternatively, a large number of investigators[174-176] have reported the use of cold wall reactors. In cold wall reactors as the substrate is heated directly, either inductively or resistively and deposition on the reactor wall can be prevented. This type of reactor was not considered in the investigation because of its complexity and high cost.

The design of the gas distributor plate is crucial as uniform distribution of the gaseous species entering into the reactor is important for obtaining uniform coatings. In general fluidised bed has mainly been used for the coating of microspheres which are either placed on a flat distributor plate, or in a conical designed base. For example, the fluid beds used for the coating of nuclear fuel particles with pyrolytic carbon[49] or with SiC[30], utilised the latter arrangement. A spray nozzle is sometimes used in the bed for the injection of reactants separately in a two component system. It has been recently shown[177] that a distribution plate with smaller holes (< 1mm diameter), provides an even distribution of incoming gaseous species during fluidisation. A proper distribution enables the majority of particles to be in contact with the fluidising gas. In the present investigation, this technique was used to fluidise sand particles, which was effective in maintaining and transferring the heat to the substrate as

described earlier.

6.3 EXPERIMENTAL RESULTS

The precursor material was fed into the preheating chamber either by bubbling nitrogen gas through a heated round-bottomed flask containing MTS, or by a liquid feed pump. The first method relies on the generation of a higher reactant vapour pressure, which permits unaided transport from the vaporiser. The vapours so generated were in fact further aided by a carrier gas pressure, i.e., N_2. Although convenient and the substrate successfully coated; it was not possible to control the feed rate. Also, it is not possible to determine reactant concentration unless it is assumed that entraining stream is fully saturated. This technique also resulted in variable time for feeding the same amount of reactant into the chamber. A liquid metering feed pump was used in the later studies which provided better control on the delivery of the material into the reactor. The pump was calibrated and finally feed rates of 2.74 ml/min and 5.5 ml/min were selected. The effect of MTS feed rate on deposition rate at the selected concentrations is shown in Fig. 57. The deposition rate at both feed rates increases with an increase in temperature. There is, however, no discernible difference on deposition rate at 1073K and 1173K. Higher feed rates were avoided as they tended to produce non-uniform coatings and

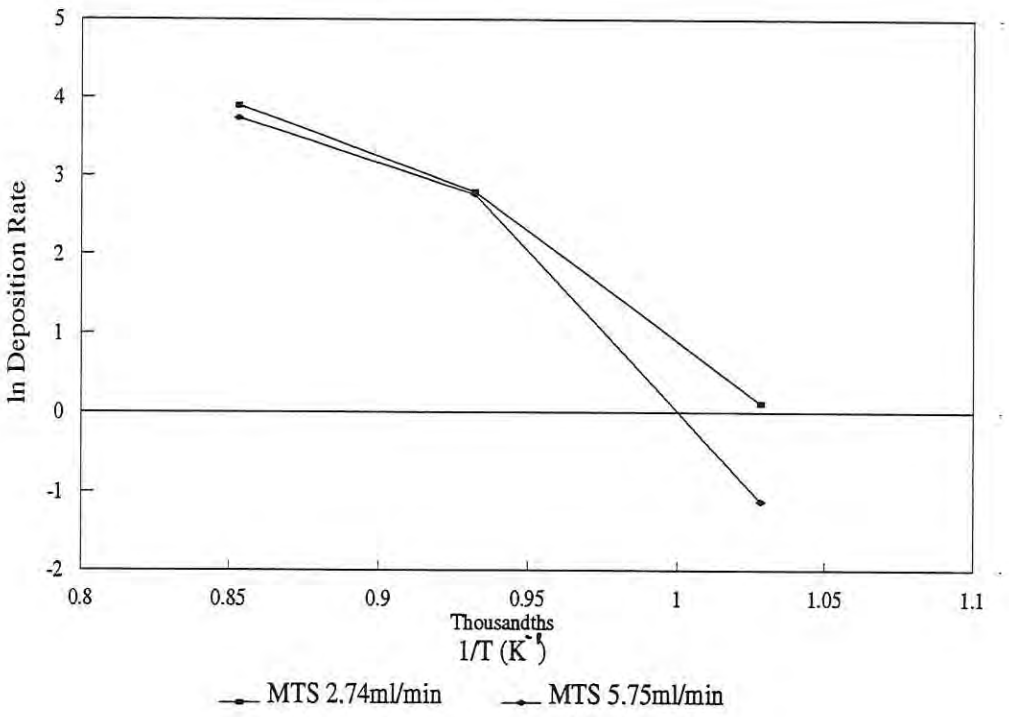

Figure 57 : Arrhenius plot showing the effect of MTS feed rate on deposition rate

sometimes partially coated substrate. It is believed that higher feed rates shortened the residence time of the reactant in the reactor, and consequently the substrate has shorter exposure time to the reactant. Also, the substrate which was unevenly coated (Fig. 58) underwent surface deterioration on exposure to air for longer periods. A rusty material appeared on the surface which probably is the result of oxidation at the substrate surface. It is envisaged that strong oxidising components, probably compounds containing chloro functionalities, were deposited on the substrate surface and these compounds in the presence of moisture produced rust. Lower feed rates which resulted in uniform surface coatings were therefore selected.

This method is also useful as the MTS vapours are toxic and very hygroscopic. It was possible to inject the MTS by generating the MTS vapours *in situ* and then transporting the vapours into the reactor. A heating element incorporated in the feed line between the liquid feed pump and the reactor ensured that MTS is vaporised and the lines leading to the reactor are kept at a temperature higher than the boiling point of MTS. This precaution is taken to ensure that MTS liquid droplets are not entrapped in the transporting lines.

The coated substrate samples with varying coating thicknesses were obtained. It was observed that even under similar deposition conditions, there was considerable variation in the deposition rates and coating

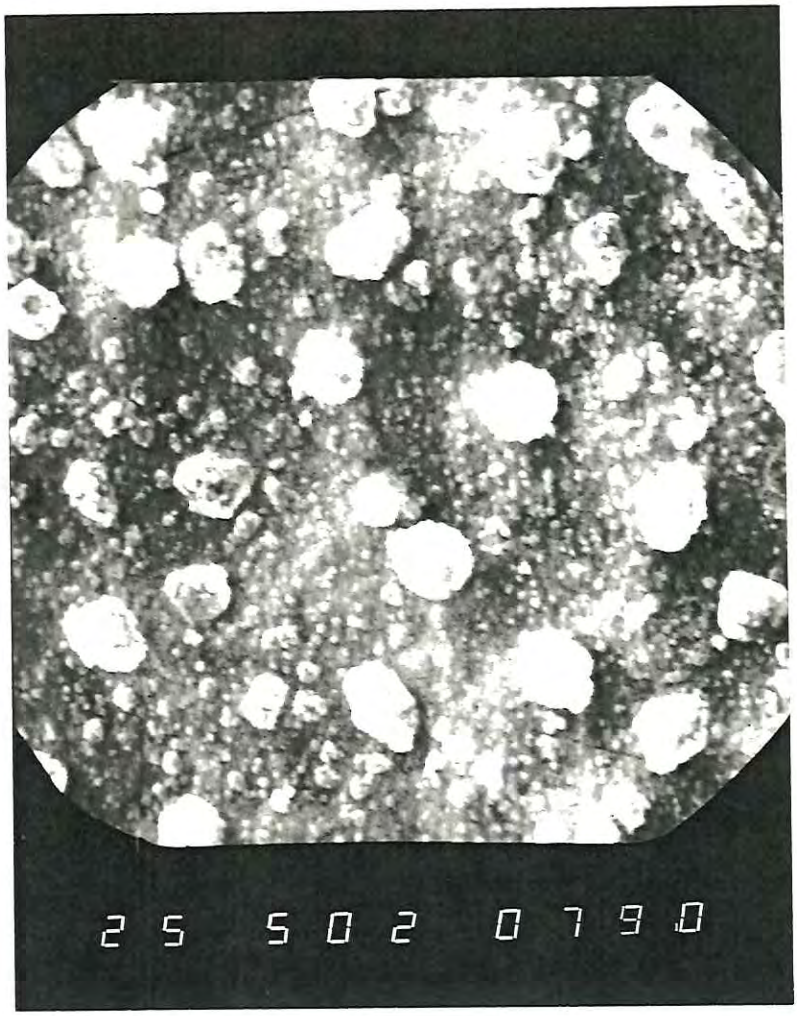

Figure 58 : SEM of coated stainless steel plate showing uneven coating upon exposure to air

thicknesses (Figs. 59). Also, there was a consistent variation of total yields of the coated material and it ranged from 0.1 to 3 %. Obviously the inner surfaces of reactor competed for deposition with the suspended substrate; and therefore no set pattern was observed in the total % yield. It is also possible that the reactor is rather too large, in comparison with the substrate size.

Since the rate of deposition is a function of reactant concentration and the reactant concentration decreases downstream as a result of reactant depletion upstream, it has been proposed that some compensation is essential if efficient use of reactant is to be attained alongwith good uniformity. Measures such as rotating axially symmetrical substrate translating the substrate relative to the reactant flow, increasing the substrate temperature downstream or constricting the flow channel downstream so as to increase the rate of gas flow and decrease the boundary layer thickness through which the mass transfer must occur, have been suggested[178]. Variation in carrier gas flow rates clearly indicate that very low gas flow rates tended to produce a partially coated substrate. Based on these observations carrier gas flow rate between 283.2l/h and 566.4l/h was selected. The effect of gas flow rate at three selected temperatures on deposition rate in a hot wall reactor is shown in Figs. 60 and 61. The results clearly indicate that gas flow rate of 400-450 l/h inside the reactor gave higher deposition rates, particularly at 1173K. The flow rate of the carrier gas therefore appears to have a

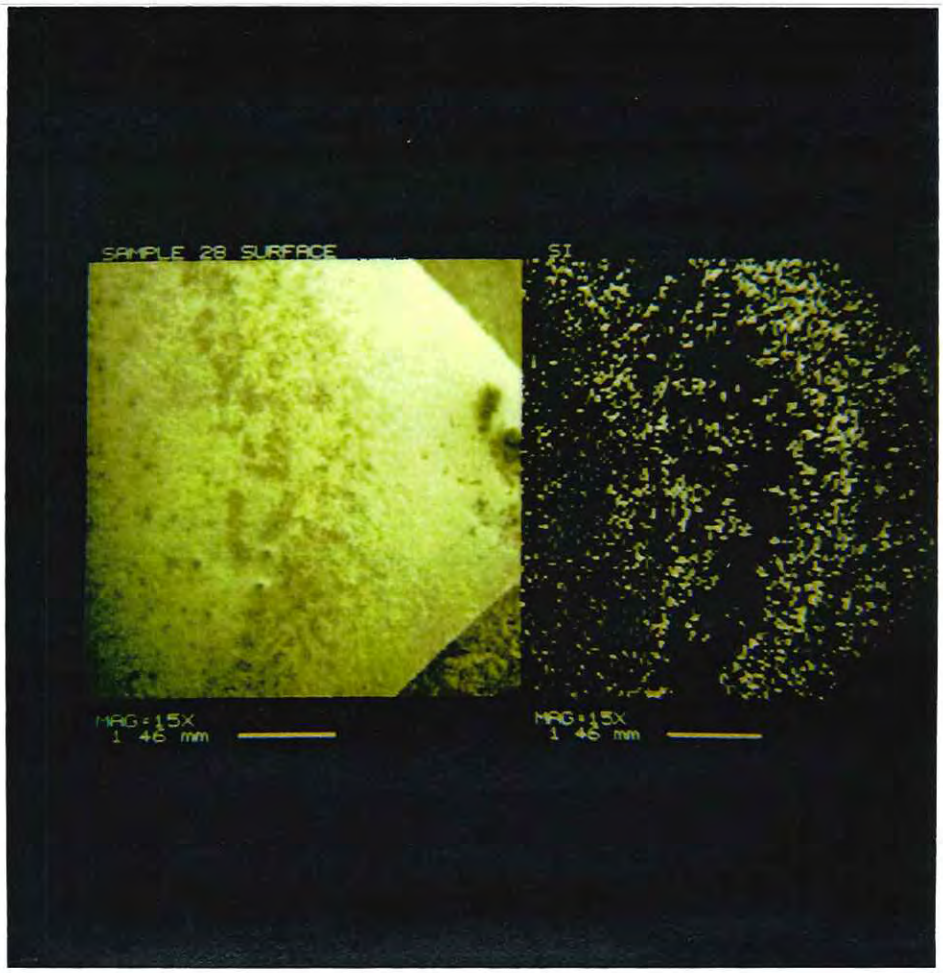

Figure 59 : SEM micrographs showing thickness and deposit variation

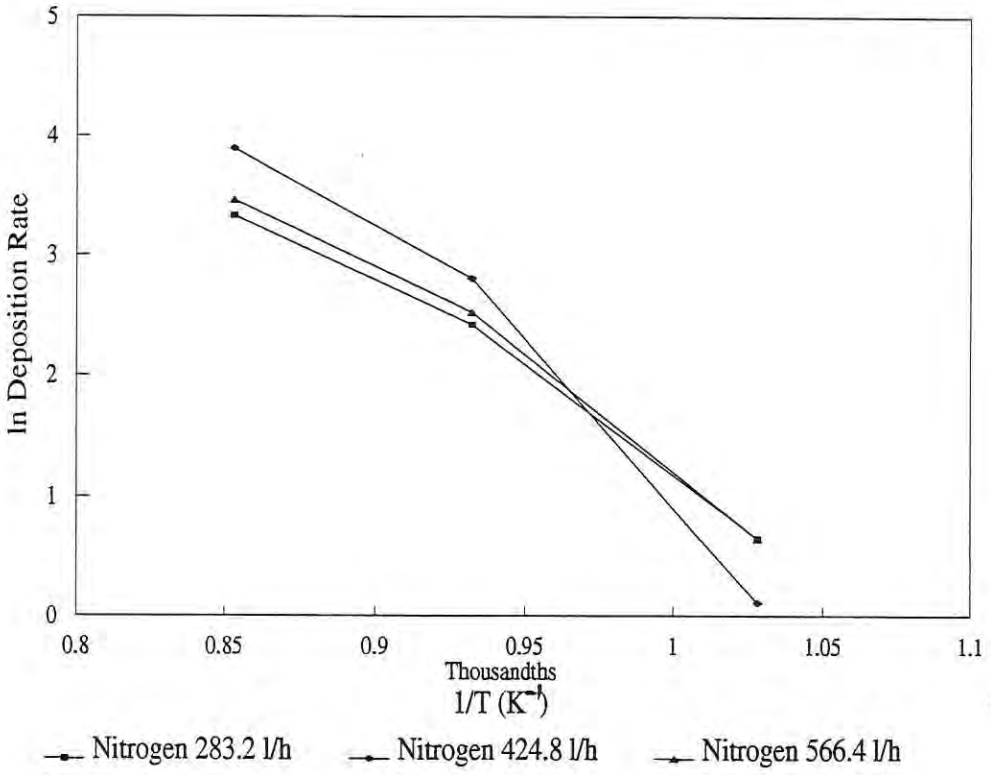

Figure 60 : Arrhenius plot showing the effect of carrier gas flow rate on the deposition rate

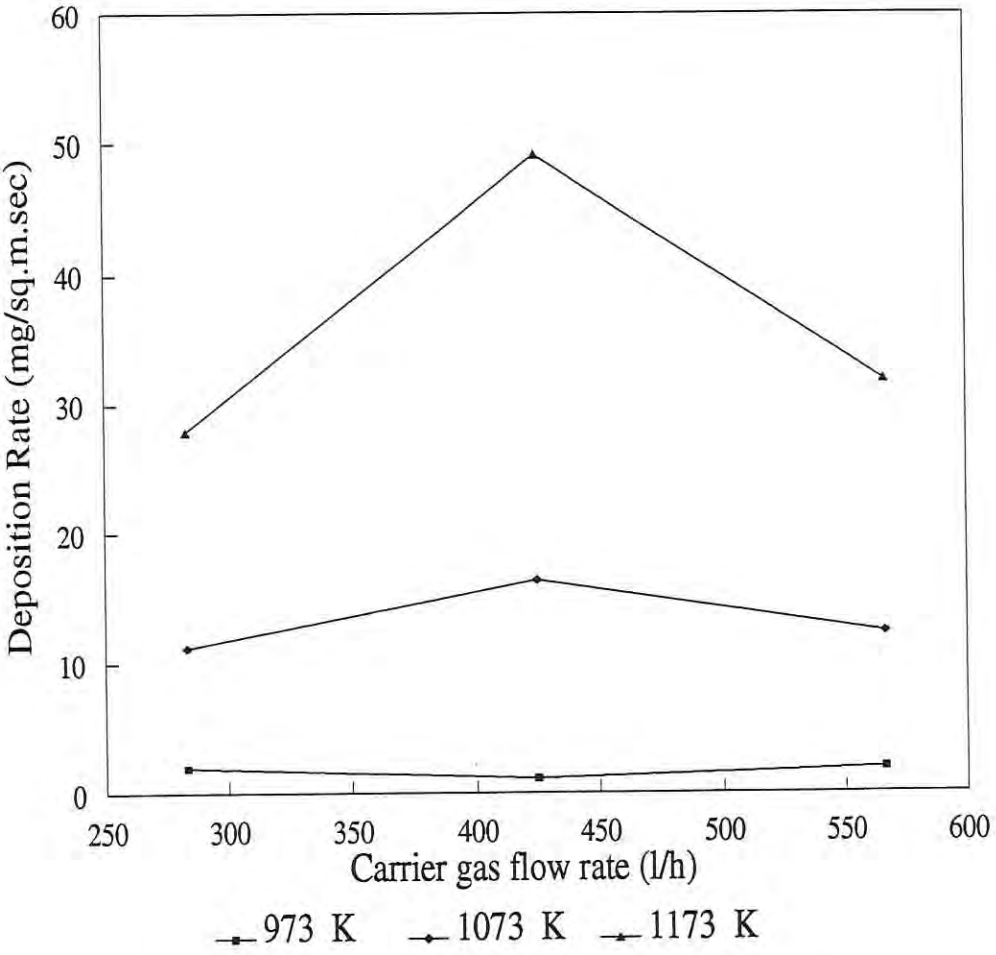

Figure 61 : Effect of carrier gas flow rate on deposition rate

significant effect on the overall reaction conditions and hence the quality of the coatings.

Substrate pretreatment is also necessary in order to attain a uniform coating and strong surface-to-film adherence. Two different techniques were used: chemical pre-treatment such as etching, and grit blasting. The chemically treated substrate showed poor film adherence and the coating was uneven (Fig. 62). SEM indicated variable thickness pattern over the entire surface. Chemical etching or pre-treatment was therefore considered inappropriate. Grit blasting was done using a mixture of sand and grit particles. This technique was found to be effective in the surface preparation of the substrate used in this investigation. Grit blasting is effective because it not only removes the surface impurities, but also produces a grooved surface (the microgrooves are only visible under microscope) which provides mechanical interlocking of coated material; the film thus grows evenly on the plate (Fig.62). The film-to-surface adherence was also found to be stronger and film was evenly spread over the entire surface of the substrate. (Fig. 63).

The deposition rate and dependence of deposition rate on gas environment are shown in Figs. 64 and 65. The deposition rate appears to increase sharply when a mixture of N_2 and H_2 gases was used as a carrier; this is particularly more pronounced in a fluidised bed reactor (Fig. 65). The introduction of pure hydrogen into the carrier gas

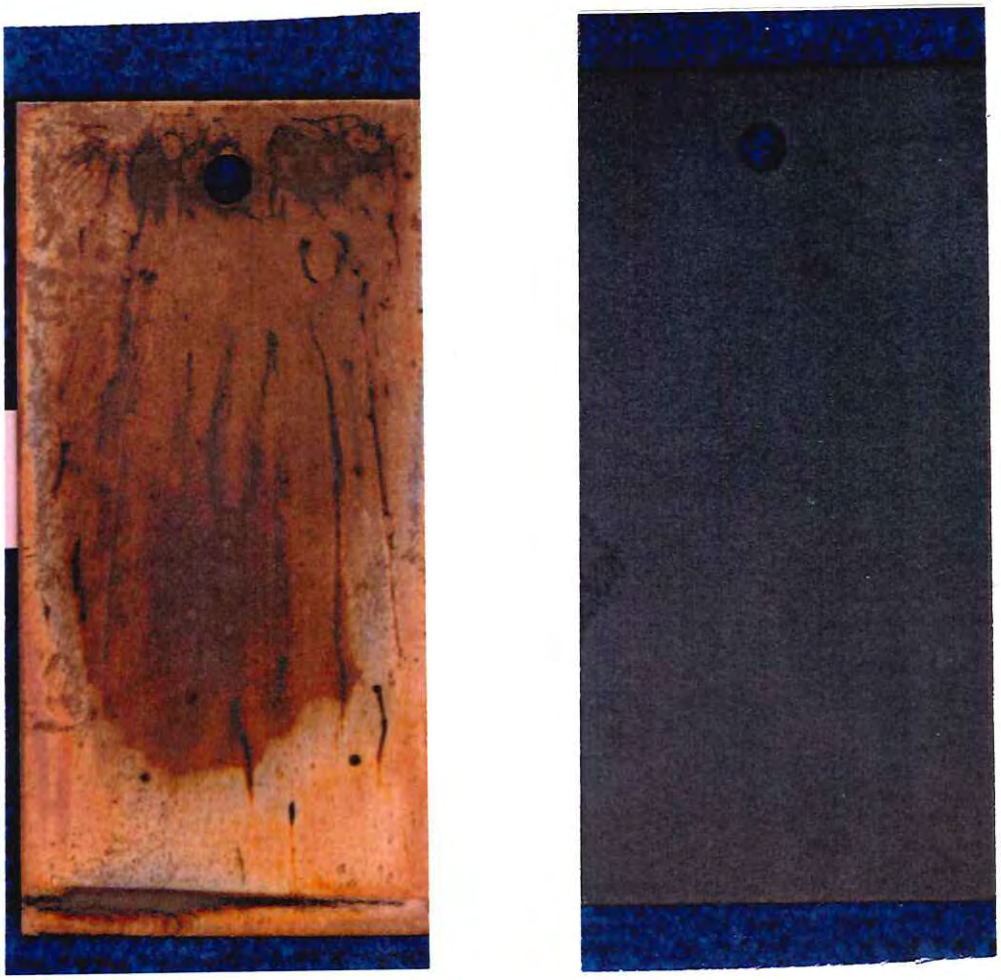

Figure 62 : Photographs of partially coated, chemically etched and grit blasted stainless steel plate

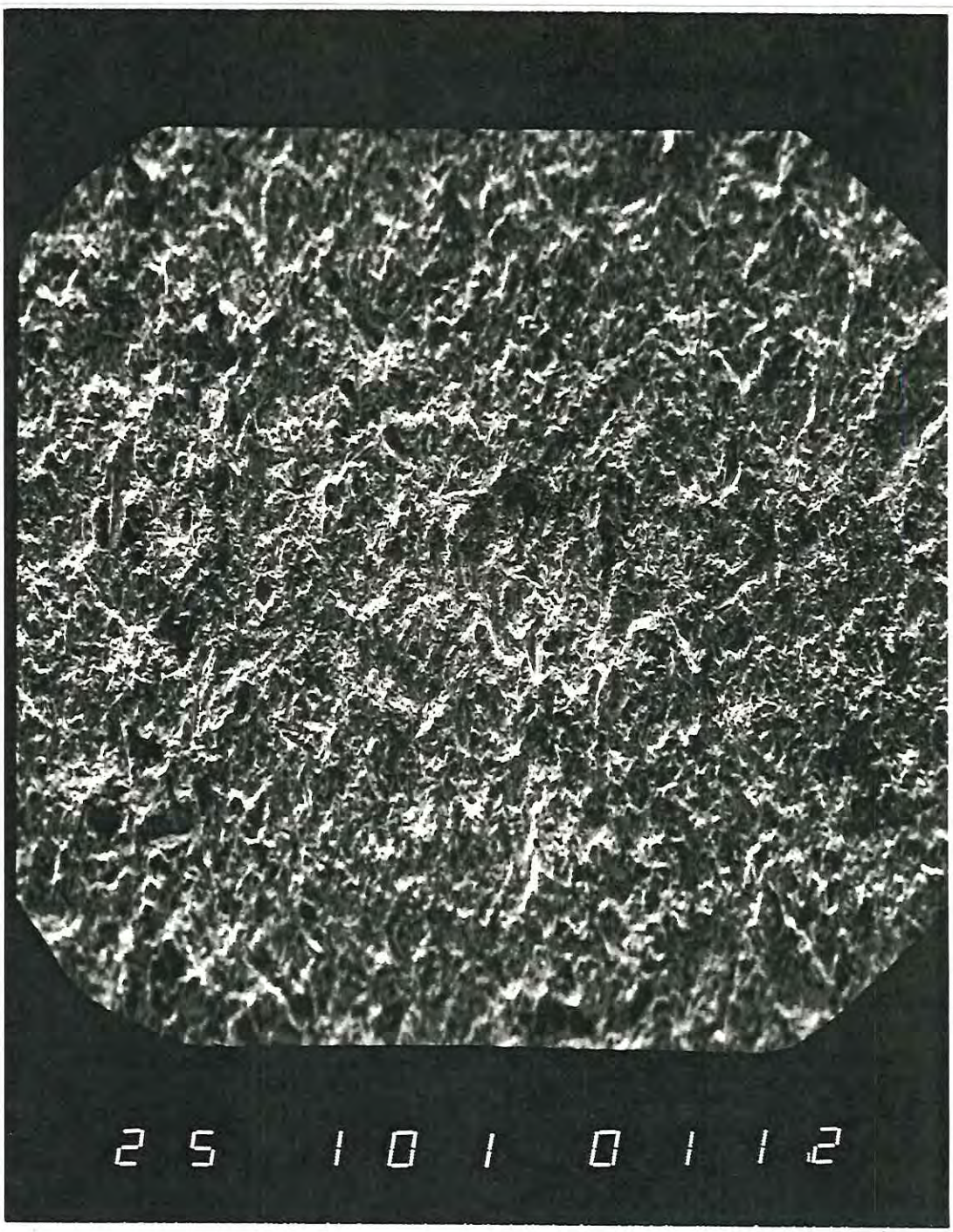

Figure 63 : SEM for grit blasted stainless steel plate

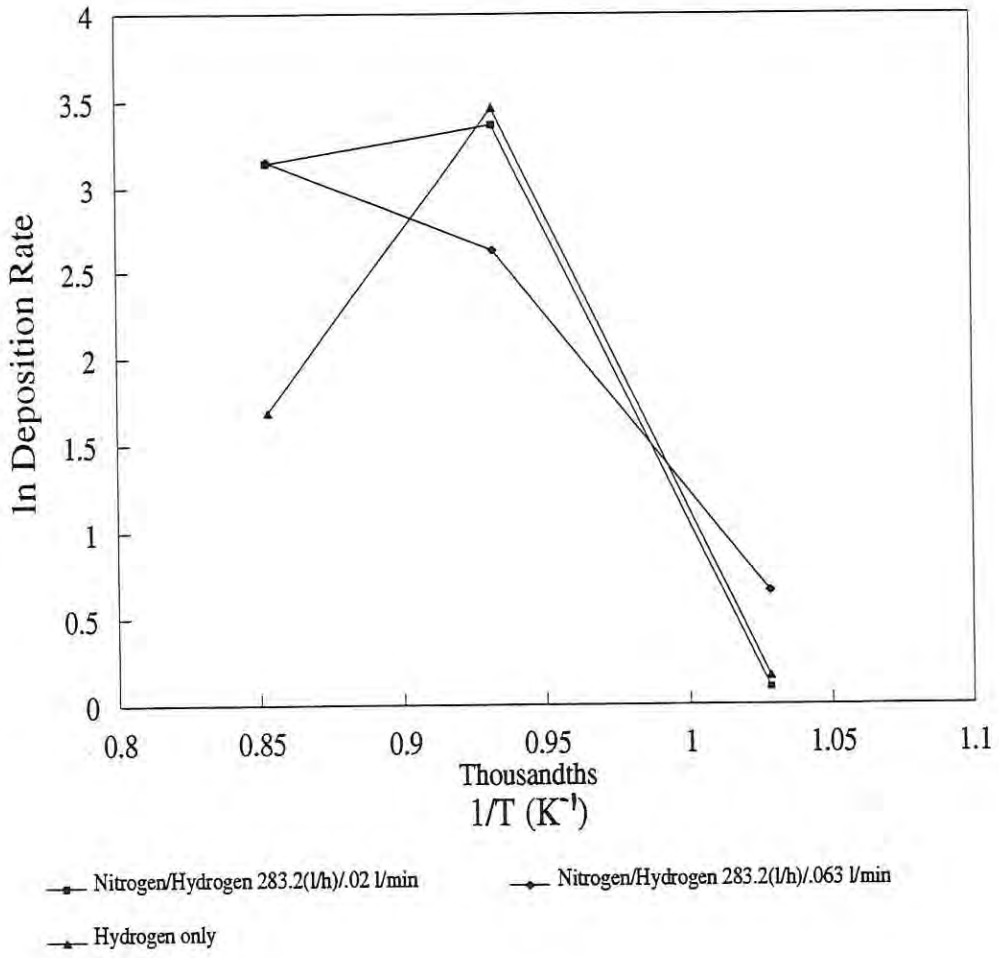

Figure 64 : Effect of H_2 concentration on deposition rate

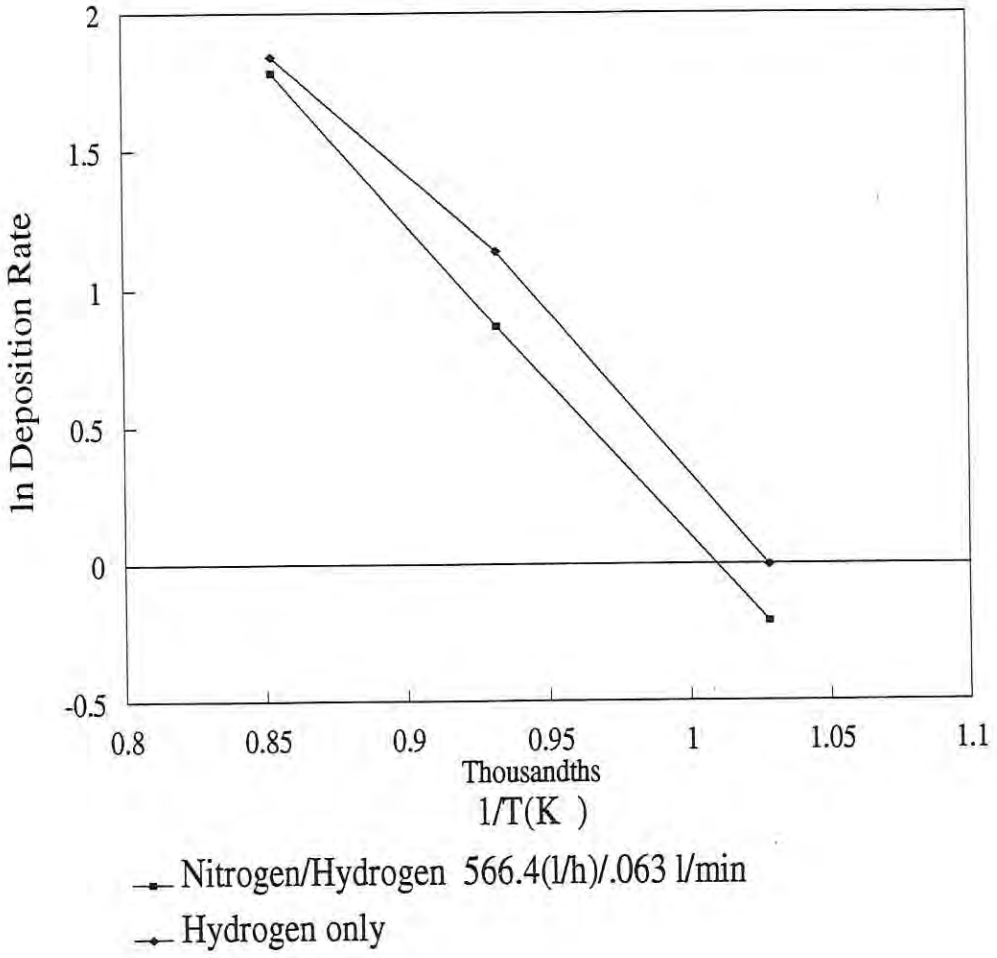

Figure 65 : Arrhenius plot showing effect of H_2 concentration on deposition rate in a fluidised bed reactor

stream also appears to enhance the surface finish of the coating. The presence of hydrogen produced a carbon free coating with low to medium silicon content (Figs. 66-67). The effect of hydrogen concentration in the synthesis of ceramic coatings from MTS has been reported widely[30,122,124]. It is considered that sufficient hydrogen concentration is essential to obtain higher yield and higher purity of SiC. The overall reaction of MTS at high temperature predicts the formation of SiC(s) and HCl(g). If it is true then HCl should be produced in quantitative yields. It has been observed in the present study that the formation of HCl ranged from 14 to 46 % (Tables 5-8), under different reaction conditions. It is therefore obvious that under studied operating conditions, the HCl yield is rather low; indicating that the reaction in the gaseous phase is not as simple. Obviously, various other chloro-species are predominant under the current experimental conditions. The excess of hydrogen helps to reduce the formation of other silicon based chloro-products and to increase the formation of HCl. The overall mechanism is discussed in detail under separate headings (Chemistry of the System). The concentration of hydrogen in the reactor is crucial as it was found that the experiments conducted in hydrogen atmosphere only produced coatings with poor surface characteristics (Fig 68). These results are consistent with the results obtained by Minato and Fukuda[30].

The coatings obtained from a fluidised bed reactor appears to have

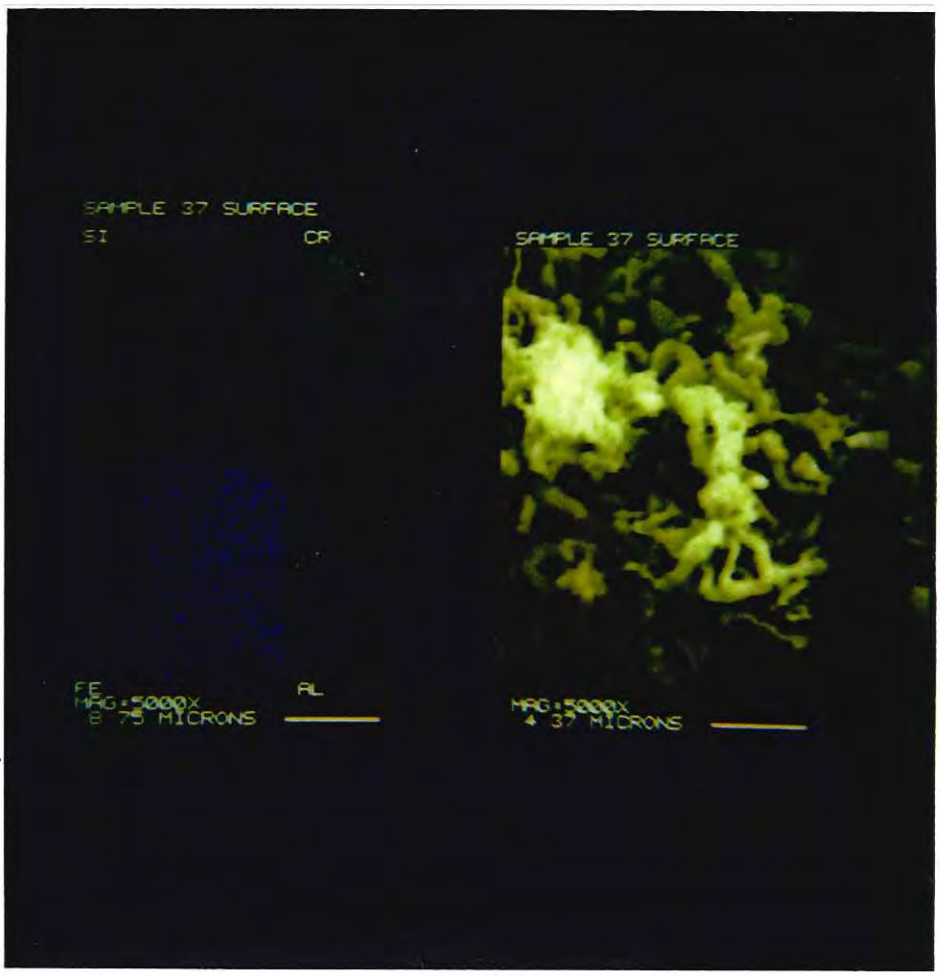

Figure 66 : SEM of coated stainless plate prepared in a N_2/H_2 atmosphere

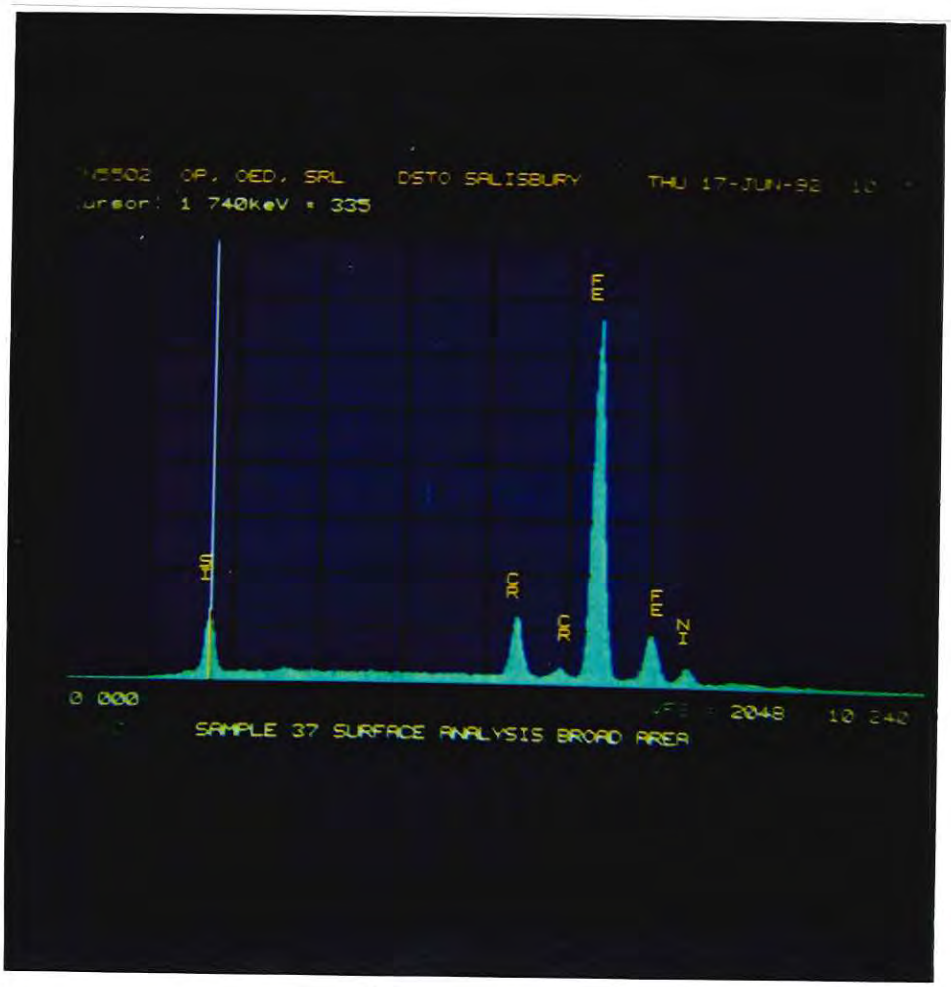

Figure 67 : SEM micrograph showing elemental distribution of a coated plate

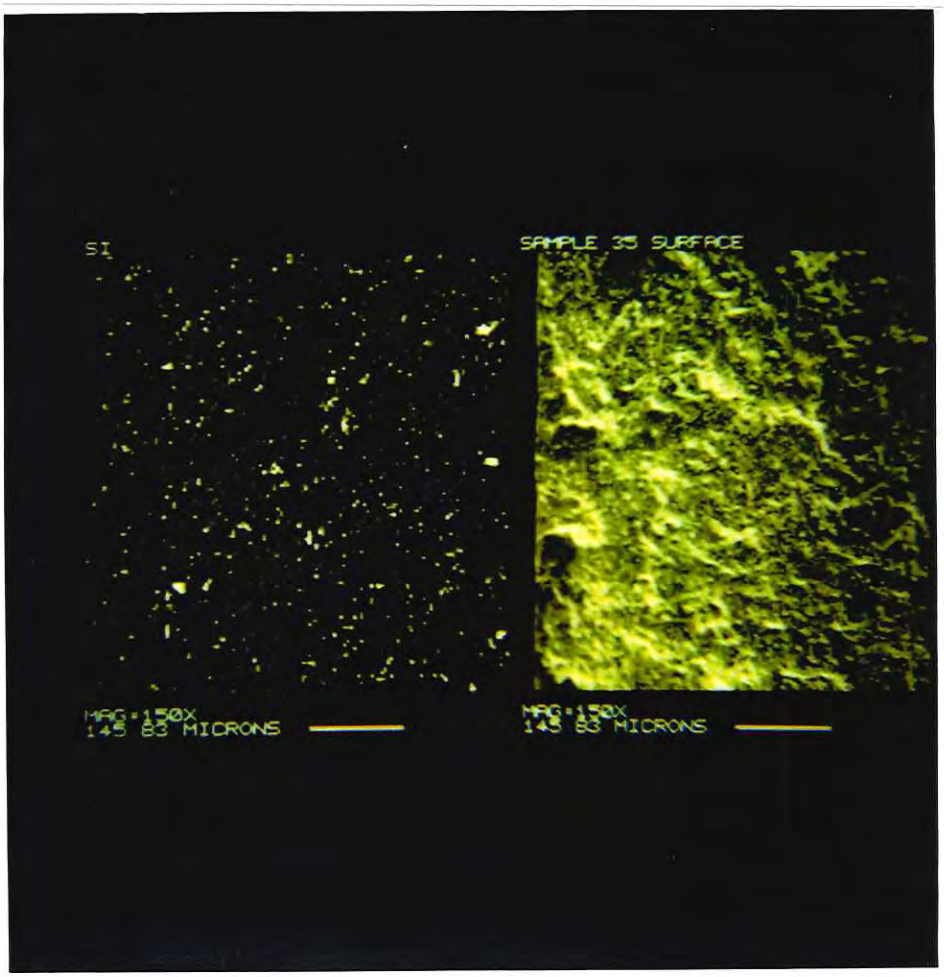

Figure 68 : SEM of a coated substrate prepared in a hydrogen atmosphere

superior surface characteristics in comparison to coatings prepared in a hot wall reactor. (Fig. 69). The best results were obtained in a fluidised bed reactor under N_2/H_2 atmosphere, using N_2 flow rate of 566.4l/h, N_2:H_2 mole ratio of 1:4 and 2.74 ml/min MTS feed rate. The effectiveness of fluidised bed can be attributed to its heat transfer characteristics, whereas in the hot wall reactor the sample may have different temperature profile over its total surface.

The effect of residence time on the deposition rate is shown in Fig. 70. The growth rate of the film decreases with time. This trend has also been observed by other workers [187]. The thickness of the coating increases to a initial minimum residence time and then drops linearly. This could be attributed to either depletion of the reactant near the surface of the substrate or most probably by the reduction in diffusion through the already formed layers of condensed phases, other products and reactant itself.

X-ray diffraction was conducted on samples to identify the coatings on the surface of the substrate. SEM studies only indicate the presence of various elements on the surface; it does not provide conclusive information as regards to the type of coatings. X-ray diffraction indicated that Si, SiO_2 and SiC were co-deposited under the majority of reaction conditions. Si and SiO_2 were the main species, while SiC deposits were extremely low. The deposition of Si and SiC have been reported by many

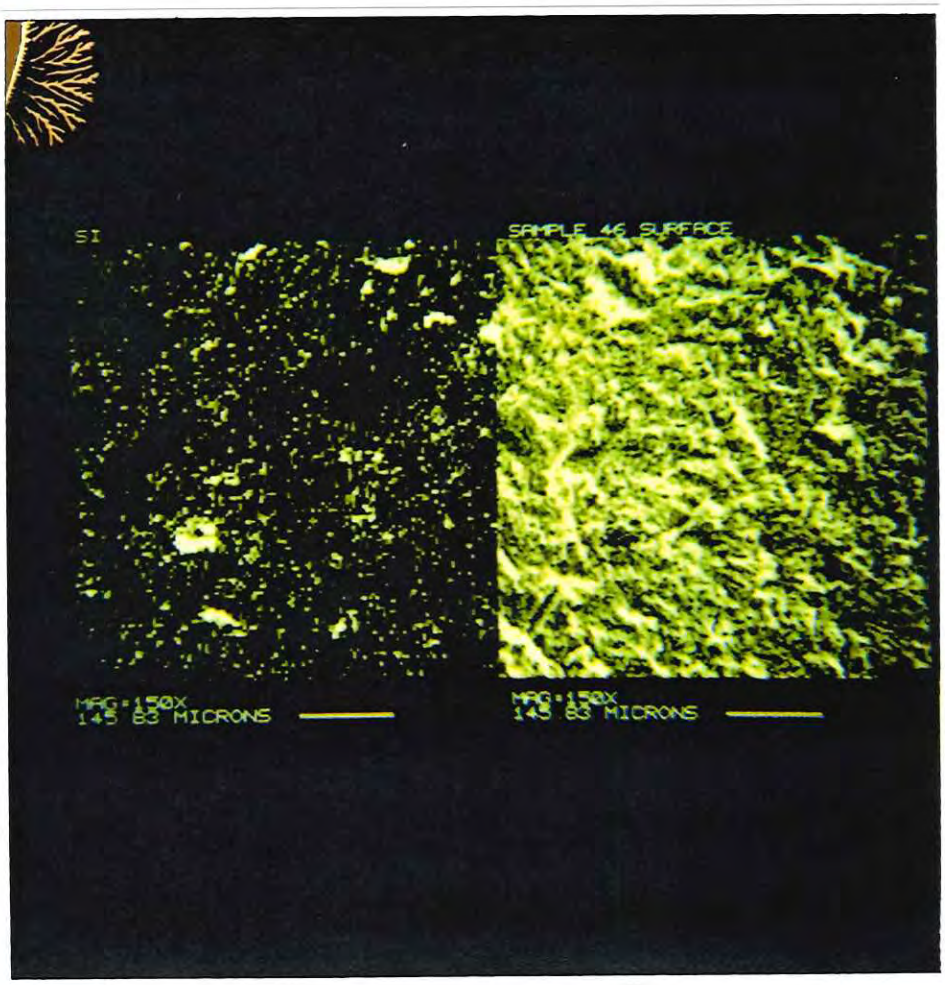

Figure 69 : SEM of a coated substrate prepared in a fluidised bed reactor under N_2/H_2 atmosphere

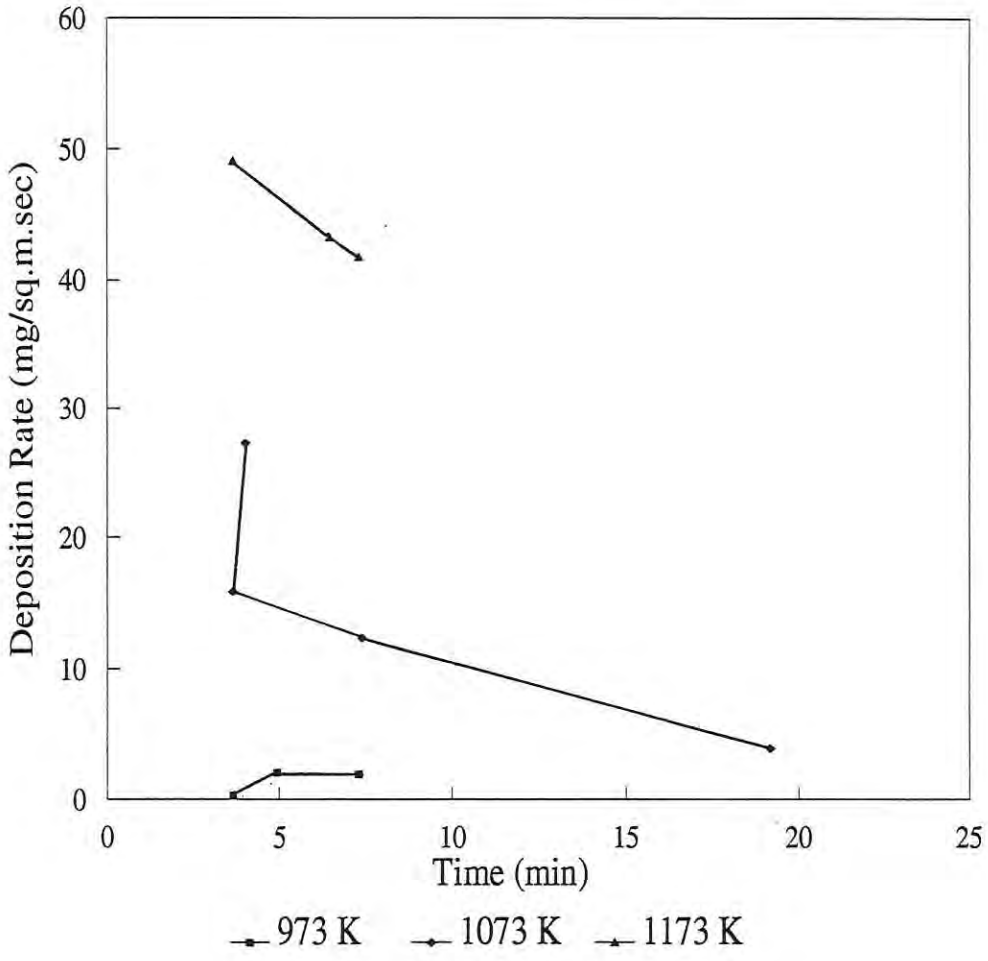

Figure 70 : Effect of residence time on deposition rate

investigators[30,122,124], and thermodynamic analysis predicts their formation. The deposition of SiO_2 as the major species as identified by X-ray diffraction, was not expected. However, the deposition of SiO_2 from MTS in the presence of water molecules is possible. MTS is an extremely hygroscopic material, and during feed by metering pump, the reactant was exposed to air. It is possible that MTS absorbed sufficient water from the atmosphere during feeding, which reacted with MTS at high temperature to produce CH_3SiCl_2OH or $CH_3SiCl(OH)_2$ intermediates, which upon decomposition and rearrangement produced SiO_2. This reaction is considered in proposing the overall reaction mechanism. Also, the data obtained by Mass Spectrometry, confirmed the presence of both of these hydroxy intermediates as indicated by m/e values.

Almost all the coated samples exhibited the presence of Si on the surface. This is consistent with the thermodynamic predictions, as the formation of Si is expected particularly at lower temperatures. As indicated separately under discussion on the chemistry of MTS, it is evident that a methyl radical is generated during first step decomposition at temperatures higher than 450°C. This radical, in the presence of hydrogen forms CH_4. The carbon needed to react with Si to form SiC type species had to be derived from CH_4. It is possible that at lower temperature (<1173 K) the decomposition of CH_4 is not complete. The temperature at which CH_4 has been reported to fully decompose is quoted at 1200 K[179]. It is therefore possible that the reaction temperature is not high enough to cause

complete decomposition of CH_4. This view is consistent with X-ray diffraction data, which indicates that the deposition of SiC species is rather low.

This view also supports the presence of various chloro-compounds, in some of the reactions, which are rather unstable and accelerated the formation of rust on the surface of the substrate. Chloro-species of Si and hydrogen are possible and are supported by thermodynamic calculations. To increase the concentration of SiC by using MTS, it appears temperatures higher than 1200 K are required or a source of carbon needs to be introduced in the system.

6.4 THERMODYNAMICS

Thermodynamic calculations for CVD of silicon based ceramic compounds have appeared in the literature since 1970's[124,166,180-182].

The majority of the data available from literature deals with calculations carried out at temperatures ranging from 1000 K to 2000 K, and pressure levels ranging from $P=10^2$ Pa to $P=10^6$ Pa. In the present investigation the temperature range of 773 K to 1273 K was taken into consideration and the total pressure of the system was maintained at 0.1 MPa (10^5 Pa). The experimental results of the present investigation indicating the Si

concentration formed and the elemental composition as determined from SEM scans are shown in Tables 15 and 16 respectively.

The experimental results indicated that SiC, Si, SiO_2 and C were the major species deposited depending on the reaction temperature and deposition conditions. The thermodynamic data, however, predicted the formation of SiC and C only at thermodynamic equilibrium under the experimental conditions used. The experimental results obtained at higher temperatures are in some agreement with the thermodynamic analysis. The formation of Si and SiO_2 was never predicted by the thermodynamic analysis. The deposition of SiO_2 was not taken into consideration during thermodynamic calculations, as water molecules were not included in the calculation. Overall the experimental results are in agreement with a majority of experimental data reported in the literature on the decomposition of CH_3SiCl_3 and the deposition of solid species. Minigawa and Gatos[180] used $SiH_4/C_3H_8/H_2$ system in their analysis and predicted three condensed phases in equilibrium. Such a system cannot represent the lowest free energy state of the system. The calculations show that all the available condensed Si and C must convert to SiC at equilibrium. Also they assumed that the α-species is the predominant SiC species, they did not consider β-SiC.

Lever[183] in his calculations considered only the formation of gaseous species using Si-H-Cl system. Most of the species predicted at lower

Table 15 : Reaction Conditions for coating a stainless steel substrate

Temp K	N_2 flow l/h	N_2:H_2 mole ratio	MTS flow ml/min	Si content	Visual assessment
973	0.3	-	10*	L	G
1073	0.3	-	10*	L	Ru
1173	0.3	-	10*	L	P
973	283.2	-	2.74	L-M	G
973	424.8	-	2.74	L	Re
973	566.4	-	2.74	L	Ru
973	708	-	2.74	L	Re
973	424.8	-	5.5	L	G
1073	283.2	-	2.74	H	G
1073	424.8	-	2.74	M	G
1073	566.4	-	2.74	vH	Ru
1073	283.2	-	5.5	M-H	Ru
1073	424.8	-	5.5	H	G
1173	283.2	-	2.74	M-H	P
1173	424.8	-	5.5	M-H	P
1173	566.4	-	2.74	H	P

1173	424.8	-	2.74	H	Re
973	283.2	1:1	2.74	L	Re
973	283.2	1:4	2.74	L	Re
973	-	0:H_2	2.74	L	Re
1073	283.2	1:1	2.74	L-M	P
1073	283.2	1:4	2.74	H	Re
1073	-	0:H_2	2.74	L	Re
1173	283.2	1:1	2.74	M	Re
1173	283.2	1:4	2.74	H	P
1173	-	0:H_2	2.74	M	G
1073	424.8	1:4	2.74	L	G
1073	566.4	1:4	2.74	L	G
1073	-	0:H_2	2.74	L	G
1173	566.4	1:4	2.74	H	G
1173	-	0:H_2	2.74	L	G

L = low, M = medium, H = high

P = poor, G = good, Re = reasonable, Ru = rusty

* using N_2 bubbler

Table 16 : Element Identification of Stainless Steel Grit Blasted Plate

No	Energy	Area	Element
1	1.472	3751	Al
2	1.744	11548	Si
3	5.401	68637	Cr
4	5.915	13026	Cr
5	6.385	163041	Fe
6	7.037	21359	Fe
7	7.454	11292	Ni
8	8.243	1271	Ni

temperature range is in agreement with his results except our analysis indicates the formation of $SiCl_3$ and $SiHCl_3$ species, however of the order of 1% by volume only.

Similarly, the calculations conducted by Turpin and Robert[159] on the CVD of $CH_3SiCl_3/CH_4/H_2$ and Christin et. al.[124], on CVD CH_3SiCl_3/H_2 system are in close agreement with our thermodynamic analysis, except that our calculation did not predict the formation of Si. The experimental data (Mass Spectrometry, X-ray diffraction and Scanning Electron Microscopy) however, supported the presence of Si.

The thermodynamic calculations along with experimental results given by Minato and Fukuda[30] for CH_3SiCl_3/H_2, CH_3SiCl_3/Ar and $CH_3SiCl_3/H_2/Ar$ systems indicated the formation of β-SiC+ C, β-SiC + Si, and β-SiC only, depending on the experimental conditions. They indicated that the experimental results below 1673 K did not agree with the thermodynamic analysis, however those obtained above that temperature were in agreement with thermodynamic calculations. They indicated that free-C was co-deposited with β-SiC at higher than 2000 K though the equilibrium composition was β-SiC and that free Si was co-deposited with β-SiC at temperatures lower than 1700 K.

Our investigations were exclusively concentrated in the temperature region below 1200 K and from the experimental data given in the literature, the

experimental and theoretical calculations clearly indicate that under applied experimental conditions it is not possible to deposit SiC species exclusively. The ceramic coatings obtained under specified experimental conditions would invariably include SiC, Si and C. It is however possible to eliminate the deposition of C by varying H_2 concentrations in the reactor, as shown in our experiments.

Also it is difficult to compare the theoretically obtained thermodynamic data with experimental data obtained in the literature in order to determine the usefulness of the thermodynamic equilibrium technique for setting up CVD processing. The problem includes: a) the range of conditions presented in the literature is very limited; b) the authors do not intentionally provide all the experimental details; and c) it is very difficult to identify small concentrations of different species that may be co-deposited during CVD reactions. However, there is one general agreement, that the thermodynamic calculations provide guidelines to set up the experimental conditions, which in turn, is helpful in the designing of the reactor.

Although there are conflicting literature reports of the phases co-deposited with SiC, with CH_3SiCl_3/H_2 system, a majority of the data closely agrees that the phases co-deposited with SiC include Si, C, and α-SiC. The predominant gaseous phase observed by various workers include $SiCl_4$, HCl and $SiCl_3$[166,184-186].

If β-SiC needs to be the major species, the results of Chin, et. al[61], Weiss and Diefendorf[187], and Minato and Fukuda[30] on CH_3SiCl_3/H_2 CVD system indicate that using the temperature range of 1400 K - 1500 K coupled with appropriate H_2 concentration, it is possible to maximise the deposition of SiC.

The experimental results of the present study indicate that for CH_3SiCl_3/H_2 or $CH_3SiCl_3/H_2/N_2$ system, fluidising method provides the deposition of SiC along with Si and SiO_2 at 800°C to 900°C. The Mass Spectrometry, DSC and IR study indicate that in our experimental set up, the water vapour was consistently taken up by the precursor material which in turn resulted in the formation of SiO_2. The details of SiO_2 formation is separately discussed under Chemistry of the System.

It should also be noted that the thermodynamic calculations allow to calculate the theoretical deposition efficiency for a given condensed phase under specified conditions. Deposition efficiency can be defined as the number of moles of a condensed phase which would deposit under thermodynamic equilibrium conditions divided by the maximum number of moles of the same phase which could be formed by the input gas if there were no thermodynamic or kinetic limitations[72]. These phase diagrams are useful in comparing the experimental data with theoretical calculation.

6.5 CHEMISTRY OF THE SYSTEM

Based on the experimental data obtained, the results reported in the literature, thermodynamic analysis and mass spectrometry data, the possible steps involved during the vapour phase decomposition of CH_3SiCl_3 and synthesis or formation of various condensed species can be followed.

The overall reaction of the formation of SiC by the decomposition of MTS is very well known and can be represented by the following equation:

$$CH_3SiCl_3 \rightarrow SiC(s) + 3HCl(g)$$

It is obvious from the above equation that the removal of chlorine from the system can be affected by the addition of H_2 to form HCl(g). Under appropriate H_2 environment, the reaction therefore will shift towards the right with the synthesis and deposition of SiC.

The gas phase reactions, however, are not that simple and involve probably, a number of steps and the formation of various other species alongside the most predicted and probably desirable final product. The results reported in the literature clearly indicate that numerous other

species involving basic elements Si, C, H and Cl are formed under different experimental conditions.

The results reported in the literature suggest that MTS decomposes into intermediates gaseous species containing hydrocarbons, possibly CH_4 and silicon chlorides. These products undergo further decomposition given favourable thermal environment. These equations can be expressed as:

$$CH_3SiCl_3 \rightarrow SiCl_3^{\cdot} + CH_3^{\cdot}$$
$$CH_3^{\cdot} + H^{\cdot} \rightarrow CH_4$$
$$CH_4 \rightarrow C + 2H_2$$

The hydrogen so formed in the reaction, reduces the silicon chloride to form HCl(g), i.e.,

$$SiCl_4 + 2H_2 \rightarrow Si + 4HCl$$
$$SiCl_3^{\cdot} + \frac{3}{2}H_2 \rightarrow Si + 3HCl$$
$$SiCl_2^{\cdot\cdot} + H_2 \rightarrow Si + 2HCl$$

Finally, it is assumed that Si and C so formed during the decomposition of silicon chlorides and methane, combine to form SiC, i.e.,

$$Si + C \rightarrow SiC(s)$$

The above reactions suggest that it is possible to deposit three species, viz., Si, C and SiC on the substrate. Thermodynamic calculations fully support this reaction path. Minato and Fukuda[30] reported that the concentration of the hydrogen and the temperature of the reactor is critical for the reaction to proceed towards the maximisation of the SiC deposit. They reported that their experimental data alongwith thermodynamic calculations, indicated that at low hydrogen concentrations, the decomposition of CH_4 to C is accelerated, therefore favouring the co-deposition of C with SiC. And if the concentration of hydrogen is adequate, it is possible to deposit pure SiC.

In the third scenario, if the concentration of hydrogen is very high, it favours the formation of hydrides with the reduction of Si formed during the reaction. This can be represented by the following equation:

$$Si + \frac{1}{2}H_2 \rightarrow SiH$$
$$Si + 2H_2 \rightarrow SiH_4$$
$$Si + HCl + H_2 \rightarrow SiH_3Cl$$

However, at extremely high concentrations of H_2, it was not possible to obtain any solid phase.

The chemistry of the reaction can be followed from thermodynamic data, if the assumption made for calculation of such data are valid and appropriate selection of species and data banks are used. It should however be noted, the thermodynamic approach is a purely theoretical approach which indicates the influence of the deposition parameters on the possible composition of both vapour and solid phases. Our thermodynamic calculations support the above reaction mechanism, except at our temperature range, no Si deposition was predicted. The experimental data however, was in agreement with this mechanism.

In addition, it is thought that there are other reactions which could be considered before a final plausible reaction mechanism is proposed.

Mass spectrometry data (Figs. 71-72) provides some information on the type and amount of species formed during decomposition. The experimental conditions, as described earlier, are such where only unimolecular decomposition are taken into consideration, assuming that there are no bimolecular collisions between the radicals formed, reactants and products of reaction. This data was therefore used to understand the first step decomposition.

Two possible decomposition reactions can be given using the m/e of species, i.e.,

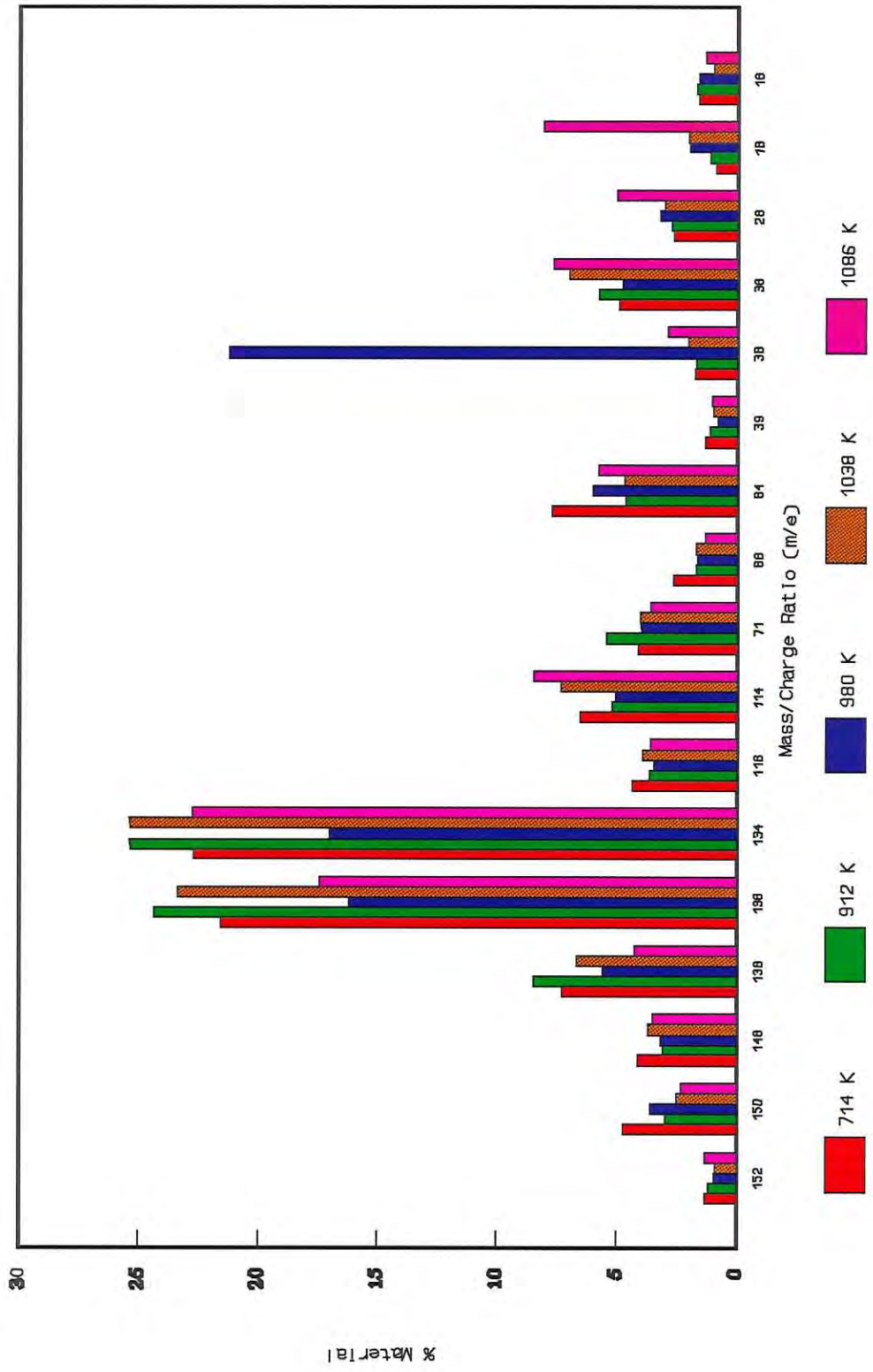

Figure 71: Comparative Mass Spectrometry data over the temperature range 714 K - 1086 K (Courtesy C. Stamatiou)

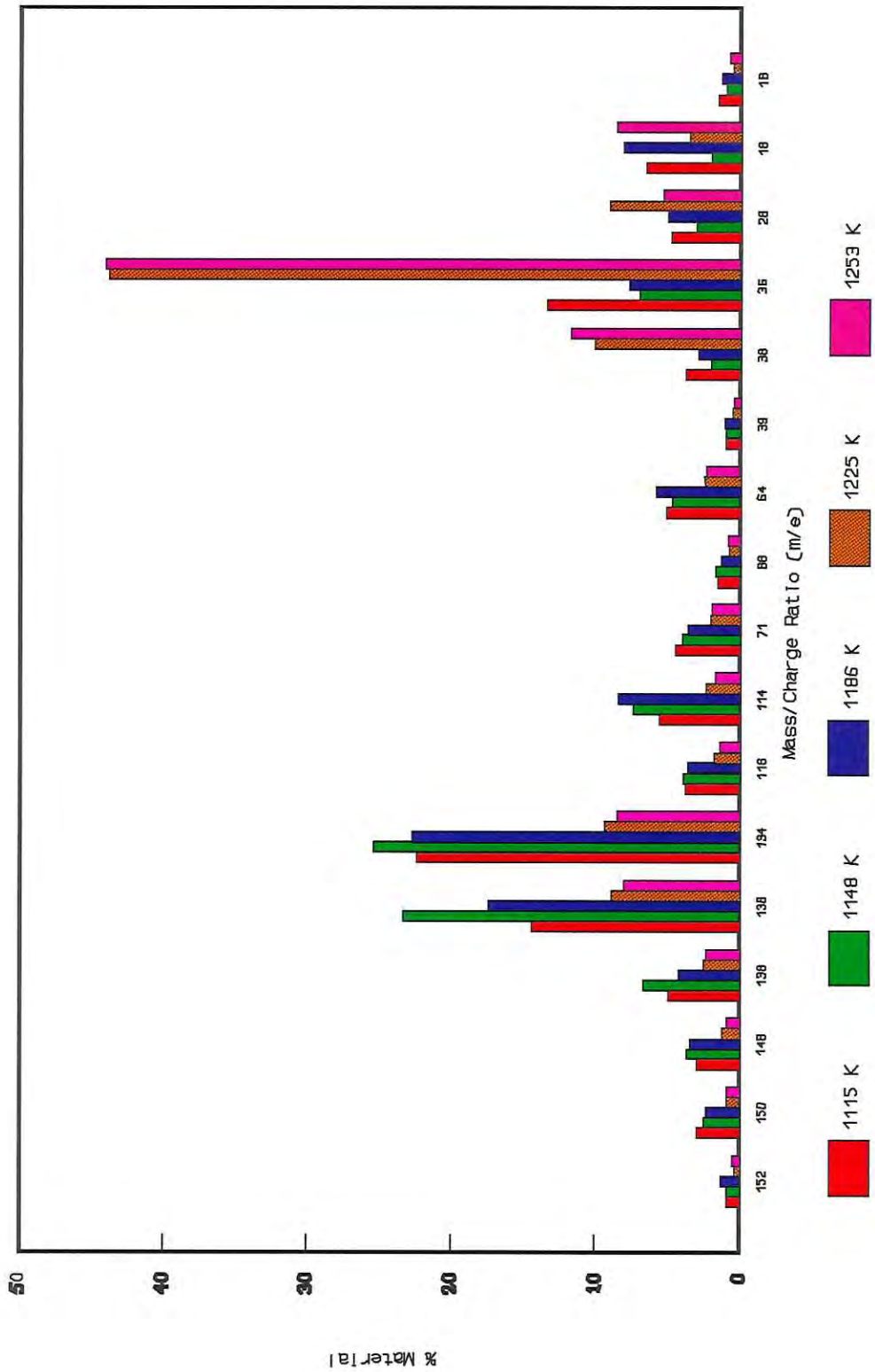

Figure 72: Comparative Mass Spectrometry data over the temperature range 1115 K - 1253 K (Courtesy C. Stamatiou)

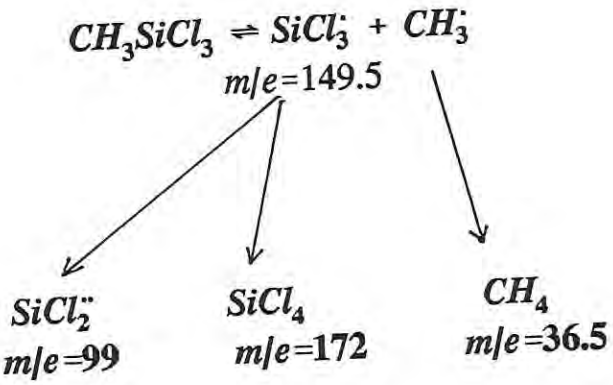

There are some other species encountered during this analysis. It is recognised that MTS, an extremely hygroscopic material, appears to have absorbed and reacted with water. This can then easily lead to the formation of hydroxides according to the following reaction:

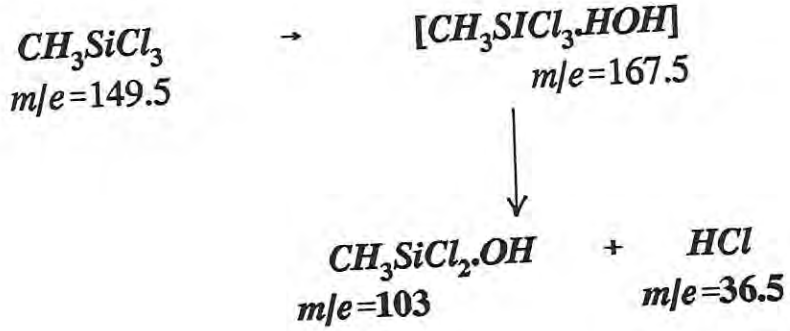

The presence of water has been detected using IR spectrometry(Fig. 73) as well as DSC data.

It is assumed that an excess of water molecules in the MTS could also lead to the formation of dihydroxides, i.e.,

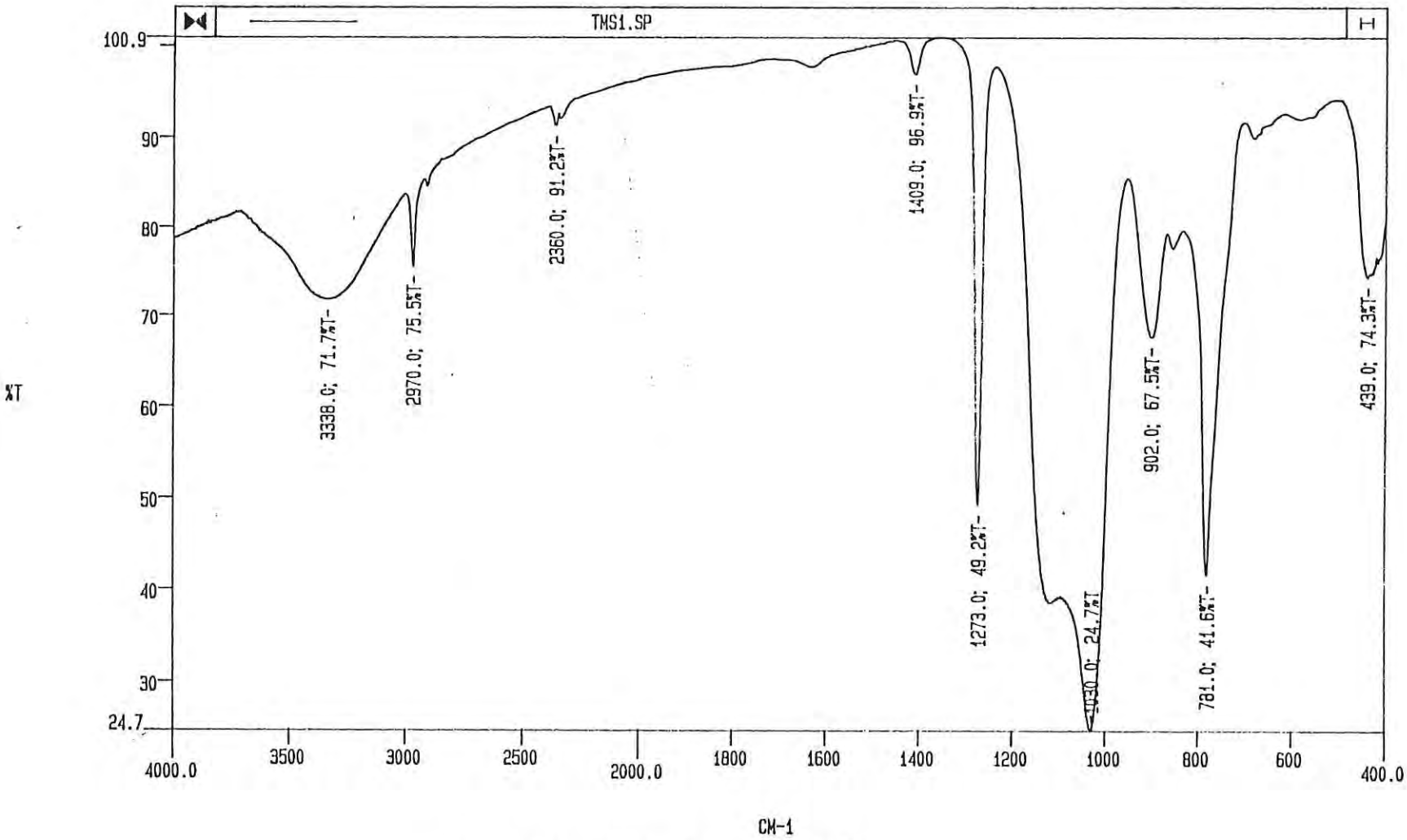

Figure 73 : Infrared scan of MTS

$$[CH_3SiCl_2.2HOH](g) \rightarrow CH_3SiCl(OH)_2(g) + 2HCl(g)$$
$$m/e = 150 \qquad m/e = 112.5 \qquad m/e = 36.5$$

Taking into consideration mass spectrometric data, experimental results, and thermodynamic calculations, a plausible reaction mechanism at 800°C -900°C is proposed (Fig. 74). It is believed that under applied experimental conditions SiC is not the only species obtained, appreciable amounts of SiO_2 and Si are also co-deposited. In some reactions, formation of C is also imminent. The reaction mechanism highlighting the pathway for the formation of SiO_2 is given in Fig. 75.

The main gaseous species, based on thermodynamic calculations include $SiCl_4$, HCl, hydroxychlorosilanes, CH_4 and $SiHCl_3$ have been taken into consideration.

6.6 REACTION KINETICS

The reaction kinetics is important to understand the overall deposition process in a CVD reactor. Papers published in the last 20 years have illustrated the value of kinetic studies for the decomposition of various organosilane compounds and the formation of Si- based final products[188-191]. It is therefore necessary that the respective

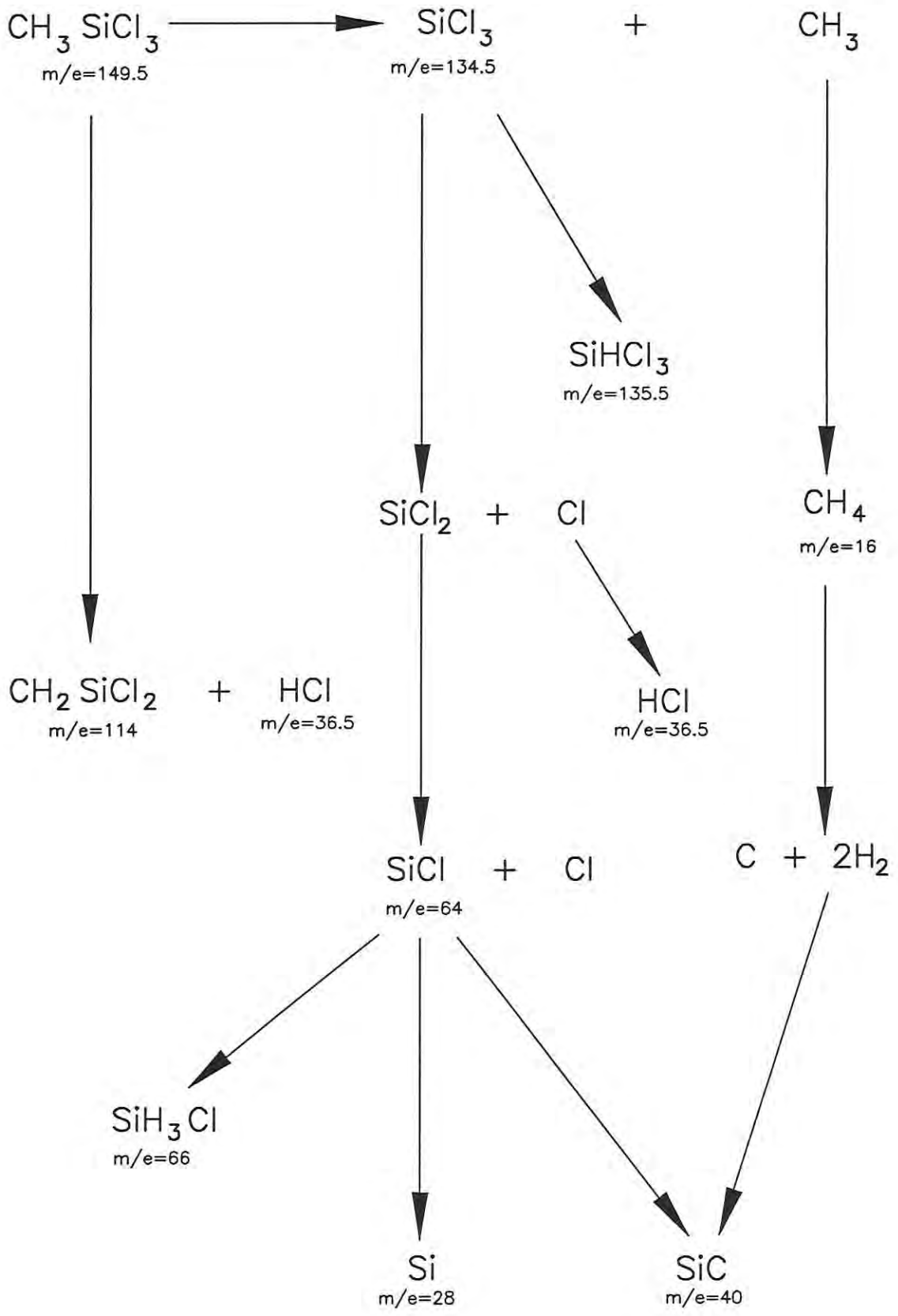

Figure 74: Plausible reaction mechanism for the decomposition of methyltrichlorosilane.

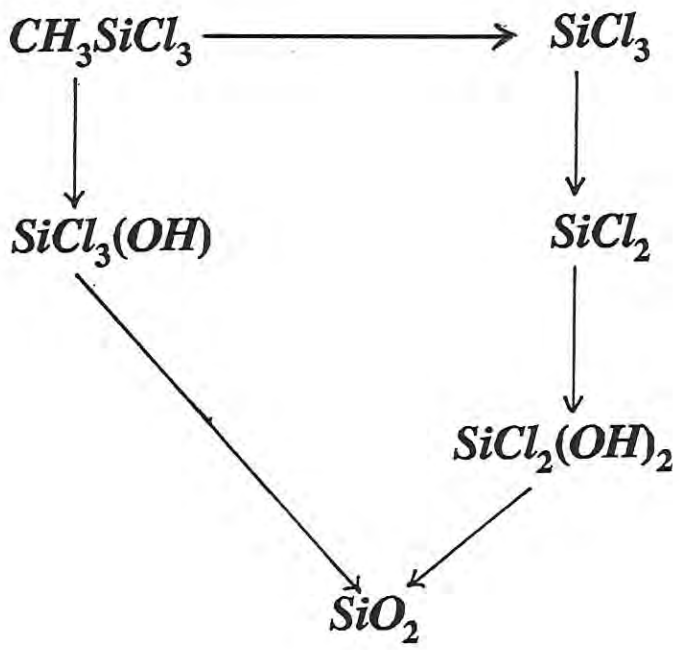

Figure 75 : Reaction mechanism for the formation of SiO_2

contributions of physical and chemical steps involved in the CVD process to the kinetics of deposition be investigated experimentally.

An attempt is therefore made to determine the kinetic parameters such as activation energy (E_a) and order of reaction (n) using Differential Scanning Calorimetry (DSC), and from the data obtained for deposition rates under different temperature conditions.

Thermoanalytical methods based on thermogravimetry (TG), differential thermal analysis (DTA) and DSC have been used increasingly in the determination of kinetic parameters[192]. In the present investigation the Perkin Elmer DSC 7, which has a built-in kinetics software for the determination of kinetic parameters has been employed. Because of the volatile nature of the material, the analysis was conducted in a stainless steel high pressure pan assuming that there was no leakage to the atmosphere, and that the decomposition products were contained, and were free to interact to form new products. In other words, the DSC pressure pan represented a small reactor, and the reaction was followed under dynamic conditions at a heating rate of 5°C per minute. The recorded data on integration with the kinetics software gave the values for E_a and n, (Fig. 37) taking into consideration the overall reaction. DSC technique is however limited to the maximum temperature of 998 K only. The deposition reactions were however conducted in the CVD reactor up to 1173 K. From the DSC scan (Fig. 37), it can be concluded that the

material has absorbed water vapour from the atmosphere (peak at 250°C). This is also apparent in IR scan (Fig. 73). The decomposition of MTS appears to commence around 460°C as indicated by a set of multiple peaks. The change in heat capacities, as observed from various peaks, is indicative of either the decomposition of materials or formation of products. Partial area analysis of the DSC scan for MTS, allows the determination of the effect of temperature on the rate co-efficient (Figs. 76-77) and depletion of reactants with time (Fig. 78). The kinetic data generated by using DSC software up to 998 K has been found to be in close agreement with the kinetic values given in the literature.

For the validation of the DSC 7 kinetic software calculations, the method suggested by Ozawa[157], which has also been adopted as an ASTM standard method for determining the Arrhenius kinetic constants for the screening of potentially hazardous materials, was employed[192]. This technique is an extension of the method originally proposed by Kissinger[156], where the variation of the peak temperature of a DTA peak with heating rate has been used to determine the activation energy of first order processes. Later workers[193] have shown that realistic values for E_a and k_o can not be obtained as the maximum rate of reaction occurs somewhere before the maximum peak point. The Kissinger method was later modified by Rogers and Smith[193], and Ozawa[157,194].

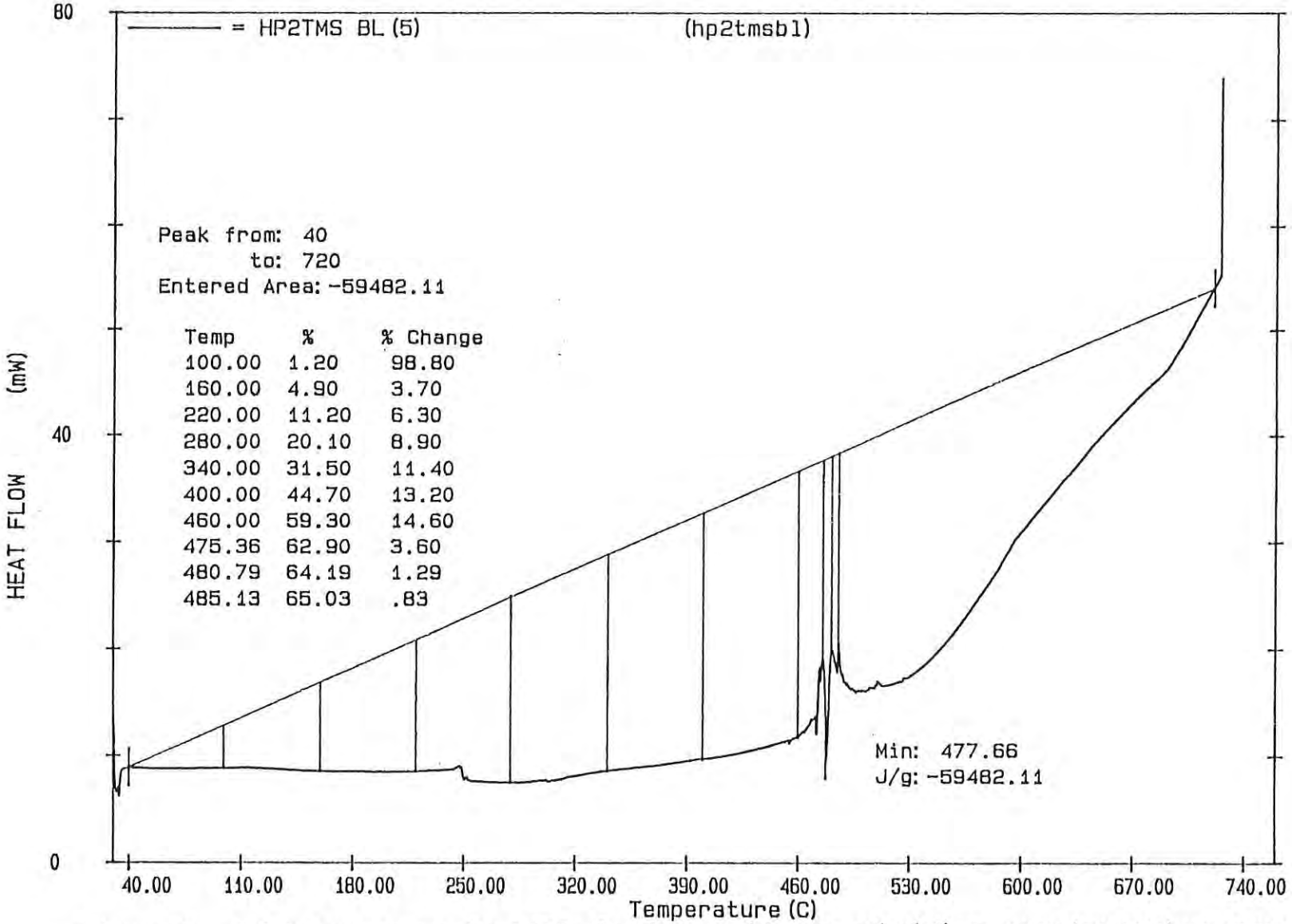

Figure 76 : DSC thermogram for MTS showing partial area calculations over temperature range 100°C - 485.13°C

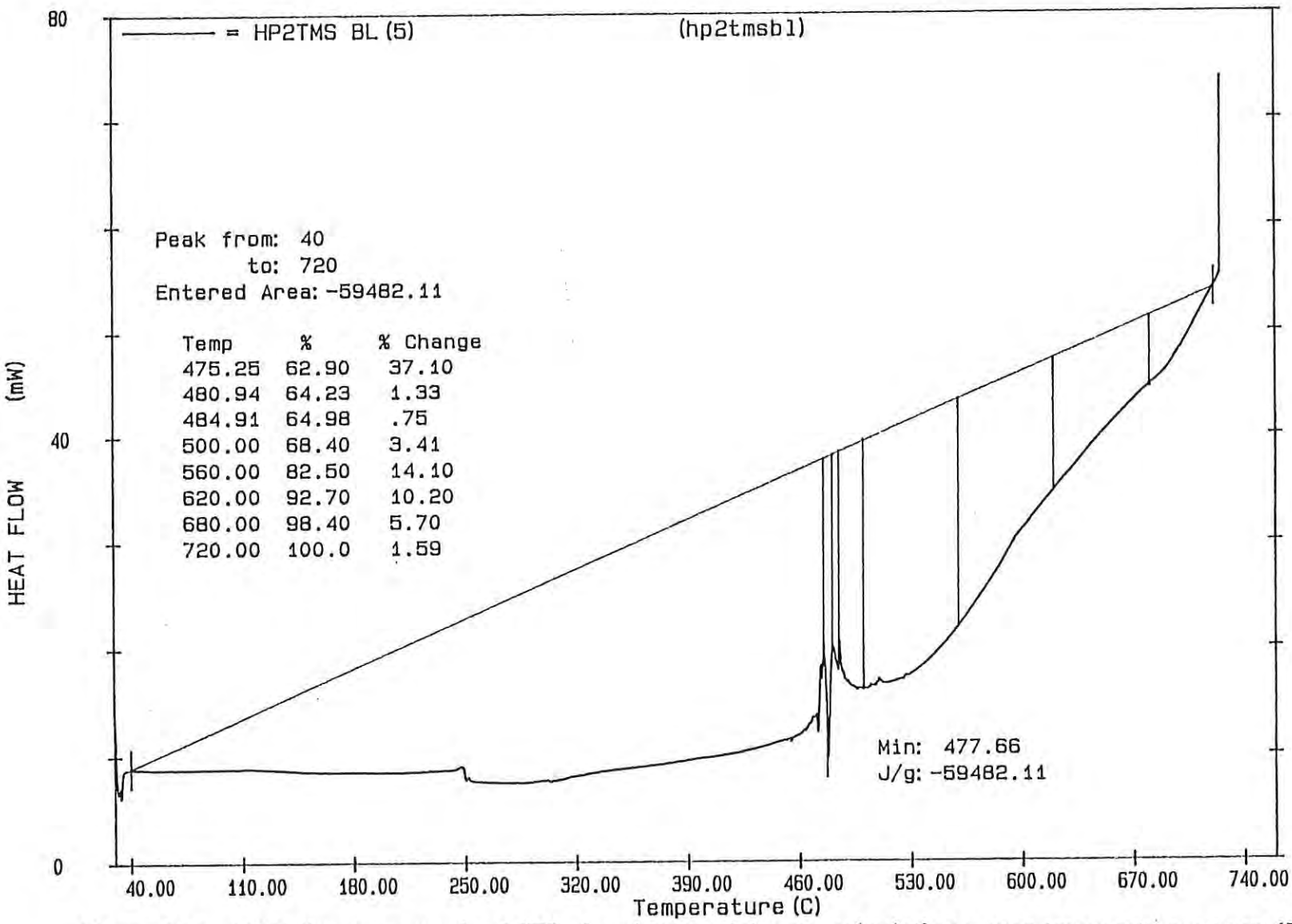

Figure 77 : DSC thermogram for MTS showing partial area calculations over temperature range 475.25°C - 720°C

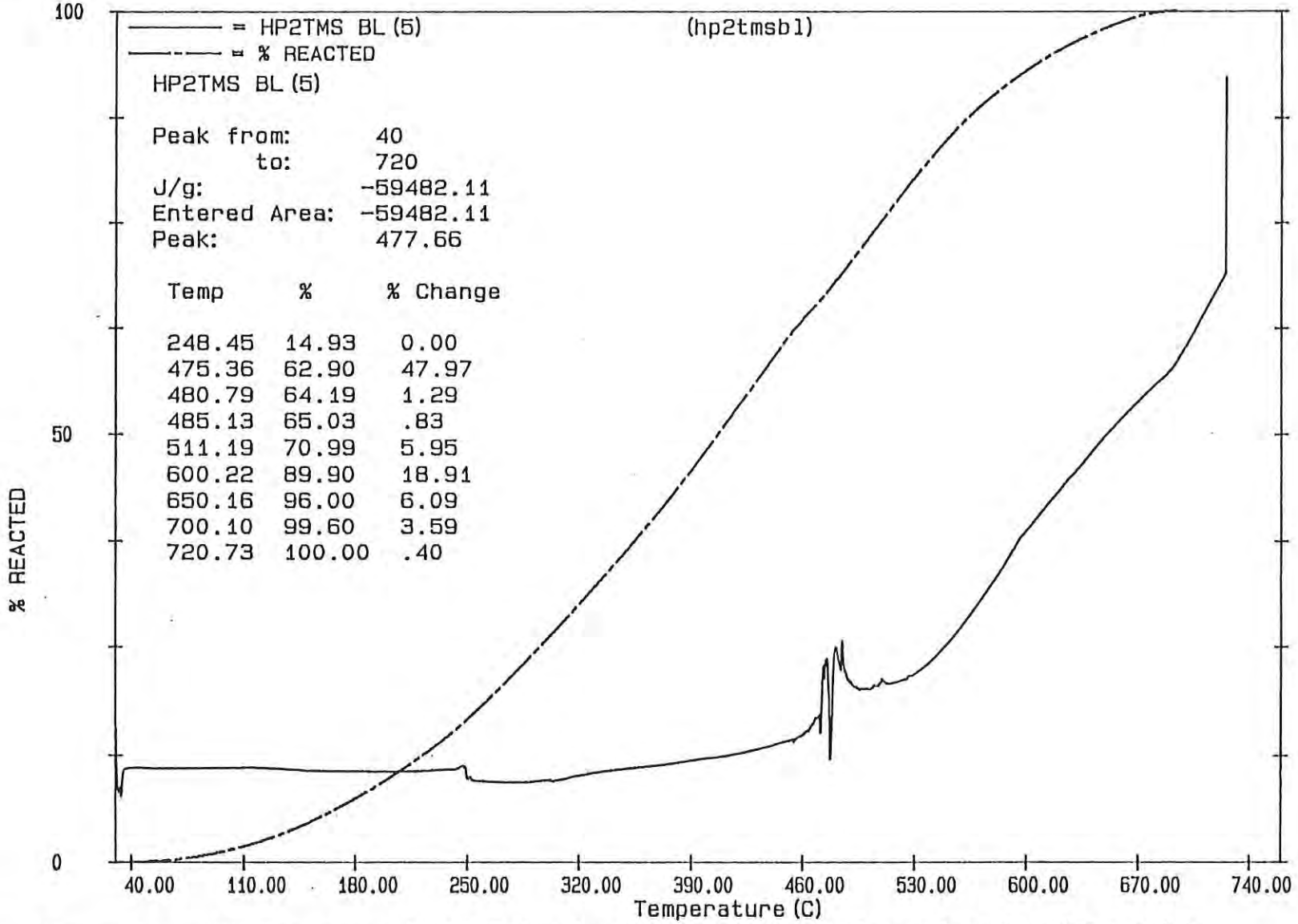

Figure 78 : DSC thermogram for MTS showing depletion of reactants as a function of time(min)

Ozawa used DSC to obtain T_{max} at a variety of heating rates and thus the E_a can be obtained from the slope of a plot of log heating rate(β) versus $1/T_{max}$, where T_{max} is the temperature of maximum reaction rate.

This technique was employed in the present study to determine the E_a (activation energy) and k_o (pre-exponential factor) for nitrocellulose; a material which is used as one of the standards chosen by ASTM E-27 committee; and the standard epoxy resin, commonly used in industry. The materials were analysed using DSC 7, and the E_a calculated from the plots of log β vs. $1/T_{max}$. MTS was also analysed by this method in order to compare the results obtained from kinetic software. The calculated values for nitrocellulose, epoxy 828 and MTS, along with literature values, are given in Table 14 and those calculated by DSC 7 kinetics software are given in Table 17.

The results clearly indicate that the E_a values obtained by Ozawa's method are in close agreement with the literature values as well as with values obtained using DSC kinetic software. It is therefore assumed that the technique using DSC 7 software is quite appropriate for the determination of E_a and n.

The kinetic parameters have also been calculated from the experimental data obtained from CVD reactor, from deposition rates at variable temperatures. The Arrhenius plots (ln R vs. 1/T K) for deposition in a hot wall reactor under nitrogen, nitrogen/hydrogen, and hydrogen

Table 17 : Kinetic Parameters as calculated using DSC 7 Kinetics Software

Material	E_a kJ/mol	k_o 1/sec	n
MTS	14.19 +/- 0.3	3.59×10^{-3}	0.6 +/- 0.01
Nitrocellulose	10.05 +/- 0.21	9.37×10^{-3}	0.35 +/- 0
Epoxy 828	67.47 +/- 1.45	3.33×10^{6}	1.06 +/- 0.02

atmosphere are shown in Figs. 60 and 64 respectively. The relationships between amount of deposition with time is shown in Fig. 70. The Arrhenius plots for the rate of deposition in a fluidised bed in N_2/H_2, and H_2 atmosphere is shown in Fig. 65. Within limits it can be deduced that the amount of deposited species is linked with the deposition time by a linear dependence. The deposition rate is higher in the initial stages and decreasing with time except for results obtained at temperature 973K. The E_a calculated from the Arrhenius plots are given in Table 18. These values vary from 120kJ/mole to 400kJ/mole and are in accordance with the literature values. The E_a for SiC deposition at temperatures above 900°C has been reported to be 15kcal/mol[195,196], 16kcal/mol[197], 47kcal/mol[29], 51.5kcal/mol[118], and 400kJ/mol[].

The X-ray diffraction and SEM study has indicated the deposition of SiO_2, SiC, Si and C, depending upon experimental conditions. These results indicate that the limiting step of the kinetic process appears to be heterogeneous. The low dependence of the deposition rate on temperature also denotes that deposition mechanism limited by mass transport through the gaseous phase. The Reynold's number values below 2000 were obtained indicating that the CVD reactor is operating in the laminar flow region. The results of Parretta et. al.,[167] (Fig. 79) are in agreement with our results.

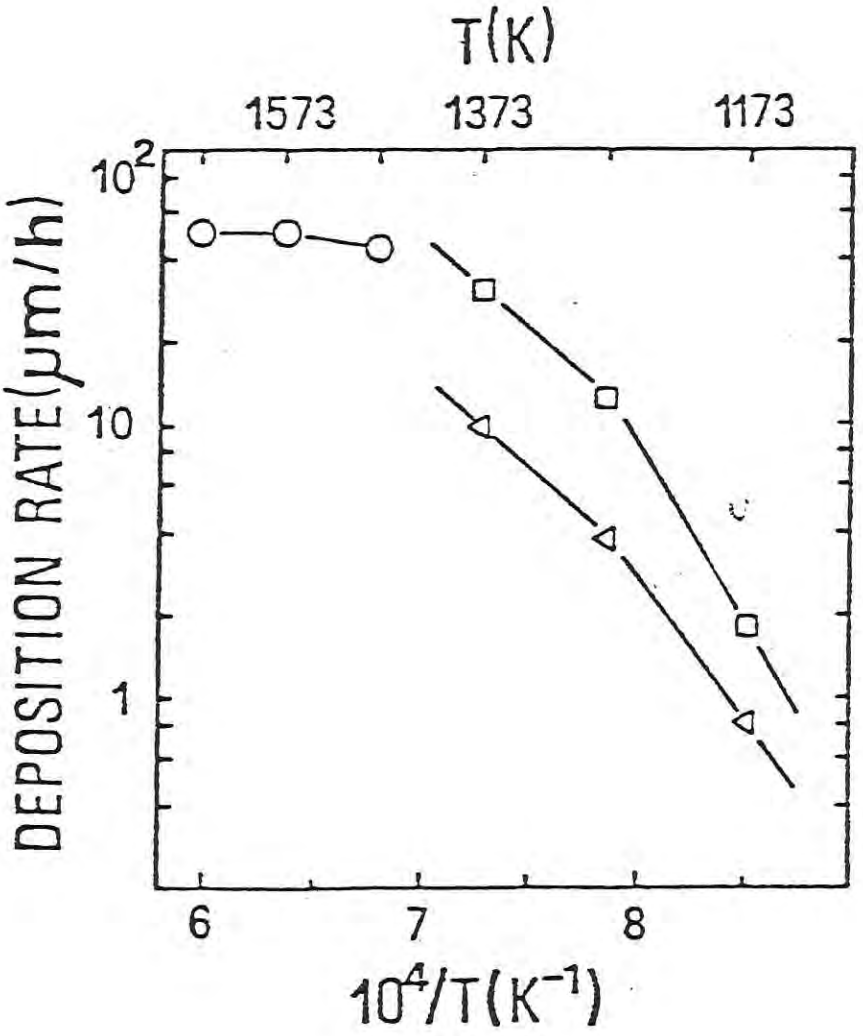

Figure 79 : SiC deposition as a function of inverse absolute temperature for $SiCl_4/C_3H_8/H_2$ system (o), and $MTS/H_2/Ar$ system at 100kPa (Δ) and 40 kPa (□)

Table 18 : Activation energies from deposition rate data

Hot Wall Reactor			
N_2 flow rate l/h		MTS feed rate mol/h	E_a kJ/mol
283.2		1.4	277.9
424.8		1.4	393.4
566.4		1.4	292.4
424.8		2.81	505.4
N_2 flow rate l/h	N_2:H_2 mole ratio	E_a^1 kJ/mol	E_a^2 kJ/mol
283.2	1:1	50.6	619.09
283.2	1:4	121.7	373.12
-	0:H_2	409.4	625.4
Fluidised Bed Reactor			
N_2 flow rate l/h	N_2:H_2 mole ratio	E_a kJ/mol	
566.4	1:4	207	
-	0:H_2	191.85	

It can also be deduced that under operating conditions the rate of deposition increases with reciprocal temperature following typical Arrhenius relation but decreases with increasing time(Fig. 70). It appears that the rate of deposition goes through two stages. During the first stage the rate of growth increases exponentially with reciprocal temperature, and follows the typical Arrhenius relationships. In the second stage, however, interdiffusion of reactants and reaction products hinders the rate of reaction at the surface, thus reducing the growth rate at the surface of the substrate with increasing surface temperature. At this stage the rate of deposition appears to become less dependant on temperature and more dependant on the rate of diffusion through the boundary layer at the surface of the substrate. The diffusion through the surface is affected by the flow dynamics of the reactor system. As the pressure is kept constant, the trend seems to continue. However, it has been reported[187] that by decreasing the pressure of the system it is possible to enhance the surface diffusion during the second stage of the reaction.

6.7 CONCLUSIONS

This investigation revealed that both hot wall and fluidised bed reactor can be applied to CVD reactions. Fluidised bed technique was however found superior to hotwall deposition technique. It is also evident that the understanding of the process fundamentals with respect to reaction

kinetics, thermodynamics and reaction mechanism is essential in order to optimise the deposition process.

CVD chemistry is quite complex. Two types of reactions predominate inside the CVD reactor: gas phase reactions and surface reactions. The type and extent of gas phase reactions is directly related to the temperature and partial pressure of the reactants. It has been reported that high reactant concentrations lead to gas phase nucleation[198]. It is very difficult to predict steps involved in gas phase nucleation.

As observed in the present investigation, and also from the data available from the literature, gas phase reactions, under different conditions, can be detrimental by forming additional species that may be classified as impurities.

CVD reaction data have been reported in terms of growth rates and its dependence on temperature. It is extremely difficult to optimise or relate the reactor design with the deposition process from this data, and not much attention is paid to the mechanistic approach in order to highlight the deposition of impurities with the desired product. The study largely indicates that the data from various analyses can be pooled together to unravel the reactions that may be operating under different conditions. It was beyond the scope of this study to optimise the reaction conditions to deposit single deposit on the substrate. In fact, this study clearly points

out the relevance of various analytical tools to achieve perceived coatings, by adopting overall mechanistic approach. It should also be considered that reaction pathways for different reactants, reactors, and substrates are not identical, but initial studies can lead to very near optimal conditions for experimental purposes. The overall modelling of processing variables of CVD to predict experimental conditions to acquire desirable results requires major attention. This will ultimately lead to cost reduction and improvement of the final product.

BIBLIOGRAPHY

[1] Somiya, S. (ed.) **Advanced Technical Ceramics**, Academic Press Inc., San Diego, California(1989).

[2] O'Bannon, L.S. **Dictionary of Ceramic Science and Engineering**, (1983)p54.

[3] Perkins, W.W. (ed.) **Ceramic Glossary**: American Ceramic Society, (1984)p13-14.

[4] Richardson, D.W. "Design, processing development and manufacturing requirements of ceramic and ceramic matrix composites", **Tech. Report**, Office of Tech. Assessment Dec. 1985.

[5] Smith, C.W. The Basic Principles of Flame Spraying. In B.N. Chapman, and J.C. Anderson, (eds.) **Science and Technology Of Surface Coating**, Academic Press, London, (1974)p262.

[6] Scott, K.T. **Materials for the Process Industries**, C79/82, (1982)p99.

[7] Moss, A.R. and Young, W.J. Arc Plasma Spraying. In B.N. Chapman and J.C. Anderson, (eds.). **Science and Technology of Surface Coating**, Academic Press, London, (1974)p287.

[8] Gadgil, V.J. and Ramesh, V.R. **Tool and Alloy Steels**, 21, No.10, (October 1987)p384.

[9] Bunshah, R.F., High Rate Physical Vapour Deposition Processes. In **Materials Coating Techniques** Lecture Series 106, (1980)L2.

[10] Bunshah, R.F. Applications of Physical Vapour Deposition Processes. In **Materials Coating Techniques** Lecture Series 106, (1980)L11.

[11] Holland, L. The Basic Principles of Sputter Deposition. In B.N. Chapman, and J.C. Anderson, (Eds.) **Science and Technology of Surface Coating**, Academic Press, London, (1974)p369.

[12] Berghaus, B., **U.K. Patent Specification**, 510, 993 (1938).

[13] Mattox, D.M., **Sandia Corporation Report**, SC-DR-218-63 (1963).

[14] Mattox, D.M. **J. Appl. Phys.** 34, (1963)p2493.

[15] Schwartz, M. Deposition from Aqueous Solutions : An overview. In R.F. Bunshah, et.al., **Deposition Technologies for Films and Coatings**. Noyes Publication, Park Ridge NY (1982).

[16] Campbell, D.S. The Basic Principles of Anodization. In B.N. Chapman, and J.C. Anderson, (eds.) **Science and Technology of Surface Coating**, Academic Press, London, (1974)p87.

[17] Cross, J.A. **Electrostatics Principles, Problems and Applications**, IOP, Bristol, England (1987).

[18] Khera, R.P. The Basic Principles of Electrolytic Deposition. In B.N. Chapman, and J.C. Anderson, (eds.) **Science and Technology of Surface Coating**, Academic Press, London, (1974)p69.

[18A] Wachtman, J.B. Jr. and Haber, R.A., Session on Advances in Ceramics Compositions, Properties and Applications, **Summer National Meeting, American Institute of Chemical Engineers**, Seattle, Washington, August 25-29, 1985.

[19] Blocher, J.M. Jr. **Vapour Deposited Materials**, Vapour Deposition. In. C.F. Powell, J.H. Oxley and J.M. Blocher, Jr., (eds.) Wiley, New York(1981).

[20] de Lodyguine, J.S. **US Patent 575,002,** (1893).

[21] Brossa, F. **Industrial Ceramics**, 9, No.3,(1989)p120.

[22] Powell, C.F., Oxley, J.H. and Blocher, J.M. (eds.). **Vapour Deposition**, John Wiley & Sons, New York, (1966).

[23] Yee., K.K., **Int. Met. Rev.**,Review No. 226,(1978) No.1.

[24] Bryant, W.A., **Journal of Material Science**, 12, (1977)p1285.

[25] Blocher, J.M. (Jr.), Vuillard, G.E. and Wahl, G. (eds.), **CVD VIII**, ECS, (1981).

[26] Bryant, W.A. **J. Crystal Growth**, 35 (1976)p257-61.

[27] Kaae, J.L. **Procs. Flat - Plate Solar Workshop on the Science of Silicon Material Preparation**, Phoenix, Ariz., USA. Aug 23-25 (1982).

[28] Guilleray, J., Lefevre., R.L.R., Price, M.T.S. and Thomas, J.P. **Fifth Int. Conf. Proc.** Fulmer, Slough, Bucks, England, Sept. 21-26 (1975).

[29] Kenigfeit, A.N., Davidov, A., Dergunova, V.S., Nabatnikov., A.P. and Surskii, G., **Fizika i Khimiya Obrabotki Materialov**, 18, No.2, (1984)p76-79.

[30] Minato, K. and Fukuda, K., **J. Nuclear Mat.**, 149, (1987)p233-246.

[31] Fatzer, E.R. and Kochka, L.E., **Ger. Offenl. 2.357.814**, (30.5.1974).

[32] Pring, J.N. and Fielding, W. **J. Chem. Soc.** 95, (1909)p1497-1506.

[33] Takabashi, T. and Kamuja, H. **High Tempertaure- High Pressure**, 9, (1977)p437-43.

[34] Motojima, S., Sugiyama, K. and Takahashi, Y. **J. Cryst. Growth**, 30, (1975)p233-39.

[35] Motojima, S. and Sugiyama, K., **J. Mater. Sci.**, 14, (1979)p2859-64.

[36] Randich, E., **Thin Solid Films**, 63, No.2., (1979)p309-14.

[37] Pierson, H.O. A Survey of Chemical Vapour Deposition Of Refractory Transition Metal Borides. In. H.O. Pierson (ed.) **Chemically Vapour Deposited Coatings**, 82nd Annual Meeting of the American Ceramic Society, Amer. Chem. Soc., Chicago, Illinois, (April 27-30, 1980)p27.

[38] Doyle, D., Titanium Nitrate Surface Technologies, Melbourne, personal communication.

[39] Rai-Choudhury, P. and Formigoni, N.P. **J. Electrochem. Soc.**, 116, (1969)p1440-1443.

[40] Nickl, J.J. and Von Braunmuhl, C., **Journal of Less-Common Metals**, 37, (1974)p317-329.

[41] Middelhoek, J. and Klinkhamer, A.J., **CVD V**, (1979)p19-29.

[42] Nagasima, N. and Kubota, N., **Japanese Journal of Applied Physics**, 14, No.8, (1975)p1105.

[43] Carlsson, J-O, **Procs. of the 17th European Solid State Device Research Conference**, ESSDERC (1987)p315-26.

[44] Watts, B.E., **Thin Solid Films**, 18, (1973)p1.

[45] Silvestri, V.J., Irene, E.A., Zirinsky, S. and Kuptsis, J.D., **Journal of Electronic Materials**, 4, No.3, (1975)p429-444.

[47] Oxley, J.H., Beidler, E.A., Blocher, J.M. Jr., Lyons, C.J., Park, R.S. and Pearson, J.H., **Nuclear Applications**, 1, (1965)p567.

[48] Oxley, J.H., Powell, C.F. and Blocher, J.M. Jr., **US Patent 3,178,308** (1965).

[49] Ikawa, K. and Iwamoto, K., **J. Nuc. Mater.**, 45, (1972)p67.

[50] Blocher, J.M. Jr., **Deposition Technologies for Films and Coatings**, Noyes Publication, Park Ridge, NY, (1982).

[51] Ogawa, K. and Katsuichi, I., **Report No. JAERI-M-82-152**, (1982).

[52] Stinton, D.P., Angelini, P., Caputo, A.J. and Lackey, W.J., **Proc. Symp. on Nucleation and Crystallization in Glasses**, Washington, DC, USA, 3 May 1981.

[53] Parr, T.R., **Powder and Bulk Engineering**, (October 1988)p15-20.

[54] Shroff, A.M., **High Temperature Materials**, 6th Planese Seminar, edited by F. Benesovsky. Metalwerk Plansee Ag Recitto, (1969)p854.

[55] Shim, H.S., Haskell, R.W. and Byrne, J.G., **CVD III**, p715.

[56] Spear, K.E., **Chemical Vapour Deposition**. In T.O. Sedgwick, et.al., (eds.), The Electrochemical Society, Princeton, (1979)p1.

[57] Bernard, C. and Madar, K., **Chemical Vapour Deposition of Refractory Metals and Ceramics**. In T.M. Besmann and B.M. Gallois, (eds.), Material Research Society, Pittsburgh, Pennsylvania, (1990).

[58] Bernard, C., Daniel, Y., Jacquot, A., Vay, P. and Ducassoir, M., **J. Less Common Metals**, 40, (1975)p165-171.

[59] Bernard, C., In J.M. Blocher, G.E. Vuillard and G. Wahl (eds.), **Eighth International Conference on CVD**, The Electrochemical Society, Pennington, (1981)p3-16.

[60] Gulden, T.D., **J. Amer. Ceram. Soc.**, 51, No.8, (1968)p424-427.

[61] Chin, J., Gantzel, P.K. and Hudson, R.G., **Thin Solid Films**, 40, (1977)p57-72.

[62] Federev, J.I., **Thin Solid Films**, 40, (1977)p81-96.

[63] Ducarroir, M., Jaynes, M., Bernard, C. and Deniel, Y., **J. Less Common Metals**, 40, (1975)p173-183.

[64] Thebault, J., Naslain, R. and Bernard, C., **J. Less Common Metals**, 57, (1978)p1-20.

[65] Schäfer, H. **Chemical Transport Reactions**, Academic Press, NY (1964).

[66] Spear, K.E. **J. Chem. Ed.** 49, (1972)p81.

[67] Spear, K.E. High Temperature Reactivity. In **Treatise on Solid State Chemistry**, 4. N.B. Hanney (ed.), Plenum Press, NY (1976)p163.

[68] Reisman, A. and Sedgwick, T.O. Chemical Vapour Deposition and Solid Vapour Equilibria. In **Phase Diagrams**, IV, A.M. Alper (ed.), Academic Press, NY (1976) p1.

[69] Stull, D.R. and Prophet, H. (1978), **JANAF Thermodynamic Tables**, Bureau of Standards and subsequent updates, (1971).

[70] Hűltren, R., Desai, P.D., Hawkins, D.J., Gleiser, M. and Kelley, K., **Selected values of the Thermodynamic Properties of the Elements**, American Society for Metals, (1973).

[71] Hajiev, S.N. and Agarunov, B.J., **J. of Organometallic Chemistry**, 22, (1978)p305-311.

[72] Spear, K.E. Applications of Phase Diagrams and Thermodynamics to CVD. In **Proc. Seventh International Conference on Chemical Vapour Deposition**, T.O. Sedgwick and H. Lydtin (eds.) Electrochem. Soc., New York, (1979)p1.

[73] Ducarroir, M. and Bernard, C., **J. Electrochem. Soc.** 123, (1976)p136.

[74] Nickl, J.J. and Scheitzer, K.K., **J. Less Common Metals**, 26, (1972), 335. Nickl, J.J., Reichle, M. and Vesper, R., CVD III,p369.

[75] Nickl, J.J., Schweitzer, K.K. and Luxenberg, P., **CVD III**,p 4.

[76] Manabe, T., Gejyo, T., Seki, H. and Eguchi, H., **CVD III**,p 25.

[77] Minigawa, S. and Seki, H., **CVD IV**, p 50.

[78] Ban, V.S., **J. Electrochem. Soc.**, 118, (1971)p1473.

[79] Klima, P., Silhavy, J., Rerabek, V., Braun, I., Cerny, C., Vonka, P. and Holub, R., **J. Crystal Growth**, 32, (1976)p165.

[80] Hunt, L.P. and Sirtl, E., **J. Electrochem. Soc.**, 119, (1972)p1741.

[81] Hunt, L.P. and Sirtl, E., **J. Electrochem. Soc.**, 120, (1973)p806.

[82] Yang, W.C., Brecher, L.E. and Cleary, J.G., **CVD IV**,p382.

[83] Wong, P. and Robinson, McD., **J. Amer. Ceram. Soc.** 53, (1970)p 617.

[84] Blocher, J.M. Jr., **Material Science and Engineering**, A 105/106, (1988)p435-441.

[85] Blocher, J.M. Jr., **J. Vac. Sci. Technol.**, 11, No.4, (1974)p680-686.

[86] Evensteijn, F.C. and Peck, H.L., **Philips Res. Rep.**, 25, (1970)p472-481.

[87] Dittman, F.W., **Adv. Chem. Ser.**, 133, (1974)p463-473.

[88] Clotrui, M.E., Kee, R.J. and Miller, J-A., **J. Electrochem. Soc.**, 131, (1984)p425-434.

[89] Oxley, J.H., Transport Processes. In J.H. Oxley, et. al. (eds.). **Vapour Deposition**, Wiley, New York, (1966)p102-125.

[90] Carlton, H.E. and Oxley, J.H., **A.I.Ch.E.J.** 13(1967)p571.

[91] Bryant, W.A. and Meier, G.H., **J. Electrochem. Soc.**, 120, (1973)p 559.

[92] Eversteyn, F., Severin, P.J.W., Vanderbrekel, C.H.J. and Peek, H.L., **J. Electrochem. Soc.**, 117, (1970)p925.

[93] Kuznetsov, F.A. and Belyi, V.I., **J. Electrochem. Soc.**, 117, (1970), p785.

[94] Lever, R.F., **J. Chem. Phys.**, 37, (1962)p1174.

[95] Vanderputte, P., Giling, L.J. and Bloem, J., **J. Crystal Growth**, 31, (1975)p299.

[96] Aggour, L., Fitzer, E., Ignotowitz, E. and Sahebkar, M., **Carbon 12** (1974)p358.

[97] Nyce, A.C., Vondra, B.L., Cline, R. and Pepkowitz, L.P., **Tr. Amer. Nuclear Soc.**, 7, (1984)p427.

[98] Gebhardt, J.J., **CVD IV**,p 460.

[99] Carlton, H.E. and Oxley, J.H., **A. I. Ch. E. J.**, 13, (1967)p86.

[100] Cadoret, R. and Cadoret, M., **J. Crystal Ground**, 31, (1975)p142.

[101] Berkeley, J.F., Brenner, A. and Reid, W.E. Jr., **J. Electrochem. Soc.**, 114, (1967)p561.

[102] Seymour, W.C. and Byrne, J.G., **CVD V**, p815.

[103] Pearce, M.L. and Mareic, R.W., **J. Am. Ceram. Soc.**, 51, (1968)p84.

[104] Bowman, M.G., USAEC, **Research and Development Report**, TID-7653, (Part II), Washington, DC, (1962).

[105] Preban, A.G. and Pleckie, H., **CVD II**,p367.

[106] Fitzer, E. and Hegen, D., **Angewardte Chemie**, 91, (1979)p316-325.

[107] Joyce, B.A. and Bradley, R.R., **J. Electrochem. Soc.**, 110, (1963)p511.

[108] Bhola, S.R. and Mayer, A., **RCA, Rev., 24**, (1963)p511.

[109] Mayer, S.E. and Shea, D.E., **J. Electrochem Soc.**, 111, (1964)p550.

[110] Armirrotto, A.L., **Solid State Technol.**, 11, (1968)p43.

[111] Richman, D. and Arlett, R.H., **J. Electrochem. Soc.**, 116, (1969)p872.

[112] **Procs. Chemical Vapour Deposition of Refractory Metals, Alloys, and Compounds**, A.C. Schaffhauser, (ed.), Amer. Nuclear Soc., Hinsdale, IL, (1967).

[113] **Procs. 2nd Int. Conf. on Chemical Vapour Deposition**, J.M., Blocher, Jr., and J.C. Withers, (eds.), The Electrochemical Soc., Princeton, NJ, (1971).

[114] **Procs. 3rd Int. Conf. on Chemical Vapour Deposition**, F.A. Glaski, (ed.), Amer. Nuclear Soc., Hinsdale, IL, (1972).

[115] **Procs. 4th Int. Conf. on Chemical Vapour Deposition**, G.F. Wakefield and J.M. Blocher, Jr., (eds.), The Electrochem. Soc., Princeton, NJ, (1973).

[116] Bloem, J., **Pure and Appl. Chem.**, 50, (1978)p435-447.

[117] Bhat, D.G., In T.S. Sudarshaw, (ed.) **Surface Modification Technologies, An Engineer's Guide**, Marcel Dekker, Inc., New York, (1989)p141-218.

[118] Langlais, J., Prebende, C., Tunide, B. and Naslain, R., **Journal de Physique**, Colloque 5, No.5, C5 - 93 - C5 - 103.

[119] Sedgwick, T.O., Smith, J.E., Jr., Ghez, R., and Cowher, M.E., **J. Crystal Growth**, 31, (1975)p264.

[120] Baw, V.S. and Gilbert, S.L., **J. Electrochem. Soc.**, 122, (1975)p1382.

[121] Amato, C.C., Hudson, J.B. and Interrante, L.V., In T.M. Besmann and B.M. Gallois, (eds.), Symposium Proceedings of **Chemical Vapour Deposition of Refractory Metals and Ceramics**, Materials Research Society, Pittsburgh, Pennsylvania, (1990) p119-24.

[122] Schlichting, J., **Powder Metallurgy International**, 12, No.3, (1980), p141-147, 196-200.

[123] Klam, C., Millet, J.P., Mazille, H. and Gras, J.M., **Journal of Materials Sci.**, 26, (1991)p4945-4952.

[124] Christian, F., Naslain, R. and Bernard, C., **Proc. Seventh Int. Conf. on CVD** (1972). In T.O. Sedgwick and H. Lydtin, (eds.), The Electrochemical Society, New York, (1979).

[125] Federer, J.T., **Thin Solid Films**, 49, (1977)p89-96.

[126] Wahl, G. and Batzies, **CVD IV**, p363.

[127] Chuzhko, R.K., Kirillov, I.V., Golovanov, Yu.N. and Zakharov, A.P., **Crystal Growth**, 3, (1968)p219.

[128] McMurray, N.D., Singleton, R.H., Muzzar, K.E. Jr., and Zimmerman, D.R., **J. Metals**,(1963)p600.

[129] Rai-Chondbury, P. and Hower, P.L., **J. Electrochem. Soc.**, 120, (1973)p1761.

[130] Theurer, H.C., **J. Electrochem. Soc.**, 108, (1961)p649.

[131] Campbell, A.E., NASA-CR-97810, Electro-Optical Systems Inc., Boston, (1968).

[132] Wicher, R., Ph. D. Dissertation, Univ. of California, (1966).

[133] Cuomo, J.J., Ziegler, J.F. and Woodall, J.M., **Appl. Phys. Letters**, 26, (1975)p557.

[134] Barnes, C.R. and Geesner, C.R., **J. Electrochem. Soc.**, 110, (1963) p361.

[135] Nagasima, N. and Kubota, N., **J. Appl. Phys.**, 14, (1975)p1105.

[136] Aboaf, J.A., **J. Electrochem. Soc.**, 114, (1967)p948.

[137] Sugawara, K., Yoshimi, T. and Sakai, H., **CVD V**, p407.

[138] Wahl, G., **CVD V**, p391.

[139] Kern, W. and Heim, R.C., **J. Electrochem. Soc.**, 117, (1970)p562.

[140] Glaski, F., **Proc. Fourth International Conference on Chemical Vapour Deposition.** In G.F. Wakefield and J.M. Blocher, Jr., (eds.) The Electrochemical Society Inc., Pennington, New Jersey, (1977), p521-535.

[141] Takahashi, T., Sugiyama, K. and Tomita, K. **J. Electrochem. Soc.** 114(1967)p1230.

[142] Bryant, W.A., M.S. Thesis, Univ. of Pittsburg, (1971).

[143] Van der Brekel, C.H.J. and Jansen, A.K., **J. Crystal Growth,** 43, (1987)p364-370.

[144] Jansen, A.K. and Van der Brekel, C.H.J., **J. Cryst. Growth,** 43, (1987), p371-377.

[145] Schaffhauser, A.C., **Report ORNL-4390**, Oak Ridge National Laboratory, Oak Ridge, Tenn., (1969).

[146] Fairchild, C.I., **CVD I**, p149.

[146A] Jensen, K.F., Fotiadis, D.I., Moffat, H.K., Einset, E.O., Kremer, A.M. and McKenna, D.R., Interdisciplinary issues in materials processing and manufacturing (Winter meeting of American Society of Mechanical Engineers), (1987),p565-585.

[147] Brinkley, S.R., **J. Chem. Phys.**, 15, (1947)p107.

[148] Brinkley, S.R., **J. Chem. Phys.**, 14, (1946)p563.

[149] White, W.B., Johnson, W.M. and Dantzig, G.B., **J. Chem. Phys.**, 28, (1958)p751.

[150] Ericksson, G., **Acta Chem. Scand.**, 25, (1971)p2651.

[151] Turnbull, A. and Wadsley, M., **CSIRO-Thermochemistry System program CHEMIX**, (version 5.1), CSIRO Division of Mineral Products, Port Melbourne, Australia, (1988)

[152] Borchardt, H.J. and Daniels, F., **J. Am. Chem. Soc.**, 79, (1957)p41.

[153] Reed, R.L., Gottfield, B.S. and Weber, L., **Ind. Eng. Chem. Fundls.,** 4, (1965)p38.

[154] Gray, A.P., **Proc. Amer. Chem. Soc. Symp. Analytical Calorimetry**, (1968)p209.

[155] Freeman, E.S. and Carroll, B.J., **J. Phys. Chem.**, 62, (1958)p394.

[156] Kissinger, H.E., **Anal. Chem.**, 29, (1957)p1702.

[157] Ozawa, T., **J. Thermal Analysis**, 2, (1970)p301.

[158] Gramberg, G. and Kőniger, M., **Solid-State Electronics**, 15, (1972) p285-292.

[159] Turpin, M. and Robert, A., **Proc. Br. Ceram. Soc.**, 22, (1973)p337-53.

[160] Price, R.J., **Nuclear Technology**, 35, (1977)p320-336.

[161] Akita, M., Iseki, T. and Suzuki, H., **Bull. of the Tokyo Inst. Technology**, No.127, (1975)p826-847.

[162] Fitzer, E., **Chemical Ing. Tech.**, 41, (1969)p331-339.

[163] Lefevre, R.L.R. and Price, M.S.T., **Ger. Offen., 2.533.135**, 12.2.(1976).

[164] Stinton, D.P. and Lackey, W.J., **Amer. Ceram. Soc.**, 57, (1978)p568-573.

[165] Pan, T.R., **Powder and Bulk Engineering**, (1988)p15-20.

[166] Von Műnch, W. and Pettenpaul, E., **J. Electrochem. Soc.**, 125, (1978) p294.

[167] Parretta, A., Giunta, G., Cappelli, E., Adonecchi, V. and Vittori, V., Influence of Substrate and Process Parameters on the Properties of CVD-SiC, In Procs. **Chemical Vapour Deposition of Refractory Metals and Ceramics**, T.M. Bessman and B.M. Gallois (eds.), Materials Research Society, Pittsburgh, Syl,vol. 168, (1990)p227-232.

[168] Aney, A.C., Cartwright, P.J. and Popper, P., **Special Ceramics**, 6, (1975),p147-157.

[169] Chappel, M.J. and Millman, R.S., **J. of Material Sci.**, 9, (1974)p1933-1948.

[170] Davis, R.F., Correlation Among Process Routes, Microstructures and Properties of Chemically Vapour Deposited Silicon Carbide, In. Symposium Procs. **Chemical Vapour Deposition of Refractory Metals and Ceramics**, T.M. Bessman and B.M. Gallois, (eds.), Materials Research Society, vol. 168, (1989)p145-158.

[171] Uny, G. and Morlevat, J.P., **J. Nucl. Mater.**, 71, (1977)p140-149.

[172] Morosanu, C.E. and Segal, E., **Thin Solid Films**, 88, (1982)p339.

[173] Parretta, A., **High Temperatures-High Pressures**, 20, (1988)p97.

[174] Bakovets, V.V., Izvest. Akademii Nauk SSSR, **Neogan. Mater.**, 12, No.7, (1976)p1312-1314.

[175] Masato, K., Nippon Kinzoku Gakkai-shi, Sendai, **J. of the Japan Institut of Metals**, 42, (1978)p131-136.

[176] Pampuch, P., Blazewicz, S. and Chlopek, J., **Szklo i Ceramika**, 29, No.10, (1978)p261-264.

[177] Linjewile, T.M., "Temperature of Burning Carbonaceous Particles in a Fluidised-Bed Combustor", **Ph. D. Thesis**, University of Adelaide, Australia, (1993).

[178] Blocher, J.M. Jr., Browning, M.F. and Barrett, D.M., **Procs. Emergent Process Methods for High Technology Ceramics**, Raleigh, NC, USA, Nov 8-10, (1982)p299-315.

[179] Finar, I.L., **Organic Chemistry: The Fundamental Principles**, Sixth Edition, Volume I, Longman Group Ltd., Hong Kong, (1973)p87.

[180] Minagawa, S. and Gatos, H.G., **Jap. J. Appl. Phys.**, 19(7), (1971)p844-49.

[181] Van Kenienade, A.C.W. and Sleinport, C.F., **J. Cryst. Growth**, 12, (1972)p13.

[182] Kobayashi, F., Ikawa, K. and Iwamoto, K., **J. Cryst. Growth**, 28, (1975)p395.

[183] Lever, R.F., **IBM**, 8(4), (1964)p460-65.

[184] Popper, P. and Riley, F.L., **Proc. Br. Ceramic Soc.**, 7, (1967)p99-109.

[185] Kobayashi, F., Ikawa, K. and Iwamoto, K., **J. Cryst. Growth**, 28, (1975)p395-96.

[186] Kingon, A.I., Lutz, L.J., Lian, P. and Davis, R.F., **J. Am. Ceramic Soc.**, 66(8), (1983)p558-566.

[187] Weiss, J.R. and Diefendorf, R.J., In **Chemically Deposited SiC for High Temperature and Structural Applications**. R.C. Marshall, J.W. Faust. Jr., and C.E. Ryan, Univ. of South Carolina, Press, Columbia SC, (1974).

[188] Vanderwielen, A.J., Ring, M.A. and O'Neal, H.E., **J. Am. Chem. Soc.**, 97, (1975)p993.

[189] Dzarnoski, J., Rickborn, S.F. and Ring, A., **Organometallics**, 1, (1982)p1217.

[190] Ring, M.A., O'Neal, H.E., Rickborn, S.F. and Sawrey, B.A., **Organometallics**, 2, (1983)p1891.

[191] Newman, C.G., O'Neal, H.E., Ring, M.A., Leska, F. and Shipley, N., **Int. J. of Chemical Kinetics**, 11, (1979)p1167.

[192] Cassel, R.B., **Perkin-Elmer Thermal Analysis Application Study 28**, Pittsburgh Conference Paper No. 688, (1979)

[193] Rogers, R.N. and Smith, L.C., **Thermochim. Acta**, 1, (1970)p1.

[194] Ozawa, T., **Bull. Chem. Soc. Jpn.** 38, (1965)p1881.

[195] Gusev, O.V., **Fiz. Khim. Obrab. Mater.**, No. 5, (1979)p51.

[196] Carten, G. and Armour, D.G., **Thin Solid Films**, 80(1), (1981)p13.

[197] Pranevicius, L., **Thin Solid Films**, 63(1), (1979)p77.

[198] Alan, M.K. and Flagan, R.C., **Aerosol Sci. Tech.**, 5(2), (1986)p237-248.